An Investigation into the Properties of Starch-Based Foams

A thesis submitted for the degree of
Doctor of Philosophy

Michael Bonin

School of Engineering & Design
Brunel University

October 2010

Abstract

This thesis reports research to investigate the mechanical, thermal and acoustic properties of biodegradable foams in block forms based on wheat starch and developed at Brunel University's School of Engineering & Design, in order to exploit the potential environmental benefits of this renewable and biodegradable class of materials.

Two emergent novel technologies have been developed based on a combination of the extrusion foaming of starch in conjunction with the natural adhesive characteristics of moistened starch to produce block foams. Regular Packing & Stacking (RPS), and Compression Bonded Loosefill (CBL), are foam fabrication technologies which have both demonstrated the potential to produce bulk foams based on wheat starch with unique structures and properties - a new class of foam materials in the form of macro-composites reinforced by a network of high-density bonding interfaces.

This thesis, as part of a Department of Trade & Industry/Technology Strategy Board funded project, reports an investigation into the following areas to address the scientific and technical issues involved in the further development of the materials and their applications.

- The basic properties of the raw materials used in the manufacture of CBL and RPS foams are outlined and the fabrication and preparation of these starch-based foams are described. The limitations of these production techniques are discussed with preliminary work and suggestions made for their enhancement.

- Research into the mechanical properties of the CBL and RPS foams includes compression, tensile, creep and dynamic impact tests, whilst the mechanical behaviour of the foams subject to high temperature and high humidity conditions is also reported.

- Research into the thermal properties of CBL and high density RPS foams includes testing of the material's thermal conductivity. This aspect of the research also involved a case study detailing the use of RPS in a commercial thermal insulation application.

- Research into the acoustic properties of CBL and RPS foams includes tests for sound absorption coefficient and sound transmission loss.

- Data obtained from these tests are benchmarked against data pertaining to the mechanical, thermal and acoustic properties of conventional polymer foams in order to provide a basis on which to identify the potential cushioning, thermal insulation and acoustic insulation applications of the starch-based materials.

The research has demonstrated the following:

- Potential cushioning applications include those limited to the range of static loads within the capabilities of the materials, taking into account the resilience of CBL and RPS which is likely to be compromised by successive impacts.

- Tensile forces tend to exploit weaknesses in the macrostructure of these materials. By implication the behaviour of the materials under shear forces would be expected to be similarly compromised.

- CBL and RPS exhibited dimensional shrinkage, density increase and significantly reduced mechanical properties under conditions of high temperature and humidity. This suggests that neither CBL nor RPS foams would be suitable for applications in regions where tropical conditions may be encountered unless used in conjunction with other protective materials which would not acutely increase the environmental burden of the products.

- Low-density RPS and CBL foams exhibit lower thermal conductivities and hence higher thermal insulation properties compared to many commercially available polymer foams of similar densities. As such these foams have the potential to be used in applications in which a measure of thermal insulation is required. A case study based on an existing commercial application in which the temperature of chilled products must be maintained over a 24 hour period reinforced these findings.

- The performance of CBL and RPS starch foams would not provide sufficient functionality to be employed in applications in which dedicated acoustic performance is required, although their sound absorption capabilities may facilitate overall marketability for applications in which a degree of acoustic performance is required if used in conjunction with other materials which demonstrate good acoustic performance.

It is anticipated that this work will make significant contributions toward advances in the development of these novel technologies, specifically in terms of establishing an understanding of the properties of the starch-based materials and in identifying potential applications. The research results should thus provide a fundamental element in the basis for the industrial development of these renewable and biodegradable materials.

Table of Contents

List of Tables

List of Figures

Acknowledgements

Chapter 1   Introduction

1.1   Background to this work

The manufacture of products made from plastics consumes a significant proportion of petrochemicals processed from finite fossil reserves. It is estimated that 4% of the world's annual oil production is used as a feedstock for plastics production requiring an additional 3 - 4% in energy use during manufacture. Consumption of plastics is estimated to be growing by approximately 4% per year in Western Europe (Waste Watch, 2006).

Packaging represents the largest single sector of plastics use in the UK accounting for 35% of plastics consumption, much of which then goes on to comprise a substantial proportion of municipal solid waste streams. Plastics comprise approximately 7% of the average household dustbin in the UK, with current annual plastics waste generation in the UK estimated to be nearly 3 million tonnes. An estimated 56% of all plastics waste is discarded packaging, three-quarters of which originates from households. It is estimated that only 7% of total plastics waste arisings are currently being recycled (Waste Watch, 2006).

The disposal of plastics products contributes significantly to their overall environmental impact. The consumption of plastics products such as packaging, which are disposed of soon after their purchase puts pressure on limited landfill space. In addition, plastic waste often becomes litter. Nearly 57% of litter found on beaches in 2003 was made from plastics (Waste Watch, 2006), whilst a 1998 survey found that 89% of the litter observed floating on the ocean surface in the North Pacific were plastics, leading to studies which estimated a global average of over 13,000 pieces of plastic litter floating on every square kilometre of ocean surface (UNEP, 2010).

These issues represent a growing set of environmental, social and economic concerns for both industrialised and developing countries. In recent years, efforts have been made to develop alternative materials from renewable raw resources into polymers which degrade easily under well-defined environmental conditions so as to facilitate waste management by biological processes. Such materials have applications in a number of niche markets in which renewability and biodegradability are desired features.

Starch is a natural polymer derived from cultivated plants including maize, wheat and potatoes, which can be plasticised into a material known as *thermoplastic starch* (TPS) and combined with other bio-plastics to produce *starch complex* (SC). Currently, successful commercial applications of TPS and SC have chiefly been in the form of sheet or film products of various types, used in the manufacture of compostable packaging and carrier bags. However, commercial applications of

block foams manufactured from TPS have thus far found a more limited market, due in part to the technical difficulties involved in the production of uniform block foams and also issues of providing adequate technical specifications for the materials.

Two emergent novel technologies have been developed at Brunel University's School of Engineering & Design which utilise the natural adhesive characteristics of moistened starch. Regular Packing & Stacking (RPS), and Compression Bonded Loosefill (CBL), are foam fabrication technologies which have both demonstrated the potential to produce bulk foams based on wheat starch with unique structures and properties - a new class of foam materials in the form of macro-composites reinforced by a network of high-density bonding interfaces.

These developments have generated opportunities for further investigation into the properties of the materials produced by the new technologies, as well as analysis into their potential commercial applications. It has also warranted research into enhancement of the technologies themselves.

As a result, this PhD work was initiated and forms part of the project; "Lightweight Eco-Composites Based on Renewable Raw Materials" (TP/2/MS/6/1/10118), funded by the UK Government Department of Trade & Industry, now known as Technology Strategy Board.

1.2   Scope of the research

1.2.1   Aims:

The primary aim of the research was to investigate the mechanical, thermal and acoustic properties of CBL and RPS foams, benchmarking the results against the properties of conventional polymer foams in order to facilitate analysis of potential applications of the starch-based materials. The secondary aim of the research was to investigate the foam fabrication processes in order to provide a basis for future enhancement of the technologies.

1.2.2   Objectives:

Overall, this work was designed to address scientific and technical issues surrounding the further development of the novel materials and to demonstrate the feasibility for applications using a case study. More specifically the objectives were:

- To understand the mechanical, thermal and acoustic properties of CBL and RPS foams.

- To understand the effects of high-humidity and high temperature conditioning on the mechanical properties of CBL and RPS foams.

- To understand the potential applications of CBL and RPS foams by means of benchmarking the test results obtained against tests conducted on conventional polymer foams, or against previously published data.

- To understand by means of a case study, the thermal insulation behaviour of RPS foam as part of an assessment of the suitability of this starch-based material in an existing commercial thermal packaging application.

- To investigate the CBL and RPS fabrication processes in order to provide a basis for future enhancement of the technologies.

1.3 Research methodology

The thesis begins by reviewing the subject and the literature covering it, before focussing on the fabrication technologies used in the production of RPS and CBL foams. The benefits and limitations of these technologies are also covered and suggestions for alternative techniques are initiated with the purpose of potential enhancement of materials processing.

The investigations focus on the mechanical, thermal and acoustic properties of starch-based foams and accordingly the work has been divided into three discrete sections corresponding to these properties. Wherever possible, tests were conducted in accordance with appropriate test standards. The results of these tests were then benchmarked against data pertaining to the properties of conventional polymer foams for purposes of comparison. In some cases data from published literature were used for benchmarking, whilst in other cases data was obtained by testing samples of conventional polymer foams alongside starch-based foams. Interpretations of datasets are given in each section of the research along with analysis of comparative data in order to facilitate mapping of the properties of the starch-based foams and thus indicate any potential commercial applications of the materials.

1) Mechanical properties

The physical performance criteria of foam materials must be specified in terms of their mechanical strength characteristics under certain conditions in order that any potential applications may be determined. As such, this section is separated into four main subdivisions relating to mechanical tests conducted on CBL starch-based foams, the mechanical properties of which are currently unspecified. The following studies were conducted to determine the mechanical properties of the materials:

- Static compression behaviour from which data including yield strength, compressive stress and elastic modulus of the materials were derived.

- Dynamic impact behaviour presented in terms of a series of cushion curves which plot peak deceleration of static loads against static stress on the samples.

- Creep behaviour in terms of material deformation over time under prolonged constant loading.

- Tensile behaviour including tensile strength and physical elongation at the point of sample break.

- Compression and creep behaviour of the materials under conditions of high temperature and relative humidity.

The results of the tests conducted should provide a basis for the full specification of these materials in terms of their mechanical properties, thus establishing their suitability for applications and environmental conditions in which a measure of mechanical strength is required. Potential applications are mainly expected to be in the field of alternative cushion packaging materials.

2) Thermal properties

In order that any potential thermal insulation applications of materials may be determined, their thermal performance criteria must be specified in terms of thermal conductivity characteristics under certain conditions. As such, this section is separated into two main subdivisions relating to thermal tests conducted on CBL and high-density RPS starch-based foams, the thermal properties of which are currently unspecified. The following studies were conducted to determine the thermal properties of the materials:

- Hot plate (heat flow meter) method conducted on CBL samples of various densities, yielding thermal conductivity values.

- Hot Disk thermal constants analysis (transient plane source) method conducted on a variety of high density RPS starch-based foam samples, yielding thermal conductivity and thermal diffusivity values, enabling an estimate of the specific heat capacity of the materials to be produced.

The results of the thermal tests conducted should provide a basis for the full specification of these materials in terms of their thermal properties, thus establishing their suitability for applications in which a measure thermal insulation is required. Potential applications are mainly expected to be in the areas of packaging for thermally sensitive products and possibly as the insulation component within composite boards for partitions and temporary structures.

A case study is also presented which investigates the potential for RPS foam to be employed in a current commercial application for the packing and transit of temperature-sensitive food products. The case study endeavours to reinforce the findings of the laboratory-based thermal conductivity tests conducted on the starch-based materials, whilst assessing RPS foam in terms of its suitability for a functional application.

3)   Acoustic properties

In order that any potential acoustic applications of materials may be determined, their acoustic performance criteria must be specified in terms of their response to certain conditions. This section is separated into two main subdivisions relating to acoustic tests conducted on CBL and RPS starch foams. The following studies were conducted to determine the acoustic properties of the materials:

- Sound absorption coefficient tests

- Sound transmission loss tests

The results of the acoustic tests conducted should provide a basis for the full specification of these materials in terms of their acoustic properties, thus establishing their suitability for applications in which a degree of acoustic functionality is required. At present it is not expected that starch-based foams would perform to the standards required of dedicated acoustic insulation materials.

1.4   Structure of the thesis

This thesis consists of eight chapters which are arranged as follows:

Chapter 1 gives an introduction to the background of this work, the aim and objectives of the project and structure of the thesis.

Chapter 2 provides a literature review in relation to the subjects considered in this project. It includes the following topics:

- An overview of the development and application of lightweight cellular polymeric materials and a summary of their characterisation.

- The general principals of cushion packaging including the mechanical properties of foams and means of testing. Examples of foams for cushion packaging applications.

- The general principals of thermal insulation and testing of thermal conductivity.

- The general principals of acoustic design. Examples of foam materials for sound attenuation applications.

- Drivers for the development of renewable bio-plastics.

- The mechanisms of biodegradation in polymers.

- Terminology and standards of plastics degradability.

- Classification of synthesised bio-plastics and starch-based plastics.

- The production of extruded starch-based foams.

- Characterisation of the structure of extruded starch.

- The properties of thermoplastic starch-based materials.

- The effects of temperature and humidity on the starch-based materials.

Chapter 3 provides the basic properties of the raw materials used in the manufacture of CBL and RPS and describes the fabrication and preparation of these starch-based foams. It then goes on to discuss the limitations of these production techniques with suggestions for improvements and some preliminary work aimed at enhancement of the technologies.

Chapter 4 describes the experimental details of mechanical, thermal and acoustic tests conducted on the starch-based foams, including sample preparation where not previously detailed, test equipment and test procedures used.

Chapters 5, 6 and 7 respectively illustrate the results of mechanical, thermal and acoustic tests conducted on the starch-based foams. Within each chapter the data obtained is compared to data pertaining to the mechanical, thermal and acoustic properties of conventional polymer foams in order to facilitate mapping of the properties of the starch-based foams and thus indicate any potential applications of the novel materials. A case study detailing the use of starch-based foam in a current commercial application is also provided in chapter 6. Interpretation and discussion of the results of the mechanical, thermal and acoustic tests is included within these respective chapters.

Chapter 8 provides a general discussion highlighting the key achievements of this research and drawing conclusions based on the previous chapters. Recommendations are made for related areas requiring further research.

Chapter 2   Literature Review

2.1   The development & application of lightweight cellular polymeric materials

Naturally occurring foams such as sponges and cork have been exploited for millennia across various cultures and geographical locations. The advent of synthetic polymers in the mid-twentieth century led to their development and production in the expanded form owing to the unique and useful properties that these new foam materials conferred (Eaves, 2004). The current use of polymer foams is extremely widespread across a diverse range of industries covering a vast array of applications including sports and leisure products, road vehicles, aircraft, furniture, construction, packaging, refrigeration, marine and military applications. The almost ubiquitous status of this class of material has come about due to the development of an outstanding range of mechanical characteristics as well as excellent thermal and acoustic insulation properties.

2.2   The formation of cellular polymer structures

The study of the formation of foams is closely linked to the mathematical problems of three-dimensional honeycombs comprising cellular structures with minimal surface areas and surface tensions, resulting in structures of maximum energy efficiency. Most synthetic polymer foams are formed by a process involving nucleation, growth and stabilisation of gas bubbles within a polymer matrix through the following phases:

1) Nucleation, involving the generation of small gas bubbles by means of blowing agents saturated within the liquid/molten polymer matrix. These come in the form of physical blowing agents - inert gasses such as carbon dioxide or nitrogen which are forced into solution in the polymer melt at high pressure and then expand as bubbles as the pressure is released. Alternatively, low-melting point liquids such as chlorofluoro-carbons or methylene chloride may be used to develop bubbles as they change state into gasses. Chemical blowing agents such as sodium bicarbonate decompose or react under the influence of heat or catalyse when mixed with other agents to form gasses (Gibson & Ashby, 1997).

2) Once the bubbles reach a critical size they continue to grow as the blowing agents rapidly diffuse into them, remaining spherical until closely packed (Naguib et al, 2004). This stage generally features the greatest density reduction in the polymer matrix. Further growth in bubble size forces distortion of closely packed cells into polyhedral structures (Eaves, 2004).

3) At this stage growth will continue until the bubbles either stabilise under atmospheric pressure or rupture resulting in open cell foams. Viscous and surface tension effects cause material to flow towards intersecting cell elements forming junctions of tricuspid cross-section (Eaves, 2004).

2.3 Characterisation of polymer foams: Foam structure

Depending on the degree of cell expansion, shape, *topology* (that is the connectivity of cell walls, pore space and cell geometry), and the particular polymer formulation, foams may have a variety or combination of structures.

2.3.1 Density

One of the most important structural characteristics of a foamed material is its density as this defines the air/polymer ratio within the foam. The density of a foam is generally defined as its mass per unit volume, usually expressed in units of kilograms per cubic metre (kg/m^3). This reflects the density of the solid material as well the porosity within the foam, but it does not account for any internal voids present within the foam as these would be averaged into the overall calculation (Eaves, 2004). This proviso is of great significance for those working with foam structures of inherent imprecise uniformity such as those which are the main focus of this research, and this issue will be covered in greater detail in this thesis.

Bulk density is a measure used for foams in the form of many discrete pieces packed together such as loosefill materials where the volume of an individual piece is difficult to measure or may not be representative. Bulk density is measured by pouring foam pieces into a container with a known volume. Bulk density is calculated as the mass of the foam pieces per unit volume occupied which includes the voids between the pieces. It therefore reflects both density of individual piece and their packing behaviour. The accuracy of bulk density measurement is thus influenced by both the dimensions of the container and the relative size and shape of the foamed samples. Bulk density may also be expressed as kilograms per cubic metre (kg/m^3). *Relative density* is the ratio of foam density to the density of the original unexpanded polymer. This term, often given as percentage, represents the volume fraction of polymer present in a foam, with examples of low density foams having volume fractions < 10% (Eaves, 2004). Clearly, porosity (volume percentage of air) of the foam can be directly derived from relative density.

Most grades of conventional low-density polymer foams have densities which range from about $12 - 40$ kg/m^3, while foams with fillers, flame retardants, or foams chemically engineered for stiffness and/or flexibility may have densities of 100 kg/m^3 or higher (Eaves, 2004).

2.3.2 Cell size

Random nucleation of cells in space and time together with the growth of cells through gas diffusion often leads to the production of foams comprising cells of widely variant size distribution. Cell size is often measured by inspection of a cross-section of foam in which a count is made of the number of cells intersecting a specific length. In practice, due to size distribution,

cell size is either expressed as an average or given as a range by foam manufacturers (Eaves, 2004).

2.3.3   Cell shape

The topology of cells in foams describes the number of cell walls or faces, the junctions between cells and the degree of curvature of cell walls or struts, all of which contribute toward the geometry of cell interfaces and space filling within a foam, which is closely linked to its density (Eaves, 2004). Foams which are not produced in conditions allowing free expansion in three dimensions may exhibit structural and property *anisotropy*, being directionally dependent and having different values when measured in different directions. This frequently occurs in cases in which foams are extruded and cells exhibit lateral distortion, resulting in a variance in measured properties along the lateral and cross directions of the foam. Manufacturers often quote properties measured in these directions (Eaves, 2004).

2.3.4   Open cell/closed cell ratio

In general, most foams have a combination of open and closed cell structures, although at either extreme of this spectrum there are foams which are comprised of only open or closed cells (Gibson & Ashby, 1997). The ratio of open to closed cells is determined by processing conditions and is important in determining foam properties, especially of low density foams (Eaves, 2004). Certain foam applications such as filters, gaskets and acoustics require that the foam either permits or blocks the passage of gasses. Since porosity can affect other mechanical foam properties, foam manufacturers use air flow to approximate the proportion of intact call walls within a foam and thus quantify its porosity. Air flow is measured in m^3/second required to maintain a pressure differential of 125 Pa through a standard 50mm x 50mm x 25mm foam sample. As is the case with other mechanical properties, porosity may vary significantly in anisotropic foams when measured in horizontal and vertical directions (Eaves, 2004).

2.3.5   Anisotropy

Almost all natural and synthetic foams are anisotropic to some degree, with a tendency for cells to be elongated, flattened or have walls of unequal thickness. Synthetic polymer foams are made by various techniques of expansion all of which tend to orientate the cells in a particular direction imparting the finished foam with *structural anisotropy*. However, *material anisotropy* can also occur within the cell walls or struts of the foam and both of these effects can combine to influence the properties of the material (Gibson & Ashby, 1997).

Whilst the structures of polymer foams have a considerable effect on their behaviour in response to external stimuli, an additional set of parameters related to the intrinsic properties of the solid material from which the cell walls are made are also of great significance in influencing the

particular properties of foams (Gibson & Ashby, 1997). The properties of polymeric foams are therefore based on the particular polymer from which the foam is comprised as well as the foaming conditions which generated the foam structure.

In this thesis, specific properties of polymer foams are discussed in terms of their behaviour in response to mechanical, thermal and acoustic stimuli as well as the functional applications of foams in these areas.

2.4   The mechanical properties of foams: general principals of cushion packaging

Foams are commonly used for cushion packaging applications in which they are primarily used to absorb energy by deformation and must exhibit the appropriate performance characteristics under given conditions. In general, cushion packaging design seeks to protect vulnerable products by reducing the stresses associated primarily with shock, vibration or compression in the distribution chain through control of energy dissipation and limitation of product freedom of movement within the package. This is achieved through deformation of the cushion in response to these stresses in order to minimise those exerted on the product. After being compressed either statically or dynamically, the cushioning material should recover approximately to its original shape and dimensions. The degree of such recovery is known as *resilience*. The material selected should have sufficient resilience to maintain the required cushioning performance.

2.4.1   Static compression

Static compression describes a condition in which compressive stress is applied at a relatively low rate. Since most products are stacked during distribution, it is important for packaging to be able to withstand static compression loads, thus avoiding damage to the product or packaging.

When subject to static compression the deformation of elastic-plastic foams typically shows three main regimes as shown in Figure 2.1:

1) Linear elastic zone - An initial linear elastic regime, where a relatively low amount of strain energy is stored in the reversible bending of the cell walls or struts. The elastic (or Young's) modulus is illustrated by the initial slope of the stress-strain curve, which represents the resistance of a foam to elastic deformation.

2) Crush plateau zone - When compression loading is increased to certain level and reaches a peak, cells start to collapse as their cell walls or struts buckle, leading to a plateau in the stress-strain curve in which small increases in load lead to very large additional strain. The foam is able to absorb energy by progressive cell buckling at approximately constant stress levels.

3) Densification zone - Finally the collapsed cell walls or struts begin to impinge upon each other and a densification regime begins. At this last stage, further strain compression will result in a rapid increase in stress as the foam starts to exhibit a rapid increase in modulus approaching that of the solid material from which it is made (ERG, 2008).
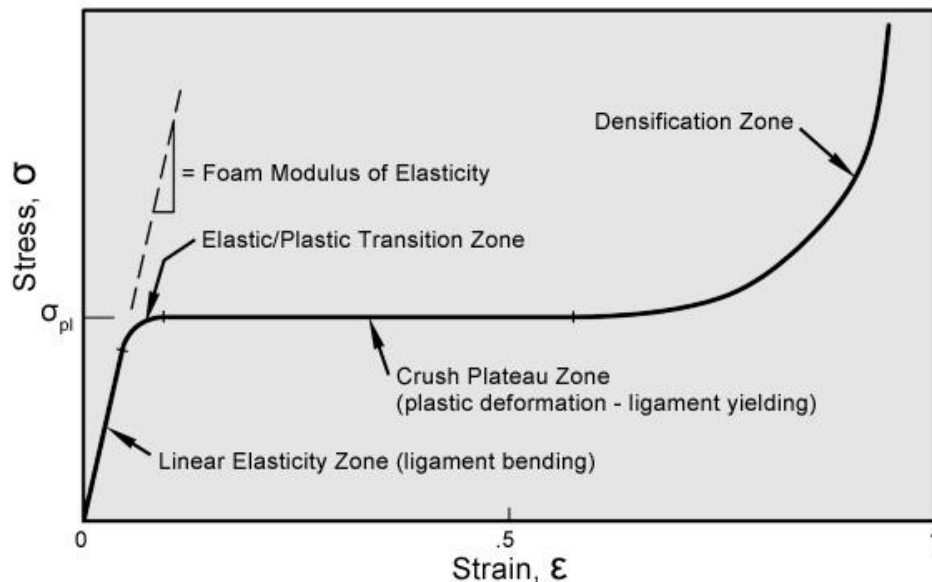
Figure 2.1: Typical static compression stress-strain curve for elastic-plastic foams
ERG, 2008

For cushion applications, the compression strength of a foam at a given compressive strain is normally defined as the stress at elastic/plastic transition zone (σ_{pl}), or for materials without a crush plateau, by stress at a predetermined compressive strain.

The work done per unit volume of the foam to a particular strain is described by the area below the stress-strain curve (Figure 2.1). The energy is absorbed by foams through the elastic buckling, plastic yielding or brittle crushing of cell walls or struts. The more energy absorbed by the foam packaging material, the less energy that is available to be transferred to the packaged product, which is thus less likely to suffer damage.

The stress-strain curve is useful in determining the overall "efficiency" of the material in terms of its static compression behaviour and it also gives some indication of the linearity of the cushion material - the relationship between deflection and applied load.

2.4.2 Dynamic compression and shock

Dynamic compression describes a condition in which compressive stress is applied at a relatively high rate, representing shocks typically occurring during warehousing operations, stack resonance, as well as normal transit conditions. The apparent compression strength of a material under static conditions can be affected by the rate of load application. Rapidly loading a visco-

elastic material normally produces a higher apparent compression strength than when a material is loaded slowly (Soroka, 1996).

Shock is defined as an impact characterised by a sudden and substantial change in velocity and may be encountered at many points in the distribution chain such as drops during manual handling, falls from conveyors, chutes or pallets, and impacts occurring as a result of uneven roads, sudden stops, or rail shunting in vehicle transportation.
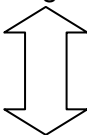
Newton's Second law of motion states that the acceleration of an object as produced by a net force is directly proportional to the magnitude of the net force, in the same direction as the net force and inversely proportional to the mass of the object. Since mass is constant for any given packaging problem, force is directly proportional to acceleration or deceleration, measured in units of gravity (G) $9.81 m/s^2$ (Soroka, 1996).

Underpinning the design of any cost-effective engineered cushion packaging structure intended to provide protection against shock damage are two principal design parameters. Firstly, the amount of mechanical shock the product can survive on its own without suffering damage. The quantified ability to withstand shock is known as a product's *fragility factor*, which is expressed in critical acceleration or G levels. The more fragile a product is, the fewer Gs it can withstand. The function of cushioning is to extend the time for the speed reduction and thereby reduce the deceleration.

Ideally, the fragility of a product is determined in a laboratory by subjecting it to a series of shocks (decelerations) of gradually increasing severity, in order to find the lowest severity impact that will damage the product. The highest deceleration which did not cause damage is then known to be the product's fragility or G factor (NEFAB, 2009).

Ideally the fragility factor of products should not be estimated, but defined through test data or obtained from the relevant Material Design Authority. If the G-factor is overestimated and the product is unable to survive as much shock as anticipated, the packaging will be under-designed and significant shipping damage is likely to occur. Conversely, if the G-factor is underestimated and the product can actually withstand more shock than anticipated, the packaging will be over-designed and thus be unnecessarily bulky, incurring unnecessary expense in production and transportation through the distribution chain (NEFAB, 2009). Table 2.1 shows some typical examples of product fragility factors.

Table 2.1: Typical product fragility factors

	Product	**Fragility Factor (Gs)**
Fragile	Aircraft altimeters, hard discs	15 – 25
	Medical diagnostics apparatus	25 – 40
	Computer terminals, printers	40 – 60
	Televisions & hi-fi equipment	60 – 85
	Major appliances & furniture	85 – 115
Durable	Table saws, machine tools	115 +

NEFAB, 2009

The second design parameter is the *design drop height* - related to the maximum height from which a package may reasonably be expected to be subject to drops in normal handling and transit. Journey hazard trials show that in general, maximum drop height is linearly related to the logarithm of package mass. Thus, the larger or heavier the package, the lower the design drop height (Campbell, 1992). Figure 2.2 shows a typical design drop height chart indicating the probability of drops from specific heights according to package weight.
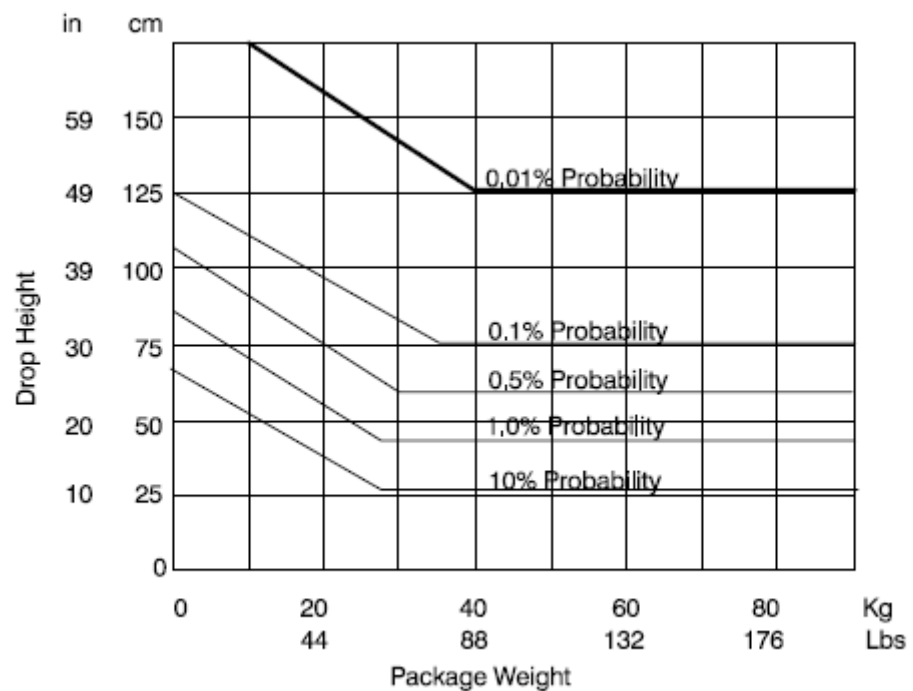
Figure 2.2: Design drop height chart
Schueneman, H H, Package Engineering, Design & Testing (Westpak Inc.)

In general, there is a lower probability of severe intensity drops to packages and an increased probability that packages will be subjected to a greater number of low intensity drops. Relatively few packages receive more than one drop from great heights.

The basic principal of cushioning against shock is to extend the time over which impact velocity is dissipated, translating the high-peak short duration shock pulse into a low-peak long duration shock pulse by deflection of a resilient cushioning material. This extension in time is achieved by the deflection of a resilient cushioning material, dissipating the deceleration energy over a longer time period and controlling deceleration to a level below the fragility level of the packaged product. Figure 2.3 compares the profile of an unprotected impact with a cushioned response.
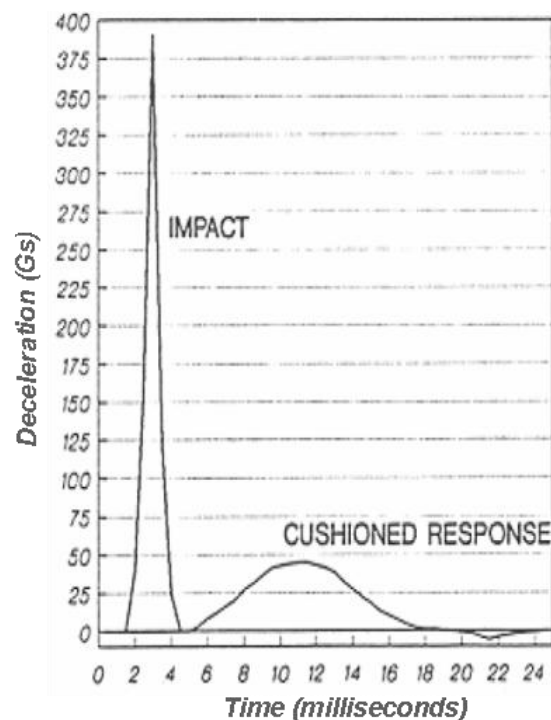
Figure 2.3: Unprotected impact vs. cushioned response
Schueneman, H H, Cushion Engineering, Design & Testing (Westpak Inc.)

In theory, an ideal cushioning material would provide constant deceleration through 100% compression to a thickness of zero. In practice however, cushioning materials cannot provide constant deceleration, nor can they be compressed to zero but will 'bottom out' at some point. Therefore the thickness of cushioning material required will always be greater than the ideal cushion by a factor C, the *cushion factor* – the ratio of a cushioning material's efficiency as a shock absorber compared to a perfect cushion with a theoretical cushion factor of 1 (Soroka, 1996). Cushion factor values are specific for each type of cushioning material. Table 2.2 shows a comparison of typical cushion factors for some common foam materials.

Table 2.2: Typical cushion factors of various foams

Material	Density (kg/m³)	Cushion Factor Range
Flexible PU Foam	30	2.2 – 2.5
EPE (A)	28	2.8 – 3.3
EPE (B)	40	2.8 – 3.5
EPS (moulded)	30	2.0 – 2.4
EPS (loose-fill)	8	3.8 – 4.2
PU chipfoam	65	3.0 – 3.3
Expanded Rubber	179	4.1 – 4.5

Schueneman, H H, Cushion Engineering, Design & Testing (Westpak Inc.)

Key to Table 2.2:   PU – polyurethane
                     EPE – expanded polyethylene
                     EPS – expanded polystyrene

Calculation of the required cushion thickness for shock protection is carried out using the following formula:

$$d = \frac{2h}{G - 2} \qquad (2.1)$$

Where: d = dynamic deflection of cushion (cm)

h = Drop height

G = required deceleration level (based on product fragility factor)

For example, if a product has a fragility factor of 50Gs and a design drop height of 90cm:

d = 2 x 90 / (50-2)

d = 3.75cm   (Schueneman[a])

The dynamic deflection of the cushion is then multiplied by the cushion factor of the particular cushion material, for example: 3.75 x 2.2 (for moulded EPS, Table 2.2) required cushion thickness = 8.25cm

As a second example: 3.75 x 3.0 (EPE) required cushion thickness = 11.25cm

Dynamic cushion performance data of foams is presented in the form of peak deceleration/optimum static loading curves (otherwise known as *cushion curves*), which are obtained by dropping a series of predetermined loads corresponding to product mass, from a specified drop height onto different thicknesses of cushioning material and recording the peak deceleration.

For each cushion curve peak deceleration has a minimum value and the cushion loading at which this occurs is known as optimum static loading - the point of maximum cushion efficiency.

Figure 2.4 shows an example of the cushion curves for two different thicknesses of the same cushioning material.
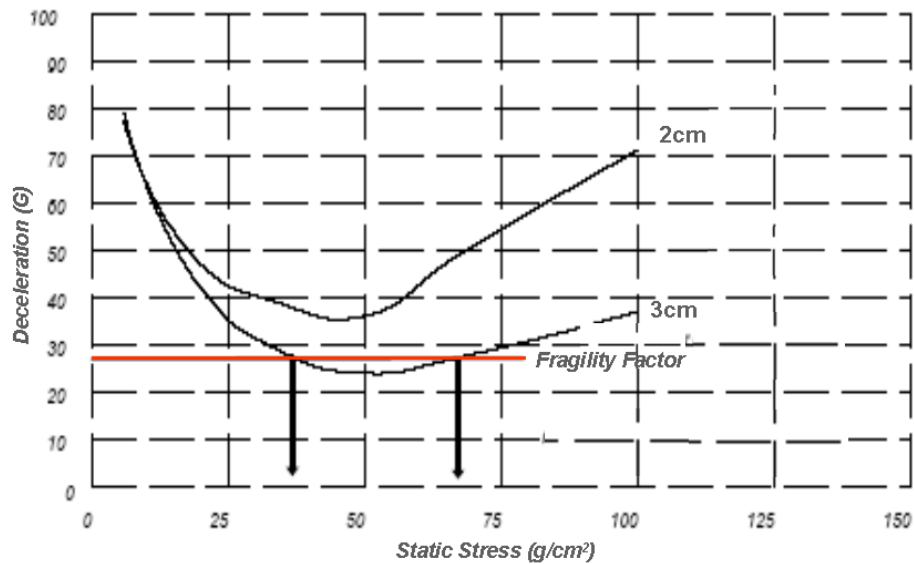
Figure 2.4: Cushion performance - peak deceleration/optimum static loading
Adapted from Schueneman, H H, Cushion Material Testing (Westpak Inc.)

Theoretically, any portion of the cushion curve below the product fragility factor will define a static stress loading capable of transmitting less than the critical acceleration to the product. For optimum material usage it is normally desirable to load the cushion to a level determined by the highest static stress allowed by the curves. However, many designers find it desirable to load the material at the low point of the cushion curve where transmitted deceleration is a minimum (Schueneman[a]).

With successive drops, some cushion materials such as expanded polystyrene (EPS) exhibit fatigue characteristics and may transmit increased levels of peak deceleration. ASTM standard D1596 therefore recommends that cushion performance tests are repeated a total of five times onto a given sample at each given static stress with the definitive cushion curve given as the average of impacts 2 - 5 (Schueneman[a]).

Figure 2.5 shows cushioning performance over a series of impacts.
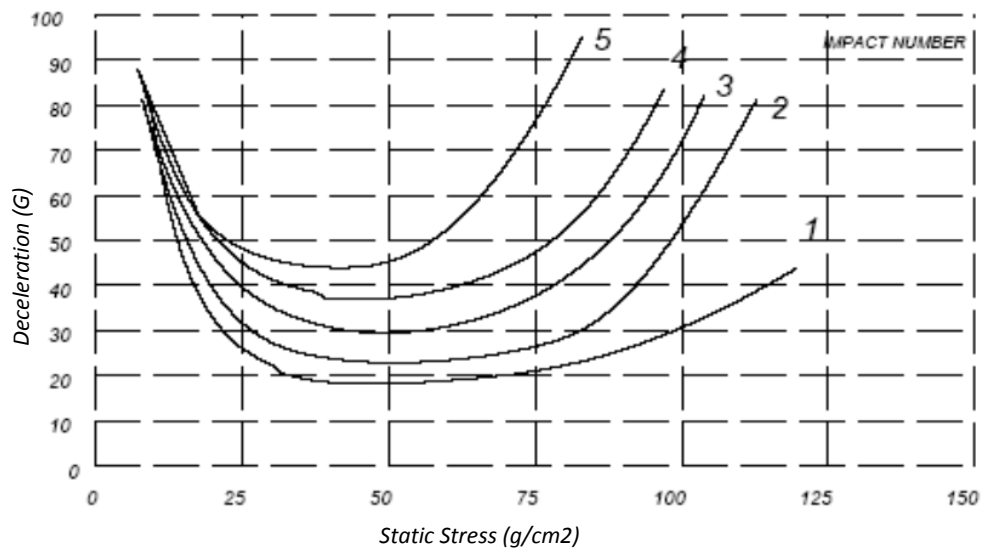
Figure 2.5: Cushion performance - multiple impacts
Schueneman, H H, Cushion Material Testing (Westpak Inc.)

Whilst heavier loadings can be used to achieve lower deceleration levels this can further increase material fatigue and have a negative effect on the cushion's ability to withstand additional impacts. Therefore, the design of an EPS pack for a single impact verification test procedure requires a different the static stress loading than would be the case if the test procedure required multiple impacts on the same face. In contrast, materials such as expanded polyethylene (EPE) are generally resilient to repeated impacts, so it would probably make little difference if the test procedure called for one impact on each face or multiple impacts (Schueneman[a]).

In practice, there is a very low risk of more than one drop per face from the design drop height and outer containers contribute significantly to protecting cushion material. Defence Packaging Authority cushion design data thus points to the use of first drop performance data (Campbell, 1992). This discrepancy in the method used therefore calls for a clearly established test procedure prior to cushion design (Schueneman[a]). Standard cushion curves are available for each type and thickness of commercially available cushioning materials. Because of the infinite number of potential combinations of masses and design drop heights, various methods have been developed relating to specific cushioning materials, which reduce the dynamic performance data into more easily used formats. Cushion curves relating to specific thicknesses of cushioning materials are also available from some suppliers. However, it should be noted that cushion curves are "best fit curves" generated from averaged data at specific loading points on specific cushion samples. The effects of sample variability, averaged data and the judgement involved in

drawing smooth curves from "non-classical" data, all point to the use of cushion curves as approximate values (Schueneman[b]).

Several papers have been published proposing methods of predicting cushion curves in order to rapidly evaluate the cushioning properties of polymer foams without the need to conduct multiple dynamic cushion tests on samples of each foam density. Loveridge and Mills (1993), base their method on the relationship between a single existing stress-strain master curve and the cushion curve, whilst Ansorge and Nendel (1998), employ a physical model developed by forming a system of equations based on energy conservation and material laws. Matthew Daum (1999) of Hewlett Packard bases his shortcut method for developing cushion curves on a stress-energy method developed by Dr. Gary Burgess of Michigan State University.

However, these prediction techniques are valid only for foams comprising a predominance of closed cells, thus they are not appropriate methods for evaluating the cushioning performance of starch foams in which structures are comprised of a significant fraction of open cells (Kang, 2006).

2.4.3   Vibration and resonance

Vibration describes an oscillation or motion about a fixed reference point. The distance moved about the reference point is the amplitude and the number of oscillations per second is the frequency. All transport modes are associated with characteristic amplitudes and frequencies of vibration, with lower amplitudes typically corresponding to higher frequencies.

Vibrations come from many sources. Road vehicle vibrations occur predominantly at the natural frequencies of the load on the vehicle's suspension system, of the unsprung mass of the tyres against the suspension system, and of the vehicle trailer and body structure. These frequencies are stimulated by the condition and irregularities of the road, tyre and wheel imbalances, and the dynamics of the load itself. For protection from vibration, the cushion system must provide attenuation of any potentially harmful vibration frequencies by means of amplitude reduction, before these can reach the product. Figure 2.6 shows how the cushion resonance attenuates the product response.
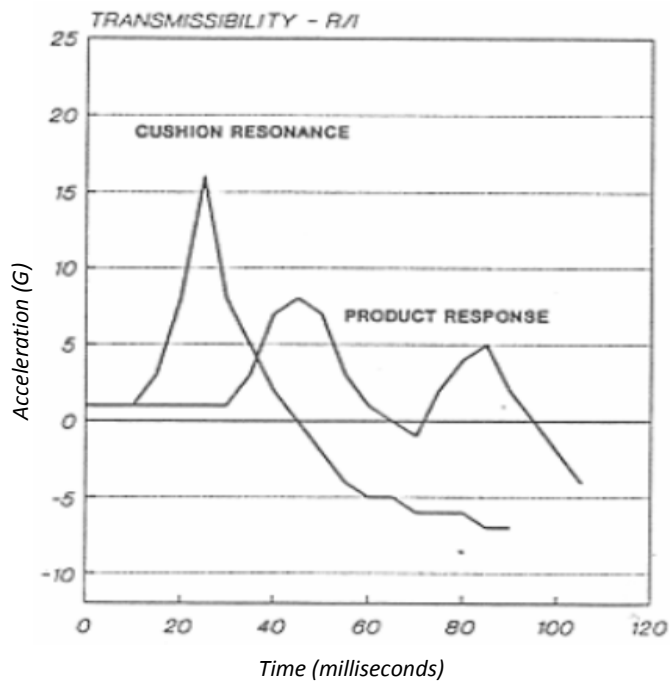
Figure 2.6: Vibration - response attenuation
Schueneman, H H, Cushion Engineering, Design & Testing (Westpak Inc.)

An ideal vibration-isolation material would provide isolation in the 3 - 100 Hz range as these are the predominant frequencies which cause damage during transportation. The most problematic frequencies in the distribution chain are those occurring below 30Hz. These are the most prevalent in road and rail vehicle transport and are difficult to isolate (Soroka, 1996).

Resonance describes a condition in which a vibration input is amplified resulting in an output value greater than the sum of all input values. Figure 2.7 shows how a cushion system may amplify the product response.

Time (milliseconds)
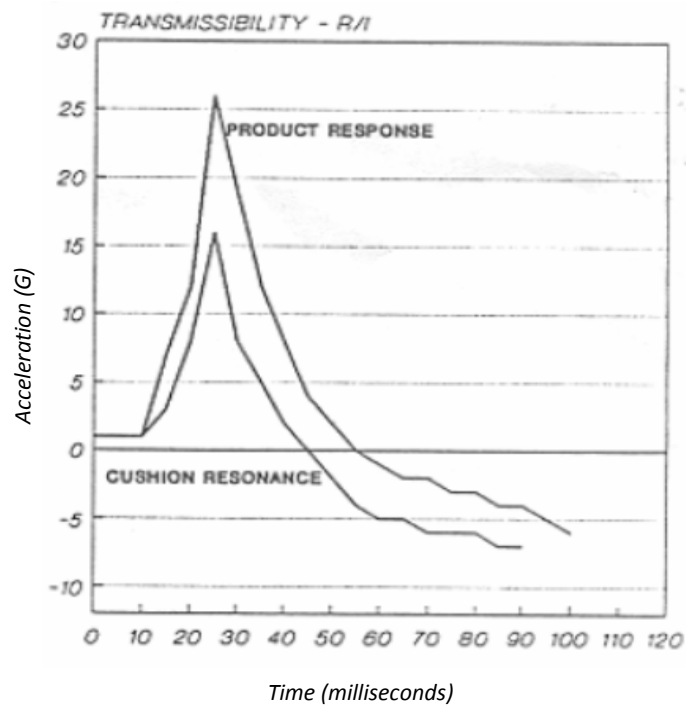
Figure 2.7: Vibration - response amplification
Schueneman, H H, Cushion Engineering, Design & Testing (Westpak Inc.)

All spring/mass systems have unique natural frequencies at which they will resonate. Vibration resonance occurs when the input frequency matches this natural frequency of the product and/or packaging system, producing an amplified vibration output. Resonance exists not only for the total assembly but also for components or subsections within the total structure including stacked loads.

For these reasons, damage caused by vibration resonance can be difficult to resolve. Whilst packaging materials used to isolate vibration are for the most part the same as those used to isolate shock, the situation is further complicated by the use of cushioning packaging materials which although acting to attenuate shock damage, may also be acting as a spring in response to vibrational inputs.

In order to alleviate resonance, all resonance points should be located and quantified by subjecting the spring/mass system to a large range of frequencies across all axes in order to identify those frequencies at which a resonance condition occurs. A properly selected isolation material resonates at an input frequency less than half of the product's natural resonance frequency (Soroka, 1996).

2.4.4   Creep resistance

Creep is a phenomenon that occurs when cushion materials are progressively compressed under a given static load (lower than the material's compression strength), during a long-term storage period. Creep is thus a relationship between dimensional change and time and is measured by the loss of thickness at given time periods. Creep data for specified materials at given static loads can be used to estimate dimensional change over periods of time so that measures can be taken (for example by increasing the initial material thickness), to compensate for this.

2.4.5   Resistance to fracture

Cushion materials are generally designed to work under compression forces. However, tensile or sheer stresses imposed on cushion materials may result in fracture from non-uniform deformation of the structure. These unpredicted forces coupled with bad structural design may cause fracture of the material and failures of the cushion packaging resulting in a loss of cushioning for shock and impact when required. Attention should be given to material selection and in design of cushion structures to prevent such failures (Kang, 2006).

2.5   Foams for cushion packaging applications

Polymer foams are widely used as cushion packaging materials in a number of industries for shipping many different kinds of products. Four types of foams are most commonly used. These are listed below along with their acronyms:

a) Expanded polystyrene (EPS or PS foam)

b) Expanded polyethylene (EPE or PE foam)

c) Expanded polypropylene (EPP or PP foam)

d) Expanded polyurethane (EPU or PU foam)

High-volume, lightweight, durable goods are often packaged in custom-moulded EPS, while lower-volume, heavier, more fragile products are commonly cushioned using PE foam. PU foams are often used to protect fragile, light-weight products regardless of sales volumes. PP foams bring additional benefits such as high thermal resistance, chemical resistance and good insulation properties. However, these generalisations are not always applicable and considerable competition and substitutions exist among all these materials which are described in further detail below.

2.5.1   Polystyrene foam

Polystyrene is an aromatic polymer made from the aromatic monomer styrene, a liquid hydrocarbon commercially manufactured from petroleum by the chemical industry. In the expanded form most EPS used in the packaging industry is moulded into custom shapes from pre-expanded beads, a process known as *steam chest moulding* (BPF, 2007). These foam shapes are used primarily by the small appliance and consumer electronics markets for shipping lightweight, relatively rugged products. EPS is rigid and lightweight, and usually provides good single-impact protection for relatively durable items such as kitchen and other electronic appliances.

EPS foam mouldings have a clean, custom-designed appearance and a lower material cost than many other foams. In addition, the manufacturing process for EPS is highly automated. Due to these advantages, more EPS foam mouldings are manufactured than any other type of foams on the market. However, EPS also has some disadvantages. For many designs, capital costs of moulding equipment and tooling may be substantial drawbacks, as well as the long lead times required for design development, tooling and delivery of moulded parts. The most critical disadvantage of these mouldings however, is reduced cushioning performance after a single impact and low fracture resistance (Wiles, 2006).

EPS is also commonly used in the form of loosefill foams known as EPS chips, which are produced by extrusion foaming and cutting the extrudate into short pieces. These are produced in a variety shapes and sizes and are mainly used to fill the packing spaces around packed goods within containers to limit their freedom of movement and provide cushion protection. EPS loosefill chips provide cost-effective protection for relatively lightweight products. Loosefill is free flowing, allowing gaps between the packaged items and the container to be easily filled, holding the products to be protected in position and eliminating any requirement to fabricate moulded cushion blocks to accommodate the shape of the packaged product.

On a volume basis loosefills are generally the least expensive polymer cushioning products and are lightweight and easy-to-use. The loosefill materials can be quickly dispensed by gravity, resulting in fast packaging rates and reduced labour costs (Eaves, 2004). However, EPS loosefill is not without its disadvantages. The chips themselves have relatively low compression strengths and suffer from problems such as settling during transit due to vibration, reducing the protection conferred to the packaged product. For these reasons it is not designed to protect heavy objects. EPS loosefill can also be messy and is easily wind blown leading to problems of litter.

In a variation of using EPS in the form of loosefills, a three-stage process in which loosefills were fabricated into moulded block foams was devised by the Dow Chemical Company. In this process a layer of adhesive-coated loosefill is dispensed into a carton which is then covered by sheet of plastic film. The product to be packed is then placed on the plastic film before being covered by a second sheet of film. The carton is then slightly overfilled with more adhesive-coated loosefill and sealed. Once the carton is sealed, the loosefill particles bond together, forming two cushions moulded to the shape of the packed product. The main advantage of bonded loosefill in comparison to ordinary loosefill products are the provision of enhanced cushioning properties mainly due to the elimination of migration of the packaged items within the container during transit. Perceived disadvantages are capital investment as well as the time required for the adhesive to set (Wiles, 2006).

2.5.2 Polyethylene foam

Polyethylene is a polyolefin (or polyalkene), produced from a simple olefin monomer (or alkene with the general formula C_nH_{2n}). In the expanded form PE foams are fabricated from extrusion foamed planks or sheets. In general, when used for cushion packaging applications, PE foam is best suited for relatively fragile products with fragility levels of up to 40 Gs (Talk Packaging, 2007).

There are many advantages in the use of PE foams. They offer lightweight protection and are more resilient and flexible than EPS. PE foams typically provide cushioning at higher loadings

than softer materials like polyurethane foams, meaning that PE foam designs will usually require less material in terms of mass or volume than designs produced from softer materials. PE foams are unaffected by most chemicals and are easily fabricated allowing greater design flexibility. They are also available with anti-static and fire-retardant additives.

Potential disadvantages of PE foams include its greater expense on a volume basis than most other common cushioning materials; its slightly abrasive finish which is unsuitable in contact with some highly polished or sensitive painted surfaces, and that it is perceived as not handling vibration as well as softer materials (Foam Design, 2008).

2.5.3   Polypropylene foam

Polypropylene is another common polyolefin made from the olefin monomer propylene. In the expanded form polypropylene foam is a tough, resilient, and lightweight closed cell material that is moisture and chemical resistant and can be used across a wide range of temperatures. Polypropylene is commonly used for cushion packaging as well as numerous other applications such as thermoformed foamed trays for packaging chilled foods, insulation materials in building construction and material for car interiors. Amongst the advantages of PP foams are its low density and good rigidity for a given weight of material. It can also be used with conventional injection moulding and extrusion equipment. Disadvantages of PP foams include low tensile strength and modulus and significantly reduced elongation at break compared with unmodified PP (Foam Design, 2008).

2.5.4   Polyurethane foam

Polyurethane is any polymer consisting of a chain of organic units joined by urethane (carbamate) links. Polyurethane polymers are formed through step-growth polymerisation by reacting a monomer containing at least two isocyanate functional groups with another monomer containing at least two hydroxyl (alcohol) groups in the presence of a catalyst. In its expanded form, PU foams are light, durable materials with many applications including cushion packaging, automotive seat mouldings, linings and furniture mouldings. Non-mechanical applications include acoustic insulation and thermal insulation for the construction industry (PFA, 2000). Disadvantages of PU foams include the release toxic fumes when burned (US Dept of Energy, Consumer Guide, 2009).

2.6   The thermal properties of foams: general principals of thermal insulation

Thermal insulation attempts to reduce or retard the flow of thermal energy or heat transfer across a temperature differential. There are only three basic methods by which heat transfer can take place:

Thermal conduction is a term applied to thermal energy transferred within a single body or between two bodies in direct contact. In metals, thermal conduction is the result of the motion of free electrons, similar to electrical conduction. In liquids or poorly conducting solids it is the oscillation of the molecules or atoms and in gasses conduction occurs through collisions between molecules (Croy & Dougherty, 1984).

Thermal convection involves the transfer of energy by the physical transport of masses of fluid or gas containing that energy from one point to another (Croy, Dougherty, 1984). Two major types of convection can occur: Free (or natural) convection in which a temperature differential results in the creation of local density differentials, causing pockets of the fluid or gas to become more buoyant or dense than the surrounding area. Forced convection is produced by mechanical means including pumps, fans and the wind. If forced convection is weak, natural convection may also occur, in what is referred to as mixed convection (Croy & Dougherty, 1984).

Thermal radiation is a portion of the electromagnetic radiation spectrum and refers to energy emitted from the surface of a thermally excited object in the form of electromagnetic waves. Whereas conduction and convection require an actual substance to carry the energy, radiation does not and this form of heat transfer may be hindered by an intermediate material (Croy & Dougherty, 1984). All bodies which have a temperature greater than absolute zero possess internal energy. At the surface of the body some of this energy is released as thermal radiation which will travel through space in a straight line until intercepted by another body (Croy & Dougherty, 1984). In most actual heat transfer situations, conduction, convection and radiation seldom occur individually and most involve combinations of the three modes of heat transfer or *combined heat transfer* (Croy & Dougherty, 1984).

2.6.1   Foams for the reduction of heat transfer

Heat is transmitted through solids by thermal vibrations and by the movement of free electrons in materials such as metals. Thermal insulation attempts to inhibit heat transfer by placing a barrier between actual or potential temperature differentials. Since the barrier itself is generally a solid, one would expect any heat transfer across it to take place solely through conduction so that the thermal insulation could be characterised by its thermal conductivity. However, although in this case thermal conduction may be the primary means of heat transfer, all three modes of contribute to some degree and it is only due to the effective suppression of convection and

radiation that efficient thermal barriers are characterised by their *apparent thermal conductivity* (Croy & Dougherty, 1984).

A warm surface exposed to cooler surroundings loses thermal energy by all three modes of heat transfer. By placing a barrier near the warm surface the radiative losses can be reduced. If a volume of air is physically decreased its mobility is constrained and thermal convection will be suppressed. Therefore, if one places a number of barriers near the warm surface so that the barriers form small air pockets, both radiation and convection will be inhibited. With an efficient distribution of barriers thermal losses from the warm surface can be reduced to the point at which it results almost entirely from pure thermal conduction through the barriers and the small pockets of still air between (Croy & Dougherty, 1984).

The best thermal insulators are highly porous materials including low density foams, certain fabrics, cork, wool, etc., all of which take advantage of the low thermal conductivity of still air (0.02 W/m.K). Foams used as thermal barriers inhibit heat transfer by utilising these phenomena. The space between the temperature differential is separated by multiple barriers containing tiny pockets of air, effectively reducing thermal radiation and convection. The remaining mechanisms of heat transfer can then be reduced by the use of foams comprising low *thermal conductivity*. The rate of thermal conduction is proportional to the temperature differential across a barrier and the area available for the heat flow to occur (perpendicular to the direction of heat flow), but inversely proportional to the thickness of the barrier (Croy & Dougherty, 1984). Figure 2.8 shows thermal conduction through a plane barrier.
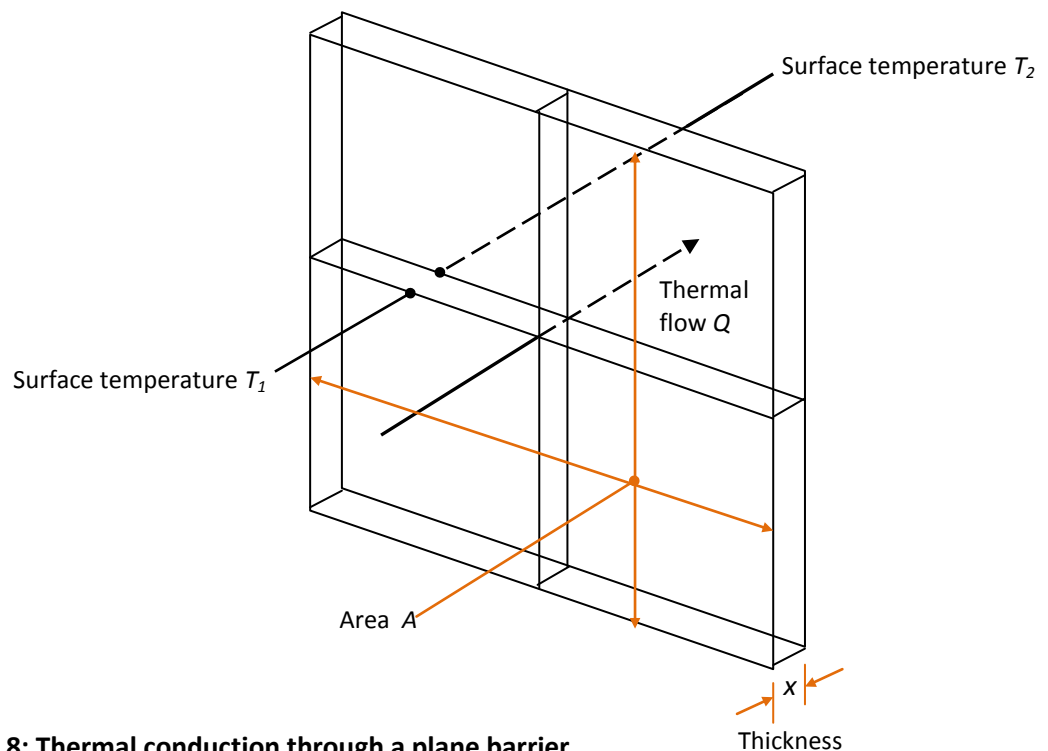
Figure 2.8: Thermal conduction through a plane barrier

Uni-axial thermal conductivity through a barrier is governed by Fourier's law of heat conduction:

$$Q = k \frac{A}{x} (T_1 - T_2) \hspace{2cm} (2.2)$$

Where: Q = thermal flow

k = thermal conductivity of the barrier

A = surface area of the barrier

x = thickness of the barrier

T = surface temperature of the barrier

(Croy & Dougherty, 1984)

Thus k gives a measure of the rate of thermal conduction which may occur through a unit area and thickness of a material when driven by unit temperature differential meaning k is a measure of the material's *thermal conductivity* which can be expressed in units of watts/metre Kelvin (W/mK).

Thermal conductivity is a material property. The greater a material's thermal conductivity, the greater the rate of thermal energy flow it will conduct and thus the poorer it will act as a thermal insulator. The inverse of thermal conductivity is *thermal resistivity* (Croy & Dougherty, 1984).

Thermal conductivity varies with temperature. For a given temperature difference, materials with a high thermal conductivity will conduct more heat and will require a smaller temperature gradient to conduct a given amount of heat than materials with lower thermal conductivity. When selecting materials for applications that are subjected to temperature changes, additional information will be required to ensure that the required level of conductivity is achieved across the operating temperature range (CES Edupack, 2010). Examples of thermal conductivity for various flexible foams of different densities are shown in Figure 2.9.
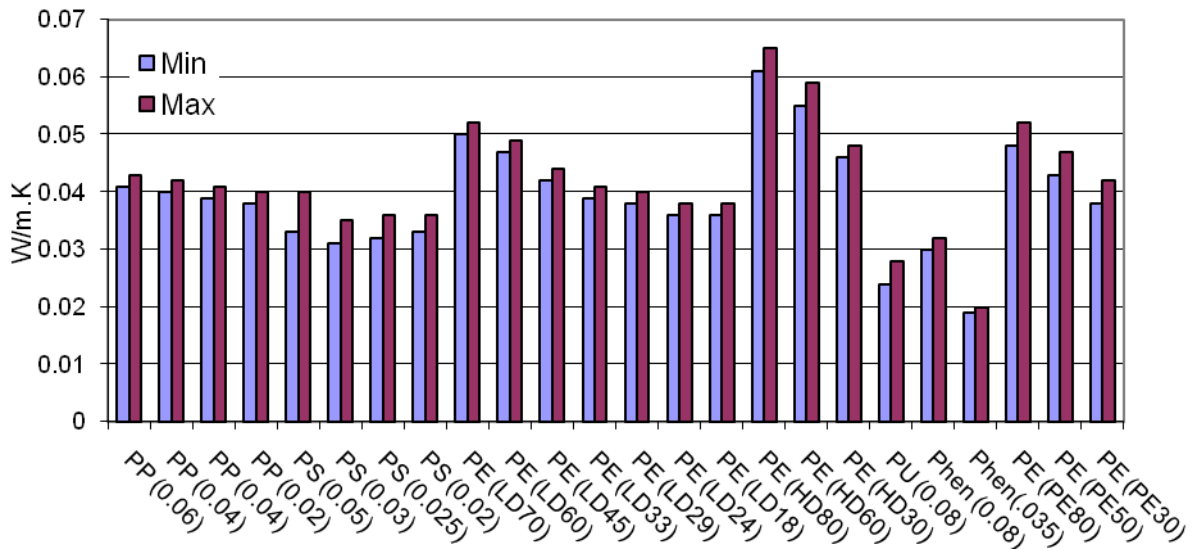
Figure 2.9: Thermal conductivity of various flexible foams of different densities

Key to Figure 2.9:

Foam abbreviation & nomenclature	Density (kg/m³)	Foam abbreviation & nomenclature	Density (kg/m³)
PP (0.06): *Polypropylene Foam: Closed Cell*	60	PE (LD29): *Polyethylene Foam*	29
PP (0.04): *Polypropylene Foam: Closed Cell*	40	PE (LD24): *Polyethylene Foam*	24
PP (0.03): *Polypropylene Foam: Closed Cell*	30	PE (LD18): *Polyethylene Foam*	18
PP (0.02): *Polypropylene Foam: Closed Cell*	20	PE (HD80): *Polyethylene Foam*	80
PS (0.05): *Polystyrene Foam: Closed Cell*	50	PE (HD60): *Polyethylene Foam*	60
PS (0.03): *Polystyrene Foam: Closed Cell*	30	PE (HD30): *Polyethylene Foam*	30
PS (0.025): *Polystyrene Foam: Closed Cell*	25	PU (0.08): *Polyurethane Foam: Flexible, Closed Cell*	80
PS (0.02): *Polystyrene Foam: Closed Cell*	20	Phen (0.08): *Phenolic Foam: Closed Cell*	80
PE (LD70): *Polyethylene Foam*	70	Phen (.035): *Phenolic Foam: Closed Cell*	35
PE (LD60): *Polyethylene Foam*	60	PE (PE80): *Polyethylene Foam*	80
PE (LD45): *Polyethylene Foam*	45	PE (PE50): *Polyethylene Foam*	50
PE (LD33): *Polyethylene Foam*	33	PE (PE30): *Polyethylene Foam*	30

Compiled from CES Edupak Database 2009

Figure 2.9 illustrates a general tendency for lower density foams to exhibit reduced thermal conductivity values.

2.6.2 Testing the thermal conductivity of materials

Using equation 2.2 given above, the measurement of thermal conductivity involves the measurement of the heat flux and temperature differential. The difficulty of the measurement is always associated with the heat flux measurement. Where the measurement of the heat flux is done directly (for example, by measuring the electrical power going into a heater), the measurement is called absolute. Where the flux measurement is done indirectly (by comparing the amount of heat input against output), the method is called comparative.

From these two main techniques several methods have been developed which yield thermal conductivity. In all cases, the entire heat flux must be uni-axial through the sample (and through

references, in comparative methods), meaning that heat losses or gains must be minimised in the transverse direction.

The configuration of a given measurement system and of the specimen itself is influenced most prominently by the magnitude of the thermal conductivity. Simple thermal considerations indicate that if the thermal conductivity of the material being tested is high, as in the case of metals, the heat flux will usually also be fairly high so that relatively speaking, heat losses from the lateral surface area of the specimen will be small. Thus, specimens are usually long (for example, in the form of cylinders). A long specimen in the direction of flow helps establish a reasonably high temperature gradient which can then be accurately measured. Conversely when the conductivity of the material is low as in the case of foams, the heat flux is correspondingly low and only a relatively small sample thickness is required to generate a large, accurately measurable gradient. Specimens of low conductivity materials are usually flat (for example, in the form of plates or disks). With low specimen heat flux, lateral losses are of concern, thus a plate-type specimen itself tends to minimize these spurious flows since the lateral surface area is small. A number of different commonly used methods are described below (Anter Corp, 2009).

1) Axial flow methods:

Axial flow methods using cylindrical samples have been long established and have produced some of the most consistent, highest accuracy results reported in the literature. Key measurement issues centre mainly on reduction of radial heat losses in the axial heat flow developed through the specimen from the electrical heater mounted at one end of the sample. The power dissipation of this heater is used in calculating column heat flux. There are three basic axial heat flow methods.

1a) Absolute axial heat flow methods. Systems of this nature are mostly used in sub-ambient environments and require very precise knowledge of the electrical power feeding the heater as losses from the heater surfaces may play a major role.

1b) Comparative cut bar (ASTM E1225). The principle of measurement lies with passing the heat flux of a known value through a known sample and an unknown sample and comparing the respective thermal gradients, which will be inversely proportional to their thermal conductivities. Most commonly, the unknown sample is sandwiched between two known reference samples to further account for minor heat losses that are very difficult to eliminate. Figure 2.10 shows a graphic representation of the cut bar method (Czichos *et al*, 2006).
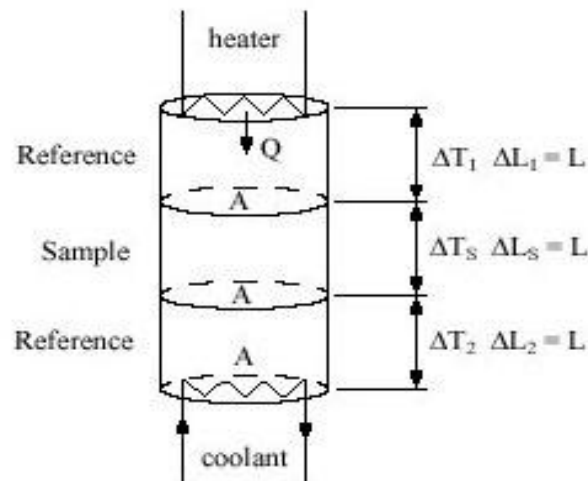
Figure 2.10: Schematic representation of sample arrangement in a comparative cut bar method
Anter Corp (2009)

Where K_R is the thermal conductivity of the references, the thermal conductivity of the sample K_s can be calculated from Equation 2.3:

$$\frac{Q}{A} = K_S \frac{\Delta T_S}{L} = K_R \frac{\Delta T_1 + \Delta T_2}{2} \frac{1}{L} \qquad (2.3)$$

(Czichos *et al*, 2006)

1c) Heat flow meter method (Test standards: ASTM C518, BS 874 – EN 12667, DIN 52612, ISO 8301). This method involves the use of a flux gauge, which has a similar purpose to the references used in the comparative cut bar method. Usually a large number of thermocouple pairs are located on both sides of the reference plate, connected differentially to yield directly an electrical signal proportional to the differential temperature across it as described by Equation 2.4:

$$K_S = K_R \frac{\frac{\Delta T_1 + \Delta T_2}{2}}{\Delta T_S} \qquad (2.4)$$

(Czichos *et al*, 2006)

The assembly is cast into a protective coating for durability. This type of flux gauge is mostly used with instruments testing very low thermal conductivity samples, such as those used for building insulations. In a similar fashion, flux gauges can be constructed from just about any material - thick or thin, depending on the material's thermal conductivity. Common requirements for all flux gauges are that the material used for the measuring section be stable and unaffected by

thermal cycling, and that the gauge be calibrated by some independent method. A very large variety of testing instruments utilise this method (Anter Corp, 2009).

2) Guarded hot plate method:

Guarded hot plate (ASTM C 177; ISO 8302:1991; EN 12667:200) is a widely used and versatile method for measuring the thermal conductivity of insulation materials. Although such specimens are often rather large this generally presents no difficulty and can provide a good representation of the material as found in functional applications.

A flat, electrically heated metering section surrounded on all lateral sides by a guard heater section controlled through differential thermocouples, supplies the planar heat source introduced over the hot face of the specimens. The most common measurement configuration is the conventional, symmetrically arranged guarded hot plate in which the heater assembly is sandwiched between two specimens (Czichos *et al*, 2006). Figure 2.11 shows a schematic representation of the setup for guarded hot plate method.
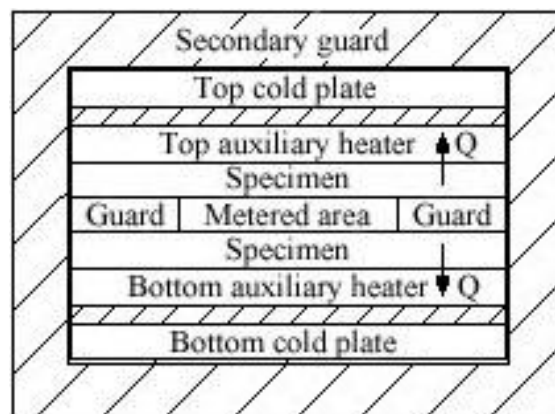
Figure 2.11: Schematic representation of guarded hot plate method set-up
Anter Corp (2009)

This is an absolute method of measurement. Amongst many parameters which may affect the unidirectional heat flux through the metered area of the specimens, the applicability of this method is dependent on:

     1) Establishment of steady-state heat flow conditions

     2) Temperatures of the hot and cold plate surfaces

     3) Accuracy of measurement of the unidirectional heat flux in the metered region

     4) Thickness of the specimens

3) Hot wire methods:

Hot wire methods (ASTM C1113) are most commonly used to measure the thermal conductivity of materials such as insulation, powder or fibrous materials. Due to the basis of technique being transient radial flow, isotropic specimens are required. The technique has been used in a more limited way to measure properties of liquids and plastics materials of relatively low thermal conductivity.

Relatively recent modifications of the hot wire method include methods utilising probes, such as the *transient plane source method* in which thermal conductivity is determined from the response of a probe in contact with the test specimen. The probe contains a heater and attached thermocouple. As a certain amount of electrical current is passed through the heater for a short period of time, the temperature history of the heater's surface will take on a characteristic form. In the initial phase, the temperature will rapidly rise and as the heat begins to soak in the rate of rise becomes constant. When the thermal front reaches the outer boundary of the sample, the rise will slow down or stop altogether due to losses into the environment. From the straight portion of the rate curve (temperature vs. time) the thermal conductivity can be calculated (Anter Corp, 2009).

2.7   The acoustic properties of foams: general principals of acoustic design

Sound is a mechanical pressure wave resulting from a longitudinal disturbance propagated through an elastic medium (gas, liquid or solid), which advances by causing molecules of the medium to vibrate. If a point source of sound is placed in an environment without reflecting surfaces, sound waves will travel outwards in a spherical front. If the point source is close to the ground the sound waves will radiate in a hemispherical pattern. In general sound travels faster through denser media.

A sound wave moving from left to right through air, will displace particles of air both rightward and leftward as the energy of the sound wave passes through it. The motion of the particles parallel (and anti-parallel) to the direction of the energy transport is what characterises sound as a longitudinal wave.

Figure 2.12 depicts the correspondence between the longitudinal nature of a sound wave and the air pressure-time fluctuations which it creates.
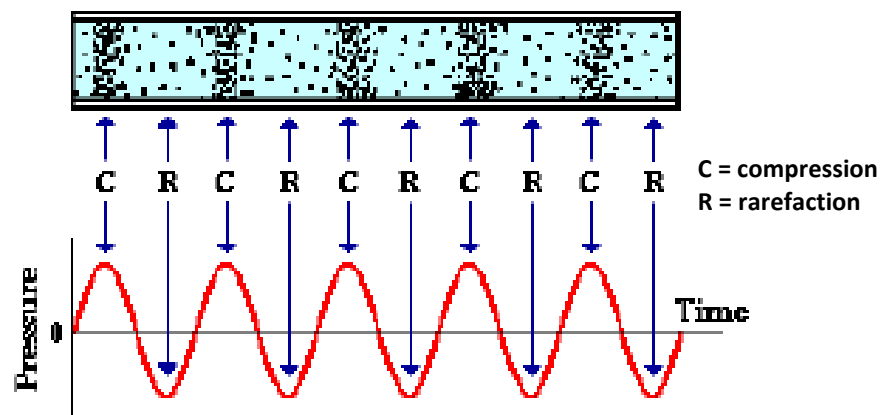
Figure 2.12: Longitudinal nature of a sound wave
The Physics Classroom (2008)

Sound has both physical and temporal dimensions. *Amplitude* is the wave height or the magnitude of oscillation of pressure (measured in Pa), and this is perceived as the *volume of the sound*, whilst *wavelength* is the distance between repeating units or periods of a wave pattern.

The number of these wave cycles or pressure variations per second is the frequency of the sound wave (measured in Hz), and is perceived as *pitch of sound*. Sounds consisting of single frequencies are known as *pure tones*. Figure 2.13 shows the physical & temporal dimensions of sound waves. It should be noted that pure tones such as those illustrated are seldom encountered in practical applications as most sounds are made up of a wide mixture of frequencies known as *broadband noise* (Silex, 2002).
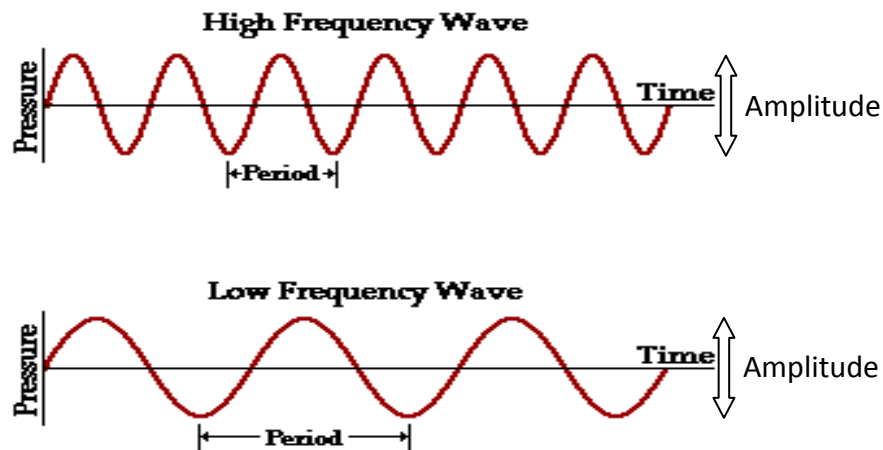
Figure 2.13: Physical & temporal dimensions of sound
Aperion audio (2008)

The human ear is a very sensitive instrument with an extremely broad range of operation. Within the audible frequency range (approximately 20 Hz - 20 kHz), the human ear is capable of detecting very faint sound pressure variations of around 20 µPa corresponding to air vibrations on the order of a tenth of an atomic diameter, whilst a very loud sound might have a pressure value of around 20 Pa (Silex, 2002).

Since the ratio of the lowest audible sound pressure to the loudest can be around 1 million, a logarithmic scale is used to compress the sound pressure range into a measure of decibels (dB). Table 2.3 shows some common sound pressure levels in decibels and their corresponding sound pressures.

Table 2.3: Common sound pressure levels (dB) and corresponding sound pressures

Common Sounds	Sound Pressure Level (SPL) dB	Sound Pressure (P) Pa
Jet Aircraft (50m away)	140	200
Threshold of pain	130	63.2
Threshold of discomfort	120	20
Chainsaw (1m away)	110	6.3
Disco (1m from speaker)	100	2
Heavy Truck (10m away)	90	0.63
Kerbside of busy road	80	0.2
Vacuum cleaner	70	0.063
Conversational speech	60	0.02
Average Household	50	0.0063
Quiet Library	40	0.002
Bedroom at night	30	0.00063
Background in TV studio	20	0.0002
Rustling leaf	10	0.000063
Threshold of hearing	0	0.00002

Sengpiel audio, 2006

Sound level measurements in decibels are generally referenced to a standard threshold of hearing corresponding to zero decibels. It represents a pressure change of less than one billionth of standard atmospheric pressure (101.325 kPa). The nominal dynamic range of human hearing is from the standard threshold of hearing to the threshold of pain. A nominal figure for the threshold of pain is given as 130 decibels (Sengpiel audio, 2006).

2.7.1   Reflection, absorption & transmission of sound

When sound hits any surface some of the sound energy will always be reflected. If an absorbing material is placed between source and receptor then depending on the particular substrate and its thickness, a proportion of the sound energy will be reflected by that material, a proportion will be absorbed and some of that sound energy will be transmitted. Figure 2.14 graphically illustrates the reflection, absorption and transmission of sound in relation to a substrate.
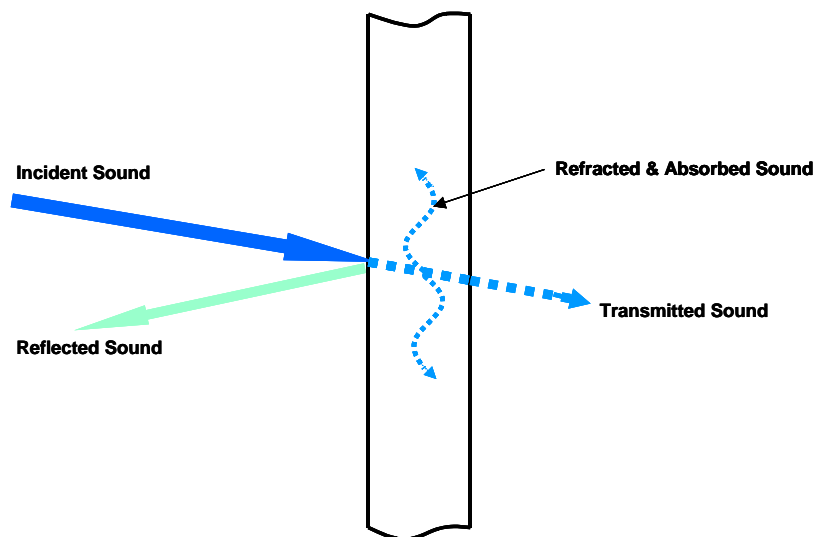
Figure 2.14: Reflection, absorption and transmission of sound

2.7.2   Sound reduction

Noise (unwanted sound) is a subjective interpretation of a physical phenomenon. Whilst noise is often thought of as simply too much volume (amplitude), a particular frequency or combination of frequencies may be low in volume but still be considered noise. The subjective nature of noise complicates sound reduction.

Reduction of sound intensity with respect to a specified source, path and receptor can take several basic approaches:

1)   Increasing the distance between source and receptor. As the area of a sound pressure front increases with its distance from the source, there is a corresponding decrease in the sound

pressure level. Most real sounds are to some degree directional and as a result sound levels at equal distances but different orientations are often unequal. Due to increased wavelengths, low frequency sounds tend to be less directional than high frequency sounds.

2) Using acoustic barriers to effectively insulate unwanted sound between source and receptor. This approach utilises dense materials known as *hard wall*s to reflect sound energy.

3) Using damping structures and materials between source and receptor to effectively absorb sound energy. This approach includes the use of sound absorbing foam materials.

4) Using softer materials to isolate solid structures from sources of unwanted sound energy which would otherwise be conducted as vibration.

5) Using active anti-noise sound generators to generate additional frequencies which cancel out unwanted frequencies.

Most construction and building materials designed to reduce unwanted sound typically utilise approaches 2), 3) and 4), or commonly a combination of all three.

2.7.3 Acoustic attenuation

When sound energy is absorbed by a substrate it is converted into another form of energy. In most cases, this takes the form of conversion to heat. This is known as *acoustic attenuation*. The heat generated results from the actions of friction and the resistance of various materials to movement and deformation. The amount of heat produced is minimal, as is the sound energy if considered in watts (Silex, 2002).

Given adequate thickness any material will eventually attenuate sound energy at all frequencies. However in practical terms most materials are effective at attenuating sound in only a limited frequency range. Achieving effective broad-spectrum sound attenuation within a limited space usually requires composites or laminates which combine the various frequency attenuation characteristics of different materials. Because of inherent space limitations in design, low frequency/longer wavelength sound can be much more difficult to attenuate. An effective sound attenuation solution in one situation may not be in another. The compromise may be space, weight, complexity, cost or any combination of factors. Decisions on trading performance for cost, or thickness for weight, is a choice manufacturers make based on their market. All sound attenuation materials are a compromise (Vickers, 2006).

2.7.4   Acoustic testing

All acoustic tests on materials are based on how a sample will modify an acoustic environment. Various tests, methods & standards exist and are briefly described below.

2.7.4.1 Sound absorption coefficient

Sound absorption coefficient (α) is the ratio of the sound energy absorbed by a medium to the incident sound energy upon its surface. This is a measure of sound energy attenuation caused by absorption by a medium. The significant factor is the unreflected sound energy, which provides the basis for calculation of the proportion of sound energy absorbed by the substrate according to test standards: BS EN ISO 15034-2: 2001, *Determination of sound absorption coefficient and impedance in impedance tubes – Part 2: Transfer function method* and ASTM E1050-98 *Standard Test Method for Impedance and Absorption of Acoustical Materials Using a Tube, Two Microphones, and a Digital Frequency Analysis System*.

Figure 2.15 shows a schematic representation of the transfer function/impedance tube method for testing sound absorption coefficient.
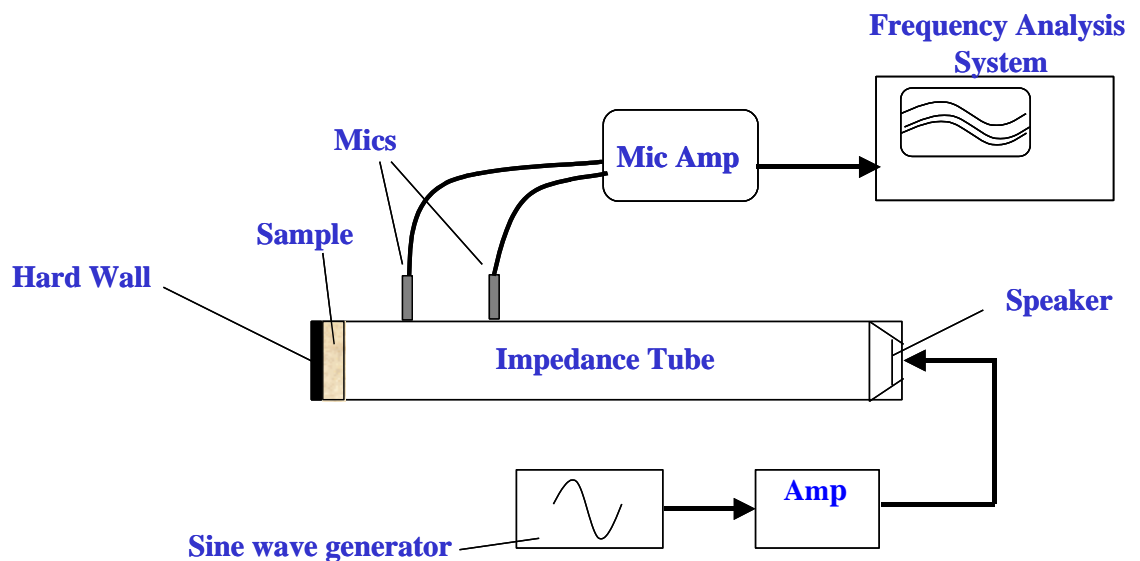
Figure 2.15: Schematic representation of the transfer function / impedance tube set-up

It is important to note that absorption coefficient (α) refers to all the sound energy that is not reflected back to the microphones. It is therefore based on the sound energy reflected from the sample to the microphones and also includes any sound energy transmitted through the sample and then reflected from the hard wall back through the sample.

Pure tones are seldom encountered in the environment as most noise consists of several frequencies. For many applications acoustic testing uses *broadband noise* - all audible frequencies at varying amplitudes.

Testing with impedance tubes exposes samples to sound waves at *normal incidence* (sound waves striking the sample at 90 degrees). Testing at *random incidence* (sound waves striking the sample at various angles) requires more elaborate reverberation room setups.

In the impedance tube setup, lower working frequencies are limited by the resolution of speakers and analysis system as well as the distance between microphones. These are set closer together for higher frequencies and further apart for lower frequencies. Upper working frequencies are limited by the cross-section of the impedance tube and the spacing between microphones. Figure 2.16 shows the two microphone transfer function/impedance tube method in more detail.
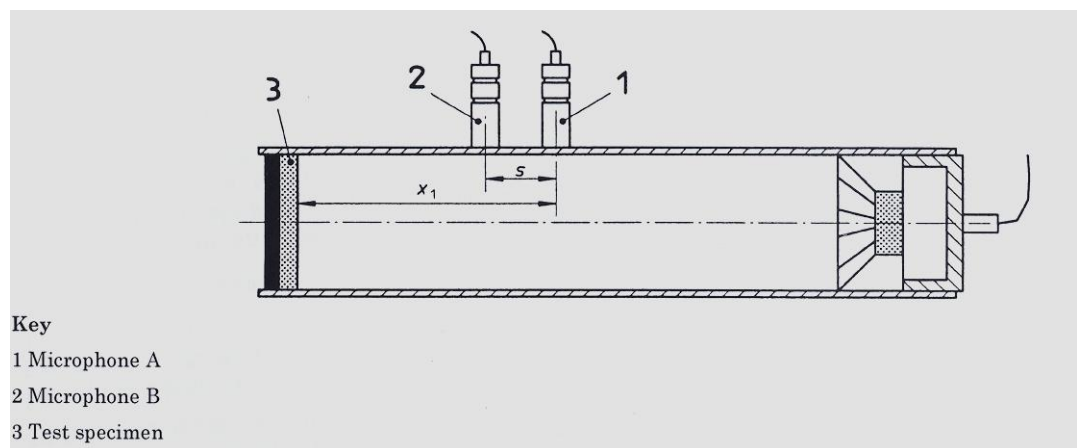
Figure 2.16: Two microphone transfer function/impedance tube method
BS EN ISO 15034-2: 2001

The normal absorption coefficient α of the specimen is given by the following Equation 2.5:

$$\alpha = 1 - |R|^2 \qquad (2.5)$$

(Suhanek et al, 2008)

Where:

R = reflection coefficient

Details of derivations for Equation 2.5 can be found in test standard BS EN ISO 15034-2: 2001.

2.7.4.2 Sound transmission loss

Sound transmission loss (*STL*) is a key quantification of the effectiveness of acoustic treatments for engineering applications. Sound transmission coefficient (τ) of an acoustic medium is a function of frequency and can be defined as the ratio of sound energy transmitted through the medium to that of the incident sound energy upon the source side of that medium (Evensen & Rao, 2002). Sound transmission loss (STL) of a partition at a specified frequency, is ten times the common logarithm of the ratio of the airborne sound power incident on the partition to the sound power transmitted by the partition and radiated on the other side. The quantity obtained expressed in decibels (dB) is 10 times the logarithm to the base 10 of the reciprocal of the sound transmission coefficient of the configuration according to Equation 2.6.

$$STL = 10.\log_{10}\left\{\frac{1}{\tau}\right\} dB$$

(2.6)

(Barnard & Rao, 2004)

Details of derivations for Equation 2.6 can be found in Barnard & Rao, 2004; Jung *et al*, 2008.

Standard test methods for determining sound transmission loss involve using two adjacent reverberation rooms with an adjoining transmission path as covered in standards BS EN ISO 140-3: 1995 (BS 2750 Part 3: 1995); BS EN ISO 717-1:1996; BS EN 1793-2:1998; BS EN 1793-3:1998 and ASTM E90. The material under test is placed between the two rooms in the adjoining transmission path and sound is generated in one room, while measurements are taken in both the source and receiver room to characterise the transmission loss (Barnard & Rao, 2004).

Unfortunately, implementing these testing methods requires large and expensive test chambers. In many situations where transmission loss tests are necessary but infrequent, this cost and space burden is unacceptable. An efficient and less costly STL testing procedure utilises a modified impedance tube comprising four microphones which measures what is known as the *transmission loss matrix* of the material, from which STL values can be extracted (Barnard & Rao, 2004).

The method utilises two pairs of microphones mounted within an impedance tube on either side of the sample being tested which are used to measure the proportion of sound energy transmitted through the sample. The anechoic termination at the end of the impedance tube is used to prevent sound reflection from the end of the tube. Currently no universally accepted standards exist for testing sound transmission loss using impedance tubes. A schematic representation of the equipment setup for testing sound transmission loss is shown in Figure 2.17.
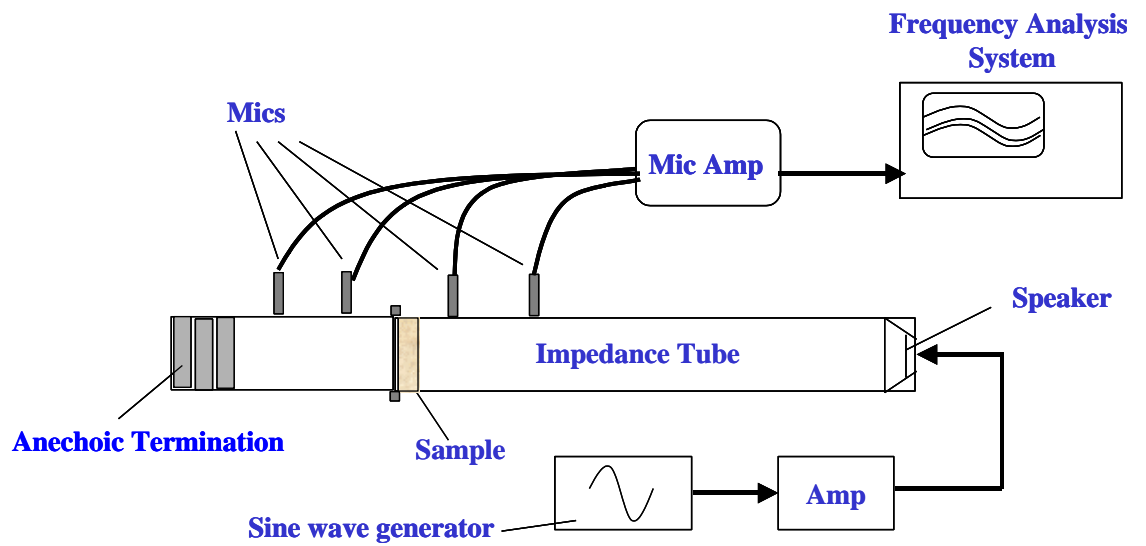
Figure 2.17: Schematic representation of set-up for testing sound transmission loss with an impedance tube

Figure 2.18 shows a detailed schematic representation of the impedance tube set-up for testing sound transmission loss, illustrating microphone positions and spacing.
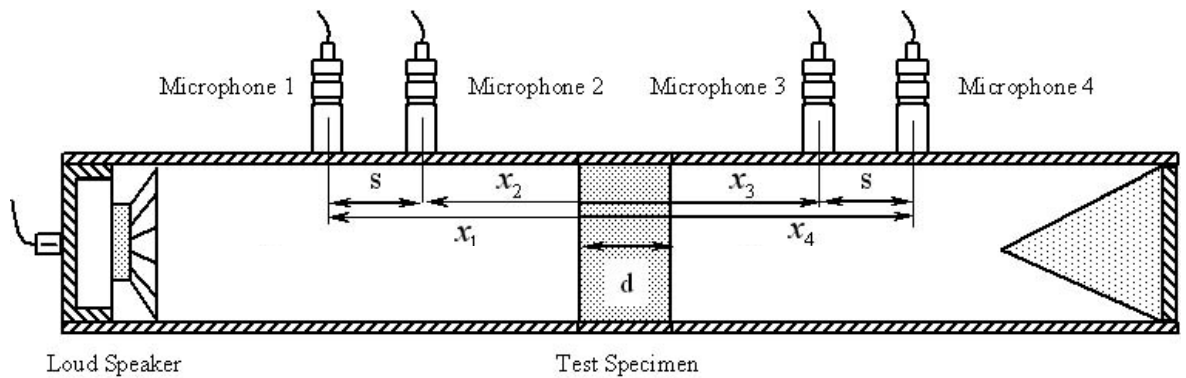
Figure 2.18: Impedance tube set-up for testing sound transmission loss
Jung, S S; Kim, Y T; Lee, Y B; Cho, S I; Lee, J K (2008). Measurement of Sound Transmission Loss by Using Impedance Tubes.

2.7.5   Foam materials for sound attenuation applications

Undesirable or harmful effects of sound can be reduced by blocking transmission paths with passive acoustic material treatments. The mechanism for reducing sound intensity within a given space is dependent upon the source of that sound. In general cellular, porous solids are good for absorbing sound. However, they are generally poor at providing insulation against sound or keeping unwanted sound out which is better achieved by utilising dense, non-porous solids. Therefore, acoustic treatments are generally multilayered, consisting of some type of dense barrier material in combination with porous, open celled absorptive materials. The barrier layers can be made of materials from rubber to hard plastic.

Typically the absorptive materials are made of polyurethane foams. Since the absorption coefficient of any material is frequency dependent, laminations of foams of different densities will generally attenuate a broad spectrum of sound frequencies better than a single foam of the same thickness. Thus, porous materials of varying densities & composition are generally used as sound absorbers to reduce sound reflection & transmission. These work by absorbing and converting sound energy into heat energy within the open pores of the material.

2.8   Drivers for the development of renewable bio-plastics

Amongst the many useful properties of plastics made from synthetic petrochemical polymers, their decomposition-resistant characteristics have been one of the inherent advantages of this class of materials. This property has been utilised by plastics manufacturers and users, particularly in the latter half of the twentieth century, resulting in the displacement of more traditional but degradation-susceptible materials such as paper, leather and wood.

The production and use of plastics has a range of environmental impacts. Firstly, plastics production requires significant quantities of resources, primarily fossil fuels as raw materials. It is estimated that 4% of the world's annual oil production is used as a feedstock for plastics production with consumption of plastics increasing at around 4% per year in Western Europe. Packaging is the largest single sector of plastics use in the UK accounting for 35% of plastics consumption, with plastics as the material of choice in almost half of all packaged goods (Waste Watch, 2006).

The disposal of plastics products also contributes significantly to their environmental impact. The average UK household dustbin comprises around 7% of plastics, generating almost 3 million tonnes of plastic waste annually. An estimated 56% of all plastics waste is used packaging, three-quarters of which is from households. It is estimated that only 7% of total plastic waste arisings are currently being recycled (Waste Watch, 2006).

In addition to the issues of plastic waste which follow appropriate disposal or recycling routes, persistent littered plastic items present further concerns both on land and in marine environments. In 1997, the US Academy of Sciences estimated the total global input of marine litter into the oceans at approximately 6.4 million tonnes per year and it has been estimated that over 13,000 pieces of plastic litter are floating on every square kilometre of ocean surface (UNEP, 2010). Figure 2.19 shows littered waste comprising of a large proportion of plastic items at a river mouth in Dorset, UK.

Figure 2.19: Littered waste at a river mouth in Kimmeridge, Dorset, UK
Marine Biological Association of the United Kingdom, 2006

Table 2.4 shows worst case estimates for degradation rates of various materials in the marine environment according to the United Nations Environment Programme (1990).

Table 2.4: Worst-case estimates for degradation rates of materials in the marine environment

MATERIAL	DEGRADATION RATE (YEARS)
Cotton rope	1
Untreated plywood	1-3
Plastic bag	10-20
Commercial netting	30-40
Foamed plastic buoy	80
Aluminium can	80-200
Plastic bottle	450
Monofilament fishing line	600
Glass bottle	1 million

Marine Biological Association of the United Kingdom 2006

The 1970s oil crisis focused the attention of the industrialised world on the political realities underpinning its energy and resource requirements, while at the same time an emerging environmental movement helped to illuminate the finite nature of fossil reserves and encouraged the development of alternatives to our dependence on these resources. As the production, use and disposal of the new plastic materials increased, it became apparent that the build up of plastic waste in landfill sites and the persistence of littered plastic items presented serious environmental concerns. This led to some extensive research programmes, the objective of which was a greater understanding of biological degradation processes and the development of biodegradable polymers made from renewable and/or petrochemical resources, in order to produce alternatives to conventional non-degradable polymers.

At this time, a concept emerged which appeared to offer a solution to the twin issues of deriving plastics feed-stocks from finite resources and of persistent plastic waste. This was the idea that disposable plastics, especially those used for single-use packaging applications could be synthesised from biomass feed-stocks - renewable plant-based resources - and furthermore, that built into these polymers would be an inherent measure of reduced durability, or more accurately, an enhanced susceptibility to degradation.

During the 1970s and 80s, the degradability of plastic packaging materials was widely regarded by sections of both popular opinion and legislators as the obvious answer to solid waste disposal. Many believed that littered items made from these materials would simply disappear and land-filled items would decompose, extending the life of landfill sites (Incpen). However, by the end of the decade there were signs of a growing disenchantment and the perception of the benefits of degradable plastics had begun to change (Bowcott, 1990).

Several factors contributed to this change in attitude. Studies of landfill contents after several years of burial documented that even readily biodegradable materials such as food do not always degrade quickly under landfill conditions. Biodegradable materials can take years to degrade in landfill; newspapers, intact and legible even after 30 years, are the main method of dating land-filled waste. Modern landfills are designed to contain and stabilise materials. Thus degradation, rather than being promoted in such an environment may actually be retarded.

The twin features of raw material renewability and end of life product degradability, viewed separately as discrete rationales or in conjunction with varying degrees of significance, are the key concepts which originally promoted and continue to drive the development of bio-based and/or biodegradable polymers, known collectively as *bio-plastics* or *biopolymers*.

2.8.1   The mechanisms of biodegradation in polymers

Polymer degradation is caused mainly by chemical bond scission reactions within macromolecules, leading to a reduction in polymer chain length and molecular weight, and ultimately in the physical breakdown of the material or of its chemical nature (Schnabel, 1981). Although there are various modes by which these reactions can be initiated - for example by absorption of UV light (photo-degradation) into the polymer; by diffusion of water molecules into water sensitive polymers and hydrolysis (hydrolytic degradation) - this section will focus essentially on biologically initiated degradation of polymers (also known as *enzymatic degradation* or *biodegradation*).

Biodegradation is a familiar process as far as natural polymers are concerned. Biopolymers, which include cellulose, wood, skin and bone, are synthesised and degraded by micro-organisms (Schnabel, 1981). The mechanism of biodegradation involves hydrolysis and scission of susceptible polymer main chain linkages by enzymes produced by micro-organisms in order to enable acquisition of a carbon energy source and also as a by-product of their metabolic functions. Commonly the nature of the products of this decomposition also allows them to be utilised by other organisms for the production of energy or the production of new compounds, including new biopolymers. Occasionally natural decomposition processes may also be forced through other routes resulting in incompletely degraded decomposition products including peat, coal or crude oil.

With the advent of synthetic polymers during the 19th and 20th centuries, questions arose as to the way in which organisms responsible for the degradation of natural polymers would behave towards the new synthetic polymeric materials, which being carbon-based should theoretically be biodegradable.

During the long evolutionary process, many micro-organisms have adapted to produce limited forms of enzymes which are quite specific in terms of the type of biopolymer substrate they will affect. Other micro-organisms produce a variety of enzymes and have shown themselves capable of further adaptation, producing new enzymes over relatively short periods of time which are then able to attack new substrates (Schnabel, 1981). The critical implications this adaptation might be expected to create for the synthetic plastics industry is offset by other factors; the first being that many synthetic polymers do not contain easily hydrolysed linkages (Selke, 1990), and secondly that most petrochemical-based plastics are inherently hydrophobic, which impedes potential enzymatic reactions (Lox, 1992).

Formative work on the subject conducted by Baptist *et al* in the early 1960s, showed that the picture is further complicated by the fact that enzymatic oxidation of hydrocarbon chains occurs

at the chain ends only and synthetic polymers are not sensitive to lateral attack at sites away from their chain ends (Sokatch, 1969). Thus, products manufactured from such materials do not lend themselves readily to many degradation processes, in part because the structure of their synthetic polymer macromolecules preclude the possibility that in a plastic item some chains will end exactly at the surface of the product (Lox, 1992). Polyethylene (PE), polystyrene (PS), and polyvinyl chloride (PVC), are but a few of the common commodity petrochemical polymers whose high molecular weights retard enzyme reaction times to such an extent that they are considered non-degradable. Although polyamides such as nylon, polyurethanes and many polyesters are somewhat more susceptible to the process, they are still considered resistant. (Klemchuk, 1989)

2.8.2   Terminology and standards of degradability of plastics

With the emergence of the concept of degradable plastics in the 1970s, there appeared to be widespread confusion surrounding the subject. Even among the scientific and technical community there were no universally accepted specific definitions relating to polymer degradation (Selke, 1996). While various organisations have worked to reconcile these issues, this situation remained unresolved until relatively recently.

The earliest interpretations of the terms *degradable* and *degradability* with reference to plastics, originated from polymer users who had historically focused on maintaining the physical properties of these materials. They therefore defined degradation in terms of the percentage loss of mechanical properties such as tensile strength or elongation. However, if assimilation into the environment was the objective then this is not an appropriate measure. From an ecological perspective the complete degradation of carbon-based materials is only achieved at the point when the carbon molecules themselves have rejoined the natural carbon cycle by conversion to carbon dioxide or other small organic molecules, or by being consumed by living organisms and converted to biomass (Selke, 1990). Conversely, virtually any material will, given a long enough period of time, degrade in some ultimate sense (Selke, 1996). For some petrochemical-based plastics, this could be in the order of decades or even longer (Lox, 1992). Thus, efforts towards the setting of standards surrounding degradability in plastics brought together the twin issues of *endpoints* - the point at which a plastic material is considered truly degraded, and *timeframes* - the period in which degradation process occurs. These twin issues operate within a third factor: *the environmental conditions of exposure* - the temperature, humidity and oxygen levels which the material comes into contact.

The key criteria then, used in defining exactly what constitutes a biodegradable plastic, is that the material is broken down by micro-organisms; within timeframes considered sufficiently rapid to

confer some meaningful benefit, and that the products of such degradation (carbon dioxide, water, inorganics and humus-type materials) result in a total loss of not simply the mechanical integrity of the plastic but also of the chemical identity of the polymeric starting material. In addition, any engineered susceptibility to accelerated degradation will always be dependent upon the environmental conditions in which the material finds itself (Incpen), since rates of biodegradation are contingent upon such factors as temperature, moisture and the presence or absence of oxygen. Other factors which need to be taken into account are other components of the material's formulation such as pigments, adhesives, fillers, inks and other additives, which will also have an effect upon rates of degradation (De Wilde & De Baere, 1990).

Developing test methods for evaluating practical environmental biodegradability is problematic, given the multitude of influencing variables. One of the original obstacles to the acceptance of starch-based plastics in the packaging industry was an inability to extrude these materials into the shapes and sizes deemed necessary for standard tests in evaluating performance. Thus, product specifications based on particular performance criteria such as barrier properties and tensile strength could not be provided. In addition, information was lacking on the additional material property of product degradability itself as this was not properly defined.

Considerable international efforts have been made in the sphere of materials testing in order to reach consensus on defining the degradability of plastics - in the US by the Degradable Polymers Council (DPC) and the American Society for Materials & Testing (ASTM), and in Japan by the Biodegradable Plastics Society (BPS). Individual European countries also have their own standards organisations, such as Germany's Deutsches Institut für Normung (DIN), and in the UK, the British Standards Institute (BSI) (Demichelli, 1996; Anon, 1998; Stevens, 2002).

One of the apparent waste treatment options for biodegradable polymers is by *composting*. In order to resolve misunderstandings and misuse of terminology surrounding compostable materials among the various organisations of EU member states, the Comité Européen de Normalisation (CEN), revised European Standards supporting the Essential Requirements of the European Commission Directive 94/62/EC on packaging and packaging waste. Harmonised European Norm (EN) 13432:2000 - *Requirements for Packaging Recoverable through Composting and Biodegradation – Test Scheme and Evaluation Criteria for the Final Acceptance of Packaging*, supersedes all previous 'sister' norms (Official Journal of the European Communities, 2001). The International Standards Organisation (ISO), has also attempted to reconcile the various interpretations surrounding biodegradability in order that international consensus on the issue can be reached.

According to ASTM D5488-84d a *biodegradable* material is "capable of undergoing decomposition into carbon dioxide, methane, water, inorganic compounds or biomass, in which the predominant mechanism is the enzymatic action of micro-organisms that can be measured by a standardised test, in a specified period of time, reflecting available disposal conditions."

A summary of ASTM definitions relating to degradable plastics is given in Table 2.5.

Table 2.5: Summary of ASTM definitions relating to degradable plastics

Degradable plastic: a plastic designed to undergo a significant change in its chemical structure under specific environmental conditions, resulting in a loss of some properties that may vary as measured by standard test methods appropriate to the plastic and the application in a period of time that determines its classification.
Biodegradable plastic: a degradable plastic in which degradation results from the action of naturally occurring micro-organisms such as bacteria, fungi and algae.
Compostable plastic: a plastic that undergoes degradation by biological processes during composting to yield carbon dioxide, water, inorganic compounds and biomass at a rate consistent with other known compostable materials and leaving no visually distinguishable or toxic residues.

Adapted from ASTM Document D883-00. Standard Terminology Relating to Plastics

A summary of CEN (and ISO) standards and test methods pertaining to biodegradability, compostability, and plastics materials conforming to these characteristics are given in Table 2.6.

Table 2.6: Summary of CEN European Standard EN 13432:2000

Biodegradability: the metabolic conversion of compostable material into carbon dioxide, measured by standard test method prEN 14046 (also published as ISO 14855: Determination of the ultimate aerobic biodegradability of plastic materials under controlled composting conditions - Method by analysis of evolved carbon dioxide). The level of acceptability is 90% (absolute or relative to the biodegradation of cellulose, which itself must reach a biodegradation of 70%), to be achieved within 6 months.
Disintegrability: the fragmentation and absence of visible contamination in the final compost, measured in a pilot scale composting test (prEN 14045). Samples of test materials to be composted with bio-waste for 3 months and the final compost screened. Residues of test materials with dimensions > 2mm to be less than 10%
Absence of negative effects: on the process of composting or of the final compost, from eco-toxins or xenobiotics either visible or invisible. To be verified with pilot scale composting tests including the reduction in agronomic values or presence of eco-toxological effects on plant growth.*
Heavy metals: to be below given maximum values. A demonstrated absence of negative effects on the final compost. To be verified with pilot scale composting tests including the reduction in agronomic values or presence of eco-toxological effects on plant growth.* *Plant growth test modified OECD 208

Adapted from EN 13432:2000. Requirements for Packaging Recoverable through Composting & Biodegradation. Test Scheme and Evaluation Criteria for the Final Acceptance of Packaging.

The points laid out in the CEN standard invoke the key criteria surrounding compostability and biodegradability (timeframes and products of degradation), but also draw a distinction between the two. A biodegradable plastic is not necessarily compostable because it must also disintegrate within the composting cycle. Conversely, a material which disintegrates during the composting cycle must also be fully biodegradable. Figure 2.20 illustrates the intrinsic set of properties and requirements comprising compostable materials.
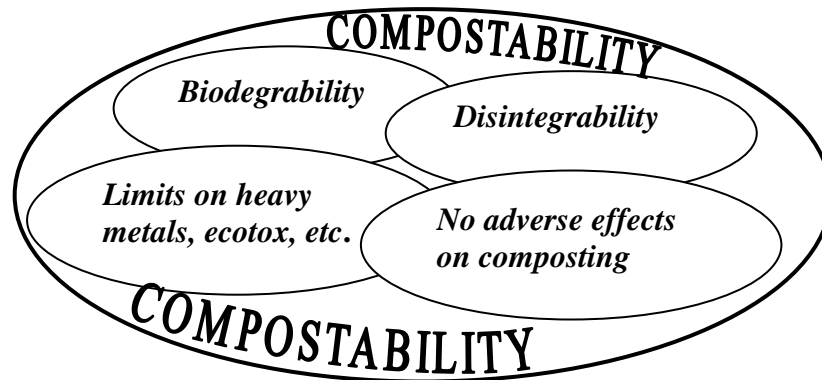
Figure 2.20: Compostability as a set of properties & requirements
The CEN activity and position of EC on sustainable polymeric materials and EDPs.

2.8.3   Classification of synthesised bio-plastics

Bio-plastics are classified in a number of ways. Perhaps the most common method of classification is according to the origin of the raw materials on which the polymers are based and synthesised. This method of classification includes three broad groups: those polymers synthesised from biological systems such as plants and microorganisms; those based on natural polymers; and those polymers derived from petrochemical sources. The latter grouping shows that not all biodegradable plastics are necessarily renewable.

For the purposes of clarity and brevity, Table 2.7 lists selected biodegradable plastics in each grouping.

Table 2.7: Selected commercially available bio-plastics and their constituent polymers

Category	Polymer	Trade Name	Manufacturer
Bio-synthetic	Poly(β-hydroxybutrate-co-β-hydroxy valerate)	Biopol	Monsanto
	Poly(lactide)	EcoPla, NatureWork, Lacea	Cargil Dow Mitsui Chemicals
	Pullulan	Pullulan	Hayashihara
Natural polymer-based	Cellulose acetate	EnviroPlastic-Z	Planet Polymer
	Starch-based polycaprolactone	Bioplast	Biotec
	Thermoplastic starch	Mater-Bi	Novamont
Chemo-synthetic	Poly(butylene succinate)	Bionelle 1000	Showa Highpolymer
	Poly(butylene succinate adipate)	Bionelle 3000	Showa Highpolymer
	Copolyester	Ecoflex	BASF
	Copolyester	Eastar Bio	Eastman Chemicals
	Polycaprolactone	Tone	Union Carbide
	Poly(vinyl alcohol)	Airvol	Air Products and Chemicals
	Poly(ester amide)	BAK	Bayer

Encyclopedia of Polymer Science & Technology (Environmentally Degradable Plastics), Stevens (2003)

2.8.4   Classification of starch-based plastics

The biodegradability of a plastic is dependent on the chemical structure of the material and on the constitution of the final product, rather than simply on the raw materials used in its production (Nolan-ITU, 2002). Biodegradable plastics can therefore be based either on carbon sources from petrochemicals, or on renewable resources such as plants. Of the latter category, a range of fully biodegradable plastics have been developed, some commercially, from a variety of sources and starting points, including the fermentation of glucose and organic acids with common soil bacteria, and others based on lactic acid. However, at present, the only biodegradable plastics that have come close to competing with conventional petrochemical plastics in terms of production costs are those based on starch - either from potatoes, maize or other cereal crops. Since the materials investigated in this thesis are exclusively starch-based, this section will focus on starch-based plastics.

Plastics comprising starch may have starch contents ranging from 6% to greater than 95%, often blended with high-performance polymers (e.g. aliphatic polyesters and polyvinyl alcohols) to achieve the necessary performance properties for a variety of applications. Starch content needs to exceed 60% before significant material breakdown occurs. As the starch content is increased, the polymer composites become more biodegradable and leave less recalcitrant residues (Nolan-ITU, 2002).

These plastics include polymer/starch blends consisting of comparatively low proportions of starch with high-performance petrochemical-based polymers and other starch-based plastics (also known as thermoplastic starch), in which proportions of starch are much higher. In this latter group the provision of many material properties of the plastic such as mechanical strength, are obtained through thermal treatment which results in the *plasticisation* of the starch itself.

Unlike petrochemical polymers which are generally resistant to lateral attack, biodegradation of starch-based polymers is a result of enzymatic attack at the glucosidic linkages between the sugar groups leading to a reduction in polymer chain length and the splitting off of sugar units (monosaccharides, disaccharides and oligosaccharides). For significant breakdown of starch/polymer blends to occur, starch contents generally need to be in excess of 60%. At lower starch contents, the starch particles act as weak links in the polymer matrix and as sites for biological attack, thus allowing the polymer matrix to disintegrate into small fragments, but not necessarily for the entire polymer structure to biodegrade (Nolan-ITU, 2002).

2.8.4.1 Starch/polymer blends

The first packaging films to be marketed as biodegradable during the 1980s were mixtures of low-density polyethylene and approximately 6% starch. Some of these films also contained pro-oxidants to enhance oxidative degradation of the polymer. The rationale behind these formulations reasoned that the starch component once consumed by micro-organisms, would leave the mechanical integrity of the film disrupted, leading to an increased surface area and decreased crystallinity of the polymer, which would then encourage the biodegradation of the remaining polyethylene. Despite claims made, principally by manufacturers, as to the degradable properties of these products, they were subsequently shown to *biofragment* rather than fully biodegrade, reducing the mechanical properties of the product, but leaving smaller fragments of the original polymer behind once the starch component had been degraded.

Modifications of these starch/polymer blends, containing typically 20% starch, were later produced commercially by the St. Lawrence Group in Canada, under the trade name *EcoStar* (Anon, 1993). Other variations under the brand were produced with starch-plastic blends of polypropylene, polystyrene, and polyurethane. These contained higher proportions of up to 50% starch (McCarthy-Bates, 1993). Films containing gelatinised starch together with a synthetic polymer and a hydrophobic copolymer serving as a compatibilising agent were further variations on the starch-polymer theme. These contained between 47-50% starch (Asche, 1994). According to the producers, Ampacet and Agri-Tech Industries, degradation of the starch component was reported to be complete in 40 days, with complete degradation of the remaining polymer components taking a minimum of 2-3 years in composting conditions in which sufficient exposure to oxygen was maintained. Given these extensive periods, it is now generally conceded that these materials were not fully biodegradable in the currently accepted definition of the term, and they are now generally regarded as *biodisruptable* plastics.

Bhatnager and Hanna used a blend of 25% amylose maize starch, polystyrene or polymethylmethacrylate to produce extruded loosefills with mechanical properties comparable to EPS (Bhatnagar & Hanna, 1996). Again, such blends are not now considered fully biodegradable materials.

Starch/polymer blends became an issue of concern to environmental groups who reasoned that by predisposing a littered plastic item to fragment, its previous potential for wildlife entrapment was simply being exchanged for problems of wildlife ingestion. Concern was also expressed over the significant lack of information about the products of degradation and their potential environmental impacts. These problems were further exacerbated by vague terminology and difficulties associated with achieving standard testing of biodegradability in plastics, resulting in

inadequate definitions surrounding the subject and helping to facilitate claims that did not reflect actual performance in terms of the extent of product breakdown within reasonable timeframes.

The new view prevalent among environmentalists in the latter part of the 1980s was that degradable plastics were being misrepresented to consumers. In several US states, the State Attorney General evidently concurred, resulting in legal action for false or deceptive advertising against some companies, notably Mobil Chemical Co. The fairly rapid demise of many of these products followed, along with more cautious and verifiable environmental claims made to promote this packaging (Selke, 1990).

Another disadvantage of plastics containing starch fillers was that these materials require an additional polymer content in order to compensate for the starch component and maintain product strength. Items made from these materials may therefore consume more resources than their original, non-degradable equivalents (Perchard, 1991).

Since that time, significant technological progress has been made in the sphere of starch-based plastics leading to the emergence of truly biodegradable starch-based plastics.

2.8.4.2 Starch-based bio-plastics

As a result of technological innovations, plastic products manufactured using starch have undergone paradigm changes since their inception, and the first generation of starch/non-biodegradable polymer blends should be contrasted from the current generation of fully biodegradable starch-based polymers (such as thermoplastic starch and starch/ biodegradable polymer blends), which have starch contents greater than 70% and are based on gelatinised vegetable starch and synthetic polymers (natural or petrochemical-based) (Nolan-ITU, 2002).

Under certain conditions of temperature, pressure, shear, limited water and sufficient time starch can be *plasticised* to produce materials with good performance properties whilst retaining its inherent biodegradability. Production of the modified starch involves *destructuring* the native starch granules. The transformation is known as the *molecular dispersion of starch and water* (MDS). The modified destructured starch loses its granular structure and is thus amorphous rather than crystalline (National Starch & Chemical, 2003[b]), rendering the material into a thermoplastic comprising an entirely new molecular structure. Starch-based products utilising MDS are thus molecularly homogeneous with amylose and amylopectin being dispersed uniformly throughout the material. Importantly, many starch-based compounds can be processed on existing plastics fabrication machinery, including extrusion equipment (Nolan-ITU, 2002).

2.8.4.3. Starch-based bio-plastic foams

Several other technologies utilising MDS have also been developed for producing starch foam products. One of the earliest members of this family of materials was *Novon*, originally produced in the US by Warner-Lambert (Churchill Technology) in the early 1990s. Novon contained up to 95% starch but tended to be moisture sensitive. With the use of additives, moisture sensitivities were controlled and water-resistant grades produced (McCarthy-Bates, 1993).

Starch may be injection moulded in a thermoforming process similar technology to that used for baking waffles to produce a material with mechanical properties suitable for particular structural packaging applications such as trays (Raynaud). Ingredients are mixed in batches consistent with their respective proportions and sequence according to the formula for the particular product being manufactured but generally containing 70–80% (w/w) moisture. The process involves injecting a metered amount of the starch mixture into heated lower platens of the product moulds which are then closed under pressure. Steam generated from the heated moisture in the dough acts as the blowing agent and the starch inside the hot mould gelatinises and expands to take the shape of the mould cavity.

Shogren et al studied this technique using a corn starch, a waxy maize starch, a high amylose maize starch containing 70% amylose and a wheat starch. These various starches were mixed with water and transferred to moulds heated to between 175 - 210°C. The dwell period in which the expanding mixture stays in the mould may be as short as several seconds, but this varies according to the particular mixture used and may be as long as 200 seconds (Shogren et al, 1998). At the end of the cycle time moulds are opened and trays are removed by vacuum suction. The finished products are then conditioned or cured to stabilise the structure. The resulting baked foam trays consist of thin wall structures comprising dense outer layers and lower density cores. Overall densities are relatively high ranging from 150 to 190 kg/m^3 The high moisture content in the mixture lengthens both processing and curing times, the latter in some cases being as long as 12 hours (Matthews, 2008), with obvious implications for any potential commercial development. However, trays manufactured by this process have been used for the packing of organic produce for sale in some UK supermarkets.

A puffing technique similar to that used for making ready-to-eat popcorn in the food industry has been studied as an alternative process for creating starch-based foams. In comparison with the baking technique previously described, the starch feedstock contains much lower moisture levels of around 10 – 15 w/w% resulting in reduced processing times in the region of several seconds at temperatures of about 180°C (Glenn, Orts, 2001). However, currently this technique has not been developed for industrial applications.

The viability of producing moulded foams shapes was studied by Zhang & Song (2003). Extruded wheat starch pellets containing approximately 10% moisture were compressed in moulds heated to 150°C – 220°C and then quickly decompressed allowing the pellets to expand and fill the mould. The expanded pellets fused to form integrated foam objects, but further work is needed to control the process in order to achieve greater precision of the finished foamed shapes. In similar method studied by Zhou et al (2004), microwave radiation was used to rapidly heat extruded starch pellets within moulds. The water within the pellets vaporises on heating, expanding the pellets to fill the mould and fuse them at their point of contact into a coherent structure. By adjusting the compositions of the extruded starch pellets, the heating and moulding conditions, a foam block with required cell structures and mechanical properties may be obtained. This novel method is referred to as Microwave Assisted Moulding (MAM).

Novamont SpA in Italy has developed extrusion technology to produce corrugated foam sheets from Mater-Bi biodegradable starch-based polymer which can then be bonded together to produce laminated block foams. The sheet is marketed under the trade name "Wave" by Mater-Bi, and used in applications such as box liners for Hewlett-Packard products. The foam is naturally antistatic and uses a special PE01/1 grade of Mater-Bi, which is 85% starch plus fillers and biodegradable polymeric additives. It's foamed with water in an unconventional extrusion line engineered by Novamont to produce 600-mm-wide sheet 12 mm thick with a density of 38 kg/m^3. Sheets can be laminated together into thicker planks. In the US, National Starch has also developed a similar technology (Plastics Technology, 2009).

In terms of extruded starch-based foams, Storopak's *Renature*, a loosefill foam cushioning material and alternative to expanded polystyrene (EPS) was one of its best-known applications (Goddard *et al.*, 1993). Research by Fang & Hanna (2001), described improvements in the mechanical properties and moisture resistance of extruded starch foams through the incorporation of Mater-Bi^{TM}, a biodegradable resin made from maize starch, into the extrusion foaming process. In the UK, Green Light Products Ltd, have marketed *Green Fill* and *Eco-Flow* since the late 1990s - loosefill cushioning products made from corn starch or wheat starch. The products are 100% biodegradable and partially water-soluble.

Green Light Products Ltd, working with the Centre for Biodegradable Materials Research at Brunel University are currently developing other techniques to fabricate various types of block foams using extruded starch. Two principal methods utilise the natural adhesive properties of moistened starch and are known as Regular Packing and Stacking (RPS), and Compression Bonded Loosefill (CBL). RPS foam technology has been reported in previous research (Kang 2006, Wang 2008), and will be discussed further in Chapter 3 of this thesis alongside CBL technology.

2.9   The production of extruded starch-based foams

Starch derived from cereal crops or tubers is the primary raw material used in the starch extrusion foaming process. Water is normally used as a blowing agent and other additives including polyvinyl alcohol and talc may also be used to modify the properties of the finished foam. This section details the physical structure and chemical characteristics of native starch and provides an overview of the production of extruded starch foam from its constituent raw materials. It then goes on to examine the structure and properties of extruded starch.

2.9.1   Starch

Different sources of starch from maize, potatoes and wheat have all been used to produce extruded starch foams. Starch is a comparatively inexpensive, renewable resource derived from agricultural production with world volumes of production approximately 48.5 million tonnes a year in 2000. Table 2.8 shows starch production by raw material in the EU, US and other countries in 2000.

Table 2.8: Starch production by raw material in the EU, US and other countries, 2000
(million tons, starch content)

	Maize	Potatoes	Wheat	Other	Total
EU	3.9	1.8	2.8	0.0	**8.4**
US	24.6	0.0	0.3	0.0	**24.9**
Other Countries	10.9	0.8	1.1	2.5	**15.2**
World	39.4	2.6	4.1	2.5	**48.5**

EU Commission (DG AGRI, Unit C2), United States Department of Agriculture (USDA), LMC Internal Database
The structure of the world starch market, LMC International 2002.

Relatively high proportions of starch are found within cereal plants as well as tubers and legumes. In cereal plants starch comprises between 65 – 80% of the plant's dry weight (Nawrath et al, 1995). Starch is a complex carbohydrate which functions as the major energy storage unit in the plant and exists as granular structures, also referred to as *amyloplasts*. These can be *lenticular* or *polyhedric* in shape depending on plant origin and are relatively dense, insoluble and hydrate only slightly in cold water (Swinkels, 1985). Amyloplasts from wheat plants generally fall into two ranges of dimension referred to as 'large' and 'small' granules. The large granules generally range from 20 to 45 µm in diameter, while the smaller granules are usually in the range of 1 to 3 µm in diameter (Atwell, 2001). Figure 2.21 shows magnified image of amyloplasts from wheat starch.
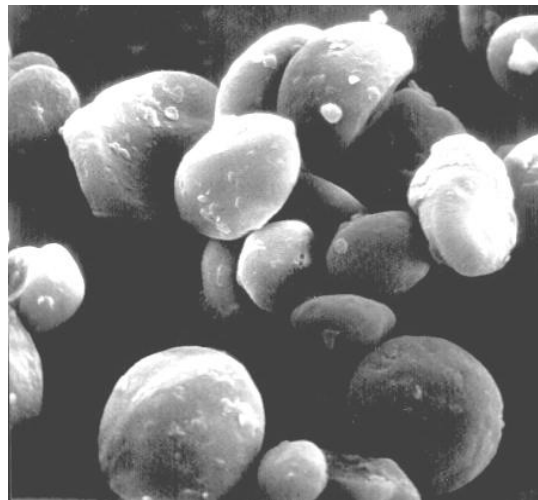
Figure 2.21: Magnified image of amyloplasts from wheat cells
Morton Satin, AGSI

Table 2.9 provides the typical characteristics of starches obtained from various plant sources.

Table 2.9: Characteristics of starches obtained from various sources

Starch	Amylose (%)	Lipids (%)	Protein (%)
Corn	28	0.8	0.35
Wheat	28	0.9	0.4
Potato	21	0.1	0.1
Tapioca	17	0.1	0.1
Mung bean	39	0.3	0.3

Wang, Y. A Study of the Structure & Properties of Starch Foam & Eco-Composites for Industrial Applications (PhD Thesis) Brunel University, 2008

In its native state, starch exists as semi-crystalline granules comprising of crystalline and amorphous regions. It is generally believed that starch granules consist of alternating 120 - 400 nm thick amorphous and semi-crystalline layers which form the amyloplast are deposited in successive layers around a central point called the *hilum* (Buleon, et al., 1998; University of York, 2008). These layers are formed as amylose molecules and outer branches of amylopectin associate through hydrogen bonding in a parallel fashion to give radially oriented, crystalline bundles known as *micelles* (National Starch & Chemical, 2003 [a]).

The highly crystalline micellular areas within the starch granules explain their ability to rotate a plane of polarised light producing characteristic interference crosses, often referred to as the *Maltese cross*. This optical effect is an example of *birefringence*, which occurs as a result of the highly ordered radial organisation of the starch granule (Rao & Hartel, 1998). Figure 2.22 shows starch granules viewed under magnification through polarised light, displaying concentric rings and the Maltese cross.
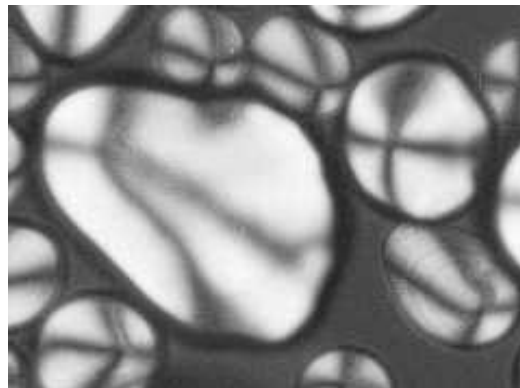
Figure 2.22: Magnified starch granules viewed under polarised light
University of York, 2001

The crystalline structure of native cereal starches produces a characteristic diffraction pattern under *X-ray diffraction*, a technique which yields the atomic structure of materials based on the elastic scattering of X-rays from the electron clouds of the individual atoms in the system. The X-ray diffraction patterns produced from cereal starches are classified as A-type, as differentiated from tuber, root and seed starches, known as B and C-types. (Zobel, 1964). The main characteristic X-ray diffraction peaks for native A-type starches are listed in Table 2.10. Small deviations from these peak positions may occur due to the sample history and moisture content (Zhou, 2004).

Table 2.10: X-ray diffraction parameters of native A-type starches

2θ (°)	Intensity
15.3	Strong
17.1	Strong
18.2	less than strong
23.5	Strong

Zhou, J. Microwave Assisted Moulding of Starch-Based Foams, PhD thesis (2004)

A-type crystal lattices consist of double helical structures. The overall crystallinity of native starch varies from 15% to 45% depending not only on the origin and hydration of starch but also on the technique used to determine it. (Buleon, et al., 1998).

Chemically, starch is a polymer of glucose $(C_6H_{10}O_5)_x$, a polysaccharide made up of repeating glucose units. A single glucose unit is shown in Figure 2.23.
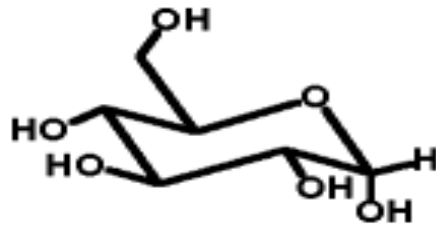
Figure 2.23: Single glucose unit
Key Centre for Polymer Colloids, 2001

Through an enzymatic condensation polymerisation reaction, one molecule of water is split out between two molecules of glucose to form a bond. These *glucosidic* linkages occur predominantly in the alpha 1-4 carbon positions, but others also occur in the alpha-1,6 carbon positions (National Starch & Chemical, 2003[a]). Both types of linkage are shown in Figure 2.24.
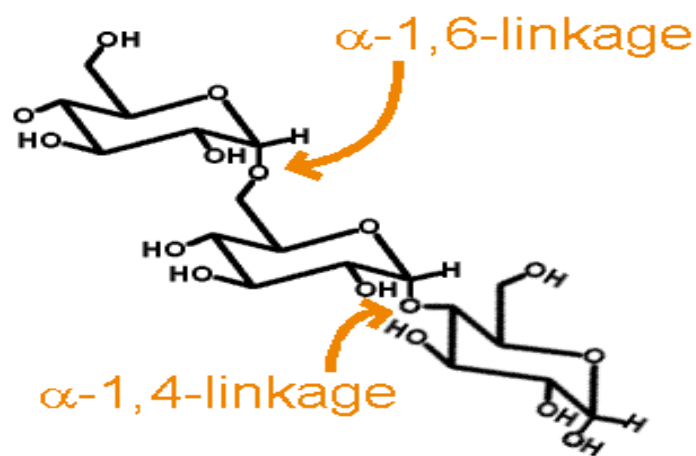
Figure 2.24: α-1,4 and α-1,6 glucosidic linkages
Source: Key Centre for Polymer Colloids, 2001

The two different linkages of this condensation polymerisation reaction result in two differentially structured starch macromolecule chains. Where linkages occur in the alpha-1 and 4 carbon positions, a linear chained homopolymer called *amylose* is produced. Figure 2.25 shows an amylose molecule.
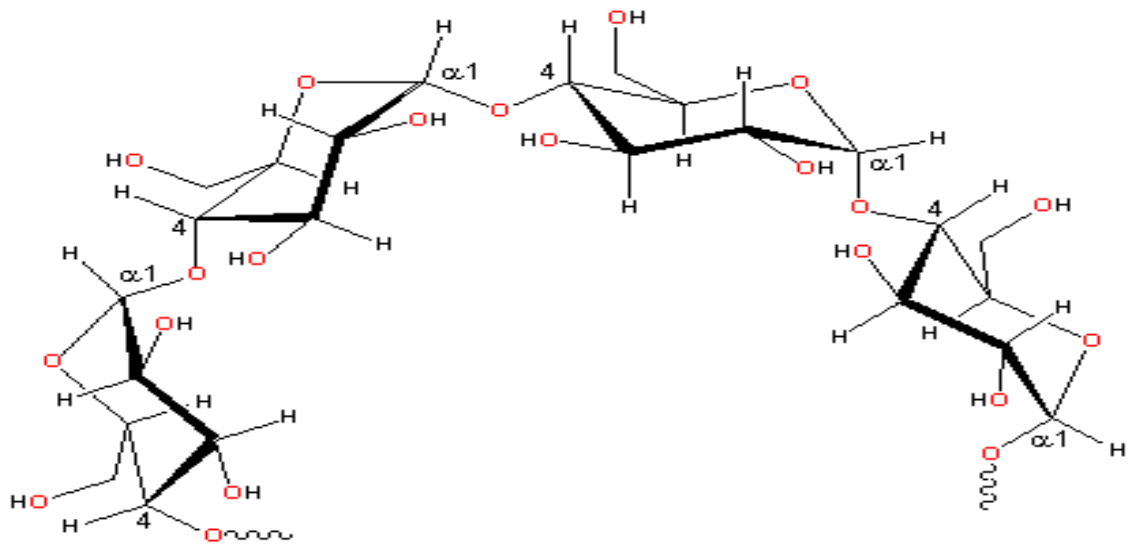
Figure 2.25: Representative partial structure of the amylose molecule
Martin Chaplin, South Bank University

The length of the amylose chains depend on the particular genetic background of the plant it comes from, but in general the average length is between 300 and 3,000 glucose units (Nolan-ITU, 2002). In contrast, *amylopectin*, the second type of polymer macromolecule found in starch, develops when, in addition to the alpha-1 and 4 carbon position linkages, the enzymatic condensation between glucose units also occurs at alpha carbon positions 1 and 6 (Swinkels, 1985). This additional linkage results in a prolific branching of chains at those positions making it much bigger than amylose and one of the largest naturally occurring molecules, but with linear chain lengths of only 10 and 60 glucose units (National Starch & Chemical, 2003[a]; Hay, 2002). An amylopectin macromolecule is shown schematically in Figure 2.26.
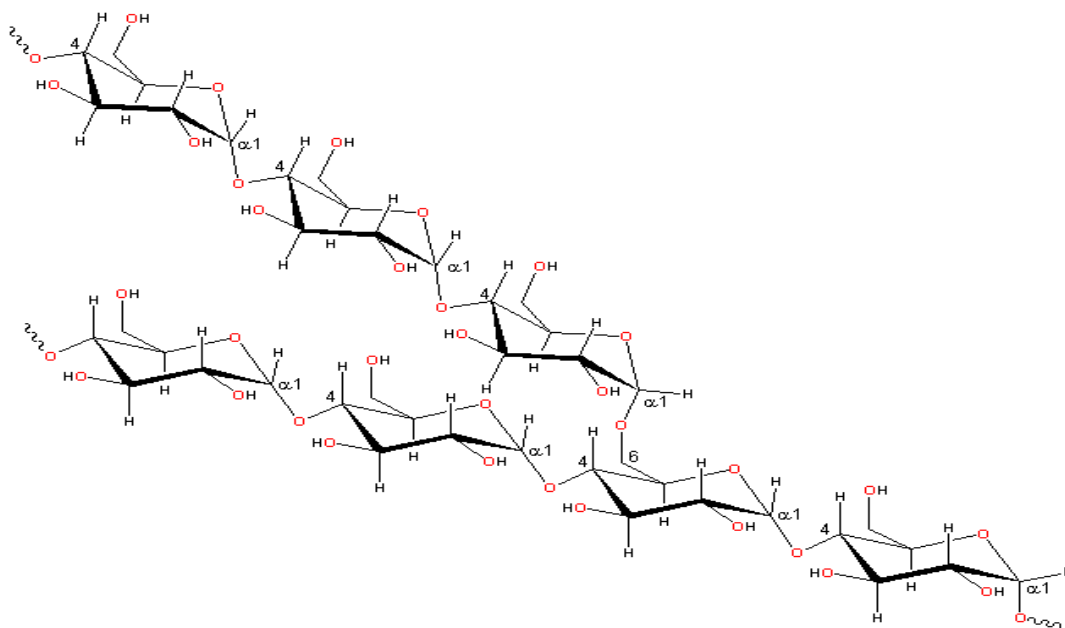
Figure 2.26: Representative partial structure of the amylopectin molecule
Martin Chaplin, South Bank University

The branched, high molecular weight amylopectin, together with the more linear amylose comprise the two major molecular components of starch. The specific arrangement of these carbohydrate chains gives starch its discrete granular structure, making it unique among carbohydrates (Hay, 2002).

The ratio of amylose to amylopectin has the greatest influence on the physicochemical properties of the starch and consequently on the range of starch applications. In most wheat crops, typical dry weight ratios are approximately 20 - 30% amylose and 70 - 80% amylopectin (Unilever Research/National Starch and Chemical, 2000), although these proportions can vary depending upon the variety of crop, the result of classical plant breeding, or through genetic modification (Europabio, 2006). In addition to amylose and amylopectin which comprise 95-97% of a typical starch granule, small amounts of proteins (0.06% - 0.4 %), lipids (0.05% - 0.9%), phosphorus (0.08%), and inorganic materials such as ash (0.4%) are also present. Other factors affecting the physicochemical properties of starch include the length and distribution of the polymer chains and moisture contents which are usually in the region of 10 - 20% based on weight (Swinkels, 1985).

Amylopectin is suited to the production of glues and pastes, while amylose is used in the manufacture of biodegradable products. Thus, for many industrial applications it is desirable to have a pure or enriched fraction of either amylopectin or amylose. Whilst scientists have been able to generate amylose-free or amylopectin-rich plants, the generation of very-high-amylose starch by genetic modification has proven much more challenging but has been achieved by the inhibition of enzymes responsible for polymer chain branching (Nature, 2000). Through this

process, starch granule morphology and composition are radically altered; high-molecular-weight amylopectin is absent, and amylose contents are increased to levels of up to 89%. Phosphorus levels are also increased by six-fold (Unilever Research/National Starch and Chemical, 2000). This unique starch offers novel properties for industrial applications and the resultant transgenic plants enable energy-consuming starch component separation process to be minimised. Scientific research organisations in many countries are actively involved in the development of *industrial starch* from purpose-grown plants specifically developed for the production of starch.

In addition to crops grown specifically for the industrial starch market, there are other routes through which starch may be obtained for industrial processing, including reclaimed by-product starch from the food processing industry (Canadian Plastics 2009).

2.9.2   The processing of starch for material applications

Although native starch is a natural polymer it is not a thermoplastic polymer because it will degrade when heated rather than forming a melt (Simmons, & Thomas, 1995). Modification of the structure of native starch is therefore necessary in order to produce a thermoplastic starch. Such modification is commonly performed by extrusion under controlled pressure and temperature using mechanical and heat energy with the addition of water or other plasticisers to destructure the starch granules and convert the starch into a homogeneous material that behaves as a thermoplastic (Lorcks, 1998).

2.9.2.1 The extrusion foaming process

Extrusion foaming is a continuous process in which foam strands of various thickness are produced. In a typical extrusion foaming process, starch is mixed with water (25% to 50% by weight), as a plasticiser and blowing agent along with other processing additives as previously outlined. The mixture is melted in the extruder barrel by heating and/or the friction generated within the pressurised material itself as it is forced along the Archimedes screw of the extruder. The extruder operates typically at temperatures of 150-180ºC and is capable of imparting intensive shear forces (McCarthy, 2001). High temperature and pressure within the extruder barrel causes swelling and destructurisation of the crystalline structure of the amyloplast in a process called *gelatinisation*. Gelatinisation is the irreversible order-disorder transition that starch undergoes when it is heated in the presence of water involving the disruption of molecular orders within the starch granule accompanied by a series of events such as water absorption, granular swelling, crystallinity loss, amylose leaching and viscosity development. As the starch breaks down it loses crystallinity and becomes plasticised with the water, resulting in a homogenous amorphous plastic melt.

The blowing agent diffuses and dissolves as a super-saturated gas within the melted polymer matrix. On exiting the die head of the extruder the polymer melt is subjected to rapid decompression causing a drop in the solubility of diffused blowing agent within the polymer matrix resulting in nucleation or bubble formation. The bubbles expand as the blowing agent rapidly diffuses into them, eventually reaching a critical size at which point the bubbles either stabilise as a result of rapid increase in viscosity of the melt or rupture.

As with conventional extruded polymer foams, the extrusion foaming of starch utilises the liquid/gas phase transitions and the bubble dynamics result in structural transformations within the material. Due to being held at a temperature higher than its boiling point, on exiting the extruder the water within the melt expands due to a sudden drop in temperature and pressure, thus serving as a blowing agent for the foaming process. The sudden decompression causes a proportion of the water in the mixture to vaporise, leading to cell nucleation, expansion, growth and stabilisation of closed pores or collapse to form open cells, resulting in porous formation. Collapse of cells at the surface will lead to rapid loss of moisture and stabilization of the cell structure. The particular foamed structure of the extruded starch based foam will depend upon factors such as the molecular weight of the starch, moisture content in the mixture and presence of plasticisers or other additives, as well as extrusion processing conditions such as extruder temperature, melt pressure and the shape of the die (McCarthy, 2001). Figure 2.27 shows a schematic representation of typical foam extrusion behaviour as it exits the extruder die.
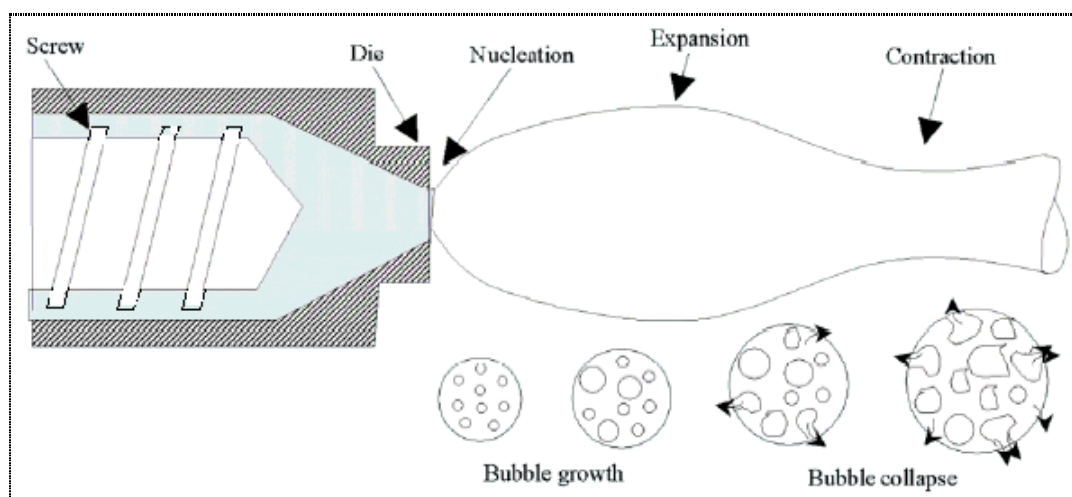
Figure 2.27: Typical foam extrusion behaviour
Kang, 2006

As the gelatinised foamed extrudate cools, starch polymer chains begin to re-associate and once again form crystalline micro-structures in a process known as *retrogradation*. Polymers of different starches re-crystallise to various degrees chiefly due to the constituent proportions of amylose to amylopectin. Amylose has a greater tendency to re-associate than amylopectin and

for amylose this re-crystallisation is irreversible. The re-crystallisation of amylopectin is reversible and this in part is responsible for the premature aging phenomena and relatively short life-span of thermoplastic starch-based products (Parker, Ring, 1995).

Extrusion foaming technology has been used since the late 1980s by organisations such as National Starch in the US, Novamont in Italy and Green Light Products Ltd in the UK to develop starch-based foams as alternatives to expanded polystyrene loosefill chips, commonly used in packaging applications.

2.9.3   Blowing agents

Any substance, which alone or in combination with other substances, is capable of generating gas and producing a cellular structure in a polymer, is known as a blowing agent. As an essential ingredient in the formation of foams, blowing agents are listed under a separate heading from other additives.

Blowing agents play an important role in both the manufacturing process and performance capabilities of the finished polymer foam. In the formation of most manufactured polymeric foam materials, the initial gaseous phase in the foaming process derives from the blowing agent(s) used.

Besides controlling density, blowing agents affect the cellular microstructure and morphology of the foam, which in turn define its end-use applications. In some applications such as insulation, the blowing agent may play a central role in the long-term performance of the foam. In these and many other cases in which the foam is closed cell, the blowing agent is retained within the cellular structure of the foam, diffusing out over comparatively long time periods, often decades. In the case of open cell foams used in packaging and cushioning applications, the blowing agent may escape the cellular structure of the foam almost immediately after the foam has been formed. In such cases, although the cellular structure and morphology imprint of the blowing agent impact upon the performance of the foam, the blowing agent itself does not. In other foam applications such as buoyancy, impact resistance, and load bearing, the role of blowing agents is intermediate (Eaves, 2004).

Blowing agents can be divided in to two main subgroups: physical and chemical. The former grouping include compressed gasses that expand when pressure is released such as nitrogen, carbon dioxide and oxygen; liquids such as pentanes with boiling points below the softening point of the polymer causing cells to develops as the liquid changes to a gaseous state, and soluble solids including chlorofluoro compounds that result in pores in the polymer as they leach out. Chemical blowing agents include exothermic, endothermic and endo-exo blends which

decompose or react under the influence of heat or a catalyst to form a gas. These include simple salts such as ammonium or sodium bicarbonate as well as complex nitrogen releasing agents (Eaves, 2004).

In the extrusion foaming of starch-based materials, water is often used both as an effective plasticiser and blowing agent. At the high pressures and temperatures within the extruder, water dissolves in the starch melt and exits the mixture as steam which acts as the blowing agent when pressure and temperature suddenly drops as the extruded material exits the extruder die head.

2.9.4   Other additives

Foams made from pure starch tend to be brittle and highly water-sensitive and do not have the satisfactory physical and mechanical properties required for applications such as foams for cushion packaging. Additives functioning as plasticisers, foaming control agents and reinforcement may be included prior to the extrusion of starch foam, either for direct modification of the properties of the finished foam or to modify processing parameters in extrusion and thus indirectly improve the foam properties.

Water is the most commonly used plasticiser in the processing of starch. However, the physical properties of starch materials are greatly influenced by the amount of inherent water. In addition, hydrophilic starch-based materials are hygroscopic meaning they are characterised by equilibrium relative humidity (ERH) - the relative humidity at which vapour pressures and movement of moisture within the material and its environment equalise, resulting in changes in moisture content according to ambient environmental conditions and hence in the properties of materials during storage and use. In addition, starch materials plasticised by water alone tend to be brittle and additional plasticisers are often included in order to extend their useful functionality (Poutanen, & Forssell, 1996).

The hydrophilic nature of many starch-based polymers is used by some manufacturers to market products based on their ability to readily disintegrate on contact with water. However, this property also results in a low moisture barrier of starch-based plastic products, which together with the consequent migration of hydrophilic plasticisers, can result in a premature ageing phenomena (Kang, 2006). For increased moisture resistance as well as mechanical property enhancements including strength and flexibility most starch foams developed for cushion packaging applications normally contain polymeric additives. These include biodegradable polymers such as polyvinyl alcohol (PVOH) (Nolan-ITU, 2002), polyethylene glycol (Cha et al, 2001), polylactic acid (PLA) and polycaprolactone (PCL) (Fang and Hanna, 2001[a]).

In order to increase flexibility and modulus as well as resistance to moisture extruded starch-based foams often incorporate polyvinyl alcohol. PVOH is commonly used as an effective oxygen

barrier layer in injection blow moulded polyethylene bottles which are increasingly being used to replace glass packaging. PVOH is also used as an additive in extruded starch foams to enhance moisture resistance as well as the flexibility and compressive strength of the foam. In extruded starch foams PVOH is added in the range of approximately 5% - 15% by weight depending on the foam properties or variations in processing parameters required (Liu & Peng, 2004).

Talc (Mg_3 Si_4 O_{10} $(OH)_2$) is an inert and hydrophobic magnesium silicate which is often added to extruded starch foams at between approximately 1-2% by weight. Due to the very weak Van der Waal's forces of attraction which bond the talc layers, the component structures slide apart under low shear stress aiding dispersion of the talc particles within the starch melt. This property is utilised in order to control the dispersion and size of cells, resulting in increased foam uniformity and a finer cell structure (Lee, 2000).

In fibre-reinforced polymer composites, strong and stiff fibres are embedded into the matrix with the aim of enhancing mechanical properties of the finished material. The length, aspect ratio, alignment of fibres and interfacial bonding between fibre and the matrix are important factors in controlling the mechanical properties of a fibre reinforced composite (Hull and Clyne, 1996). Natural fibres generally combine good mechanical properties with low density and are the obvious choice of reinforcement for foams made from renewable and biodegradable raw materials. In fibre reinforced foams, fibre contents are commonly between 20–35% by weight (Wollerdorfer, Bader, 1998).

2.10 Characterisation of the structure of extruded starch

As a result of the thermal and mechanical energy imparted to starch granules during extrusion, the processes of gelatinisation and subsequent retrogradation result in a range of modifications in extruded starch materials at both the molecular and macroscopic levels. Modifications to the structure and properties of native starch by extrusion have been investigated by several methods. These include optical microscopy; *scanning electron microscopy* (SEM) - a technique that images a sample by scanning it with a high-energy beam of electrons in a raster scan pattern, causing the electrons to interact with the atoms that make up the sample and producing signals that contain information about the sample's surface topography and composition; *differential scanning calorimetry* (DSC) - a thermo-analytical technique in which the difference in the amount of heat required to increase the temperature of a sample and reference is measured as a function of temperature, and also *X-ray diffraction* (XRD) - a family of non-destructive analytical techniques which reveal information about the crystallographic structure, chemical composition, and physical properties of materials, based on observing the scattered intensity of an X-ray beam hitting a sample as a function of incident and scattered angle, polarization, and wavelength or energy.

During gelatinisation, several phenomena occur at different structural levels including fragmentation of the starch granules, hydrogen-bond cleavage between starch molecules leading to loss of crystallinity, and partial depolymersation of the starch polymer chains. Depending on the processing conditions, extrudates may be comprised of residual swollen granular starch comprising partially broken and partially melted granules (generally formed under conditions of inadequate energy input in terms of temperature and/or applied shear), completely molten starch, and recrystallised starch (Ollett, et al., 1990).

When starch is thermally and mechanically treated it often exhibits diffraction patterns classified as V-type or E-type (as differentiated from A, B and C-types typically found in native starches from different plant origins). These are formed upon the complexing of amylose with lipids and other polar organic molecules (Cairns, et al., 1997).

Following retrogradation, the crystalinity of extruded cereal starches may be characterised by residual A-type crystallinity (due to incomplete gelatinisation during extrusion), along with processing-induced V and E-type crystallinity within the recrystallised extrudates to varying degrees depending on processing conditions (van Soest, et al., 1996[a]).

Whilst DSC has also been used to investigate the crystallinity of starch extrudates, due to the issues associated with maintaining humidity and moisture content within samples this technique cannot provide further information about the changes in crystallinity or structure that occur in

starch during extrusion processing or under conditions of high atmospheric humidity (Zhou, 2004) .

Using X-ray diffraction to characterise the crystallinity of processed starch-based materials, two different types of crystallinities denoted V type and E type structures have been observed, as distinct from the A, B or C type crystalline structures of native starch previously described. These modified V and E type crystallinities are produced by the rapid recrystallisation of single-helical structures of amylose during retrogradation (van Soest & Vliegenthart, 1997). Whilst the most frequently observed structure is the V type crystallinity, the actual proportions of these types of crystallinity depends on the composition of the starting materials including the amounts of amylose and lipids as well as the processing conditions. (van Soest, et al., 1996 [a]).

The diffraction parameters of the processing induced crystallinities in extrudates are summarised in Table 2.11.

Table 2.11: X-ray diffraction parameters of V and E type crystallinity in extruded starches

Type	2θ (°)	Intensity
V	7.1/7.4	Strong
	12.6/13.0	Strong
	19.4/20.0	Very strong
	22.1	Medium
E	6.6/6.9	Medium
	11.6/12.0	Medium
	18.0/18.5	Strong

Zhou, J. Microwave Assisted Moulding of Starch-Based Foams, PhD thesis (2004)
van Soest, et al. Crystallinity in starch bioplastics. Industrial Crops and Products 1996

2.11   The mechanical properties of thermoplastic starch-based materials

The mechanical properties of thermoplastic starches are dependent on several factors including the origin of the starch, moisture content and processing conditions. Most of the research to characterise the mechanical properties of starch based materials and investigate the ways to improve mechanical properties has focused on blending starch with plasticisers and synthetic polymers (Zhou, 2004).

Moisture content has an important effect on the mechanical properties of starch materials. Flexural modulus, strength and visco-elastic behaviour of extruded starch were found to be a function of moisture content, with a transition from brittle to ductile behaviour occurring at water contents in the range of 9 - 10% (w/w) in studies conducted on extruded maize starch (Kirby et al, 1993). The significance of moisture content was also demonstrated in a thermoplastic waxy maize starch extruded at 140°C with water and glycerol, where the glass to rubber transition characteristics typical of amorphous polymers at different moisture contents was shown. Below moisture contents of 10% (w/w) the materials were brittle with a modulus of approximately 1000 MPa and an elongation at break of less than 20%. Moisture contents of 11 - 13% (w/w) resulted in decreases in the elastic modulus and tensile strength with an increase in elongation at break. At higher moisture contents of between 13 - 20% (w/w) the materials behaved in a rubbery fashion with moduli of only 0 - 10 MPa, tensile strengths of 0 - 2 MPa and ultimate elongation of 300 - 500% (van Soest et al, 1996[b]).

The mechanical properties of extruded high-amylose (70%) and standard cornstarch extruded at 170°C and 20 - 30% (w/w) moisture content were studied as a function of time and humidity conditioning. (Shogren & Jasberg, 1994). Tensile strengths for the extruded high-amylose starch samples were observed to stabilise over time at higher levels than those for standard cornstarch whilst elongation at break declined gradually over time for the high-amylose starch compared to the more rapid declines seen for standard amylose cornstarch samples. It was therefore shown, that thermoplastic starch-based materials prepared from high-amylose cornstarch have greater strength and flexibility alongside slower physical ageing than those prepared from standard cornstarch.

The molecular mass of the starch has also influence on the properties of resultant thermoplastic starches. The mechanical properties of extruded thermoplastic starch samples comprising different mean molecular masses in the range of ~1900 kgmol[-1] - ~37000 kgmol[-1] and moisture contents ranging from 5 - 30% (w/w) were investigated (Van Soest et al, 1996[c]). In the rubbery state of the studied materials (14% moisture content), the elongation at break of the high molecular mass material was reported as 100 - 125%, whilst the low molecular mass material had

elongation at break values of 30 - 50%. Tearing tests conducted on the materials showed a maximum energy of 0.15 and 0.1 Jmm^{-2} at a moisture content of 9 - 10% (w/w) for the high and low molecular mass materials respectively. Above water content of 15% the materials became weak and soft and values for elongation at break decreased.

2.11.1 The mechanical properties of starch-based foams

Previous work conducted at Brunel University, Dept of Mechanical Engineering has sought to establish the mechanical properties of extruded starch-based foams and has focussed mainly on a group of macro-composite foams known collectively as RPS. (The manufacture of RPS starch-based foams is summarised in Chapter 3 of this thesis). Figure 2.28 shows stress-strain curves from compression tests conducted in the horizontal and vertical axis on various macro-structure arrangements of RPS starch-based foam blocks.
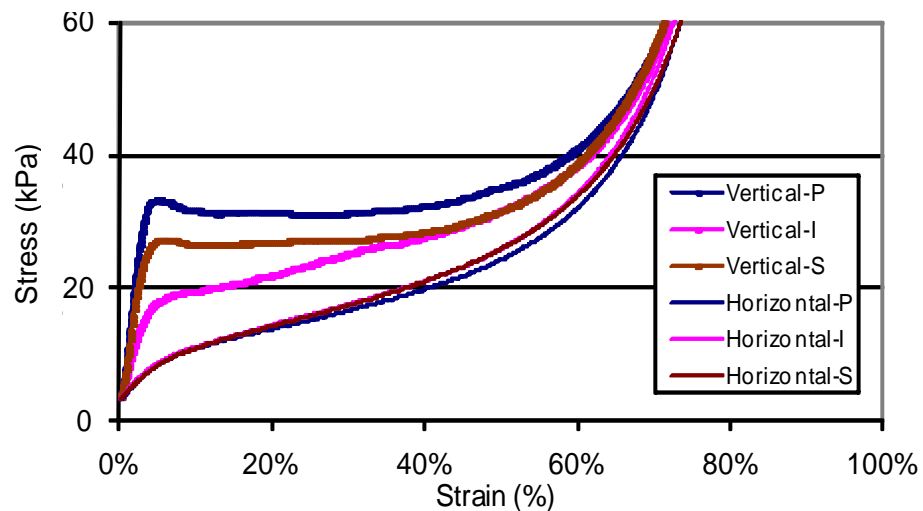
Figure 2.28: Stress-strain curves from compression tests conducted on RPS starch foam blocks
Lightweight Eco-composites Based on Renewable Resources (Song, J. Brunel University, 2006)

This work showed the contribution of the arrangement and orientation of the foam macro-structure and its significance to the mechanical strength of RPS foams.

Some previous work was also conducted to determine the dynamic impact performance of RPS starch-based foams compared to expanded polystyrene. Figure 2.29 shows the cushion curves produced from these dynamic impact tests.
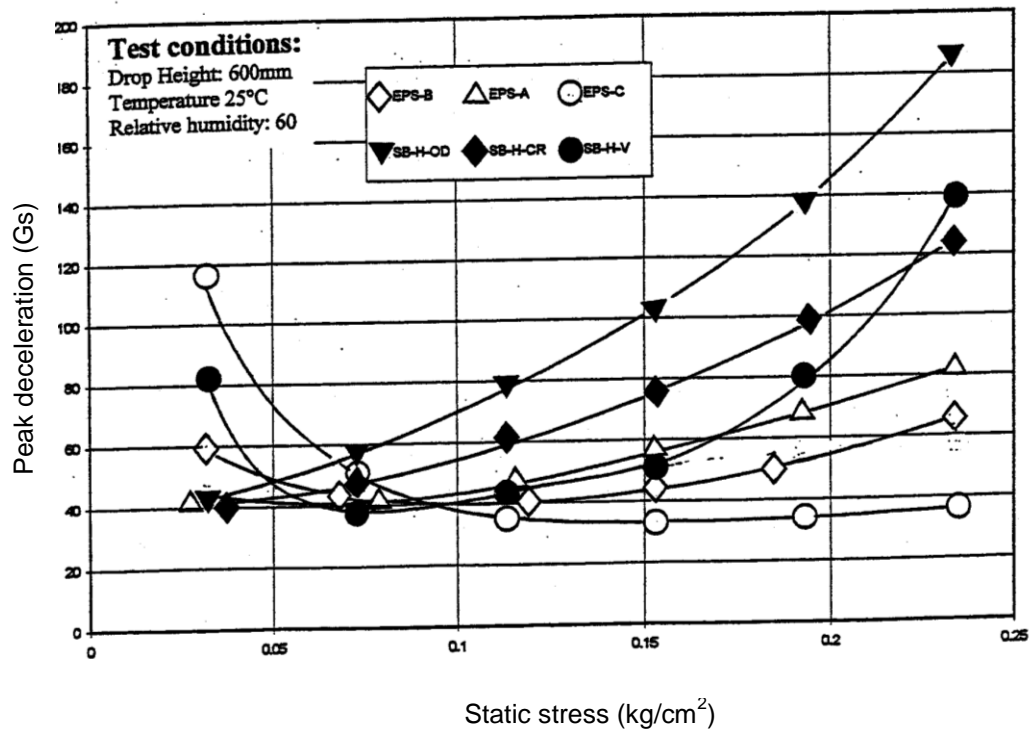
Figure 2.29: Dynamic impact cushion curves conducted on RPS v. EPS
Foam density (kg/m^3)
▼◆●RPS foams: SB-H-OD (23); SB-H-CR (23); SB-H-V (31)
◇△○EPS foams: EPS-A (10.1); EPS-B (15.4); EPS-C (25.5)
Lightweight Eco-composites Based on Renewable Resources (Song, Brunel University, 2006)

The results of this work showed that the softer RPS foams exhibited reduced peak deceleration values and provided superior cushioning performance at lower static stresses whilst, EPS foams provided lower peak deceleration values and superior cushioning performance at higher static stresses.

2.11.2   The thermal properties of starch-based foams

Previous work was conducted at the National Physical Laboratory (NPL), to determine the thermal conductivity of extruded starch-based foams (Wang, 2008). These macro-composite starch-based foams (known collectively as RPS), have an average density of 23 kg/m^3. (The manufacture of RPS starch foams is summarised in Chapter 3 of this thesis).

Tests were conducted using the guarded hot plate method according to standard ISO 8302:1991 and EN 12667:200. Specifications of the samples and the test conditions are summarised in Table 2.12

Table 2.12: Thermal conductivity of starch-based foam - samples & test conditions

Sample ID	QM316A	QM316B
Mean length x width (mm)	304.1 x 303.6	303.8 x 303.9
Mean thickness (mm)	38.57	
Mass before testing (kg)	0.084	0.085
Mass after testing (kg)	0.082	0.082
Density during test/(kg/m³)	23.38	
Laboratory temperature (℃)	19 to 25	
Laboratory relative humidity (%RH)	18 to 38	

Wang, Y. A Study of the Structure & Properties of Starch Foam & Eco-Composites for Industrial Applications (PhD Thesis, 2008)

Samples were conditioned at 23 º C and 50%RH for 13 days before testing. Thermal resistance was measured using a pair of precision double-sided 305 x 305 mm guarded hot-plates (NPL305GHP3), between which the specimens were mounted horizontally with the heat flow in the vertical direction. Thermocouples and a differential thermocouple were used to monitor the temperature balance between the guard and metering areas of heater plate. Temperatures used for the measurement of the foam samples were selected as -5 ^{0}C; 5 ^{0}C; 20 ^{0}C and 30 ^{0}C (Wang, 2008). From the temperature differentials across the materials and the heat flow recorded, the thermal conductivity of the materials at the mean temperatures were calculated and are shown in Figure 2.30.
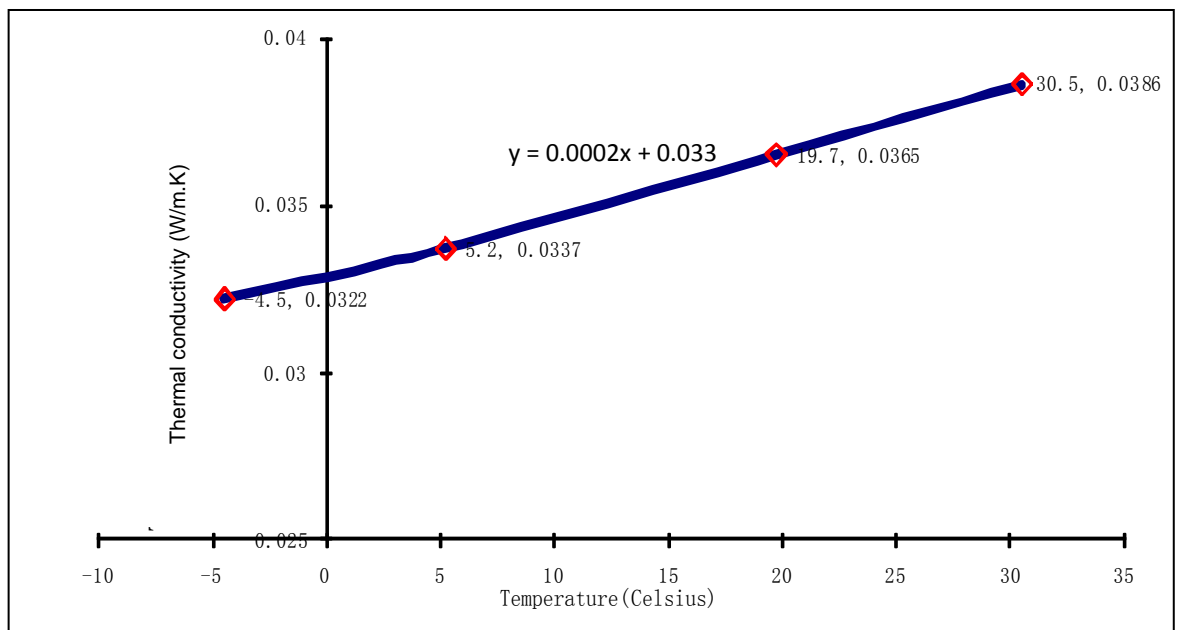
Figure 2.30: Thermal conductivity of RPS starch-based foams
Wang, Y. A Study of the Structure & Properties of Starch Foam & Eco-Composites for Industrial Applications (PhD Thesis, 2008)

Figure 2.30 shows a general tendency for RPS starch based foams to display greater thermal conductivity values at higher test temperatures. A trendline generated by linear regression is shown in Figure 2.30, while the *thermal conductivity constant* equation is also given which describes the gradient of the trendline.

2.11.3   The acoustic properties of starch-based foams

Previous work to measure the airborne sound absorption coefficient of extruded starch-based foams was conducted by Malith Sumanasekera, a Mechanical Engineering student at the University of Manchester under the supervision of Dr. Bin Wang in 2006. This work utilised the *Standing Wave Ratio* method to test the absorption coefficient of the materials at a frequency range of 100 – 5000 Hz, and compared the results obtained to absorption coefficient tests conducted using the transfer function/impedance tube method at a frequency range of 100 – 500 Hz. Due to the very limited range of test frequencies reported as produced from the transfer function/impedance tube method, only those tests conducted using the broader range of frequencies as conducted by the standing wave ratio method are discussed here.

The standing wave ratio method as detailed in part one of test standard BS EN ISO 10534, is a traditional method used for measuring the sound absorption characteristics of materials. The sample is mounted at one end of a rigid smooth tube at the other end of which is a speaker used to generate a pure tone sound wave inside the tube. If 100% of the incident sound wave is reflected, both incident and reflected sound waves have the same amplitude and a standing wave is created. In this case the *nodes* (where the two sound waves clash destructively to create a minimum sound pressure), will have zero pressure whilst the *antinodes* (where the sound waves combine constructively to create a maximum pressure), will have double the sound pressure. Conversely, when part of the incident sound energy is absorbed by the sample the incident and reflected sound waves differ and the nodes and antinodes will no longer be at zero and maximum pressures respectively.

The sound pressures at the nodes and the antinodes are measured using a probe tube which is attached to a movable microphone which slides along a graduated ruler. The ratio of the maximum to minimum sound pressure is measured and is known as the Standing Wave Ratio (SWR). These measured values are used to determine the sample's reflection coefficient amplitude R, absorption coefficient α, and its impedance Z.

Figure 2.31 shows a schematic representation of the Bruel & Kjaer Standing Wave apparatus model 4002.
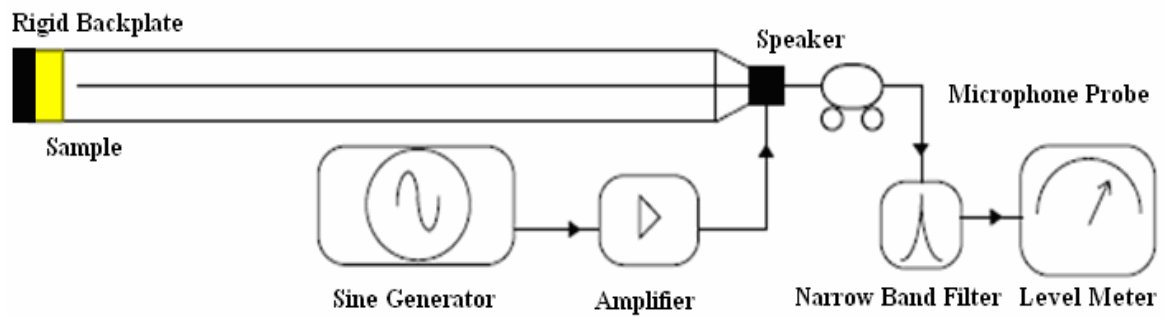
Figure 2.31: Schematic representation of Bruel & Kjaer Standing Wave apparatus model 4002

Figure 2.32 shows the sound absorption coefficient of an extruded, macro-composite starch-based foam (known as RPS), with a density of 23 kg/m^3 at three different sample thicknesses (approximately 13mm, 26mm & 39mm). Sound absorption coefficient values were obtained using the standing wave ratio method. (The manufacture of RPS starch-based foams is summarised in Chapter 3 of this thesis.) An ideal acoustic sound absorbing material would absorb 100% of all audible frequencies tested and would be represented in Figure 2.32 by a straight horizontal line at 1 (or 100%) on the *y* axis ranging from zero to 6,400 Hz on the *x* axis. Thus, for sound absorption coefficient, units of measurement are given as a proportion of the ideal and as such the scale is linear.
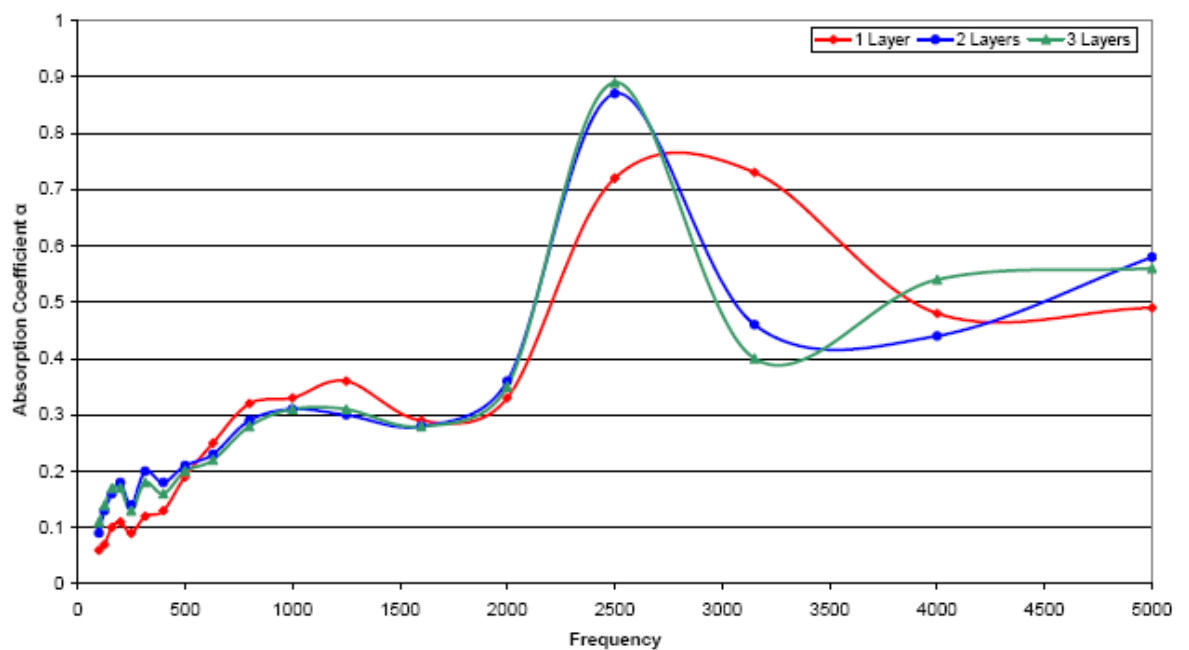
Figure 2.32: Sound absorption coefficient of RPS foam – Standing Wave Ratio method
Malith Sumanasekera, Dept of Mechanical Engineering, University of Manchester (2006)

The sound absorption coefficients plotted in Figure 2.32 are seen to increase with the thickness of the material, although the 2 and 3 layer RPS show only a slight difference in values peaking at 2500 Hz with absorption coefficient values of almost 0.9. The behaviour of the material in the low frequency region is seen to have relatively low absorption coefficient values, whilst frequencies above 3000 Hz display absorption coefficients below 0.6.

Figure 2.33 shows the sound absorption coefficient of a macro-composite starch-based foam known as CBL at three different sample thicknesses (20mm, 40mm & 60mm). Sample density was not given in the report. Sound absorption coefficient values were obtained using the standing wave ratio method. (The manufacture of CBL starch foam is covered in Chapter 3 of this thesis.)
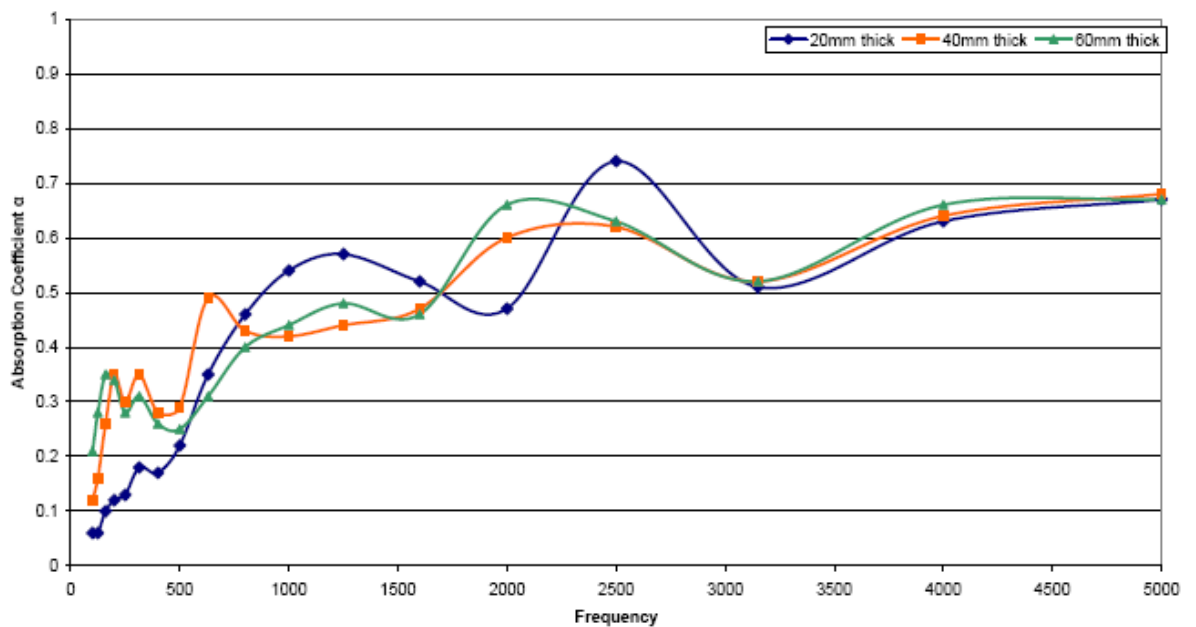
Figure 2.33: Sound absorption coefficient of CBL foam – Standing Wave Ratio method
Malith Sumanasekera, Dept of Mechanical Engineering, University of Manchester (2006)

The sound absorption coefficients plotted in Figure 2.33 show peak values of between 2000 Hz and 2500 Hz. The absorption coefficient values are seen to differ with changing thicknesses according to the frequency tested, although no clear correlation between sample thickness and sound absorption coefficient values can be inferred across all frequencies. In general, the low frequency range tested corresponds to low of sound absorption coefficient values while at frequencies above 3000 Hz sound absorption coefficient values stay below 0.7.

Figure 2.34 shows sound absorption coefficient values of 3 layer RPS (extrudate) starch foam and 60mm thick CBL (loosefill) starch foam compared to 50mm thick expanded polystyrene (EPS) and a specialist acoustic foam manufactured by Auralex Acoustics (Auralex, 2010). Results for EPS

were obtained using the standing wave ratio method, whilst data for Auralex foam was obtained from the manufacturer. Sample densities for CBL, EPS and Auralex were not given in the report, whilst details of the particular Auralex foam tested and method of determination of sound absorption coefficient data for this foam are also not stated.
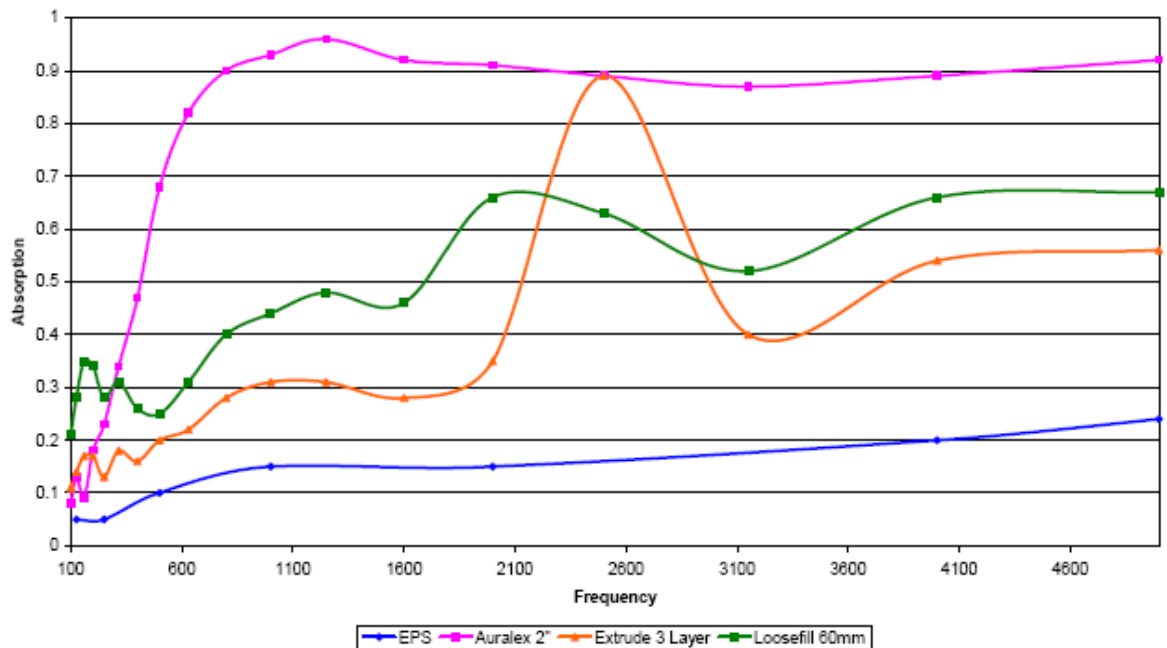
Figure 2.34: Sound Absorption coefficient – RPS & CBL starch-based foams compared to EPS & Auralex foams
Malith Sumanasekera, Dept of Mechanical Engineering, University of Manchester (2006)

Comparison of sound absorption coefficient values for the materials tested show that both the RPS and CBL starch foams perform significantly better than the EPS foam across all frequencies tested. EPS is a foam comprising a closed cell structure which results in poor sound absorption characteristics, whilst both starch foams tested are comprised of a significant fraction of open cell structures.

As a specialist acoustic foam the Auralex foam performs significantly better than both RPS or CBL starch foams across all frequencies above approximately 400 Hz, although at frequencies below 400 Hz the sound absorption coefficient values for Auralex are relatively low. At frequencies above 600 Hz Auralex foam has absorption coefficient values of above 0.85 throughout the frequency range. Since foams such as Auralex are designed primarily as a sound absorbing materials they are capable of absorbing a wide range of sound frequencies. From Figure 2.34 above, RPS starch-based foam can be seen to perform well in only a relatively narrow frequency range, whilst CBL starch-based foam displays a better overall performance across the frequency range tested.

2.12   Effects of temperature and humidity

Specific conditions for the testing of materials are specified in relevant test standards including ASTM E 171 - 63 *Standard atmospheres for conditioning and testing materials*. Standard conditions for material pre-conditioning and testing are generally given as 23°C and 50% r.h. However, moisture sensitive materials such as starch foams should have their performance tested under expected humidity conditions in order to identify any effect on their properties.

Fluctuations in temperature may affect the properties of foamed plastics which tend to become stiffer at temperatures lower than the *glass transition point* (T_g) of the material and softer at temperatures higher than its T_g. Whilst high atmospheric humidity has a limited effect on many hydrophobic petrochemical-based plastic materials, hydrophilic starch-based materials are hygroscopic and exhibit equilibrium relative humidity (ERH). Absorption of moisture plasticises starch-based materials (Kang, 2006). Therefore, high atmospheric humidity is likely to significantly affect the performance of starch-based materials, potentially compromising their mechanical properties.

Studies on sections of extruded starch foams by Kang *et al* showed that starch foams shrink under high-humidity conditioning due to relaxation of the cell structure, previously "fixed" in a meta-stable state during extrusion foaming. High-humidity conditioning results in gradual and uniform moisture penetration into the starch foam, reducing the cell dimensions, decreasing the volume of the foam and increasing foam density. The degree of shrinkage is a function of the atmospheric relative humidity and exposure time (Kang, 2006).

Figures 2.35 (a, b & c) present a series of scanning electron microscope (SEM) images showing starch foam cell structure at equivalent magnification before and after high-humidity conditioning.
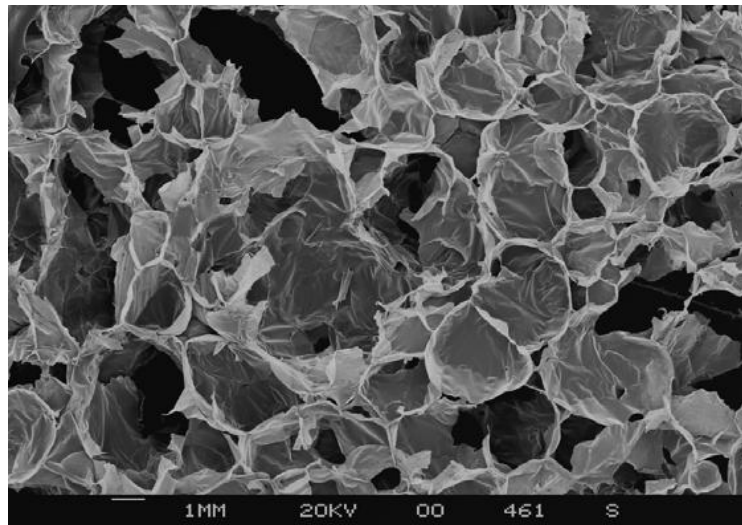
Figure 2.35 (a): Original sample under standard conditions 23°C/50% r.h.
Kang, Y G, Biodegradable Starch-Based Foam Block for Cushion Packaging (PhD Thesis, 2006)
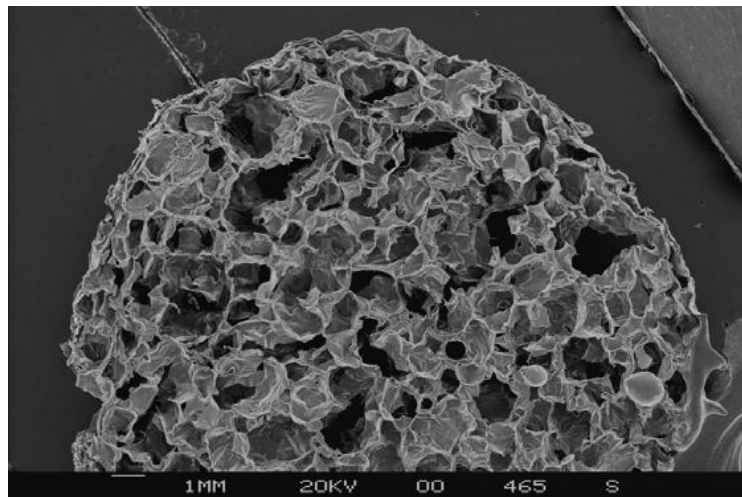
Figure 2.35 (b): Sample shrinkage after conditioning at 23°C/96% r.h. for 16 hrs
Kang, Y G, Biodegradable Starch-Based Foam Block for Cushion Packaging (PhD Thesis, 2006)
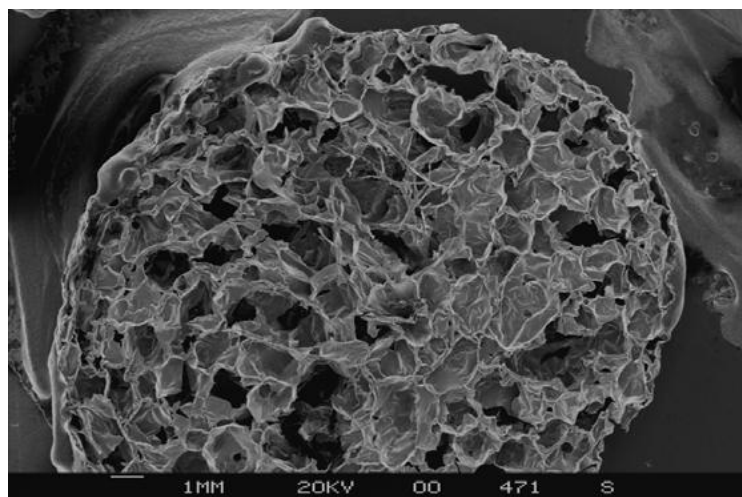
Figure 2.35 (c): Sample after conditioning at 40°C/76% r.h. for 48 hrs
Kang, Y G, Biodegradable Starch-Based Foam Block for Cushion Packaging (PhD Thesis, 2006)

Figures 2.35 (a, b & c) show that average cell size is considerably reduced by the high humidity treatments. Samples treated under different high-humidity conditions (Figures 2.35 b & c), attain a similar degree of cell shrinkage, rendering final sample volume reduction and foam density comparable. Over a 24 hour period cell shrinkage may result in average reductions of 30% - 40% in overall sample dimensions relative to the original sample size and an increase in sample density of up to 5 - 5.5 times (Kang, 2006).

Similar studies by Kang to determine the effects of high humidity conditioning on the behaviour of RPS starch foam blocks showed that the samples underwent significant shrinkage when conditioned under a high humidity environment leading to modification of cell sizes and an increase in overall foam density. The shrinkage rate of the RPS starch foam blocks was found to be dominated by the relative humidity to which they were exposed. The higher the relative humidity, the faster the foams shrank to reach an equilibrium dimension. At relative humidity of 96% at room temperature (approximately 23°C), samples took approximately 8 hours to reach maximum shrinkage. Shrinkage of the blocks to a final stage after 12 hours treatment resulted in samples of approximately 85% of their original dimensions and density increases of around 3.5 times their original density. Intermediate densities were achieved by controlling the exposure time to the high humidity environment. At elevated temperatures, equilibrium relative humidity was reduced and the shrinkage process was slowed. At 40°C and 76% r.h., longer exposure to the conditioning regime was required for the samples to reach maximum shrinkage (Kang, 2006).

After samples were removed from the high humidity environment and allowed to recondition at standard conditions (23°C and 50% r.h.) for a minimum of 72 hours. The increase in density as a result of the high humidity conditioning was found to have enhanced the mechanical properties of the foams. The compression strength of the conditioned RPS foam blocks had increased about by 8 - 10 times compared with untreated RPS foam blocks. Dynamic impact tests conducted on treated samples found that stress levels at peak deceleration were extended from 33 kPa for untreated samples to 360 kPa for treated samples. The treated samples were therefore suitable for higher loading cushion applications (Kang, 2006).

The enhanced mechanical strength of high relative humidity treated starch foams is chiefly due to foam shrinkage which produces a material with a greater number of cell walls per unit volume of foam. However, another factor which may contribute to these enhanced mechanical properties may be the re-ordering of the material's crystalline arrangements during high relative humidity treatment, resulting in a less amorphous and more crystalline molecular structure.

The study suggested that the high humidity treatment and shrinkage phenomenon may potentially be applicable as a cost-effective process to manipulate foam density and enhance

mechanical properties by refining the cell structure of starch foams (Kang, 2006). However, this work also highlighted issues potentially compromising these materials when utilised under high-humidity service conditions.

An Investigation into the Properties of Starch-Based Foams
Chapter 3. The Fabrication of CBL & RPS Starch-Based Foams

81

Chapter 3   The Fabrication of CBL & RPS Starch-Based Foams

Extrusion foaming is a well-established technology for commercial manufacturing of starch foams predominantly used for loosefill packaging (Green Light Products Ltd, 2010). Figure 3.1 shows a starch extrusion foaming line at Green Light Products Ltd. (UK). In this case the rotating cutter normally used to chop the extrudate into loosefill chips has been removed and continuous foamed strands are being produced. With the rotating cutter in place the extruded foam strands are cut into short chips to produce what is known as loosefill foams.

Figure 3.1: Continuous starch foam strands being extruded (rotating cutter removed)

Figure 3.2 (a) shows the extruded rods in more detail, while Figure 3.2 (b) shows a scanning electron microscope (SEM) image of the extruded starch foam.
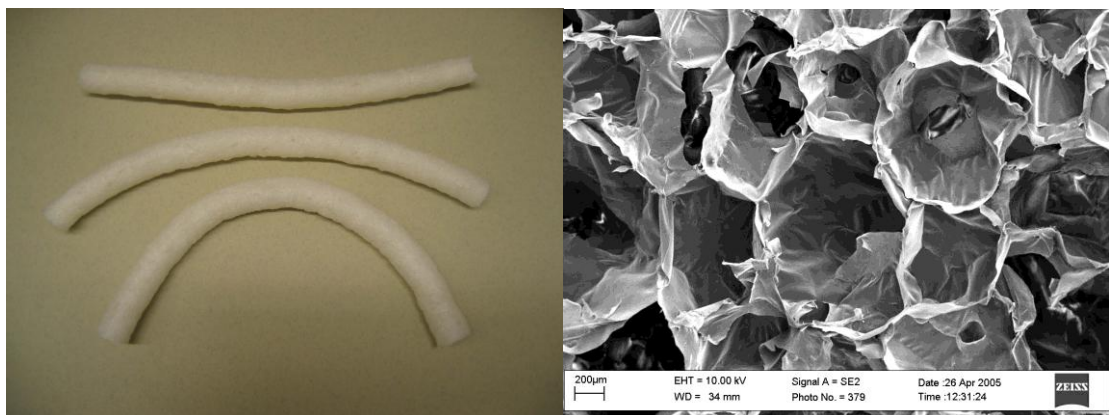
Figure 3.2 (a) Extruded starch foam rods   **Figure 3.2 (b) Cross-section SEM of extruded starch foam showing cell structure (14 kg/m^3)**

Wang, Y (2008) A Study of the Structure & Properties of Starch Foam & Eco-Composites (PhD Thesis)

An Investigation into the Properties of Starch-Based Foams
Chapter 3. The Fabrication of CBL & RPS Starch-Based Foams

82

3.1   Raw materials

Depending on the processing methods used, typical compositions of raw materials prepared from wheat grain used in the production of starch-based materials such as extruded starch foams are shown in Table 3.1.

Table 3.1 Typical composition of raw materials prepared from wheat grain (wt % of dry solids)

Component	Whole grain	Milled Flour	Purified Starch
Starch	75	80	90
Protein	12	11	0.2
Fibre	8	1.5	0.5
Lipid	2.5	1.5	1
Ash	1.5	1	0.5

Typical moisture content of wheat flour 10 - 14 % dependent on environmental humidity.
Data Sheet: Heygates Limited

Polyvinyl Alcohol (PVOH) is typically added to starch in extrusion foaming as a plasticiser to provide plasticity to the foam extrudates, making them more flexible and suitable for cushioning. PVOH was added to the wheat flour at 12 wt% (Green Light Products Ltd, 2010).

3.2   The fabrication of block starch-based foams

As discussed in the previous chapter, loosefill materials have some limitations in terms of their relatively low compression strengths as well as the problems associated with settling during transit which may allow migration of the packaged product within the container, thereby further reducing the protection offered by the packaging. Loosefills can also be messy and easily wind-blown leading to problems of litter.

These issues underpin the rationale behind efforts made to produce block foams from extruded starch. In order to further capitalise on the environmental benefits of these renewable and biodegradable materials, two novel technologies were originated at the School of Engineering & Design at Brunel University.

A technique known as Regular Packing & Stacking (RPS) has been developed in a previous work at Brunel University to fabricate block starch foams using the continuous foam strands (Kang, 2006).

RPS technology is briefly described in this chapter which then goes on to focus mainly on the development of a new technique known as Compression Bonded Loosefill (CBL) for manufacturing a novel type of block foam utilising loosefill starch foams as a raw material. A feasibility study of the CBL method is included alongside a study on some key processing factors associated with development of the CBL technique towards an industrial process.

3.2.1   The fabrication of regular packing & stacking (RPS) foams

RPS is a process developed jointly by the Centre for Biodegradable Materials Research at Brunel University and Green Light products Ltd., in which continuous starch foam extrudate is fabricated into planks or block foams.

With the cutter is removed from the end of the extruder, continuous foam strands can be produced, as shown in Figure 3.1. This led to the concept of arranging starch foam strands into block foams utilising the self-adhesive property of their moistened surfaces. This section summarises the fabrication process on which this technology is based.

The properties of RPS foam have been characterised in previous work providing a background of the materials (Kang, 2006, Wang 2008). Some further characterisations have been carried out in this work in order to provide a basis for comparison with CBL foams.

3.2.2   The RPS process

RPS is a process by which continuous extruded foam strands are processed into planks and laminated into block foams. Utilising the self-adhesive property of surface-moistened starch foams, continuous foam strands are packed in parallel and adhere to each other under compression to form foam planks. These planks can then be stacked and bonded in a similar way following chosen stacking patterns into block foams.

The bonding interfaces within RPS block foams form regular internal macrostructure networks which have a relatively higher density and thus higher mechanical strength and stiffness. The RPS block foams are thus macro-composites with the bonding interface network functioning as reinforcement. In addition to altering the microstructure of individual foam strands through controlling the extrusion process, the subsequent packaging and stacking patterns of pre-extruded strands may also be varied in order to arrange the interface network to obtain required mechanical properties from the RPS block foams.

The RPS concept was developed in several stages. Initially, lengths of cylindrical strands were manually wetted using a hand-held water spray gun and lateral pressure was then applied manually to bring the strands together. However, the non-uniform water coverage over the cylindrical surfaces of each strand proved problematic resulting in inconsistent bonding between strands.

In order to resolve these issues an RPS machine was developed (Kang, 2006). The RPS machine brings together separate extruded strands, joining them into single layer planks through a three stage process of heating/pultrusion, wetting and bonding.

An Investigation into the Properties of Starch-Based Foams
Chapter 3. The Fabrication of CBL & RPS Starch-Based Foams

84

In the heating/pultrusion stage each extruded strand is pulled through a heated pultrusion die which reshapes the cylindrical cross-section of the thermoplastic starch strands into a square cross-section by applying heat and pressure at the contact surface with die-wall. This facilitates uniform surface wetting and increases the bonding surface between the strands. The entrance of the die accommodates the shape of original strand whilst the die exit defines the shape of the required cross-section. Square-section rods are generally used to form RPS planks, although other cross-sectional shapes can be made by means of alternative pultrusion dies. Figure 3.3 shows a graphic representation of the reshaping of extruded starch as it is passed through a pultrusion die.

Section A–A, Extruded cylindrical strand entering the pultrusion die
Section B–B, Modified cross-section of the strand after pultrusion
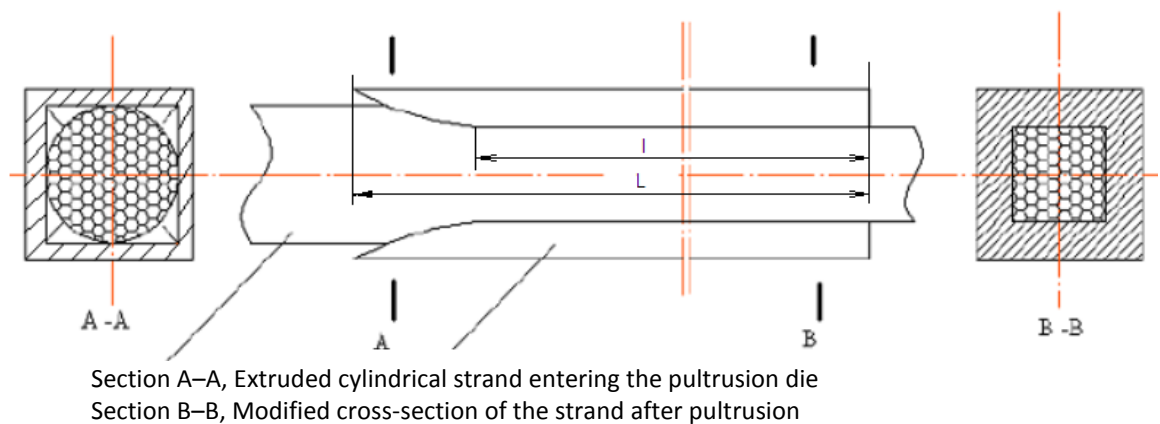
Figure 3.3: Extruded starch being reshaped by pultrusion
Kang, YG (2006). Biodegradable Starch-Based Foam Block for Cushion Packaging (PhD Thesis)

Pultrusion is a continuous process in which the strand is pulled through the heated pultrusion die set at a temperature greater than the softening temperature of the foam but below the point above which thermal degradation of the foam material takes place (Kang, 2006). The pultruded, square-section rods enable a more uniform application of moisture on their flat surfaces. In addition, subsequent stacking of the reshaped rods is also enhanced resulting in block foams with good dimensional definition and a regular interface arrangement.

The ratio of the pultruded rod cross-sectional area to that of the original strand, known as area reduction ratio, defines the degree of plastic deformation of the cross-section resulting from pultrusion. Given that there is no appreciable change in length of a strand during pultrusion, the area reduction of starch foam strands is attributable to the densification of the foam cells within its cross-section. Therefore, pultrusion increases the density of each strand (Kang, 2006). This increase in foam density contributes to a change in the mechanical properties of the individual extruded strands and also that of the RPS block foam. Different area reduction ratios can be achieved according to the particular die selected. The area reduction ratio is thus one aspect which can be utilised to control the overall mechanical behaviour of the RPS foams (Kang, 2006).

An Investigation into the Properties of Starch-Based Foams
Chapter 3. The Fabrication of CBL & RPS Starch-Based Foams

85

Following pultrusion, the reshaped rods then pass through a wetting unit on the RPS machine which applies a thin film of water to the sides of the rods. The wetted rods are then brought together under lateral pressure to form a plank. Figure 3.4 shows a schematic illustration of the three processing stages of the RPS machine as viewed from above, while Figure 3.5 provides a more detailed view of the pultruded, wetted rods being brought together and bonded by lateral pressure to form a plank.
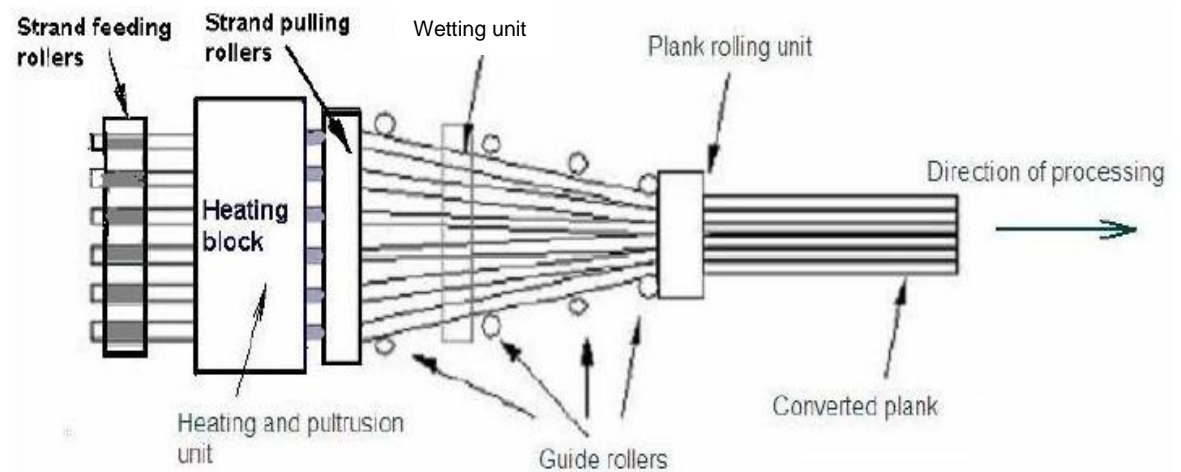
Figure 3.4: Processing stages of the RPS machine
Kang, YG (2006). Biodegradable Starch-Based Foam Block for Cushion Packaging (PhD Thesis)
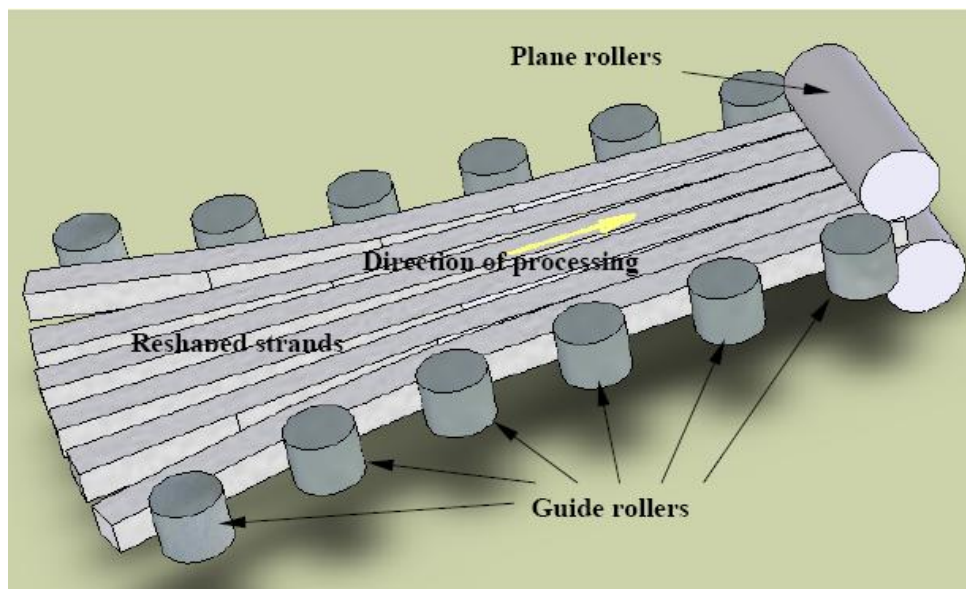
Figure 3.5: Pultruded, wetted rods brought together and bonded by lateral pressure to form a plank
Kang, YG (2006). Biodegradable Starch-Based Foam Block for Cushion Packaging (PhD Thesis)

An Investigation into the Properties of Starch-Based Foams
Chapter 3. The Fabrication of CBL & RPS Starch-Based Foams

86

Single-layer planks produced by this technique can then be stacked and bonded as required into a chosen stacking pattern to form block foams as shown in Figure 3.6.
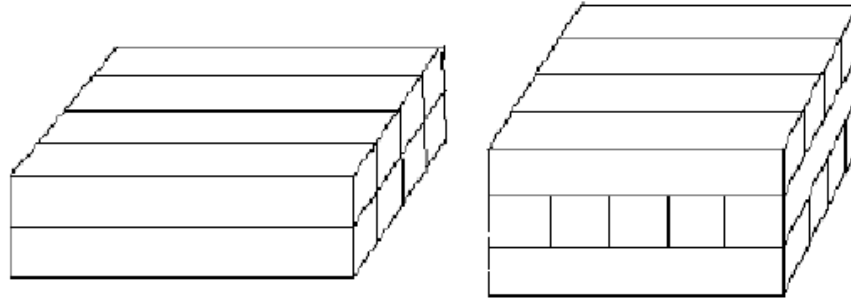
Figure 3.6: Schematic diagram showing typical stacking patterns of RPS block foams
Kang, YG (2006). Biodegradable Starch-Based Foam Block for Cushion Packaging (PhD Thesis)

The RPS technique confers several benefits in terms of manipulation of foam structure and properties.

- The regular packing and stacking of pultruded and reshaped rods eliminates the majority of gaps occurring between unpultruded foam strands and thus forms a more uniform structure.

- The bonding interfaces between larger contact surfaces results in enhancement of strength and stiffness of the resulting block foam.

- The process gives rise to greater dimensional control and stability of the foams and a good surface finish.

However, the current RPS technique is not without its limitations. Despite extensive work conducted to develop the RPS process, there remain problems associated with the considerable disparity between the rate of starch foam rod leaving the extruder at a velocity of several metres per second, compared to the relatively slow speed of pultrusion, wetting and bonding on the RPS machine at a velocity of approximately 1.3 metres per second (Kang, 2006).

The difficulty in automation of handling the multiple foam strands on the RPS machine whilst ensuring that all strands of foam rod do not break before entering the pultrusion die is an additional issue affecting production rate. The subsequent and entirely separate process of bonding single planks together to form thicker planks is an additional time-consuming and labour-intensive procedure which may hinder the successful commercial application of this block foam production technique.

These production bottlenecks represent, in the opinion of the author, a major obstacle to the development of block foams made from extruded foamed starch strands, necessitating the

development of alternative and more efficient methods for manufacturing these types of block foams.

One example of a variation of the RPS method which may warrant investigation is the Rolled Bonded Extrudate (RBE) concept, in which starch foam extrudate is fed directly from the extruder die onto a square mandrel revolving at a speed equivalent to the velocity of the extruded starch. Simultaneous side-to-side oscillation of the mandrel would be required in order to distribute the foam strand evenly across its width, whilst a water mist spray adjacent to the mandrel could be used for surface wetting of the foam strands. A soft pressure applicator could aid compression and adhesion of each successive layer of the coiled foam strands, although since the extrudate arriving at the mandrill would still be warm, moist and flexible shortly after exiting the extruder, it is possible that sufficient adhesion between adjacent rods may occur without the application of additional moisture or pressure.

This type of high speed spooling process is already well established in several industries including pipe coiling and cable winding (Auto Reel, 2010). However, these processes generally utilise a measure of the tensile properties of the spooled substrates to ensure tension control and tight coiling, which in the case of extruded foamed starch is comparatively limited. Assuming such issues could be resolved, the potential exists for the process to be utilised to produce unique block foams at high speed.

The RBE concept is schematically represented in Figures 3.7 (a) and 3.7 (b).

An Investigation into the Properties of Starch-Based Foams
Chapter 3. The Fabrication of CBL & RPS Starch-Based Foams

88

Water mist spray

Figure 3.7 (a)

Square-section
teflon mandrill

Pressure
applicator

Rotation

Extruded starch
foam rod

Lateral oscillation

Figure 3.7 (b)

Corner areas trimmed to produce RBE blocks
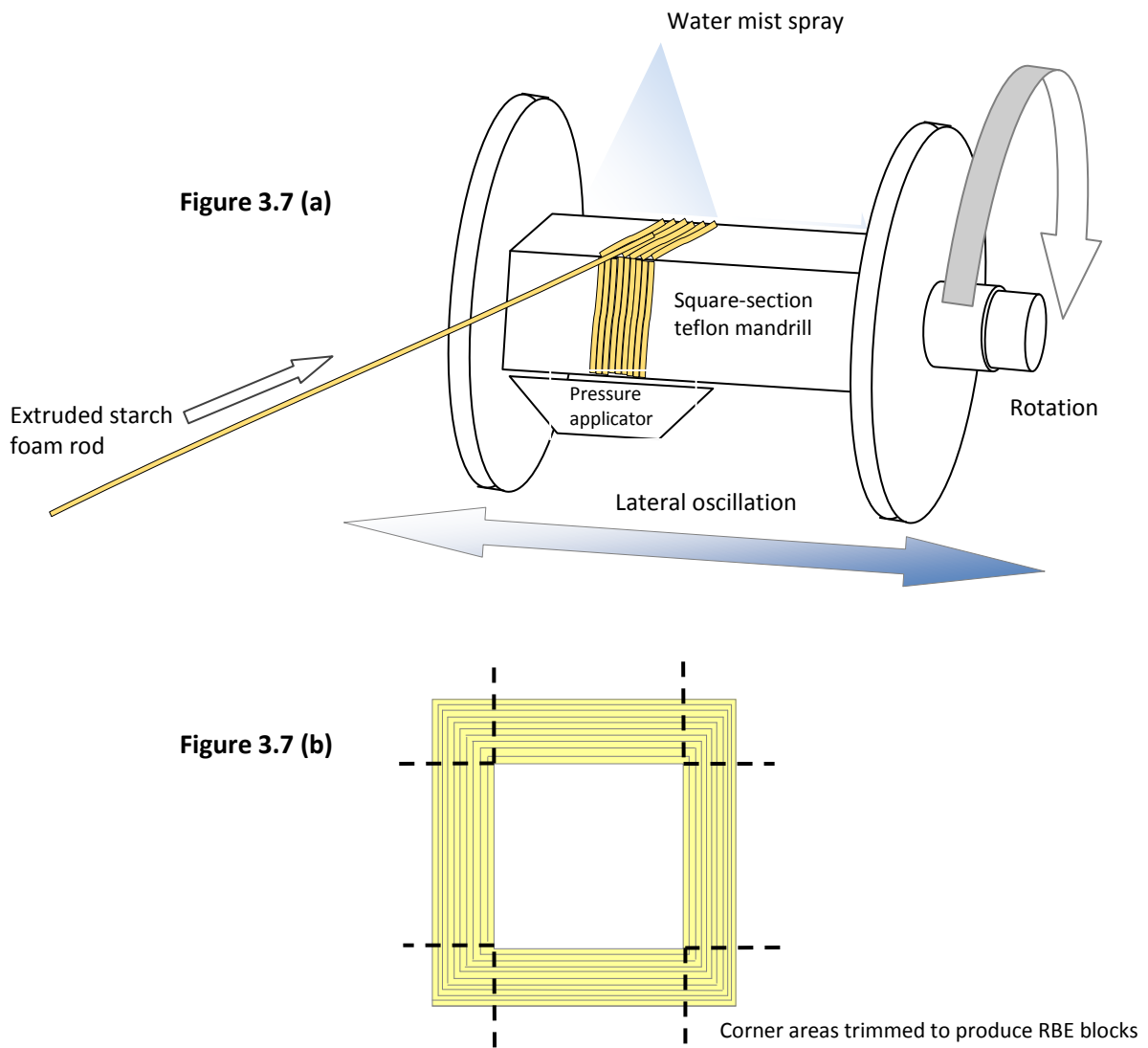
Figure 3.7 (a): Schematic representation of rolled bonded extrudate (RBE) concept

Figure 3.7 (b): Cross-section of RBE block after removal from mandrill

An investigation into the Properties of Starch-Based Foams
Chapter 3. The Fabrication of CBL & RPS Starch-Based Foams

89

3.2.3 The development of CBL technology for the manufacture of starch-based block foams

Although offering some advantages in terms of cost and ease of filling as outlined in the previous chapter, loosefill products are subject to some limitations in terms of the protection they offer to packaged goods due to their relatively low compression strength combined with a propensity for settling during transit which may allow migration of goods within the package to occur thus reducing the efficacy of the overall packaging system. Block foams made from extruded starch loosefill have the potential to offer several advantages over starch loosefill for packaging applications and may also provide the possibility of applications in other commercial areas.

3.2.4 Loosefill starch foams as raw materials for CBL

Most extruded starch foam currently manufactured is used for loosefill packaging applications. Immediately after extrusion, the foam is cut at high speed to produce loosefill chips of different lengths depending on the speed of the cutter. Starch foam loosefills have loose bulk densities of approximately 7 - 8 kg/m^3 (pers.com, Lewis, 2010).

Previous studies (Kang, 2006), to determine the mechanical properties of extruded starch foams were conducted on three grades of commercial foam samples obtained from Green Light Products Ltd as listed in Table 3.2.

Table 3.2: Average dimensions of loosefill produced at Green Light Products Ltd

Sample ID	Sample description	Diameter of extrudate (mm)
GLH	Heavy duty	21
GLS	Standard	17
GLT	Thin	11.5

Kang, Y G (2006)

Since these products are mainly used for cushion packaging applications, the compression behaviour of the loosefill foams was studied by Kang in 2006. Samples from each grade were cut into short lengths for compression tests conducted in the extrusion direction under standard conditions of 23 degrees Centigrade, 50% relative humidity. Averaged data from these test results were used to produce stress-strain curves and cushion factors as shown in Figure 3.8.

An investigation into the Properties of Starch-Based Foams
Chapter 3. The Fabrication of CBL & RPS Starch-Based Foams

90
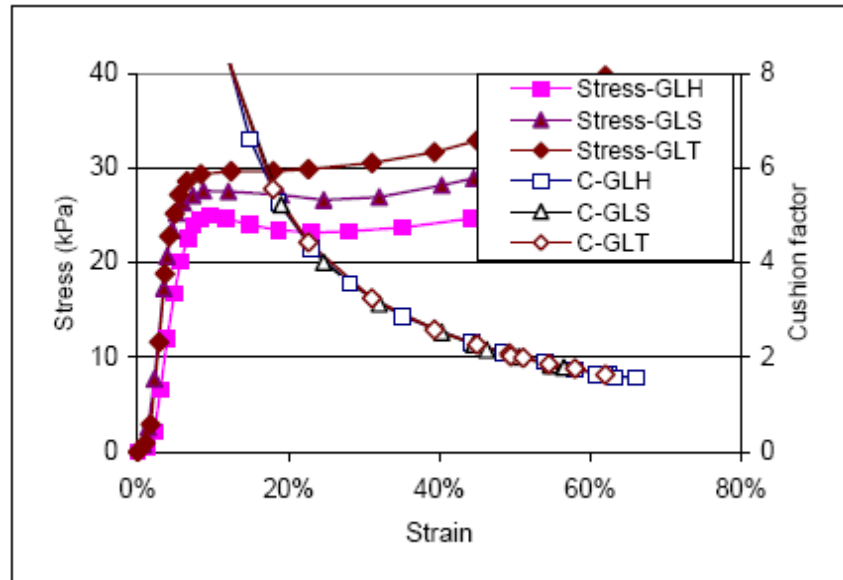
Figure 3.8: Averaged stress-strain curves and cushion factors for GLH, GLS and GLT samples
Kang, Y G (2006), Biodegradable Starch-Based Foam Block for Cushion Packaging (PhD Thesis)

In general, these tests illustrated that foam density is the predominant factor affecting the compression strengths (indicated by the high compressive strength of GLT grade foams compared with lower density GLS and GLH grades). In addition the study found that cell size, distribution and uniformity of the cell structure also play an important role. GLT grade foams are reported to possess more uniform, finer cell structures than the other grades tested. Cushion curves revealed that all three foams have equivalent cushion efficiencies for a given strain. The stress-strain and cushion curves also show that optimum cushion efficiency of the foams is approximately 60% of strain (Kang, 2006).

In this thesis, unless otherwise stated, loosefills made from standard GLS grade extrusions were selected for the preparation of CBL block foams and for the studies of various properties of CBL foam samples. These loosefill chips are generally cylindrical in shape with average dimensions of 26.33mm (length) and 17.53mm (diameter).

3.2.5 Feasibility of the CBL concept

In order to prove the feasibility of fabricating starch block foam from loosefills, an experimental study was carried out based on previous experience in the RPS process (Kang 2006), in which it was shown that small pieces of starch foams moisturised at their surfaces can achieve adequate adhesion and form block foams if assisted by applying a low compressive stress at the contact areas. Starch at the surface of moistened loosefill foam chips partially dissolves thus allowing the natural adhesive property of the material to be utilised. As moistened starch loosefill chips are brought into contact with each other under compression, their contact areas adhere and a

An investigation into the Properties of Starch-Based Foams
Chapter 3. The Fabrication of CBL & RPS Starch-Based Foams

91

block foam is formed. This combination of moisture and pressure is the basis for the compression bonded loosefill technique.

Figure 3.9 shows the wetting of loosefill chips using a hand-held spray gun. Once moistened, the loosefill chips lose their free-flowing characteristic and adhere to each other at points of contact despite the absence of application of any compressive force. This feature may prevent uniform packing of the loosefill chips and gives rise to uneven distribution and voids within the resulting block foam if not adequately controlled.

Figure 3.9: Manual wetting of loosefill chips showing immediate adhesion at contact points

Figure 3.10 shows the set-up for manual compression of the moistened loosefill within a compression jig.

Figure 3.10: Set-up for compression of the moistened loosefill

An investigation into the Properties of Starch-Based Foams
Chapter 3. The Fabrication of CBL & RPS Starch-Based Foams

92

Figure 3.11 shows an example of a CBL block with dimensions of 150mm x 150mm x 150mm after removal from the compression jig. (In this example a mixture of white and brown loosefills were used for the purpose of picture contrast).

Figure 3.11: Example of compressed CBL block

After the CBL blocks were allowed to dry for 48 hours under controlled conditions (23° Centigrade, 50% relative humidity), an equilibrium moisture content of approximately 10% was reached and they were machine cut to the particular sample sizes required for specific tests. The CBL samples were then individually weighed and their dimensions measured in order to calculate sample density.

The density of CBL block foams can be controlled using different proportions of materials and degree of compression. CBL block foams can be produced with average densities of approximately 30 – 150 kg/m^3. Below this density range, voids within the blocks tend to be too large for the foams to be reliably machine cut, whilst foams of a higher density tend to be characterised by hard, highly-densified areas in which adhered loosefill chips have absorbed excessive amounts of water causing these areas of the foam to congeal. In these areas the macrostructure of the foam dominates.

Certain practical difficulties exist in achieving uniform surface wetting and close packing of moistened loosefill chips prior to compression, due to the loss of the loosefill's free-flowing property at the moment the surfaces of the chips come into contact with each other. Consequently, the manual fabrication process described above gives rise to difficulties in reproduction of CBL block foams of prescribed densities and hence problems in duplication of

An investigation into the Properties of Starch-Based Foams
Chapter 3. The Fabrication of CBL & RPS Starch-Based Foams

93

samples for testing. Samples produced for the tests described in successive chapters of this thesis were therefore prepared within certain density tolerances.

In addition, since the fabrication of each CBL block is carried out by a series of manual compressions, the density within each block may vary, such that the average density of a CBL block may not accurately represent the specific density within the material at any given point within that block.

In order to demonstrate this issue, CBL block foams of various densities with dimensions of 150mm x 150mm x 150mm were vertically cut into two smaller blocks (Sample A and Sample B), each with dimensions of 50mm x 100mm x 100mm. Figure 3.12 shows the density variations between the two smaller CBL blocks in comparison to the larger CBL blocks from which they were cut.
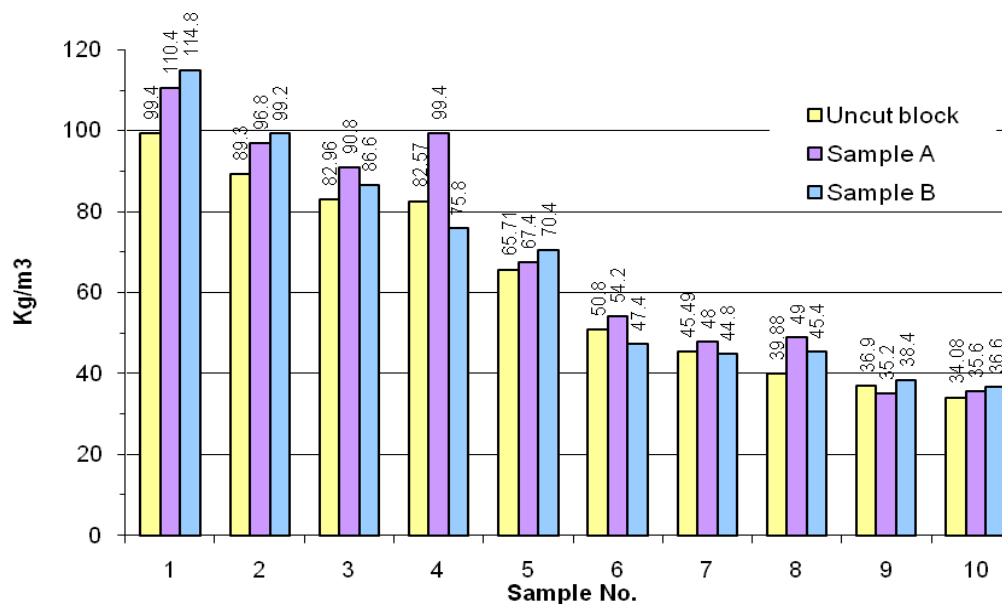
Figure 3.12: Density variation within CBL blocks

In order to further illustrate this issue, Figure 3.13 shows the structure of a vertically cut cross-section of CBL foam which exemplifies the arbitrary nature of compressive stresses from fabrication acting on individual loosefill chips, resulting in localised densification of areas of the block foam. In this example the macrostructure interfaces between adjacent bonded loosefill chips can be seen within the foam along with voids of various dimensions. The cellular microstructure within compressed loosefill chips can also be seen.

An investigation into the Properties of Starch-Based Foams
Chapter 3. The Fabrication of CBL & RPS Starch-Based Foams

94
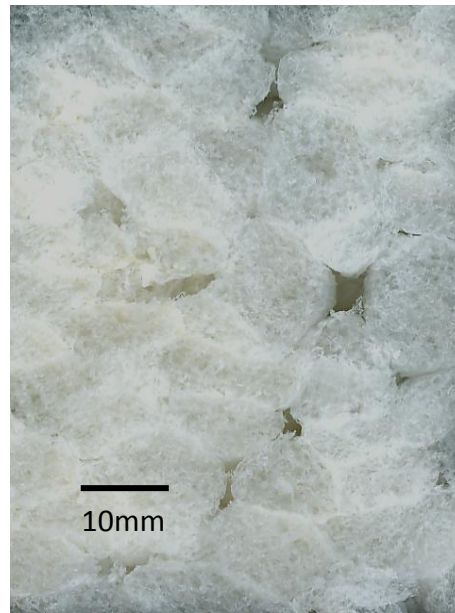
Figure 3.13: Vertical cross-section scan of CBL foam (43 kg/m^3)

The bonded interfaces within both CBL and RPS block foams form three-dimensional internal macrostructure networks. These block foams are thus macro-composites, consisting of foamed domains enclosed by a network of higher density interfaces. In addition to control of their cellular microstructures, such macro-composites also allow additional management of their finished properties via manipulation of the foam macrostructure during fabrication. Figure 3.14 shows a scanning electron microscope (SEM) image of an internal interface within RPS foam.
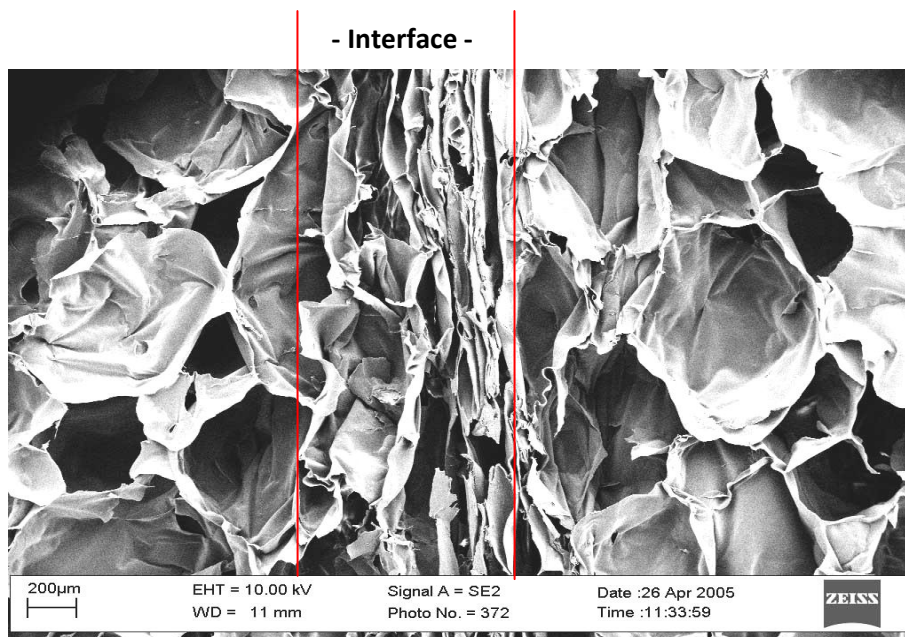
Figure 3.14: SEM image showing the cell structure at the site of a bonded interface within RPS foam (23 kg/m^3)

Wang, Y (2008) A Study of the Structure & Properties of Starch Foam & Eco-Composites (PhD Thesis)

An investigation into the Properties of Starch-Based Foams
Chapter 3. The Fabrication of CBL & RPS Starch-Based Foams

95

The structures of CBL and RPS starch-based foams comprising integral macrostructures can be contrasted with the uniform cell structures of typical open-cell polymer foams such as that shown in Figure 3.15 below.

1mm
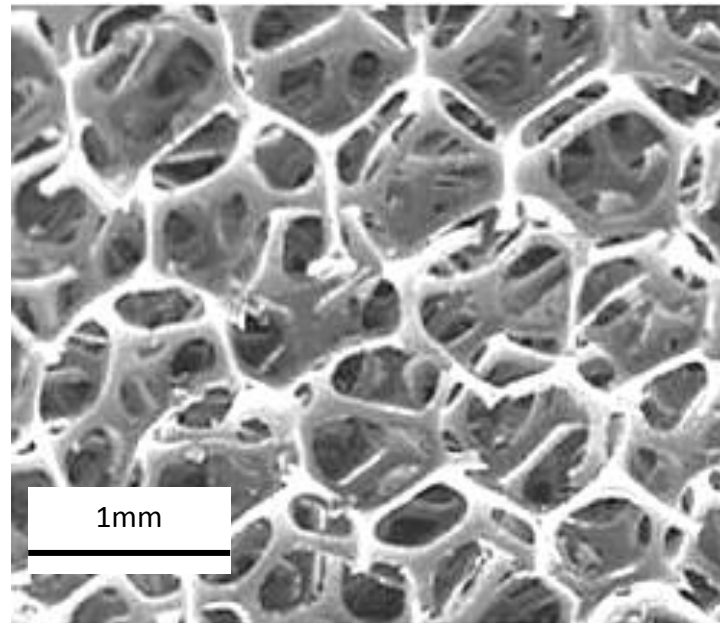
Figure 3.15: SEM image showing uniform cell structure of open-cell polyurethane foam
Gibson and Ashby, 1997

The RPS and CBL techniques have a number of distinct features.

a) The regular packing and stacking of strands in the RPS block foams do not lead to the cavities or voids often found between bonded loosefill chips and hence RPS foams benefit from a greater consistency of density and better surface finish than CBL foams.

b) The bonding interfaces within RPS foams are regular and ordered, giving rise to orientation in the foam structure and properties, whilst the interfaces within CBL foams are more randomly distributed and thus are likely to exhibit greater isotropic structure and properties.

c) The density of RPS foams are generally in the region of 23- 25 kg/m^3 (Kang, 2006), whilst it is difficult to produce CBL foams with densities lower than 30 kg/m^3. However, CBL is more versatile in terms of producing higher-density block foams than the RPS process.

Any comparative assessment of the benefits or disadvantages of these technologies and resultant materials must take into account the potential for development in the automation of processes. To this end, the CBL method has a number of advantages. Firstly, as a feedstock for CBL processing, starch loosefill is currently a commercially available product which can be stored and supplied as required, whereas the feedstock for producing RPS is not in current commercial

An investigation into the Properties of Starch-Based Foams
Chapter 3. The Fabrication of CBL & RPS Starch-Based Foams

96

production. Secondly, any automation of the CBL process has the potential to be much less complex than the RPS process, without the need for awkward handling of multiple foamed strands.

An investigation into the Properties of Starch-Based Foams
Chapter 3. The Fabrication of CBL & RPS Starch-Based Foams

97

3.3   Study of the key controlling factors in CBL processing

The difficulties described in controlling the density of CBL block foams as described in section 3.2.5, result in potential problems in terms of density control and reproducibility, which place limitations on research into the characterisation of CBL foams.

For the further development of the CBL method into a viable process for industrial production there is clearly a need to overcome these problems and to automate the process. The key problems are density variation and structural non-uniformity, both of which are associated with non-uniform wetting and/or poor flow and packing of the moistened loosefill. Therefore, fabrication of high-quality CBL foams requires:

a) uniform moistening/wetting of the surface area of the loosefill.
b) good packing and compression of the moistened loosefill.

This section of the thesis covers some fundamental work conducted in an attempt to address these two key issues by means of investigations into methods of wetting and packing of moistened loosefill.

3.3.1. Steam treatment for surface wetting of loosefill

Steam treatment was investigated as a potential loosefill wetting method based on the principle of absorption of moisture via condensation from saturated water vapour, in which a layer of loosefill chips was placed on mesh above a duct emitting steam from a vessel of boiling water. However, this investigation quickly eliminated this potential method due to loosefill shrinkage and subsequent lack of adhesion.

Reasons for the failure of this wetting method are likely to be due to the comparatively small steam water droplet sizes compared to sprayed water droplets, leading to absorption and penetration of moisture into the foam interior, resulting in softening and shrinkage of the loosefill chips. Despite the water penetration, this method resulted in insufficient water adsorption onto the surface of the loosefill chips for good adhesion to occur.

Figure 3.16 shows steam treated loosefill chips compared to untreated chips, showing significant shrinkage of treated chips with insufficient adsorption of moisture necessary for self-adhesion to occur under pressure.

An investigation into the Properties of Starch-Based Foams
Chapter 3. The Fabrication of CBL & RPS Starch-Based Foams

98

Figure 3.16: Steam treated loosefill chips (top/left) compared to untreated chips (bottom/right)

In order to ameliorate the issues of moisture penetration rather than desired surface adsorption, chilling of the loosefill prior to the application of steam was considered in order to create condensation on the surfaces of the loosefill chips. However, this idea was considered too inefficient in terms of energy usage to pursue.

3.3.2   Development of mist chamber for wetting of loosefills

Aggressive air currents caused by equipment such as spray guns tend to blow lightweight foams into each other causing premature contact and adhesion of loosefill chips, leading to non-uniform packing. Based on the experience of using a spray gun as a preliminary wetting method as previously described, the proposal of free-falling loosefill chips passing through a mist chamber containing a high density of fine water droplets was considered as the most appropriate method of wetting in order to overcome such issues and achieve uniform water coverage and thus improved packing of loosefill chips.

A graphic representation of the experimental setup for studying the effectiveness of mist chamber wetting of loosefill chips is shown in Figure 3.17.

An investigation into the Properties of Starch-Based Foams
Chapter 3. The Fabrication of CBL & RPS Starch-Based Foams

99
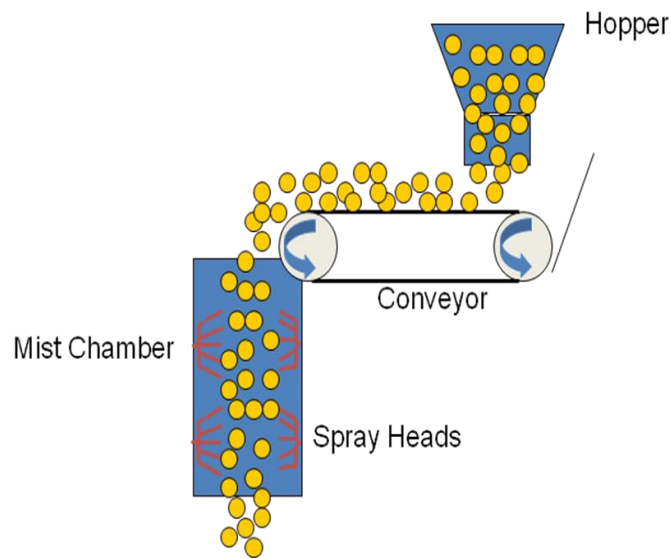
Figure 3.17: Graphic representation of experimental set-up for mist chamber wetting of loosefill

Various chamber coating methods can be used depending upon the particular coating application. These methods fall into two main categories: *counter-current* methods in which the direction of the spray is opposite to that of the passing media are generally used to increase the residence time of contact, whilst *co-current* methods feature media falling through a mist passing in the same direction. Co-current coating methods tend to protect the nozzle head from a build up of falling debris, thus reducing the potential for blockage (Beynon, 2008). The co-current method is graphically represented in Figure 3.18.
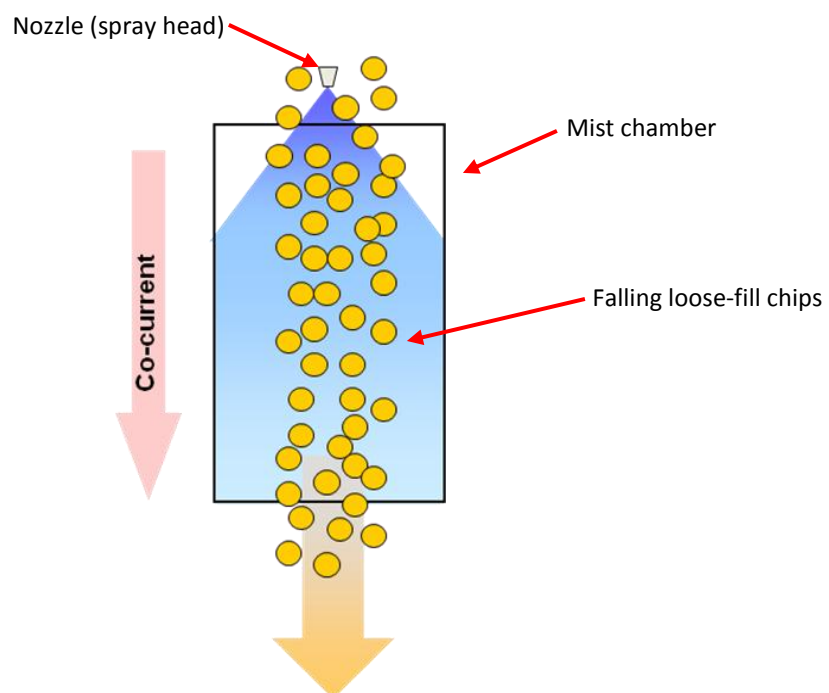
Figure 3.18: Graphic representation of Co-current loosefill mist chamber wetting method

An investigation into the Properties of Starch-Based Foams
Chapter 3. The Fabrication of CBL & RPS Starch-Based Foams

100

Co-current methods also benefit from the elimination of obstructions to the falling media from the nozzle itself, thus for reasons of simplicity this method was considered as the most appropriate for setting up lab-scale equipment. Based on the concepts shown in Figures 3.17 and 3.18, a lab-scale co-current mist chamber wetting unit was set up as shown in Figure 3.19, in order to test the concept of automated wetting.
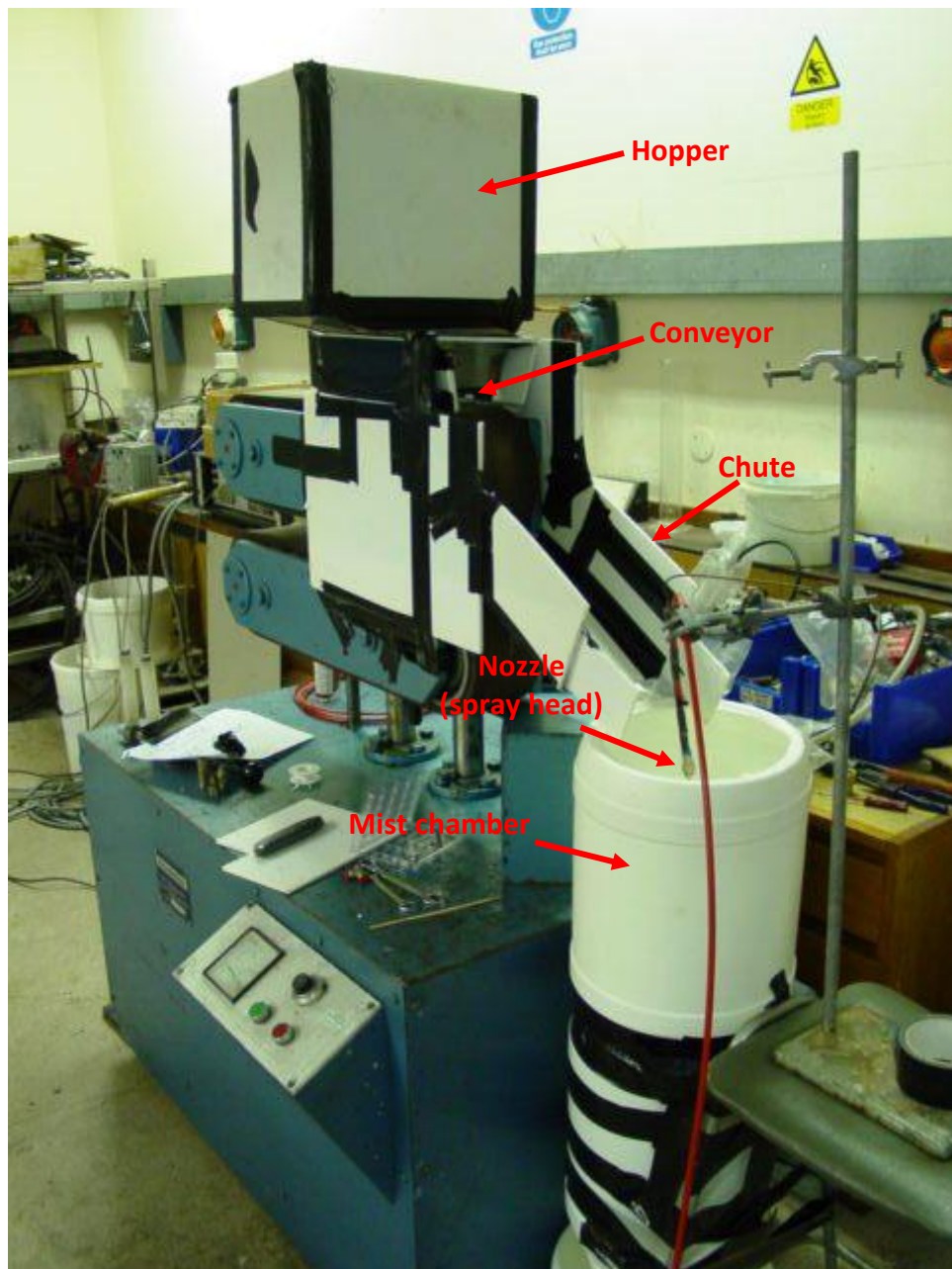
Figure 3.19: Set-up of experimental lab-scale mist chamber wetting unit

This lab-scale setup utilised a 110mm width conveyor which was run at the various speeds and loosefill chip throughputs. This data is shown in Table 3.3.

An investigation into the Properties of Starch-Based Foams
Chapter 3. The Fabrication of CBL & RPS Starch-Based Foams

101

Table 3.3: Loosefill chip throughput on lab-scale automated wetting unit

Conveyor speed (mm/sec)	Loosefill chip throughput (g/min)
5 mm	45
10 mm	67.8
15 mm	91.7

At all conveyor speeds tested on the lab-scale automated wetting equipment, sufficient water was delivered in the mist chamber to achieve adhesion of the wetted loosefill chips. However, the key to achieving efficient and uniform wetting or coating is for loosefill to fall through a mist chamber containing densely populated and uniformly distributed fine water droplets. This would result in a greater uniformity of water coverage over the surface of each loosefill chip.

The amount of water coverage on the surface area of each loosefill chip must be sufficient to ensure good adhesion between chips during the subsequent compression process. Whilst in the mist chamber, the loosefill chips are not expected to come into contact with each other as they enter the chamber at different times and from different positions and travel in the same direction under constant gravitational acceleration. This is expected to help minimise premature formation of loosefill networks which should engender greater packing uniformity of the wetted loosefill than the manual spray gun wetting method previously described, in which premature loosefill contact is inevitable. An effective mist chamber wetting method requires all inherent process variables to be taken into account and controlled. These variables are discussed below.

A) Water delivery

Water delivery at the nozzle is pressure dependent. Whilst the flow rate or the amount of water exiting the nozzle rises as water pressure is increased, mean droplet diameter will decrease with the rise in water pressure producing a finer water mist. Figure 3.20 and Figure 3.21 show water delivery from the PJ6 nozzle in terms of flow rate and mean droplet diameter respectively, as function of pressure.

An investigation into the Properties of Starch-Based Foams
Chapter 3. The Fabrication of CBL & RPS Starch-Based Foams

102
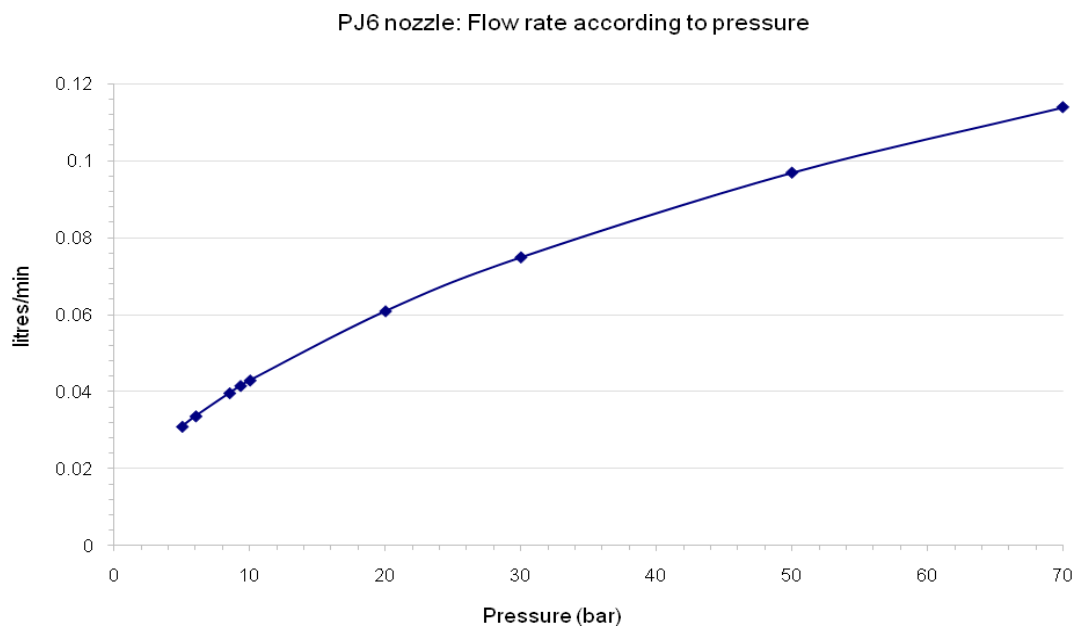
Figure 3.20: Flow rate as function of pressure (PJ6 nozzle)
Data compiled from PJ6 nozzle specifications (BETE)
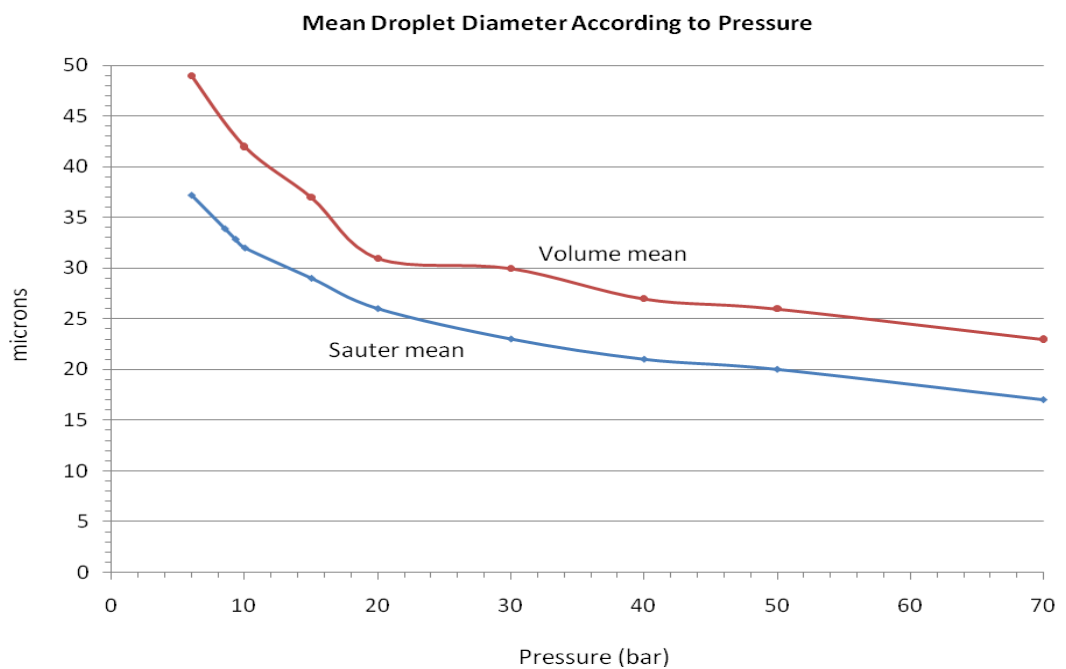
Figure 3.21: Mean water droplet diameter as function of pressure (PJ6 nozzle)
Data compiled from PJ6 nozzle specifications (BETE)

Although the PJ6 nozzle can operate at pressures of between 5 to 70 bar, for reasons of safety

the lab-scale equipment described was only deemed suitable for more moderate pressures. For

An investigation into the Properties of Starch-Based Foams
Chapter 3. The Fabrication of CBL & RPS Starch-Based Foams

103

this reason testing was conducted at pressures of between 6 to 9.3 bar. Figure 3.22 shows water flow rates in litres/minute from the PJ6 nozzle at 6 bar, 8.5 bar and 9.3 bar pressures.
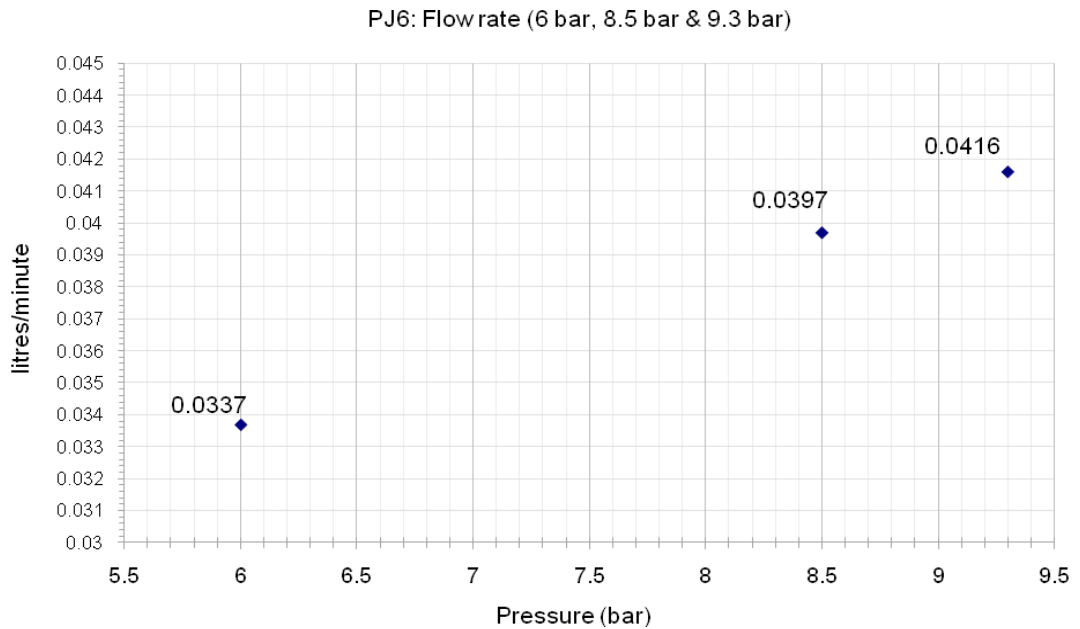
Figure 3.22: Water flow rates from PJ6 nozzle according to pressure
Data based on PJ6 nozzle specifications (BETE)

Mean water droplet diameters at the given nozzle pressures are shown in Figure 3.23.
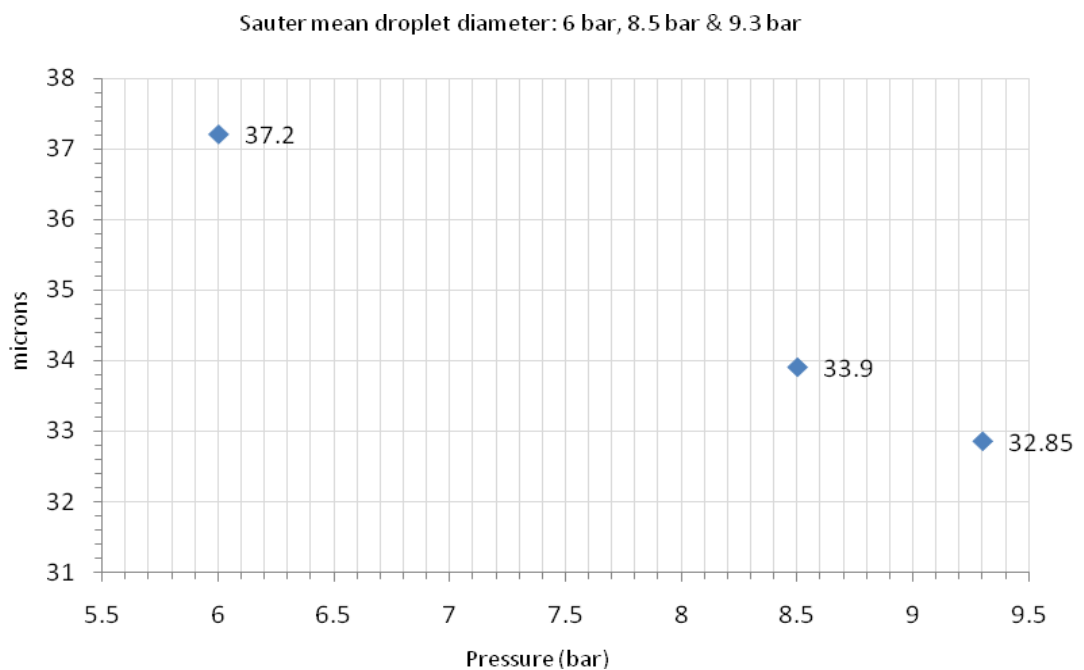
Figure 3.23: Mean water droplet diameter from PJ6 nozzle at given pressures
Data based on PJ6 nozzle specifications (BETE)

An investigation into the Properties of Starch-Based Foams
Chapter 3. The Fabrication of CBL & RPS Starch-Based Foams

104

At any given pressure mean droplet volume (V_d) can be calculated from the mean droplet diameter (d).

$$V_d = \frac{\pi d^3}{6}$$

(3.1)

Figure 3.24 shows mean water droplet volumes according to the three given pressures.
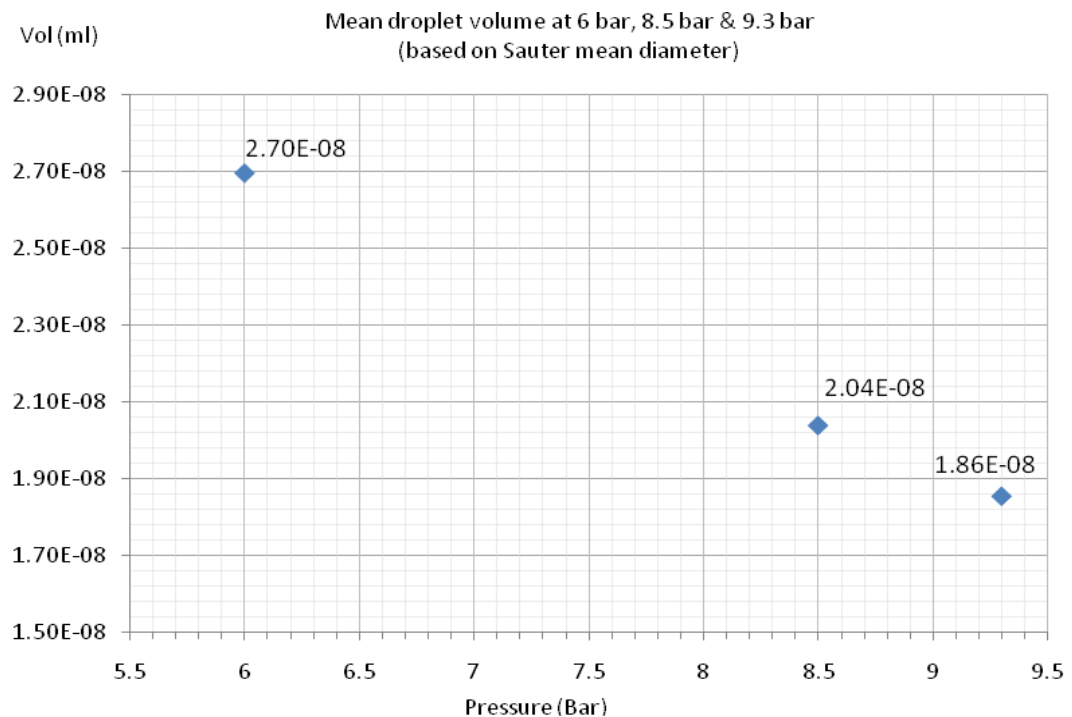
Figure 3.24: Mean water droplet volumes from PJ6 nozzle at given pressures
Data based on PJ6 nozzle specifications (BETE)

B) Loosefill chip water adsorption/absorption

In order to determine the amount of water adsorbed onto the surface of each loosefill chip passing through the mist chamber, the weights of single chips were measured before and then immediately after passing through the mist chamber at water pressures of 6 bar and 9.3 bar. Multiple chips (x 10) were also passed through the mist chamber simultaneously in order to obtain mean water mass coverage/absorption values for each batch and each chip. Figure 3.25 shows the mean water mass per loosefill chip after passing through the mist chamber, based on measurements of approximately 50 single chips and 50 multiple chips tested simultaneously.

An investigation into the Properties of Starch-Based Foams
Chapter 3. The Fabrication of CBL & RPS Starch-Based Foams

105
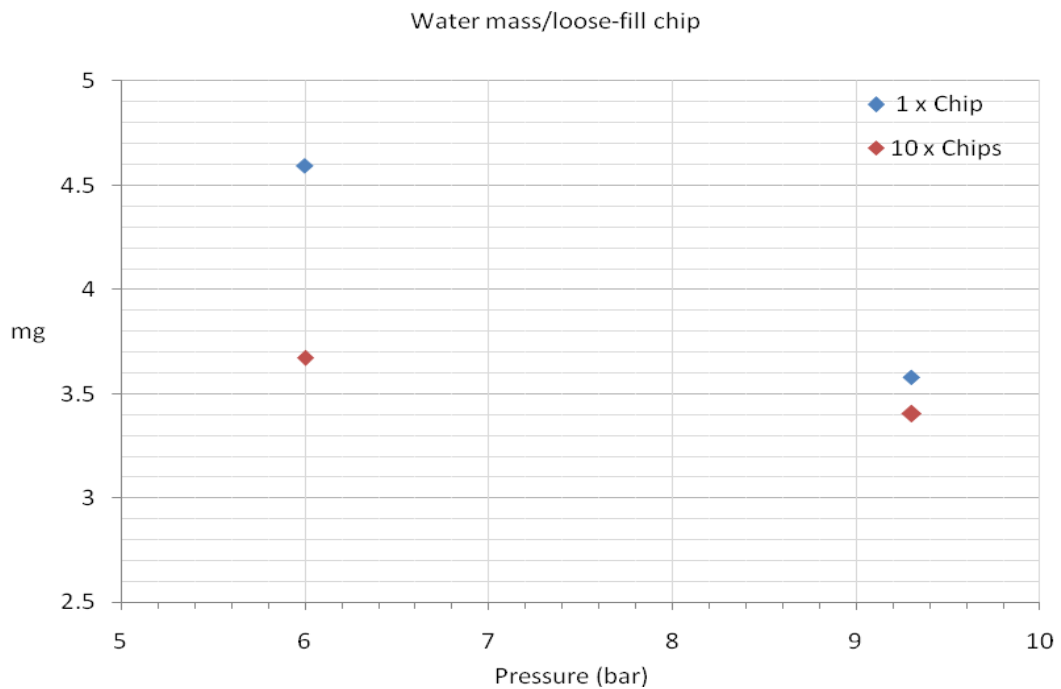
Figure 3.25: Mean water mass per loosefill chip after passing through mist chamber

Figure 3.25 shows that at both pressures tested, single chips passing through the mist chamber adsorb a greater mean water mass per loosefill chip (and thus a greater number of water droplets), than the mean water mass per chip of multiple chips passed through the mist chamber simultaneously. This phenomenon may occur due to the possibility that the increased number of water droplets adsorbed onto multiple chips passing through the mist chamber results in fewer freely available droplets for accompanying chips to adsorb. The diminishing availability of water droplets within the mist chamber in response to an increase in loosefill chips passing through the chamber therefore represents an additional variable which would require further research in order to achieve optimisation of the droplet/loosefill chip ratio.

Figure 3.25 also shows that testing at the higher water pressure of 9.3 bar reduces the mass of water adsorbed onto each chip compared to testing at the lower pressure of 6 bar. This is due to finer mist produced by higher water pressure at the nozzle and the subsequent smaller droplets which are adsorbed onto the loosefill chips.

From the measured water mass per chip values and the mean droplet volumes given above, it is possible to calculate the quantity of water droplets adsorbed onto each chip after passing through the mist chamber at any given water pressure. Figure 3.26 shows the average number of water droplets per loosefill chip at water pressures of 6 bar and 9.3 bar.

An investigation into the Properties of Starch-Based Foams
Chapter 3. The Fabrication of CBL & RPS Starch-Based Foams

106
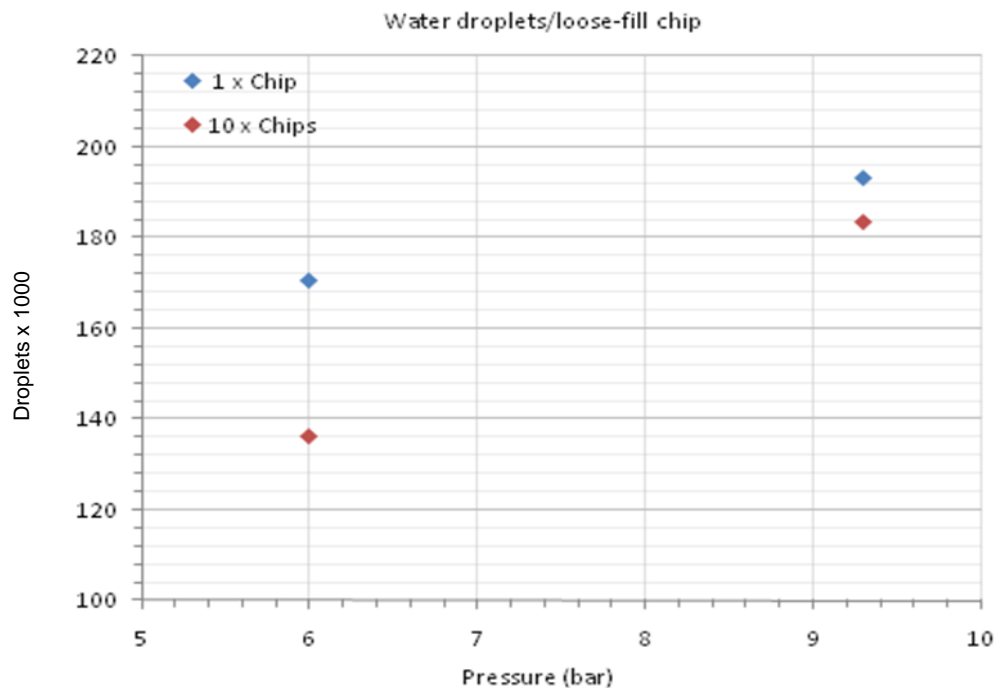
Figure 3.26: Average quantity of water droplets per loosefill chip after passing through mist chamber

Figure 3.26 shows that for both single and multiple loosefill chip passed through the mist chamber, the number of water droplets adsorbed onto the surface of each loosefill chip increases as water pressure at the nozzle is increased due to the finer mist and smaller droplet sizes produced at greater water pressures. Again, at both pressures tested, multiple chips passing through the mist chamber simultaneously result in fewer water droplets adsorbed onto each loosefill chip.

The results of these tests indicate that as water pressure is increased the mass of water adsorbed onto each loosefill chip is reduced due to a finer mist comprising smaller droplets. At higher water pressures an increased quantity of droplets is adsorbed onto each chip, but at a reduced overall water mass, which suggests that higher water pressure at the nozzle would result in a more uniform wetting of loosefill chips, which is preferable for this application. Testing at greater water pressures would be required to support these findings.

To take account of the variation in water adsorption onto chips of different volumes and surface areas, the average surface area of loosefill chips must be established. Since loosefill chips can be produced in a variety of extruded diameters and lengths depending on the particular extrusion die and cutter speed used, the dimensions of each particular batch were manually measured. Figure 3.27 and Figure 3.28 show the dimensions of two different batches of loosefill chips based on 40 samples taken from each batch, with average dimensions and standard deviation given below each figure.

An investigation into the Properties of Starch-Based Foams
Chapter 3. The Fabrication of CBL & RPS Starch-Based Foams

107

Loose-fill chip dimensions (Batch A)
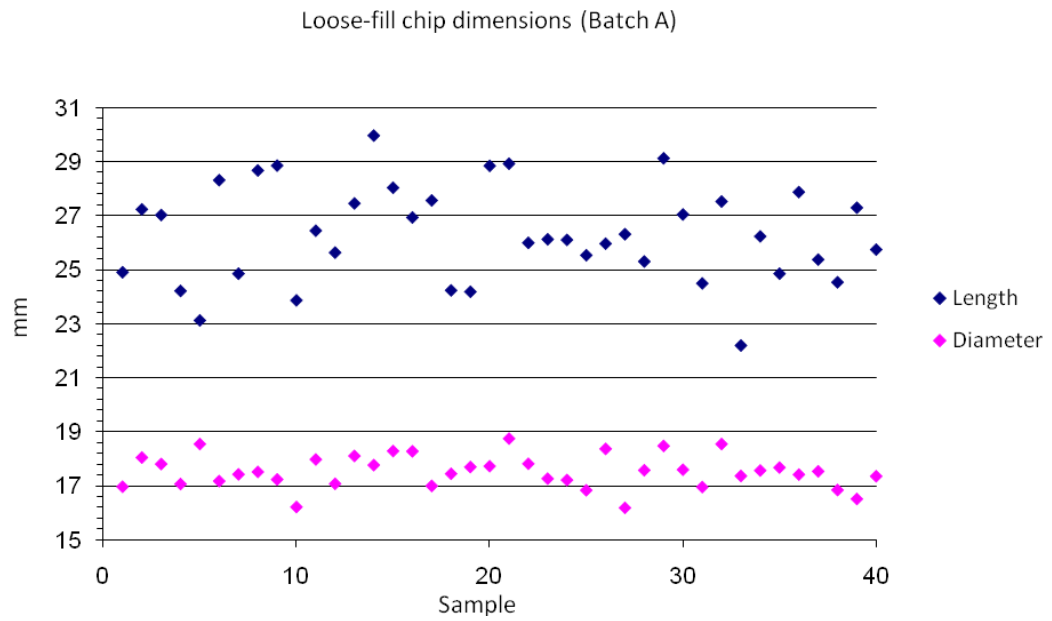
Batch A	Length (mm)	Dia. (mm)
Average	26.338	17.534
Std. Dev.	1.798	0.614

Figure 3.27: Loosefill chip dimensions – Batch A (short cut standard GLS extrusion, bulk density approx. 8 kg/m³)

Loose-fill chip dimensions (Batch B)
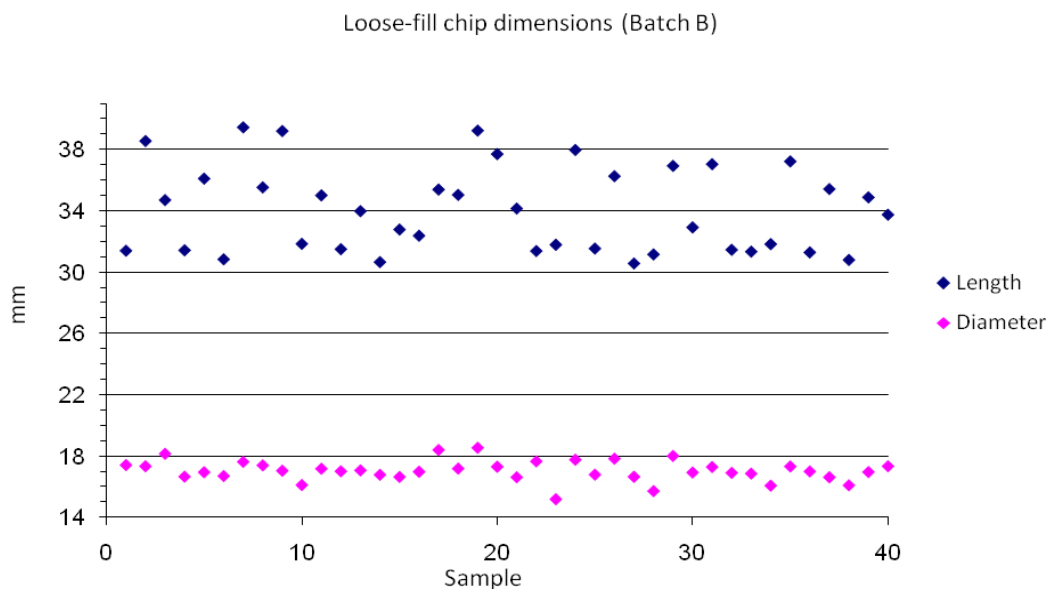
Batch B	Length (mm)	Dia. (mm)
Average	34.040	17.054
Std. Dev.	2.799	0.680

Figure 3.28: Loosefill chip dimensions – Batch B (long cut standard GLS extrusion, bulk density approx. 8 kg/m³)

An investigation into the Properties of Starch-Based Foams
Chapter 3. The Fabrication of CBL & RPS Starch-Based Foams

108

In both batches of loosefill chips, the standard deviation of chip length is far greater than the standard deviation of chip diameter. This is due to loosefill chip production in which deviation of diameter (or transverse dimension), is limited by the fixed diameter of the extruder die head. Standard deviation of loosefill chip diameter is therefore a function of foam expansion. The length of loosefill chips is governed by the velocity of extrudate leaving the die (influenced by the extruder screw speed and material feeding rate), and the speed of the rotating cutter. These variables are responsible for the greater standard deviation in loosefill chip length.

From the data above, calculation of the volume and surface area of both batches of loosefill chips was made based on approximation of the cylindrical chips. Table 3.4 shows these calculated values.

Table 3.4: Average loosefill chip volume & surface area

		Vol. (mm^3)	SA (mm^2)
Batch A	**Average**	6376.792	1935.437
	Std. Dev.	716.817	149.391
Batch B	**Average**	7817.813	2284.882
	Std. Dev.	1133.305	233.073

It should be noted that these results are approximate figures based on cylindrical volumes calculated from the manual measurement of loosefill chips. However, starch loosefill chips do not have smooth surfaces and therefore in the case of surface area the results obtained may not accurately reflect the true surface area if the convoluted surfaces of chips at the microscopic level are taken into account, in which case these values are likely to be far greater. Since the application of loosefill chip surface area data is to be utilised to assess coverage and adsorption of minute water droplets with diameters in the region of 35 microns, clearly there is a need for further work to more accurately establish the surface area of loosefill chips.

3.4 Discussion of CBL foam fabrication techniques

This chapter focused mainly on development of a new technique known as Compression Bonded Loosefill (CBL) for manufacturing a novel type of block foam utilising loosefill starch foams as a raw material, comprising a feasibility study of the CBL method alongside studies on some key processing factors associated with development of the CBL technique towards an industrial process.

The study proved the feasibility of producing samples of block foams in a range of densities from manually wetted and compressed loosefill chips, but it also highlighted key issues surrounding inconsistencies in sample density due to inadequate control of the technique.

An investigation into the Properties of Starch-Based Foams
Chapter 3. The Fabrication of CBL & RPS Starch-Based Foams

109

As such, some preliminary studies were conducted with the objective of establishing an automated method to achieve greater uniformity of loosefill wetting which is a prerequisite of facilitating the efficiency of any subsequent automated compression system.

Whilst many issues remain unresolved, this objective was accomplished to some degree. The lab-scale equipment proved the overall feasibility of the wetting method despite the limitations of the relatively low water pressures used. The wetting system also indicated that adequate adhesion of wetted loosefill chips could be achieved through the use of such a system.

The study of water delivery through the spray nozzle showed the significance of using higher water pressures in order to produce a greater number of smaller droplets and thus achieve better uniformity of wetting.

Data representing the quantity of water droplets within the mist chamber at any given water pressure would help provide a more accurate method of determining the water coverage of a continuous stream of loosefill chips passing through the chamber and is thus an essential element in the development of any chamber-based wetting system.

Droplet density within the mist chamber is dependent on the velocity of the droplets exiting the nozzle and slowed by air drag as they pass through the mist chamber. However, the initial velocity of water droplets exiting the nozzle is unavailable from technical specifications from the nozzle manufacturer and thus represents an unknown variable, although methods such as *laser Doppler* may be used to measure this. In addition, the number of droplets colliding with each other to form larger droplets as well as droplets 'lost' on contact with chamber walls would need to be determined.

If accurate distribution of water droplets within the mist chamber can be calculated it may be used to optimise chamber dimensions, water pressure, loosefill throughput and thus water adsorption onto loosefill chips - the surface area of which must also be accurately defined. These are all areas of research requiring further work.

Chapter 4   Experimental details

Experimental details for tests conducted on CBL and RPS foams are detailed in this chapter which has been divided into three main subsections: mechanical tests, thermal tests and acoustic tests.

4.1   Sample preparation

Unless otherwise stated, all CBL and RPS samples tested were prepared according to procedures described in the previous chapter detailing the fabrication of these foams.

In order to determine the pressures required to produce CBL samples at a range of densities, other variables were eliminated by using an identical mass/volume of extruded starch loosefill foam and water while compressing the material to a range of peak displacements on the Hounsfield testing machine (Model H10K-T), in conjunction with 1kN and 10kN force transducers (Model HTE- 1kN & 10kN). Figure 4.1 shows a CBL sample being produced by this method on the Hounsfield testing machine at Brunel University.

Figure 4.1: CBL sample being produced on the Hounsfield testing machine

CBL samples were fabricated according to the production parameters shown in Table 4.1 which provides data for a selection of uncut CBL blocks fabricated from standard GLS extruded loosefill with an approximate bulk density of 8 Kg/m^3.

Table 4.1: Production parameters of selected CBL blocks

Loosefill mass (g)	Loosefill vol. (cm3)	Water vol. (approx.) (ml)	Applied peak pressure (kPa)	Crosshead displacement (mm)	Crosshead speed (mm/sec)	Sample dimensions (mm) *	Sample density (Kg/m3) •
48.3	5888	14	4.15	50	10	130 x 130 x 28	38.6
48.3	5888	14	5.68	70	10	130 x 130 x 35	46.2
48.3	5888	14	8.93	90	10	130 x 130 x 48	51.6
48.3	5888	14	16.17	110	10	130 x 130 x 63	74.1
48.3	5888	14	89.99	140	8.3	130 x 130 x 95	143.8
48.3	5888	14	220.64	145	8.3	130 x 130 x 110	166

* After 48 hours conditioning at 23 C/50% r.h.   • Data pertains to trimmed CBL blocks after conditioning

Figure 4.2 (a) shows fabrication compression curves recorded from 3 samples produced by this method as a function of equipment displacement. This illustrates how each sample produced was subjected to similar pressures over the same displacement range, but to different peak displacements.
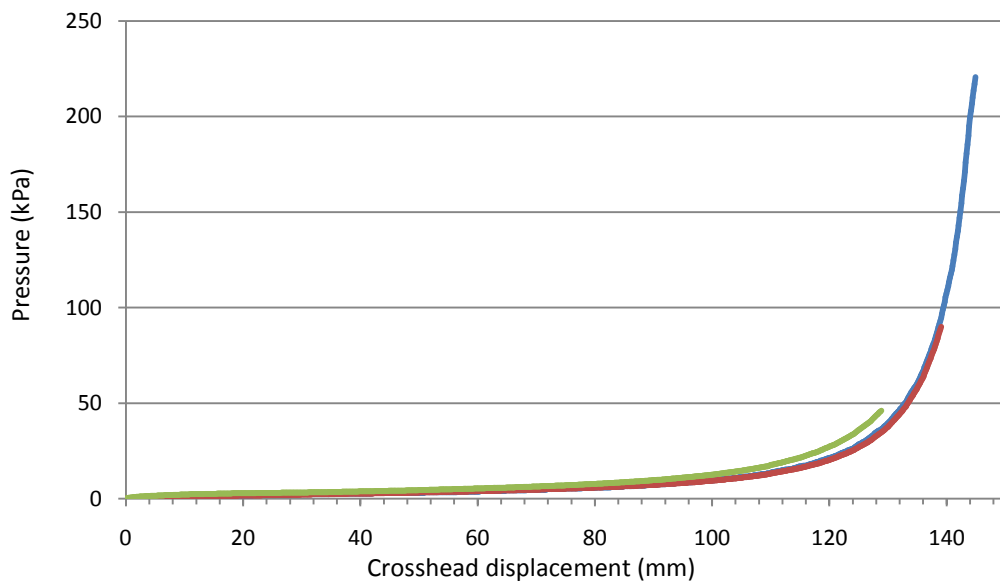
Figure 4.2 (a): CBL fabrication compression curves as a function of equipment displacement

Figure 4.2 (b) shows the relationship between applied peak pressure and the resultant density of samples produced after 48 hours conditioning.
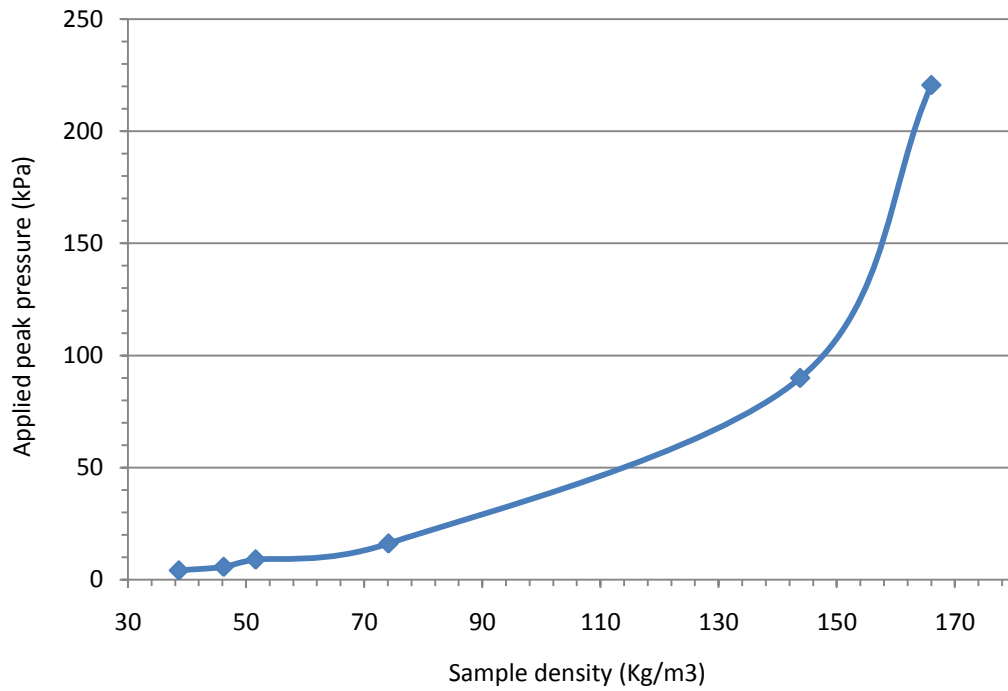
Figure 4.2 (b): Density of CBL samples as a function of applied peak pressure
Density data pertains to trimmed CBL blocks after 48 hours conditioning at 23 C/50% r.h.

4.2   Mechanical Tests

Since foams are generally subject to some different types and degree of mechanical stress during applications such as packaging, an understanding of their mechanical behaviour is of great significance. This subsection covers experimental details pertaining to static compression tests, dynamic compression tests, tensile tests and creep tests. It also covers mechanical tests conducted under high-humidity and temperature conditions.

4.2.1   Compression tests

Compression tests were conducted in accordance with BS ISO 844:2001 *Cellular plastics - Compression test for rigid materials* on CBL samples with a dimension of 100mm x 100mm x 50mm (length x width x thickness) and densities ranging from 32 kg/m^3 to 99 kg/m^3. The CBL samples were conditioned at 23°C & 50% r.h. for a minimum of 48 hours prior to testing. These conditions were maintained throughout the tests in a conditioned laboratory environment.

Samples were tested on Hounsfield mechanical testing machine (Model H10K-T) at Brunel University in conjunction with a 10kN force transducer (Model HTE-10kN), at a crosshead speed of 5mm/minute using QMAT 4.58 series data processing software. Accuracy of this equipment is specified as follows:

- Load measurement accuracy: +/- 0.5% of the applied load

- Position measurement accuracy: +/- 0.01% of reading or 0.001 mm

- Speed accuracy: +/- 0.005% of the set speed   (Tinius Olsen, 2010)

From displacement of the crosshead and the applied load, stress and engineering strain can be derived. Figures 4.3 and 4.4 show the test set-up and a CBL sample undergoing a compression test.
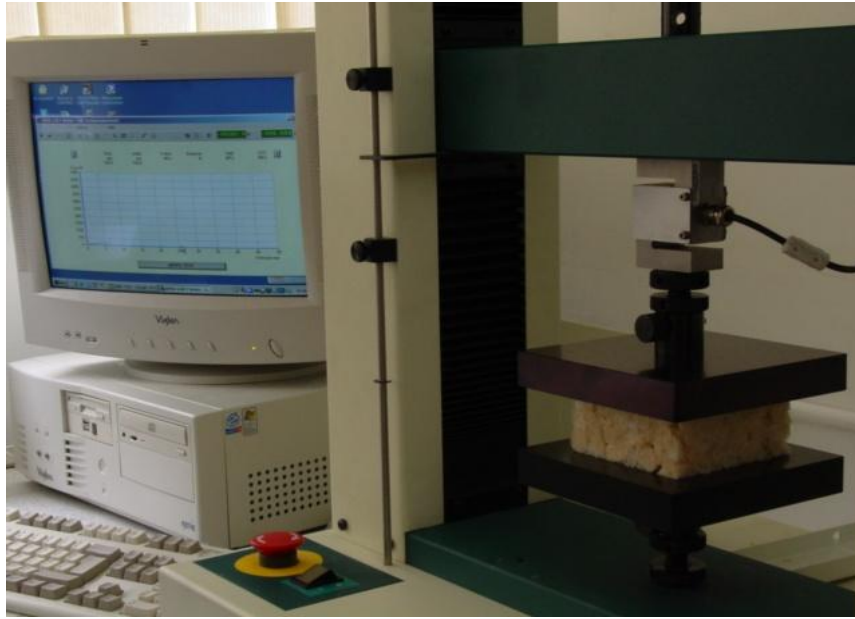
Figure 4.3: Set-up of the compression test equipment
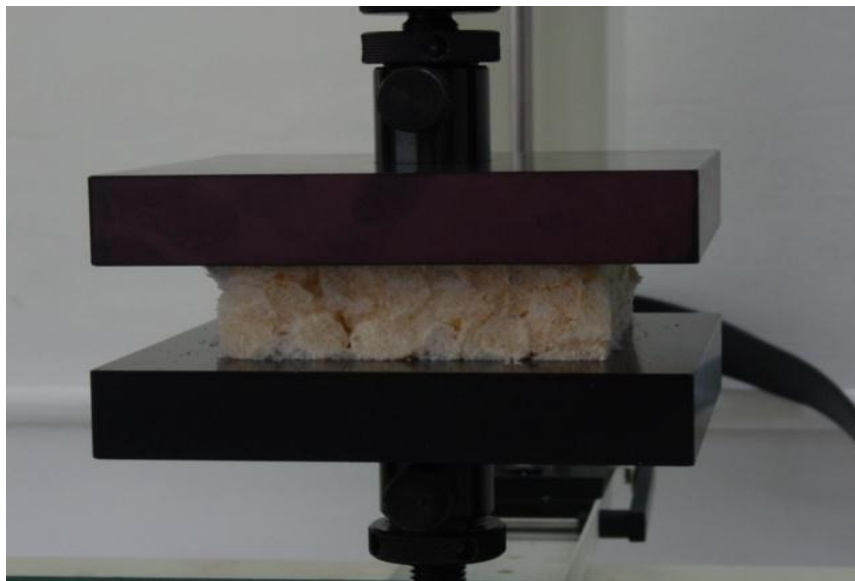
Figure 4.4: CBL sample undergoing a compression test

4.2.2   Dynamic impact cushion tests

Dynamic impact cushion tests involve conducting a series of drops of weights of various masses from a specified drop height onto a selection of foam samples. On impact, an accelerometer attached to the weight measures peak deceleration in terms of multiples of gravitational acceleration coefficient (9.81 ms^{-2}) known as G values.   The peak deceleration values for successive impacts are then linked to produce cushion curves representing peak deceleration across a range of static stresses (as mass in kg per nominal impact area of the sample in cm^2).

Dynamic impact cushion tests were conducted on a range of CBL foam samples with approximate mean densities of 40 kg/m^3, 60 kg/m^3 and 80 kg/m^3. In each group of samples, density tolerance was set at +/- 5 kg/m^3 from the mean density due to the difficulty of controlling density in CBL sample production as previously reported. All CBL samples were cut to dimensions of 100mm x 100mm x 50mm and were conditioned at 23°C/50% r.h. for a minimum of 48 hours prior to testing. These conditions were maintained throughout the tests in an environmentally conditioned laboratory. Figure 4.5 below shows the dynamic impact testing set-up used for all tests reported.
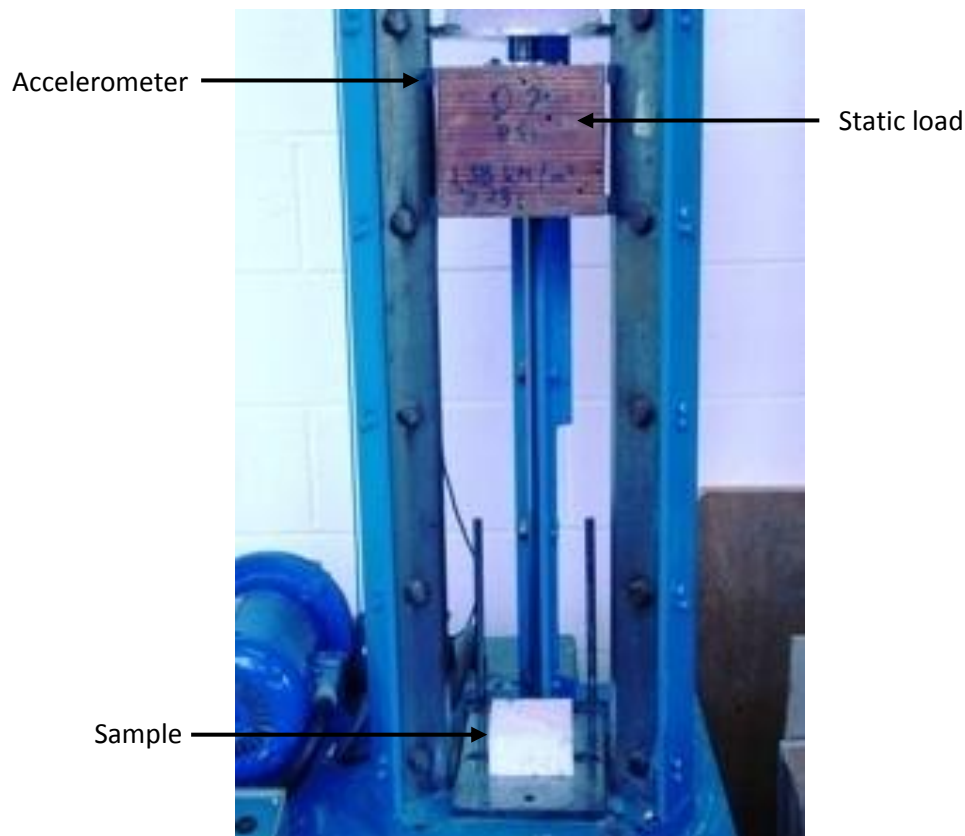
Figure 4.5: Dynamic impact testing set-up

Dynamic impact tests were conducted according to ASTM D1596 - 97(2003), *Standard Test Method for Dynamic Shock Cushioning Characteristics of Packaging Materials*, on Pira International Dynamic Impact Cushion Test equipment using a 500G ICP accelerometer in conjunction with Lansmont - Test Partner data acquisition USB 4 x 4 software (Lansmont Corporation, Monterey CA. USA) at Pira International Ltd, Leatherhead, Surrey, UK.

Drop heights for all dynamic impact tests were set at 600mm. Each sample was subject to 5 successive impacts using a particular weight, with a period of approximately 45 seconds between each impact. A total of 25 samples were tested in each of the 40 kg/m^3 and 60 kg/m^3 density ranges while a total of 20 samples were tested in the 80 kg/m^3 density range.

4.2.3   Creep tests

The compressive creep properties of materials are determined by subjecting samples to prolonged constant uni-axial compression loading. Material deformation is recorded at specified time intervals and a creep (sample thickness change) vs. time diagram is plotted. The slope of the plotted curve at any point corresponds to the creep rate.

All creep tests described in this section were conducted at Pira International Ltd, Leatherhead, Surrey on CBL foam samples in the 40, 60 and 80 kg/m^3 density ranges as specified previously (section 4.2.2). Sample sizes of 100mm x 100mm x 50mm were tested on creep rigs according to BS 4443: *Part 3:1975 Methods of test for Flexible cellular materials. Part 3. Method 8. Determination of creep.*

1.5kg loads were hung from the end of each creep rig arm corresponding to a total load of 5,394g on each sample (3.2 x load on the end of the arm + 894g for top plate and arm assembly), equivalent to 5.286 kPa. All samples were conditioned at 23° C, 50% r.h. for a minimum of 48 hours prior to testing. These conditions were maintained throughout the tests in a conditioned laboratory. Figure 4.6 shows two CBL samples in rigs undergoing a creep test.
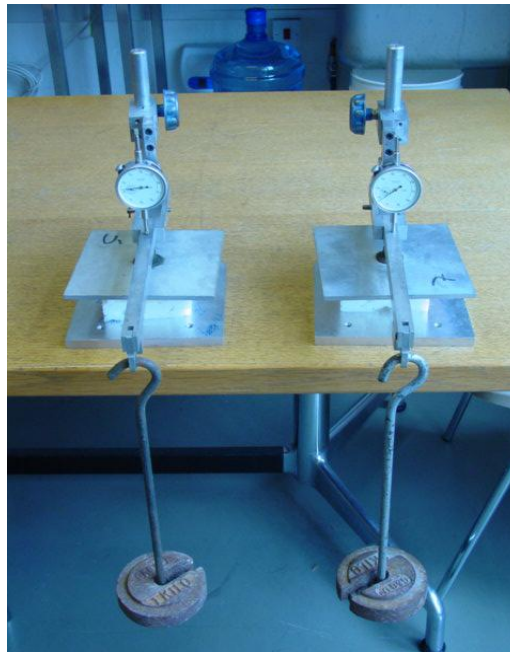
Figure 4.6: CBL samples undergoing a creep test

In order to gain greater confidence in these results, further creep tests were conducted on samples of CBL foams and RPS foam (23 kg/m3), alongside a selection of conventional polymer foams. The polymer foams selected for the purposes of these tests were as follows:

- ETAS 40: anti-static expanded polyether with a density of 40 kg/m^3, manufactured by the Vita Group (Pall Mall, London, UK), commonly used as a cushion packaging foam.

- TMS 50: flame-retardant furniture grade polyether with a density of 50 kg/m^3, manufactured by the Vita Group, commonly used as a load bearing foam by the furniture industry.

- PEN 35: polyethylene with a density of 35 kg/m^3, manufactured by Pregis Corp (Deerfield, IL, US), commonly used as a cushion packaging foam. (Wiles, 2010)

Experimental details for these tests are identical to those previously described in this subsection.

4.2.4   Tensile tests

For the majority of applications requiring mechanical strength characteristics, converters and users of polymeric foam materials are chiefly concerned with the ways in which a foam material will withstand compressive stresses. However, on occasion, polymer foams may be subjected to tensile stresses and thus their behaviour under tensile conditions should also be characterised as a secondary foam property.

Tensile tests were conducted at Brunel University on CBL sample densities ranging from 33 kg/m^3 to 94 kg/m^3. Samples were cut to dimensions of 100mm x 100mm, with a gauge height of between 40mm and 80mm. Samples were attached at each end to mild steel plates of 130mm x 130mm using hot melt adhesive and then conditioned at 23°C/50% r.h. for a minimum of 48 hours prior to testing. These conditions were maintained throughout the tests in a conditioned laboratory. Tensile tests were conducted on a Hounsfield universal mechanical testing machine (Model H10K-T) in conjunction with a 1kN force transducer (Model HTE-1000N) at a crosshead speed of approximately 1.3mm/minute for each 25mm of sample gauge height, using QMAT 4.58 series data processing software. Accuracy of this equipment is specified as follows:

Load measurement accuracy: +/- 0.5% of applied load

Position measurement accuracy: +/- 0.01% of reading or 0.001 mm

Speed accuracy: +/- 0.005% of set speed   (Tinius Olsen, 2010)

Tests were conducted in accordance with ASTM D 1623-03 *Standard test method for tensile and tensile adhesion properties for rigid cellular plastics (2003).* Type C samples were prepared according to the test standard. Figure 4.7 shows a CBL sample in the Hounsfield testing equipment undergoing a tensile test. The steel plates attached to the CBL foam samples are pulled apart by grips made at Brunel University specifically for such tensile tests.

Figure 4.7: CBL sample undergoing a tensile test

4.2.5   Mechanical tests conducted at high humidity & temperature

One characteristic of all foams which may potentially affect their mechanical strength is their susceptibility to high temperature and humidity. This is especially true for hygroscopic materials such as CBL and RPS starch-based foams. Due to this inherent susceptibility further mechanical tests were conducted on pre-conditioned samples (according to ASTM D4332 - *Standard practice for conditioning container, packages or packaging components for testing*), at high temperature and relative humidity in order to simulate the tropical conditions in which these materials might realistically be expected to function according to *ISTA 2 Series Partial-Simulation Performance Test Procedure*, in which 38°C and 85% r.h. are given as standard test conditions.

The dominant effect of tropical conditioning on the mechanical strength of hygroscopic materials such as starch-based foams is high humidity, with high temperature having a second order effect (Shires, 2009). The reported mechanical tests conducted under high temperature and relative humidity conditions are compression tests and creep tests.

4.2.5.1 High temperature & humidity compression tests

CBL and RPS samples with densities ranging from 23 kg/m^3 to 93 kg/m^3 were cut to dimensions of 100mm x 100mm x 80mm (length x width x thickness) and conditioned at 38°C and 85% r.h. for a minimum of 48 hours prior to testing in a Delta 190-40HS (Design Environmental, UK) conditioning chamber for a minimum of 48 hours prior to testing. These conditions were maintained throughout the tests. Figure 4.8 shows samples during conditioning in the Delta 190-40HS conditioning chamber.

Figure 4.8: Samples during conditioning in the Delta 190-40HS conditioning chamber

Samples were tested on Hounsfield mechanical testing machine (Model H10K-T) at Brunel University in conjunction with a 10kN force transducer (Model HTE-10kN), at a crosshead speed of 5mm/minute using QMAT 4.58 series data processing software in accordance with BS ISO 844:2001 Cellular plastics - *Compression test for rigid materials*.

Figure 4.9 shows the Hounsfield mechanical testing machine fitted with a Design Environmental auxiliary testing chamber in which the conditioned samples were tested in order to maintain the specified high temperature and humidity conditions during testing.

Figure 4.9: Hounsfield mechanical testing machine fitted with Design Environmental auxiliary testing chamber

4.2.5.2 Sample changes during high temperature & humidity conditioning

During conditioning samples exhibited dimensional shrinkage. Figure 4.10 shows the non-uniform nature of shrinkage of a CBL sample exposed to high temperature and high humidity conditioning, alongside an untreated sample for comparison purposes.

Figure 4.10: Non-uniform shrinkage of CBL sample subjected to high temperature and high humidity conditioning (right), alongside an untreated sample
(Sample densities approx. 46 Kg/m^3. Post-conditioned sample density 73 Kg/m^3)

Figure 4.11 shows the overall volume reduction of conditioned samples as a percentage of their original volume.
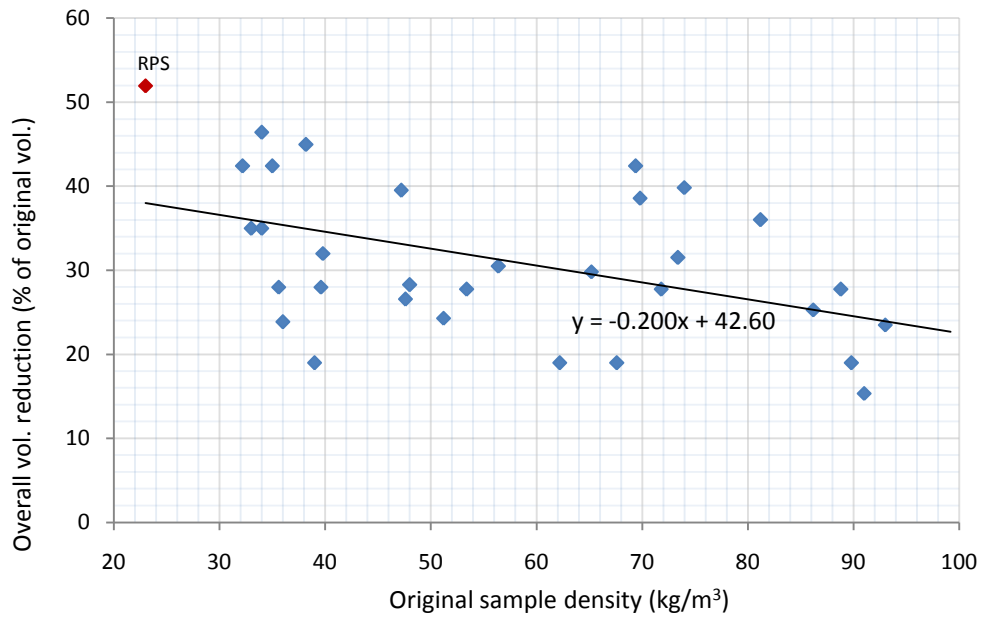
Figure 4.11: Overall volume reduction of 38°C & 85% r.h. conditioned samples as % of original volume (trendline generated by linear regression)

Figure 4.11 shows that lower density samples have a tendency for greater shrinkage during conditioning. The average volume reduction across all samples was 31.27% as a percentage of their original volume. The dimensional shrinkage of conditioned samples was accompanied by an increase in their mass as a result of moisture absorption from exposure to high-humidity. Figure 4.12 shows the increase in the mass of samples conditioned in the Design Environmental chamber as a percentage of their original mass.
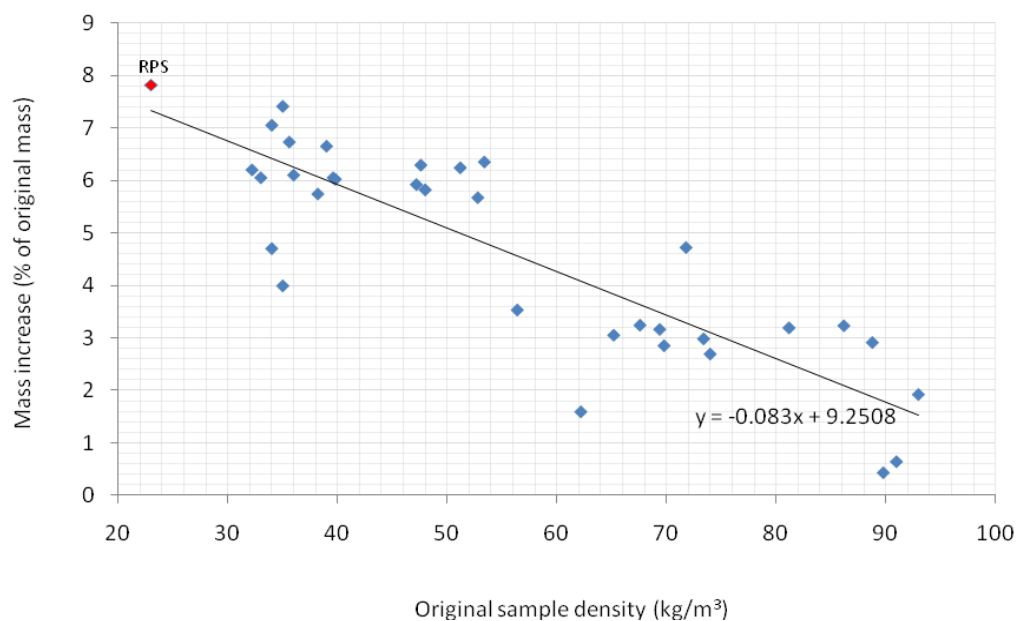
Figure 4.12: Mass increase of 38°C & 85% r.h. Design Environmental chamber conditioned samples as % of original mass (trendline generated by linear regression)

Figure 4.12 illustates that conditioning resulted in increases in the mass of samples of between 0.44% - 7.82% of their original mass, with an average mass increase across all samples of 4.62%. The data also shows that in general, lower density starch foam samples were subject to greater mass increases when viewed as a percentage of their original mass.

In order to determine the origin of sample shrinkage and mass increase during conditioning, Figure 4.13 shows the density variations of samples before and after conditioning based on the original mass of samples. Densities of conditioned samples were re-calculated on a wet and dry basis to show the effects of absorbed moisture on sample density.
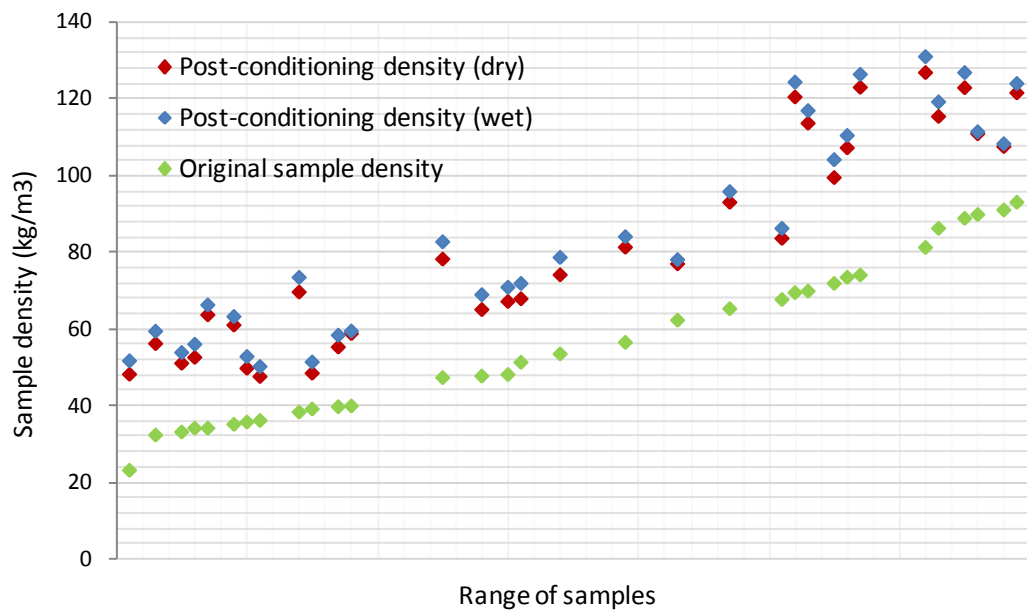
Figure 4.13: Density variation of samples before and after 38°C & 85% r.h. conditioning

Average density increase across all samples as calculated on a dry basis was 25.2 kg/m^3. Comparison of the wet and dry post-conditioned sample densities shown in Figure 4.13 illustrates that moisture absorbtion was responsible for a relatively minor proportion of the density increases observed. Thus it can be concluded that the vast majority of the density increases of conditioned samples must originate from shrinkage in the sample dimensions rather than from absorbed moisture.

In order to better understand the changes taking place within samples exposed to high temperature and humidity conditioning, scanning electron microscopy (SEM) and X-ray diffraction (XRD) techniques were used to further analyse samples. The details of the techniques used are given below.

4.2.5.3 Scanning electron microscopy (SEM)

Two sets of CBL foam samples with similar densities of approximately 43 Kg/m^3 were used for scanning electron microscope (SEM) observations at the Experimental Techniques Centre, Brunel University, in order to further analyse the mechanisms behind the shrinkage of samples subjected to high temperature and high humidity conditioning.

One set of samples were conditioned at 23°C and 50% r.h. for a minimum of 48 hours, while the other set of samples were conditioned at 38°C and 85% r.h. for a minimum of 48 hours in a Delta 190-40HS conditioning chamber (as previously described in section 4.2.5.1) before being allowed to recondition at 23°C and 50% r.h. for a minimum of 48 hours. The modified density of high temperature and high humidity conditioned samples was measured at approximately 75 Kg/m^3.

Samples were sectioned after freezing with liquid nitrogen using a single-edged razor blade and then mounted on aluminium stubs with a graphite filled double side adhesive tape and coated with gold in a SEM sputter coating unit. SEM examinations were conducted with a Cambridge Stereoscan scanning electron microscope (250 MK2 Cambridge, England).

4.2.5.4 X-ray diffraction (XRD)

Two sets of CBL foam samples were used for X-ray diffraction (XRD) analysis in order to characterise the crystallinity of CBL foams. One set of samples were conditioned at 23°C and 50% r.h. for a minimum of 48 hours, while the other set of samples were conditioned at 38°C and 85% r.h. for a minimum of 48 hours in a Delta 190-40HS conditioning chamber (as previously described in section 4.2.5.1) before being allowed to recondition at 23°C and 50% r.h. for a minimum of 48 hours. Table 4.2 provides specifications of CBL samples analysed by XRD.

Table 4.2: Specifications of CBL samples analysed by XRD

	Conditioning regime	
	CBL 23°C & 50% r.h.	CBL 38°C & 85% r.h.
Density (Kg/m^3)	43.6	42.6 (75)
	70	72 (104)

Figures in parenthesis represent post-conditioning density of high temperature & high humidity conditioned samples

Wide angle X-ray spectra of CBL samples were collected using a diffractometer employing Cu Kα radiation (PW1050, Phillips). The generator was operated at 36 kV and 26 mA. Samples were mounted on sample stages and scanned over the 2θ range from 3° to 30° or 50° with step size

0.02° and a scan rate of 0.02 °/sec. The collected data were analysed using the software, Traces (version 3.0, Diffraction Technology Pty Ltd) installed in the machine. The areas under the diffraction peaks (crystallised areas) and total area under the diffraction spectrum were calculated using the "measure peak area" function in the Traces software, which automatically generated and subtracted the background pattern from each diffraction spectrum. The crystallinity (%) was obtained from the ratio of the areas of the diffraction peaks to the total area of diffraction spectrum.

4.2.5.5 High temperature & humidity creep tests

Creep tests were conducted on creep rigs according to BS 4443: Part 3: 1975 *Methods of test for Flexible cellular materials. Method 8. Determination of creep* at Pira International Ltd, Leatherhead, Surrey on CBL starch foam samples in the 40, 60 and 80 kg/m^3 density ranges (specified previously, section 4.2.2), and the three conventional polymer foams previously used for comparison purposes (as specified, section 4.2.3).

1.5kg mass were hung from the end of each creep rig arm corresponding to a total load of 5,394g on each sample (3.2 x load on the end of the arm + 894g for top plate and arm assembly), giving rise to an equivalent pressure of 5.289 kPa on each sample, calculated using the pre-conditioned sample dimensions.

Sample sizes of 100mm x 100mm x 50mm were conditioned at 38°C and 85% r.h. in a Climatec tropical chamber for a minimum of 48 hours prior to testing. These conditions were maintained throughout the creep tests within the chamber. Although pertaining to 1000 hour creep tests, ASTM D3575 Suffix BB states that tests may be conducted at a range of temperatures and relative humidities in order to simulate actual conditions. Figure 4.14 shows samples undergoing creep tests in the Climatec tropical chamber at Pira International Ltd.

Figure 4.14: Samples undergoing creep tests in the Climatec tropical chamber at Pira International Ltd.

Table 4.3 shows weights and densities of samples prior to and after conditioning in the Climatec tropical chamber.

Table 4.3: Weights and densities of samples prior to and after 38°C & 85% r.h conditioning

Sample	Pre-conditioning Density (kg/m^3)	Pre-conditioning mass (g)	Post-conditioning mass (g) (wet)	Post-conditioning density (kg/m^3) (wet)
CBL 47 (H)	47.2	23.6	24.5	49
CBL 67 (H)	67	33.5	34.2	68.4
CBL 85 (H)	85.2	42.6	43.4	86.8
RPS 23 (H)	23	11.5	12.2	24.4
ETAS 40 (H)	40	20	20	40
TMS 50 (H)	50	25	25	50
PEN 35 (H)	35	17.5	17.5	35

(H): Sample conditioned & tested under high temperature & high humidity conditions

Table 4.3 gives post-conditioning masses and densities of samples including any absorbed moisture. Conditioning increased the masses of the CBL foam samples by an average of 1.46g and RPS foam by an average of 1.1g, which in turn increased sample density. In contrast to the conditioning of samples for the high temperature and humidity compression tests outlined in section 4.2.5.2, sample dimensions were generally unaffected by conditioning in the tropical chamber, such that in this case it can be concluded that the observed increase in sample mass was largely due to absorbed moisture. Despite previous work conducted on the effects of humidity on the shrinkage of RPS starch foam strands (Kang, 2006) as outlined in Chapter 2 (section 2.12), the reasons for this discrepancy are currently unclear.

In order to investigate this further, Figure 4.15 compares the mass increases of CBL and RPS samples conditioned in the Design Environmental chamber at Brunel University, against samples conditioned at high temperature and relative humidity in the Climatec Tropical chamber at Pira International (as previously shown in Figure 4.12), as a percentage of their original mass.
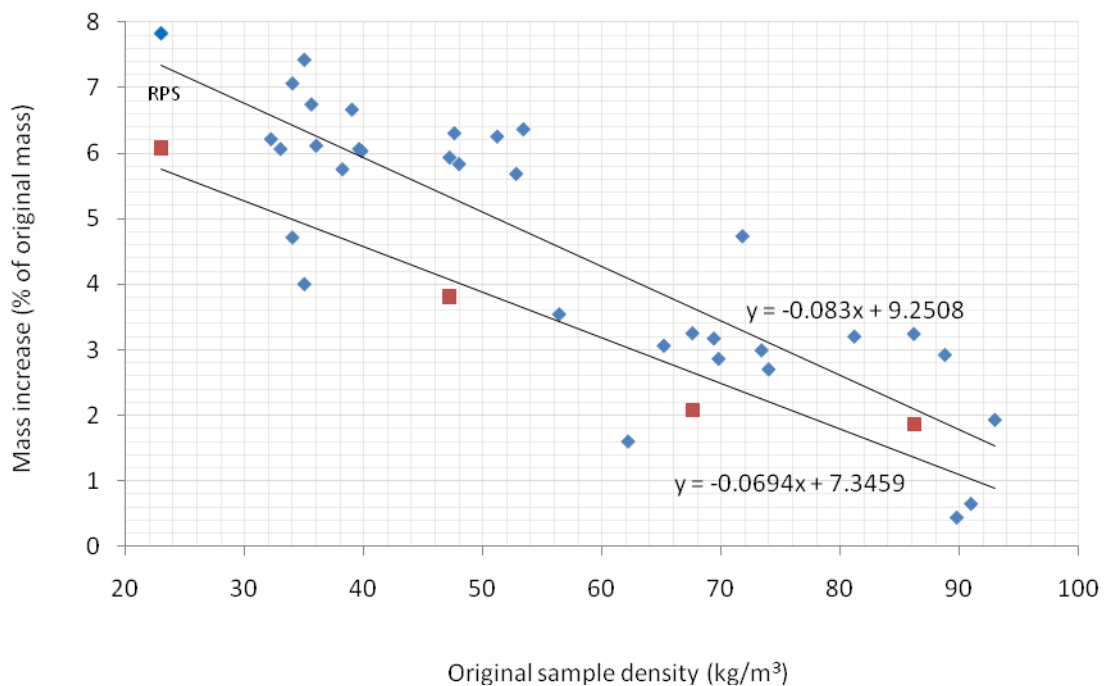
Figure 4.15: Mass increase comparison of 38°C & 85% r.h. Design Environmental chamber conditioned samples & Climatec Tropical chamber conditioned samples as % of original mass (trendlines generated by linear regression)

Key to Figure 4.15:
◆   Samples conditioned in Design environmental chamber
■   Samples conditioned in Climatec Tropical chamber

Figure 4.15 shows that in general, the CBL and RPS starch foam samples conditioned in the Climatec Tropical chamber have slightly lower mass increases indicating a smaller proportion of absorbed moisture compared to the samples conditioned in the Delta 190-40HS Design Environmental chamber. Since the samples were conditioned at different facilities it is likely that the much larger volume of the Climatec Tropical conditioning chamber may result in a more moderate intensity of initial conditioning which in turn may also be responsible for the reduced degree of sample shrinkage observed in the samples conditioned in this chamber. Clearly the conditioning of numerous additional samples at various facilities would be required in order to further investigate this issue.

4.3 Thermal Tests

Foam applications such as insulation require an understanding of the material's thermal behaviour. This subsection covers experimental details pertaining to thermal conductivity tests on CBL conducted using facilities at Gearing Scientific Ltd, Ashwell, Herts.; tests to assess the thermal properties of high-density RPS performed at the Polymer Characterisation Lab, Materials Science Department, University of Cambridge, and a case study conducted using facilities at Brunel University together with assistance from the Technical (Quality Assurance) Department at Hydropac Ltd, Aylesbury, Bucks, UK.

4.3.1 Thermal conductivity of CBL foams

In order to examine the relationship between the density of CBL foam and its thermal conductivity, three different densities of CBL foam were characterised using the Fox 200HT™ Thermal Conductivity Instrument, manufactured by LaserComp, Massachusetts, USA.

Three CBL foam samples were prepared to approximate dimensions of 170mm x 170mm x 40mm and densities of 39, 62 and 83 kg/m³.

The Fox 200HT thermal conductivity instrument was used to measure the thermal conductivity of the three CBL foam samples at three mean temperatures of 0°C, 30°C, 60°C. The Fox 200HT uses the heat flow meter method (according to test standards: ASTM C518, BS 874 − EN 12667, DIN 52612, ISO 8301), in which a 75mm^2 high-output thin film heat flux transducer is bonded to the surface of each plate with a type E thermocouple bonded to the centre of each transducer. These directly yield an electrical signal proportional to the differential temperature across the sample thickness. The Fox 200HT uses the same thermocouples to monitor sample surface temperatures and to control plate temperatures (LaserComp). Figure 4.16 shows the Fox 200HT thermal conductivity instrument.

Figure 4.16: Fox 200HT thermal conductivity instrument
Lasercomp.com

Each sample to be tested was first weighed and then placed between two plates in the test stack within the test chamber of the Fox 200HT instrument which also measures thickness of the samples. Samples were tested at mean temperatures of 0°C, 30°C, 60°C and finally at 30°C again in order to assess any effects of moisture variation within samples on thermal conductivity measurements.

The Fox 200HT controls the temperatures of the upper and lower plates using Peltier liquid heating/cooling in order to generate a 20°C temperature differential between the plates, typically at an accuracy of +/- 0.04°C. Heat flux differential measurements between the two plates are then automatically carried out by the instrument and these data are digitally recorded every half second via Win_Therm software interface. Every four minutes the average is stored as one block and once equilibrium is achieved readings are taken for a minimum of one hour before the final five block readings are averaged. (pers.com, Gearing Scientific, 2010)

Accuracy of the Fox 200HT thermal conductivity instrument is reported to be +/- 1%. Displacement transducers are zeroed before each measurement and the equipment is calibrated using NIST 1495 glass fibre calibration standard. (pers.com, Gearing Scientific, 2010) The laboratory environment temperature and humidity were 10 - 15°C and 64 – 72% r.h., respectively during the tests. Table 4.4 shows the mean thickness of samples along with pre-test and post test masses and densities.

Table 4.4: Sample thickness, pre & post-test mass & density

Sample ID	Mean thickness (mm)	Pre-test mass (g)	Post-test mass (g)	Post-test mass loss (g)	Pre-test density (kg/m^3)	Post-test density (kg/m^3)
CBL 39	39.95	45.4	44.2*	1.2	39.32	38.28
CBL 62	39.06	70.2	68.9	1.3	62.18	61.03
CBL82	40.60	96.3	95.2	1.1	82.07	81.13

*Adjusted post-test weight to compensate for 24 hr delay in measurement

4.3.2 Thermal properties of high-density RPS foams

Previous work on RPS foams (as described in Chapter 2, section 2.11.2), examined the thermal conductivity of RPS at a density of around 23 - 25 kg/m^3.

In order to further examine the relationship between the density of RPS foams and its thermal properties, samples of high density RPS were tested using the Hot Disk^{TM} Thermal Constants Analyser, Model TPS 2500, (Mathis Instruments, Ltd., Fredericton, New Brunswick, Canada), based on the principle of dissipation of thermal energy (generated from a temperature pulse) trough materials – *the transient plane source technique* (Michigan Tech, 2010).

In comparison to the hot plate method previously described, much smaller samples are required (> approximately 3 times the disc sensor diameter used). However, the sensor used in conjunction with this equipment requires good contact with the surfaces of samples to be tested. Therefore this method is not suitable for the testing of low-density CBL foams, typically characterised by internal voids exposed at the surfaces of cut samples, which may inhibit good contact with the sensor.

The Hot Disk^{TM} thermal constants analyser was used to measure the thermo-physical properties of a series of high-density RPS samples ranging in density from 200 kg/m^3 to 584 kg/m^3. The Hot Disk^{TM} thermal constants analyser measures thermal conductivity (λ) and thermal diffusivity (Td), simultaneously enabling an estimation of the sample's specific heat capacity (Cp) per unit volume of the material tested. Figure 4.17 shows the Hot Disk^{TM} Thermal Constants Analyser Model TPS 2500 with its covered sensor to the left.
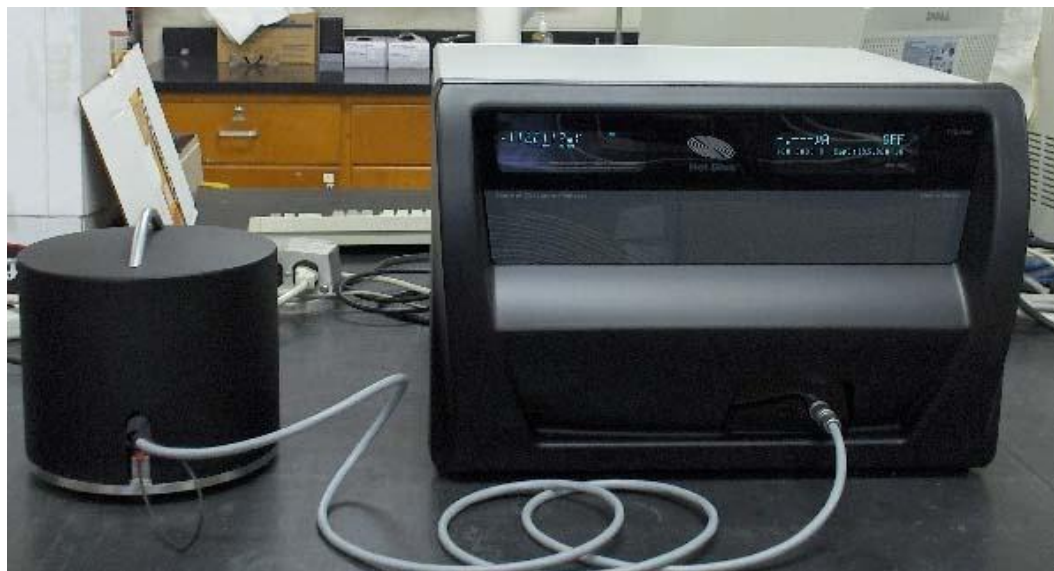
Figure 4.17: Hot Disk^{TM} Thermal Constants Analyser equipment with covered sensor

The Hot Disk system is based on the *transient plane source* method designed for thermal conductivity and thermal diffusivity measurements on various sample types. The transient plane source technique utilises a probe (as shown in Figure 4.18) comprising a flat sensor with a continuous double-spiral of electrically-conducting nickel etched out of thin foil and sandwiched between two layers of kapton, a polyimide film developed by DuPont which retains good stability over a wide range of temperatures.
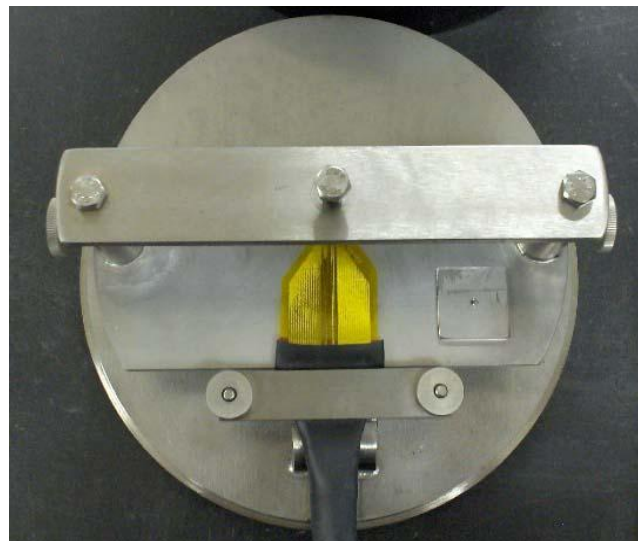
Figure 4.18: Hot Disk ^{TM} thermal constants analyser sensor (cover removed)

The kapton film enclosing the double nickel spiral is 0.013 - 0.025mm thick and provides electrical insulation from the sample and mechanical stability for the probe. The sensor is normally placed between the surfaces of two pieces of the sample to be measured. Different sizes and formats of sensor are available. During measurement, an electrical current passes through the nickel spiral creating an increase in temperature. The heat generated dissipates through the sample on either side at a rate dependent on the thermal transport characteristics of the material. By recording the response of temperature versus time in the sensor, these characteristics can be calculated (Michigan Tech, 2010).

Precision of the instrument is rated at λ: +/- 2%, *Td*: +/- 4% and *Cp*: +/- 5% (Log & Gustafsson, 1991). However, other sources suggest that specific heat capacity estimates are subject to +/- 20% accuracy and should only be used as a general guide (Cornell, 2007). The sensor size used for the tests was 2mm radius. Other parameters for these tests are as follows: Power: 0.05 watts. Dwell time: 20 seconds. Test conditions: temperature 25-27°C; relative humidity 60%. Reported results are based on averages of three measurements taken from different locations of each sample tested.

4.3.2.1 High density RPS sample preparation

High density RPS samples were prepared by exposure of standard 25 kg/m³ RPS block foams in a high-humidity chamber (Figure 4.19 a), followed by compression (Figure 4.19 b). The RPS foams were plasticised by absorption of water at 23°C, 96% r.h., which gave rise to shrinkage of the foams. Conditioning was maintained for a period of several hours depending on the sample size. Changes to the physical dimensions of samples was monitored and occurred mostly within the first two hours of exposure, but exposure was terminated when sample dimensions had stabilised and no further significant changes in the sample dimensions could be observed. By means of this conditioning method, the shrinkage of extruded starch foam rods with density of 14 kg/m^3 used to fabricate RPS foams were reported to be 65.6% and 71.3% in diameter and length respectively (Kang, 2006).

Application of physical pressure on the humidity treated RPS planks facilitated further increase in the density of the foam. The samples were compressed between two parallel steel plates to a desired thickness and then permitted to dry at conditions of 22-25°C, 45%-65% r.h. for one week to produce the resultant block samples (Figure 4.19 c) (Wang, 2008).

Figures 4.19 a), b) & c): Preparation of high-density RPS block foam samples utilising high-humidity conditioning and compression *(Wang, 2008)*

   a) **Standard RPS blocks being treated in the high-humidly chamber**
   b) **Compression of softened foam**
   c) **Resultant high-density RPS foam blocks**

Test specimens were then cut from these blocks and conditioned at 23°C and 50% r.h. for a period of two weeks before density measurement and testing of thermal conductivity. Six samples were tested ranging in density from 200 kg/m^3 to 584 kg/m^3.

4.3.3   Case study: Comparison of polyethylene & RPS starch foam in commercial thermal packaging application

A case study was conducted in order to compare the thermal insulation performance of RPS starch foam in place of an existing commercial coolbox system based on a polyethylene (PE) foam liner used to deliver premium chilled foods under ambient transport conditions without refrigeration. The conditions of delivery require the contents packed within the coolboxes to be maintained below 5 °C over a 24 hour period in order to reach recipients in a safe consumable condition.

The existing coolbox system (Shipper Code: CUIS002) as marketed by Hydropac Ltd, High Wycombe, consists of a C - flute corrugated board outer carton lined with a polyethylene (PE) foam inner with a thickness of 32mm and a density of approximately 32.7 kg/m^3. Internal dimensions of the shipper are 375mm x 230mm x 120mm giving a volume of 10.35 litres. Shipper capacity is given as 6kg.

The function of the outer carton is mainly containment and protection, whilst the foam liner provides the majority of thermal insulation for the packaged product as well as offering a degree of cushion protection in the event of a drop or an impact. Figure 4.20 shows the existing coolbox system as received from the supplier.

Figure 4.20: Existing PE foam-lined coolbox supplied by Hydropac Ltd

Standard procedure for packing coolboxes is to place ice sheets cooled to approximately minus 18 °C directly below and above the packed product which is itself chilled to approximately 1 - 3 °C. The boxes are then sealed and shipped in ambient conditions, arriving at their destination within a 24 hour period. Packing of the coolboxes was carried out in accordance with the recommendations of Fairfax Meadow, a UK supplier of chilled meats and regular commercial user of these coolboxes (Billington, 2006).

4.3.3.1 Preparation of the coolboxes

Coolboxes lined with the RPS starch foam were made using the standard Hydropack outer carton, but instead of the PE foam liner, a two rod layer RPS starch foam liner together with a C - flute corrugated fibreboard inner liner was substituted. The function of the inner corrugated fibreboard liner was to prevent condensation inside the container from affecting the RPS foam during the 24 hour test period.

The density of the PE foam coolbox liner was approximately 32.7 kg/m^3 whilst the density of RPS foam was approximately 23 kg/m^3. However, the basis for any functional comparison of the coolboxes is the thickness of the insulation material rather than its density. The total thickness of the two rod layer RPS plus corrugated fibreboard inner liner was 29mm in comparison with the 32mm thick PE foam, therefore the thickness of the standard Hydropac PE foam liner was reduced to 29mm in order to provide an equivalent basis for comparison. The PE foam lined coolbox as shown in Figure 4.20 and the RPS foam lined coolbox as shown below in Figure 4.21 were used for testing as part of the case study.

Figure 4.21: RPS foam-lined coolbox

The case study on the performance of the coolboxes entailed two main elements:

1) The ability of the coolboxes to maintain the required temperature of packed product over a 24 hour period - tested by means of a static test monitored within a controlled laboratory environment.

2) The ability of the coolboxes to maintain the required temperature of packed product over a 24 hour period – tested by means of a transit trial in order to replicate the realistic shipping environment incorporating the effects of other influences such as vehicle vibration, temperature variation and handling during shipping. During the transit trial the temperatures inside the boxes was monitored. Although, unlike laboratory testing within a controlled environment such transit trials are not replicable, they do conform to standard industry procedure.

4.3.3.2 Static laboratory test procedure

In order to evaluate the performance of the coolboxes in a controlled environment, tests were first conducted in the environmental chamber at the School of Engineering and Design, Brunel University.

A mild coloured cheese of 500g per unit was selected as representative of the products often shipped via coolboxes and suitable as a test media owing to its uniform density and regular shape. The cheese was chilled to 0 °C and then packed into the coolboxes along with the ice sheets (as supplied by Hydropac Ltd), which were cooled to minus 18°C and positioned directly below and above the product.

Nine T-type thermocouples were calibrated using an Omega thermo-regulator (Omega Engineering Inc. Delaware, US), in conjunction with LAB F250 precision thermometer (Automatic Systems Laboratories, Surrey, UK).

Four thermocouples were placed in one quadrant of each box at approximately half the depth of the product load. Figures 4.22 and 4.23 show the positions of numbered thermocouples. The packed (RPS-lined) coolbox is shown in Figure 4.24 prior to being closed and sealed.
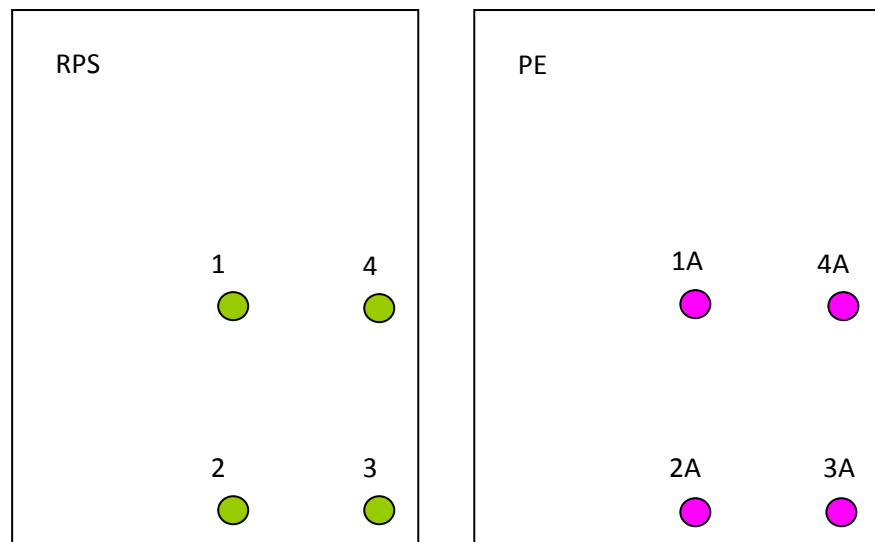
Figure 4.22: Thermocouple positions within the RPS and PE foam-lined coolboxes

Figure 4.23: Thermocouple positions within the PE foam-lined coolbox (prior to sealing)

Figure 4.24: Packed goods within the RPS foam-lined coolbox (prior to sealing)

The coolboxes were placed in the environmental chamber set at 25 °C which was monitored throughout the tests by means of an extra thermocouple placed outside the boxes. The relative humidity was measured at between 60% and 65% during the tests. All thermocouples were connected to a LABTECH digital interface which was set to monitor the thermocouples once per minute, providing high resolution results. Figure 4.25 shows the setup in the environmental chamber.

Figure 4.25: Set-up of laboratory tests in the environmental chamber

4.3.3.3 Transit trials

As part of the case study, two transit trials of the RPS and PE foam lined coolboxes were conducted in order to reinforce the findings of the laboratory tests as previously described in section 4.3.3.2 and to test the RPS foam in a functional, commercial application. In the transit trials the coolboxes were shipped by road over a 24 hour period in order to replicate a realistic transit situation. For these transit trials the dimensions of coolboxes and thicknesses of the RPS and PE foam liners remained unchanged from the specifications previously given in section 4.3.3.1.

4.3.3.4 First transit trial

One PE foam-lined 6 kg coolbox and one RPS foam-lined 6 kg coolbox (details of each coolbox as previously given), were each packed with two ice sheets chilled to 5 °C which were used as alternative product loads. The ice sheets were wrapped in bubble-wrap and then sandwiched between two additional ice sheets cooled to -18 °C used as refrigerants. Miniature temperature data-loggers known as *Tinytags* were inserted inside the boxes next to the chilled product to monitor the core product temperature, and on the outer edge of the product to monitor temperature in the airspace between the product and the coolbox insulation. The Tinytags were programmed to monitor temperatures every 10 minutes and were calibrated prior to insertion. Figure 4.26 shows the packed RPS-lined coolbox prior to sealing and shipping.

Figure 4.26: Packed RPS-lined coolbox prior to sealing and shipping

Table 4.5 gives details of the coolbox packing procedure and probe locations.

Table 4.5: Details of coolbox packing procedure

Insulated Container	1 x RPS foam-lined 6 kg coolbox (with internal corrugated fibreboard liner). Total liner gauge: 29mm
	1 x PE foam-lined 6 kg coolbox. Total liner gauge: 29mm
Product Load	2 x ICES012 ice sheets wrapped in bubblewrap
Product Conditioning	Stored and stabilised at 5°C
Cooling Media	2 x ICES012 500g ice sheets
Quantity of cool charges and positioning	1 x ice sheet under + 1 x ice sheet above product load
Cooling Media Conditioning	Frozen and stabilised at -18°C
Product Temp Probe location	Outer edge + core
Cooling Media Temp Probe Location	None

The packed coolboxes were shipped by road from Hydropac, High Wycombe, Bucks. to Brunel University, Uxbridge, Middx. at ambient temperatures over a 24 hour period. On arrival at Brunel University the coolboxes remained stored at ambient temperatures overnight before return shipment by road to Hydropac Ltd.

4.3.3.5 Second transit trial

Due to the issue of refrigerants coming into proximity of data-loggers and causing them to register sub-zero temperatures in the first transit trial, a second transit trial was conducted to improve the validity of the data and to extend the parameters to be studied.

Although 6 kg shippers as previously described were used for these trials, the second transit trial differed from the first transit trial in the following respects:

a) In order to test the resistance and durability of the RPS foam to moisture and condensation no internal corrugated fibreboard liner was used within the RPS coolbox, the interior of which is shown in Figure 4.27.

Figure 4.27: The unlined RPS coolbox

b) 2 kg of sausages chilled to 3° C were used as the product loads. Figure 4.28 shows the packed RPS coolbox prior to sealing showing the location of temperature monitor.

Figure 4.28: Packed RPS coolbox prior to sealing showing the location of temperature monitor

c) The focus of temperature monitoring with Tinytags was the outer edge airspace between the packed product and the insulation which constitute "hot spots" in the coolbox. Tinytags were also located on the outside of the boxes to monitor the ambient temperature. Figure 4.29 shows both coolboxes sealed and ready for commencement of the second transit trial.

Figure 4.29: Sealed coolboxes prior to the second transit trial

Table 4.6 gives details of the coolbox packing procedure for the second transit trial.

Table 4.6: Details of coolbox packing procedure (second transit trial)

Insulated Container	1 x RPS foam-lined 6 kg coolbox (no internal corrugated fibreboard liner). Insulation gauge: 26mm
	1 x PE foam-lined 6 kg coolbox. Insulation gauge: 29mm
Product Load	2kg chilled sausages in each coolbox
Product Conditioning	Stored and stabilised at 3° C
Cooling Media	2 x ICES012 500g ice sheets in each coolbox
Quantity of cool charges and positioning	1 x ice sheet under + 1 x ice sheet above product load
Cooling Media Conditioning	Frozen and stabilised at -18°C
Product Temp Probe location	Outer edge + ambient
Cooling Media Temp Probe Location	None

4.4   Acoustic tests

In order to determine the potential for starch foams to be used in applications in which a degree of acoustic attenuation may be required, CBL and RPS foams were tested for airborne sound absorption coefficient and airborne sound transmission loss in the audible frequency range of 50 – 6,400 Hz. In addition, two polymer foams, one of which is designed for specialist acoustic applications were also subjected to the same tests in order to serve as benchmarks against which the starch foams could be compared. All acoustic tests were conducted using the facilities at Bruel & Kjaer UK Ltd, Stevenage, Hertfordshire, UK.

Three different densities of CBL and two densities of RPS starch foams were tested for sound absorption coefficient and sound transmission loss. High-Density RPS was made by compressing single layers of RPS foam to approximately 5mm thick before bonding the layers together.

Two 'benchmark' polymer foams were also tested. These were ET 21/250, a load bearing open-cell polyurethane foam produced by the Vita Group with a density of 19 kg/m^3, and Basotect ^{TM}, a specialist acoustic open-cell foam made from melamine resin and produced by BASF with a density of only 8 kg/m^3. These foams were selected as benchmarks for testing due to their open-cell structures. Low-density open-cell PU foams such as ET 21/250 are known to possess good acoustic properties, whilst the specialist acoustic foam Basotect $^{(TM)}$, was expected to out-perform all other foams subjected to the tests.

Two cylindrical samples of different diameters were cut from each material in order to fit into devices designed to characterise sound in different frequency ranges. Samples of 100mm diameter were used to test a frequency range of 50 – 800 Hz, whilst samples of 29mm diameter were used to test a frequency range of 800 – 6,400 Hz. Since these acoustic tests are non-destructive, the same samples were used for testing sound absorption coefficient and sound transmission loss.

All samples were made to a thickness of 40mm. Since both sound absorption coefficient and sound transmission loss measurements are dependent on the thickness of the material being tested, this dimension was selected to represent that typically found in some acoustic attenuation applications. Table 4.7 shows specification details of the samples tested for sound absorption coefficient and sound transmission loss.

Table 4.7: Specifications of samples tested for sound absorption coefficient and sound transmission loss

Material	Density (kg/m^3)		
RPS	26		
High Density RPS	68		
CBL	50	86	110
ET21	19		
Basotect $^{(TM)}$	8		

Various acoustic test methods and standards exist, however all acoustic tests on materials are based on how a sample will modify the acoustic environment. The following sections describe sound absorption coefficient and sound transmission loss coefficient tests.

The standards governing sound absorption coefficient tests is covered in ISO 15034-2, *Determination of sound absorption coefficient and impedance in impedance tubes – Part 2 transfer function method*, and ASTM E1050.

The standards governing sound transmission loss tests are covered in ASTM E90 *Standard test method for laboratory measurement of airborne sound transmission loss of building partitions*. Sound transmission loss is also covered in the standard ASTM E2249 and ASTM E336. The corresponding ISO standard is ISO 140/111 *Laboratory measurement of airborne sound insulation of building elements* (NRC Canada). Other methods exist such as that defined by the Society of Automotive Engineers (SAE) in the standard SAE J1400.

These standards cover the testing of sound transmission loss in reverberation rooms. However, implementing such test methods reliably requires large and expensive test chambers and in many situations in which sound transmission loss testing is necessary but infrequent, this space and cost burden is unacceptable. For this reason, the use of a modified impedance tube comprising four microphones for testing sound transmission loss has been implemented and validated by several studies including those conducted at Michigan Tech University by Barnard & Rao (Barnard & Rao, 2004). Although the application of this method is widespread in acoustic testing, at the time of writing no standards currently exist for the testing of sound transmission loss using impedance tube equipment.

4.4.1 Airborne sound absorption coefficient test

(Two microphone transfer function/impedance tube method)

Sound absorption coefficient can be defined as the ratio of the sound energy absorbed by a medium to the incident sound energy upon its surface. Figure 4.30 shows a schematic representation of the two microphone impedance tube test equipment used to test sound absorption coefficient as specified by ISO 15034-2 and ASTM E1050.
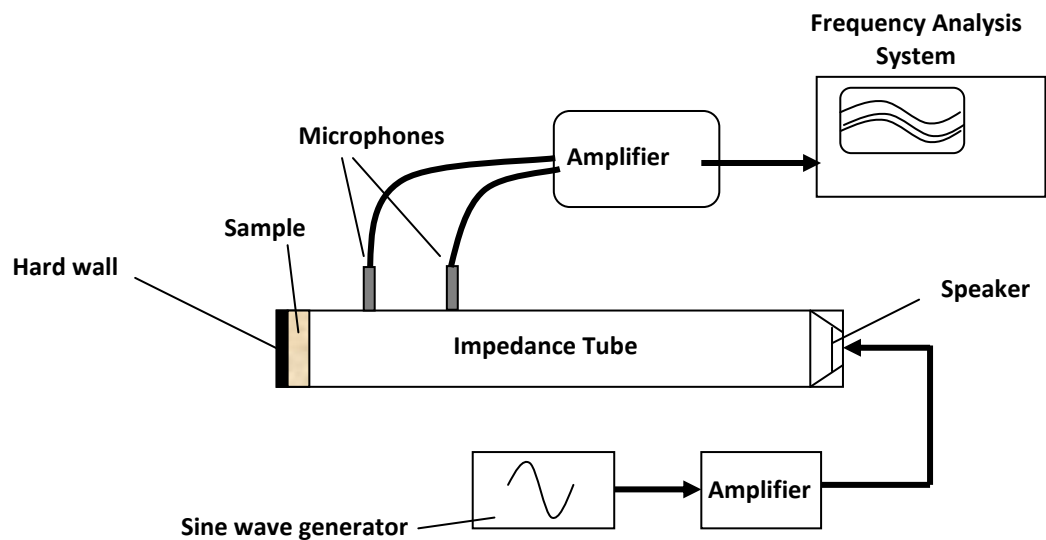
Figure 4.30: Schematic representation of sound absorption coefficient test equipment (Transfer function / impedance tube method ISO 15034-2 & ASTM E1050)

Acoustic sine waves at the specified frequency range are generated, amplified and emitted from a speaker positioned at one end of the impedance tube. The sample tested is positioned at the other end of the impedance tube directly in front of an acoustic hard wall - a non-absorbing material. The frequencies produced by the sine wave generator and emitted from the speaker consist of *random broadband noise* – all audible frequencies at varying amplitudes within the frequency range of 50Hz – 6400 Hz. These sound waves propagate as plane waves inside the tube and given a sufficient time period the equipment would generate all frequencies at all amplitudes.

As shown in Figure 4.31, sound waves travelling towards the sample strike the sample at normal incidence - perpendicular to the sample. In other variations of sound absorption coefficient tests, sound waves may strike the sample at random incidence. However such tests require reverberation room equipment.
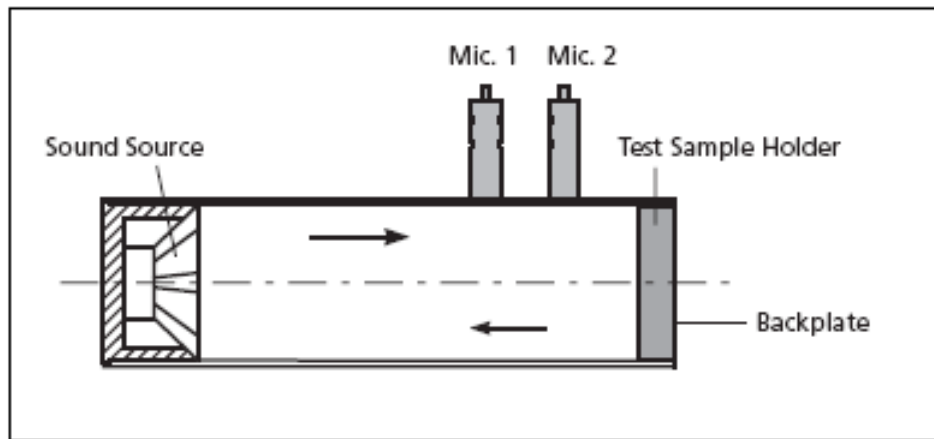
Figure 4.31: Schematic representation of the impedance tube for the two-microphone transfer-function method
Brüel& Kjær

After striking the sample any sound energy not absorbed by the sample is reflected, by the hard wall behind. Depending on the way in which the sample has modified the acoustic environment, particular sound frequencies will be absorbed or reflected in varying degrees. The propagation, contact and reflection result in a standing-wave interference pattern due to the superposition of forward and backward travelling waves inside the tube. By measuring the sound pressure at two fixed locations and calculating the complex transfer function using a two-channel digital frequency analyzer, it is possible to determine the sound absorption and complex reflection coefficients and the normal acoustic impedance of the material (Brüel &Kjær, 2008).

From the known incident sound power level and the proportion of the sound energy reflected towards the microphones, the Brüel& Kjær PULSE software is able to calculate the ratio of the sound energy absorbed by the sample to the incident sound energy upon its surface at any given frequency in the range tested.

In impedance tube tests, lower working frequencies are limited by the resolution of the speaker and analysis system as well as the distance between the microphones. Upper working frequencies are limited by the cross-section of the impedance tube and the spacing between the microphones. Microphone spacing can be set closer to increase the resolution of high frequency measurements or set further apart for the accurate measurement of low frequencies. Fixed microphone spacing is therefore a compromise.

Brüel& Kjær impedance tube type 4206 was used for all absorption coefficient tests conducted on samples given in Table 4.6. Figures 4.32 and 4.33 show type 4206 large tube and small tube setups.

Figure 4.32: Brüel& Kjær impedance tube type 4206, large tube set-up
Brüel& Kjær

Type 4206 large-tube setup comprised a 100mm internal diameter impedance tube and measured parameters in the frequency range from 50 Hz to 800 Hz. In the large-tube setup, the large extension tube (as shown on the right in Figure 4.32), was coupled to the main tube and the sample holder or backplate was mounted directly at the open end of the large extension tube as illustrated.

Figure 4.33: Brüel& Kjær impedance tube type 4206, small tube set-up
Brüel& Kjær

Type 4206 small-tube setup comprised a 29mm internal diameter impedance tube and measured parameters in the frequency range from 800 Hz to 1.6 kHz. In the small-tube setup, the small extension tube (as shown on the right in Figure 4.33), was coupled to the open end of the large tube which contained the loudspeaker. The sample holder was mounted in the small tube as illustrated.

Sound absorption loss test equipment included couplers for mounting microphones flush with the inside of the impedance tubes. These coupled the microphones to the sound field in the tube and prevented both leakage and obstructions that would otherwise cause measurement error. Measurements were made with 1/4" Condenser Microphones Type 4187, designed to reduce errors due to pressure leakage at high frequencies (Brüel &Kjær, 2008).

Impedance tube diameters and microphone spacings were as follows:

Large tube diameter: 0.1m

Microphone spacing: 0.05m

Distance to sample from microphones: 0.1m and 0.15m

Small tube diameter: 0.029m

Microphone spacing: 0.02m

Distance to sample from microphones: 0.035m and 0.37m.

4.4.2   Airborne sound transmission loss test
(Four-microphone transfer-function/impedance tube method)

Sound transmission loss can be defined as sound energy transmitted through a medium, divided by the incident sound energy upon that medium and expressed in decibels (dB).

In situations in which reverberation room equipment cannot be used to test for airborne sound transmission loss, impedance tubes can be used. However, as yet there are no accepted ISO or ASTM standards for this method. Figure 4.34 shows a schematic representation of the sound transmission loss test equipment used.
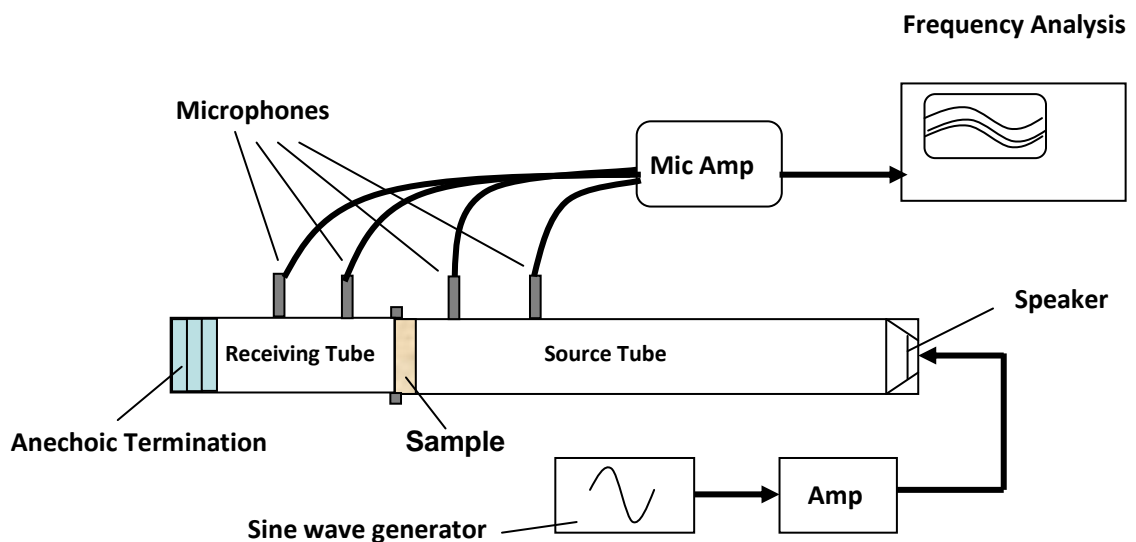
Figure 4.34: Schematic representation of sound transmission loss test equipment

The impedance tube equipment used to test for sound transmission loss is similar to that used to test for sound absorption coefficient as previously described. However, an extension to the impedance tube and two additional microphones are fitted.

Acoustic sine waves at the specified frequency range are generated, amplified and emitted from a sound source (loudspeaker) which is mounted at one end of the impedance tube (source tube). At the other end of the source tube a sample is mounted in a sample holder. As shown in Figure 4.35, the loudspeaker emits sound waves, which strike the sample at normal incidence (A), perpendicular to the sample. A proportion of the sound energy is reflected back into the source tube (B), whilst a proportion of the sound energy is either absorbed by the material or passes through the sample to the receiving tube (C). The portion of the sound energy passing through the sample then encounters the end of the receiving tube where a proportion of that energy is reflected (D), and some is absorbed by the anechoic termination which consists of several layers of sound absorbing material.
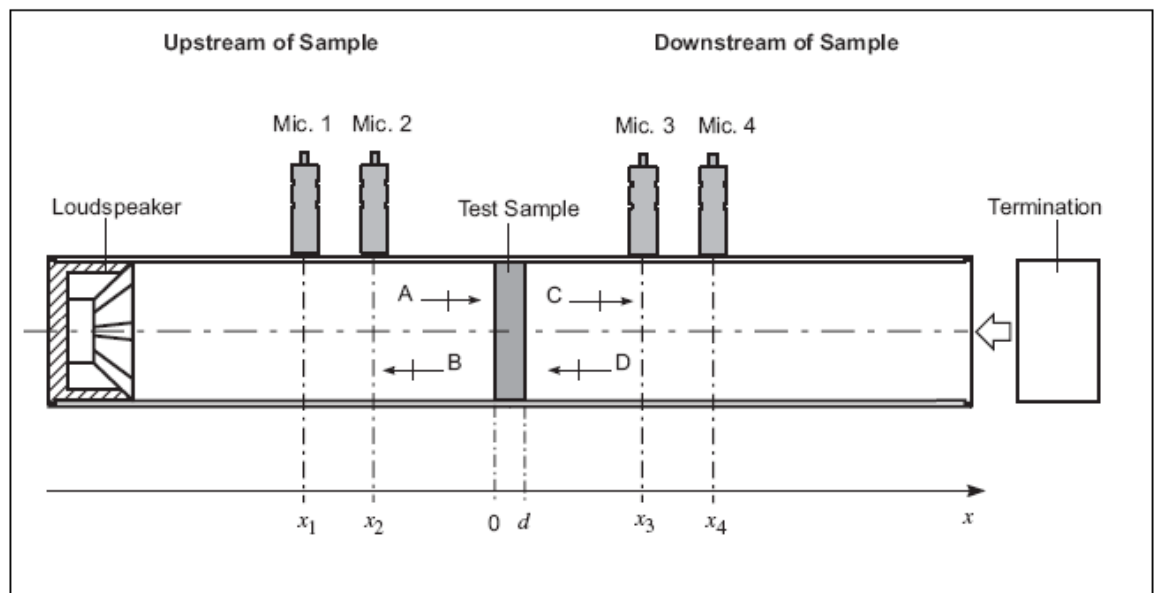
Figure 4.35: Schematic representation of the transmission loss impedance tube for the four microphone transfer function method
Brüel& Kjær

By measuring the sound pressure at four fixed locations, two in the source tube (x_1 and x_2) and two in the receiving tube (x_3 and x_4), and calculating the complex transfer function using a four-channel digital frequency analyzer, it is possible to determine the transmission loss of the material. The usable frequency range depends on the diameter of the tube and the spacing between the microphone positions (Brüel &Kjær, 2008).

Figures 4.36 and 4.37 show the large and small sound transmission loss impedance tube setups (Type 4206-T), which were used to measure airborne sound transmission loss at frequency ranges of 50 Hz to 800 Hz and 800Hz to 6.4 kHz respectively.

Figure 4.36: Large sound transmission loss impedance tube setup (Type 4206-T)
Brüel& Kjær

Figure 4.37: Small sound transmission loss impedance tube setup (Type 4206-T)
Brüel& Kjær

Transmission loss test equipment included couplers for mounting microphones flush with the inside of the tubes. These coupled the microphones to the sound field in the tube and prevented both leakage and obstructions that would otherwise cause measurement error. Measurements were made with 1/4″ Condenser Microphones Type 4187, designed to reduce errors due to pressure leakage at high frequencies (Brüel &Kjær, 2008).

Impedance tube diameters and microphone spacings were as follows:

Large tube diameter: 0.1m

Microphone spacing: 0.05m

Distance to sample from microphones: 0.1m and 0.15m

Small tube diameter: 0.029m

Microphone spacing: 0.02m

Distance to sample from microphones: 0.035m and 0.37m.

Chapter 5   The Mechanical Properties of CBL & RPS Starch-Based Foams

The vast majority of foam products must conform to certain physical performance criteria and as such the foams from which these products are made must be specified in terms of their behaviour under certain conditions including characterisation of their mechanical properties.

This chapter is separated into four main subdivisions relating to the characterisation of mechanical properties, based on tests conducted on CBL starch foams. These include: static compression, dynamic Impact, creep and tensile properties, the results of which should provide a basis for the full specification of these materials in terms of their mechanical properties. In each subdivision, the results of characterisations are then compared to previously published data or data from commercial sources relating to petrochemical-based polymer foams of similar densities. These comparisons were conducted in order to form a better understanding of the areas in which the new materials may find applications as alternatives to commercially available polymer foams. Where library data was unavailable, samples of conventional polymer foams were obtained and subjected to the same mechanical tests for direct comparison.

In addition, the results of compression and creep tests conducted on starch foam samples condition and tested at high temperature and relative humidity are also presented. Analysis of the results includes the use of scanning electron microscopy and X-ray diffraction techniques.

5.1   Results of compression tests

Stress-strain curves are an extremely important graphical measure of a material's mechanical properties. The engineering measures of stress and strain are determined from the measured load and deflection using the original specimen cross-sectional area and thickness. When the stress is plotted against the strain an engineering stress-strain curve is obtained (Roylance, 2001).

A selection of stress-strain curves from the static compression tests conducted on CBL samples of varying average densities are shown in Figure 5.1 which illustrate the various zones or regimes of foam deformation as described in Chapter 2 (section 2.4.1).

An Investigation into the Properties of Starch-Based Foams
Chapter 5. The Mechanical Properties of CBL & RPS Starch-Based Foams

152
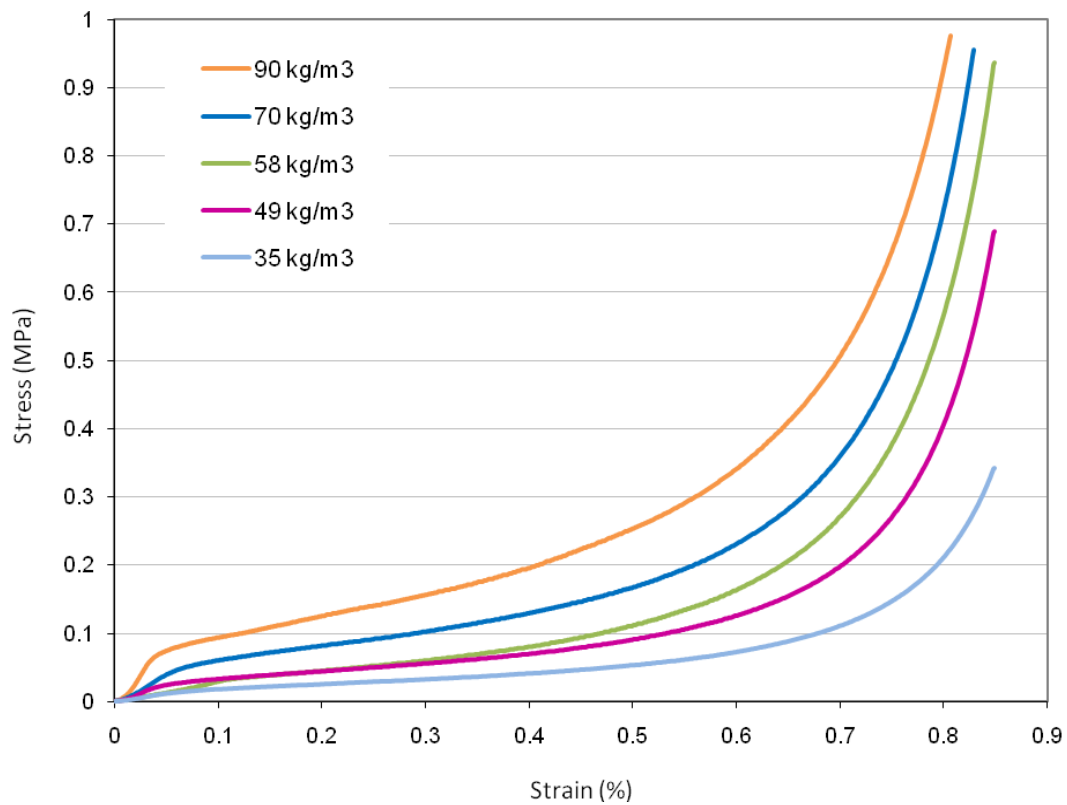
Figure 5.1: Selected stress-strain curves from static compression tests of CBL foams

Several properties of foam materials can be derived from compression tests. These include:

- Yield strength - the point at which cell walls within foams buckle as characterised by the elastic/plastic transition zone in the stress/strain curve.

- Compressive strength - stress at predetermined strain levels.

- Compressive elastic modulus - a measure of foam stiffness in the elastic region.

As cell walls within the foams collapse under compression, the elastic-plastic transition zone at which the initial linear-elasticity phase of the stress-strain curve develops into the plateau phase provides the basis at which the yield strength of the foams is determined. This is the point of stress at which material strain changes from elastic deformation to plastic deformation, causing it to deform permanently (CES, 2009). Figure 5.2 shows the yield strength of a range of CBL foams tested according to their average densities.

An Investigation into the Properties of Starch-Based Foams
Chapter 5. The Mechanical Properties of CBL & RPS Starch-Based Foams

153
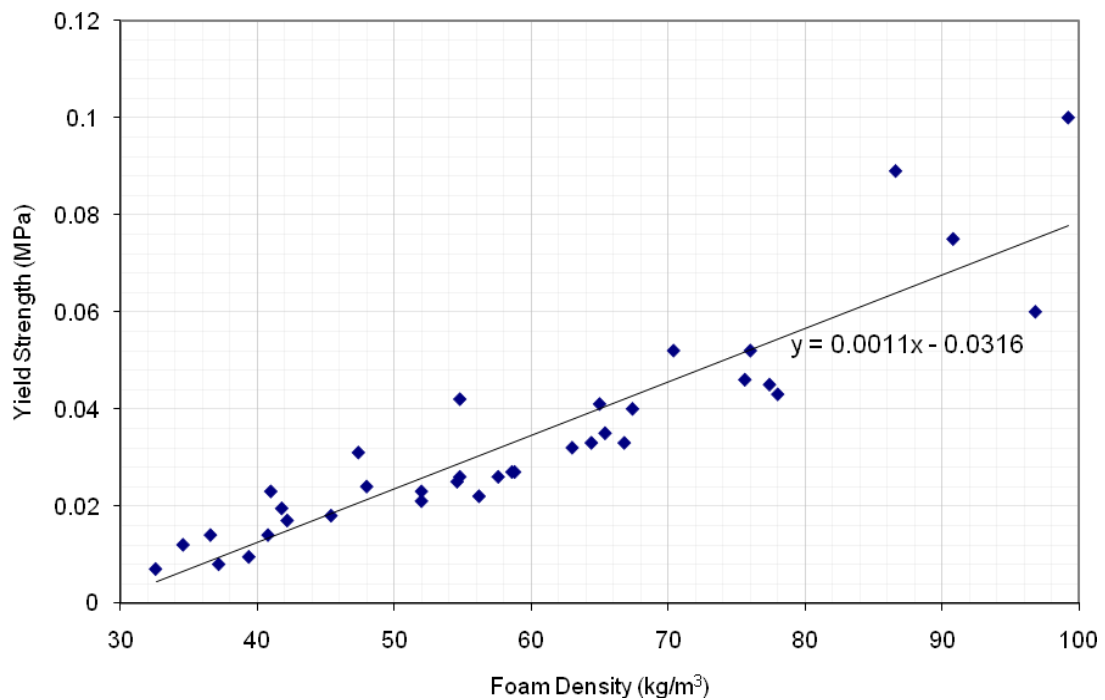
Figure 5.2: Variation of yield strength of CBL foams according to foam density (trendline generated by linear regression)

5.1.1   Interpretation of compression test results

Figure 5.2 indicates a clear correlation between the density of CBL foam and its yield strength. An increase in the yield strength of CBL foam samples was observed according to the increased density of samples tested.

The yield strength of foams under compression is a function of their linear elasticity, which is itself governed by particular mechanisms depending on whether the cells are open or closed (Gibson & Ashby, 1997). In their simplified model, Gibson & Ashby describe the deformation mechanism of open-cell foam structures. The mechanisms which contribute to the linear-elastic response of open-cell foams are schematically shown in Figure 5.3 in response to a uni-axial stress *F*. They occur as subsequent but overlapping phases with varying degrees of significance depending on the particular foam. At low relative densities open-cell foams deform primarily as a result of cell wall bending.

As the relative density of the foam increases, the contribution to deformation by simple extension and compression of cell walls or struts becomes more significant. In contrast to closed-cell foams, fluid flow between the cells of an open-cell foam generally only contribute towards its elastic modulus if the fluid has a high viscosity or if the strain rate is exceptionally high (Gibson & Ashby, 1997).

An Investigation into the Properties of Starch-Based Foams
Chapter 5. The Mechanical Properties of CBL & RPS Starch-Based Foams

154
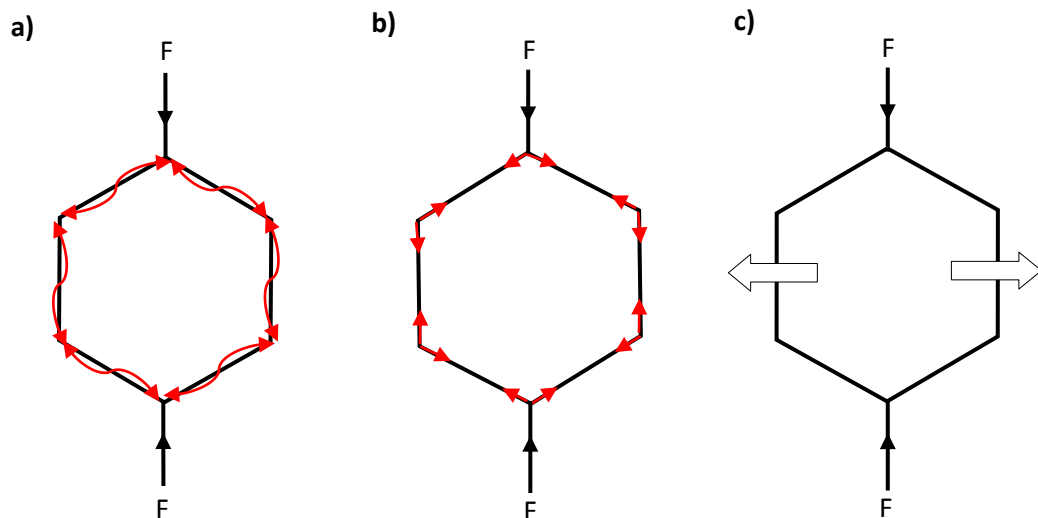
Figure 5.3: Schematic representation of mechanisms of linear-elastic deformation in open-cell foams
  a)   Cell wall bending
  b)   Cell wall axial deformation
  c)   Fluid flow between cells
  Adapted from Cellular Solids – Structure and Properties, 2nd Edition, Gibson & Ashby 1997

Open-cell foams are modelled by Gibson & Ashby in their most basic form as a cubic array of members of length ℓ with square cross-sections of thickness t. Adjoining cells are staggered so that their members meet at their midpoints.

Figure 5.4 shows the cubic model demonstrating cell edge bending in open-cell foams during linear-elastic deformation. The elastic modulus for the foam is calculated from the linear-elastic deflection δ of a beam loaded at its midpoint by a load *F*. *Standard beam theory* (Timoshenko & Goodier, 1970), is used to demonstrate that when subject to uni-axial stresses, deformation during the linear-elasticity zone of low-density open-cell plastic-elastic foams occurs primarily as a result of axial cell strut bending as cell edges (struts lying perpendicular to the applied stress), transmit a force resulting in bending of the cell edges (Gibson & Ashby, 1997).

An Investigation into the Properties of Starch-Based Foams
Chapter 5. The Mechanical Properties of CBL & RPS Starch-Based Foams

155
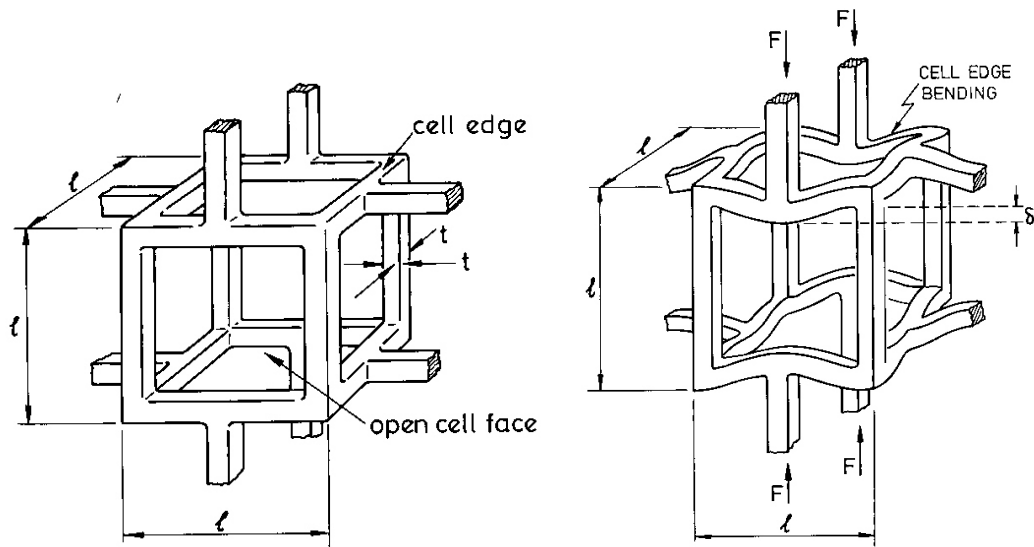
Figure 5.4: Cubic model showing cell edge bending in linear-elastic deformation of an open-cell
Cellular Solids – Structure and Properties, 2nd Edition, Gibson & Ashby 1997.

Elastic modulus is a measure of the resistance of a material to be deformed elastically (non-permanently) when subjected to a stress. The elastic modulus of a material is defined as the gradient of the linear-elastic deformation zone of its stress/strain curve and represents a constant ratio of stress and strain. Figure 5.5 below shows the elastic modulus of CBL foams according to density.
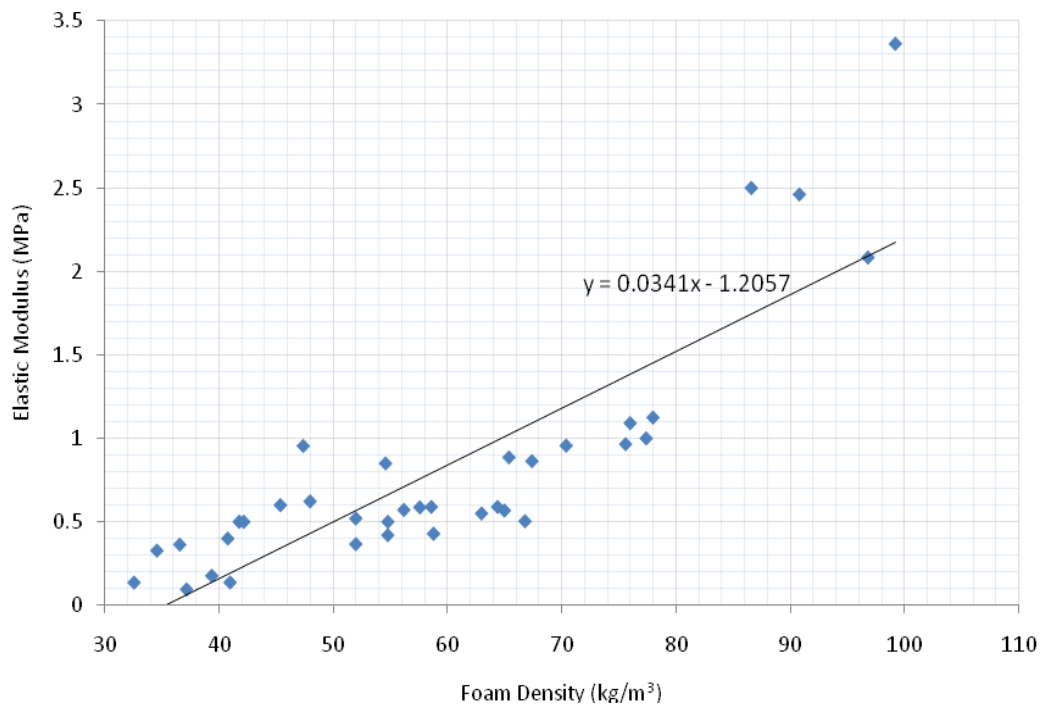
Figure 5.5: Variation of elastic modulus of CBL foams according to foam density (trendline generated by linear regression)

As with most polymeric foam materials, elastic modulus under compression is in part a function of foam density. Figure 5.5 indicates a clear correlation between the density of CBL foam and its elastic modulus. An increase in the elastic modulus of CBL foam samples was observed according to the increased density of samples tested.

At greater strains represented by the crush-plateau zone on the stress/strain curve, deformation is still elastic and thus recoverable to some degree. However, this deformation occurs as non-linear elastic buckling of cell walls or struts lying along the axis of the applied stress (Gibson & Ashby, 1997). Figure 5.6 shows non-linear elastic buckling of an open-cell in addition to the linear-elastic cell strut bending previously described in Figure 5.4.
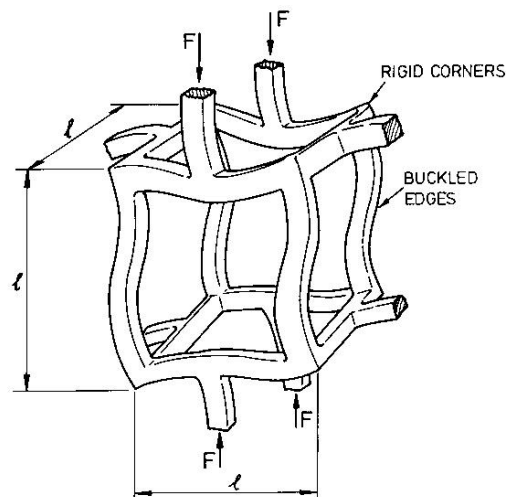
Figure 5.6: Cubic model showing additional cell edge buckling in non-linear elastic deformation of an open-cell *Cellular Solids – Structure and Properties, 2nd Edition, Gibson & Ashby 1997.*

Cell shapes in real foams are more complex than the Gibson & Ashby models propose and although alternative models are provided to account for anisotropic foams for example, it should be borne in mind that these are also simplified models. Nevertheless, if the cells of foams such as CBL (which feature a significant proportion of open-cells), behave by such mechanisms in response to applied stresses, their properties can be better understood using dimensional arguments which omit all constants arising from specific cell geometries (Gibson & Ashby, 1997).

Reviewing the shape of a typical static compression stress/strain curve for an elastic-plastic foam shown in Figure 5.7 below, it can be observed that this differs in some respects from stress-strain curves for CBL foams previously given in Figure 5.1.

An Investigation into the Properties of Starch-Based Foams
Chapter 5. The Mechanical Properties of CBL & RPS Starch-Based Foams

157
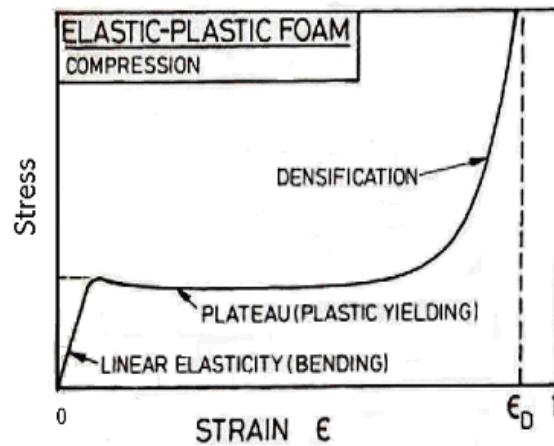
Figure 5.7: Typical deformation behaviour of an elastic-plastic foam
Cellular Solids – Structure and Properties, 2nd Edition, Gibson & Ashby 1997.

This is illustrated by a less pronounced *plateau zones* in the stress-strain curves for of CBL foams as compared to those of typical elastic-plastic foams. In the case of CBL foams the plateau zones are far more inclined with less distinct regime transformations into the subsequent *densification zones*, indicating a hardening of the foams as stress in increased. An initial analysis using the Gibson & Ashby model represented in Figure 5.6, may suggest that the non-linear elasticity of CBL is significantly reduced by more limited buckling moments of cell edges when compared to typical elastic-plastic foams. However, it seems more likely that this characteristic is influenced by the dense macrostructures of the CBL foams and this inference is supported by previous compression tests conducted on starch-based RPS foams (Chapter 2, Figure 2.28), in which the arrangement and orientation of the foam macrostructure played a significant role in determining the stress-strain profiles of the samples tested.

In other respects too, the results of the compression tests conducted on CBL foams may differ from that predicted by the Gibson & Ashby model due to specific microstructure and macrostructure features of this starch-based foam. Previous research into the microstructure of extruded starch foams from which CBL foams are fabricated has found widespread variation in cell size and non-uniform cell shapes. Figure 5.8 provides a SEM image showing a cross-section of extruded foam alongside redrawn cell boundaries for the purposes of image analysis.

An Investigation into the Properties of Starch-Based Foams
Chapter 5. The Mechanical Properties of CBL & RPS Starch-Based Foams

158
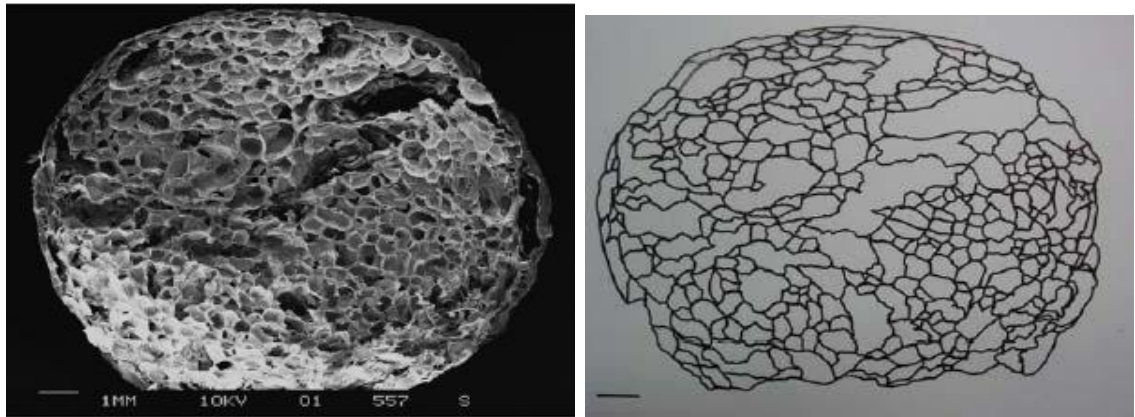
Figure 5.8: SEM image showing cross-section of extruded starch foam, alongside redrawn cell boundaries   *Kang, Y G (2006), Biodegradable Starch-Based Foam Block for Cushion Packaging (PhD Thesis)*

Figure 5.8 illustrates irregular cell shapes and cell size variation. Besides the widespread cell size variation shown in this cross-section, the larger voids shown were found to be elongated along the axis of the extrusion direction giving the starch foam extrudate anisotropic characteristics (Kang, 2006).

The other factor which may differentiate the behaviour of CBL foams from the Gibson & Ashby model is the density variation within CBL foams from compression and bonding of loosefill chips which results in a macrostructure of irregular, dense interfaces (previously discussed in Chapter 3). Whilst the high-density macrostructure of CBL foams may assist their compression strength performance, the effects of the foam macrostructure on the compression behaviour of CBL may be seen in the distribution of yield strength values previously shown in Figure 5.2. As the density of tested CBL samples are increased, the results show a greater distribution of yield strength values away from the trendline. This apparent decrease in the consistency of results may be due to an increase in local density variation due to inadequate control during fabrication of the foams, resulting in increased non-uniformity of the macrostructure within higher density CBL samples.

Standard industry data from compression tests on polymeric foam materials includes compressive strength at specified levels of strain. Figure 5.9 show stresses on a range of CBL foams at 10%, 25% and 50% strain which are commonly specified for foams (CES, 2010), according to foam density.

An Investigation into the Properties of Starch-Based Foams
Chapter 5. The Mechanical Properties of CBL & RPS Starch-Based Foams

159
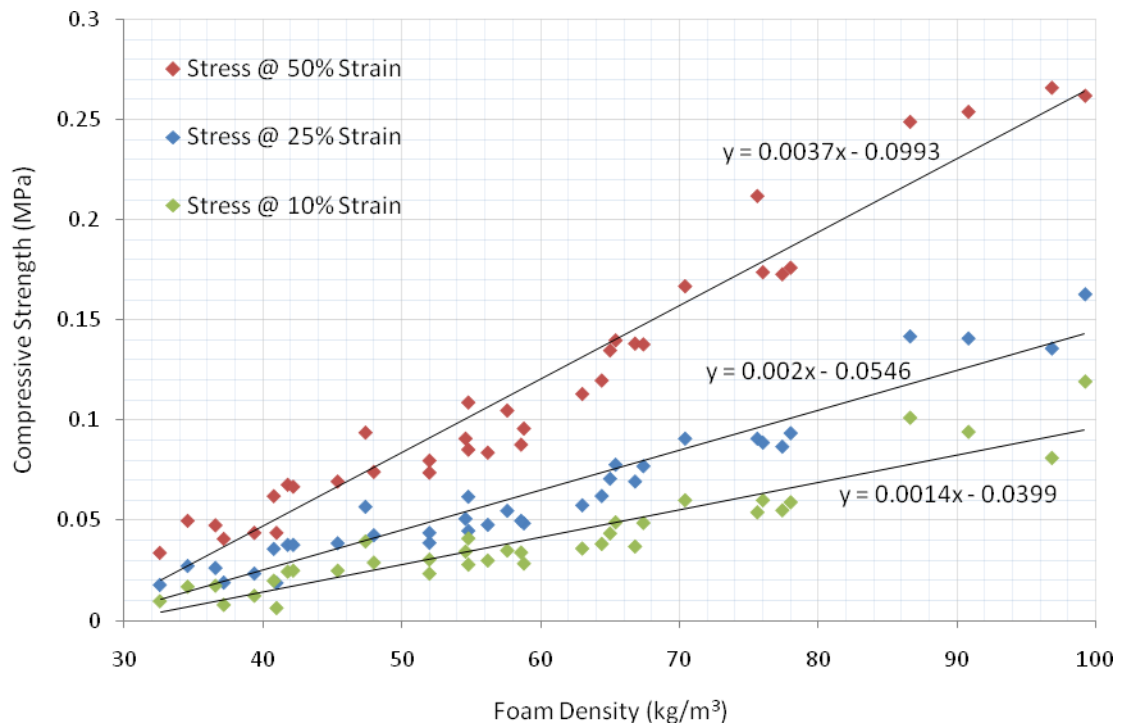
Figure 5.9: Compressive strength of CBL samples according to density at 10%, 25% and 50% strain (trendlines generated by linear regression)

As with most polymeric foam materials, compressive strength under given levels of strain is in part a function of foam density (Gibson & Ashby, 1997). Figure 5.9 indicates a clear correlation between the density of CBL foam samples and their compressive strengths at predetermined strain rates. An increase in the compressive strength of CBL foam samples was observed according to the increased density of samples tested, whilst greater levels of strain on individual foam samples also resulted in increased compressive strength.

An Investigation into the Properties of Starch-Based Foams
Chapter 5. The Mechanical Properties of CBL & RPS Starch-Based Foams

160

5.1.2 Compression performance - comparison with polymer foams

The results of the static compression tests are compared with published data for petrochemical-based polymer foams of similar densities. Figure 5.10 shows the yield strengths of RPS and CBL starch foams compared to petrochemical-based polymer foams of similar densities.
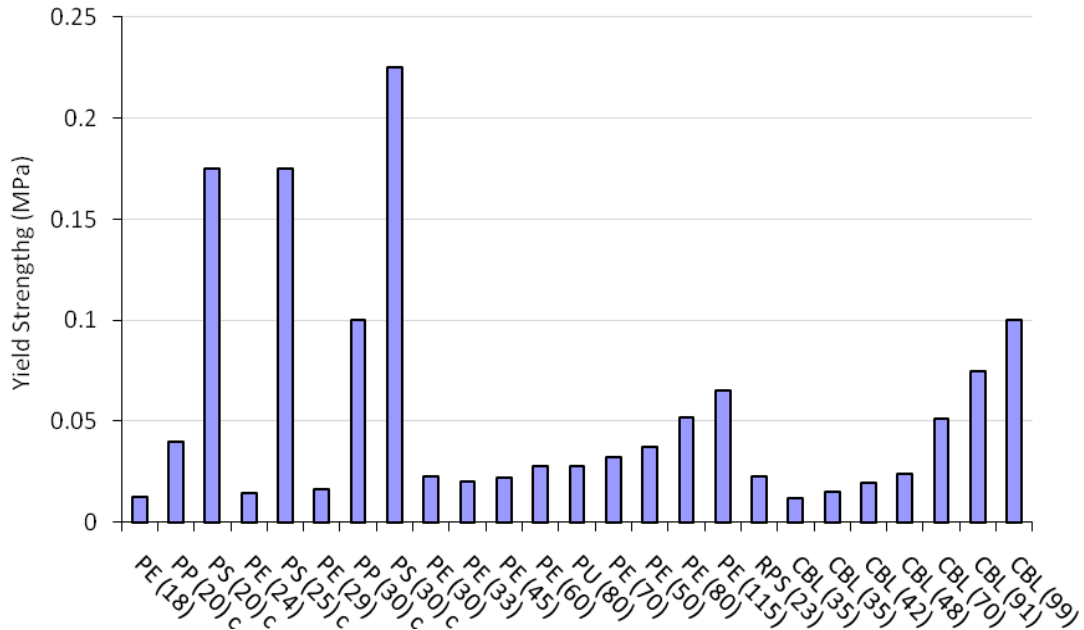
Figure 5.10: Comparison of yield strength of low/medium density foams

Key to Figure 5.10: All figures given in parenthesis refer to foam densities (kg/m^3).
C denotes closed-cell foams.

PE - Polyethylene foam
PP - Polypropylene foam
PS - Polystyrene foam
PU- Polyurethane foam
RPS - Regular Packing & Stacking starch foam
CBL - Compression Bonded Loosefill starch foam

Data for petrochemical polymer foams compiled from CES Edupack database (2008).
RPS data courtesy of Prof. Jim Song, Brunel University

The comparison of foams in Figure 5.10 indicates that the yield strengths of the starch-based foams are comparable to many grades of polyethylene and polyurethane, whilst the yield strengths of other grades of polyethylene, polypropylene and polystyrene are markedly higher. Figures 5.11 and 5.12 show the elastic modulus of a range of CBL foams compared to petrochemical-based polymer foams of similar densities.

An Investigation into the Properties of Starch-Based Foams
Chapter 5. The Mechanical Properties of CBL & RPS Starch-Based Foams

161
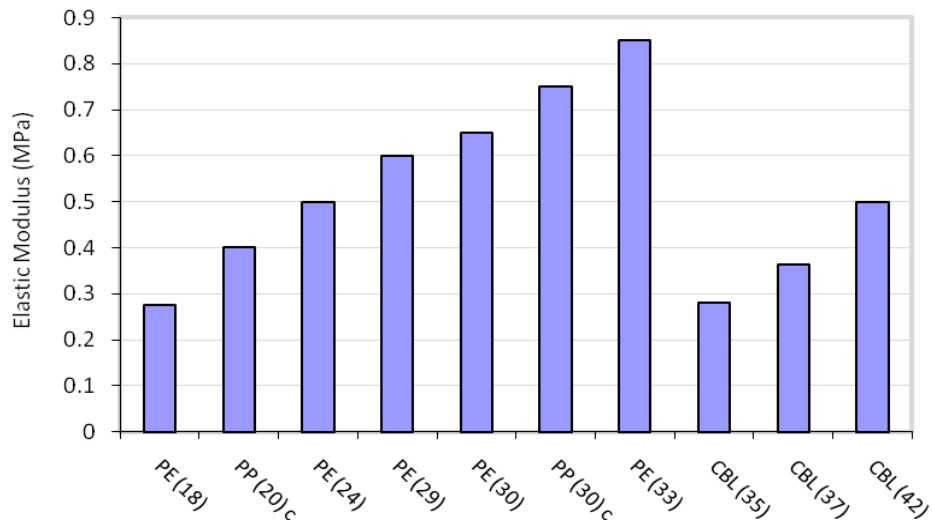
Figure 5.11: Comparison of elastic modulus of low density foams
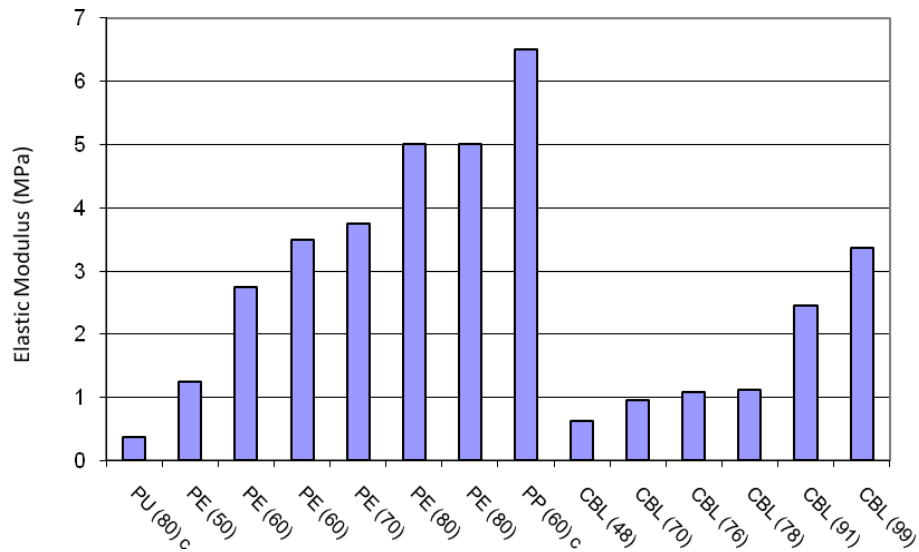
Figure 5.12: Comparison of elastic modulus of medium density foams

Key to Figures 5.11 & 5.12: All figures given in parenthesis refer to foam densities (kg/m^3).
C denotes closed-cell foams.
PE – Polyethylene foam
PP – Polypropylene foam
PU - Polyurethane Foam
CBL - Compression Bonded Loosefill starch foam
Data for petrochemical polymer foams compiled from CES Edupack database 2008

The comparison of elastic modulus given in Figure 5.11 and 5.12 clearly show that the elastic modulus of foams is in part dependent on foam density. With the exception of polyurethane foam, it can also be seen that the elastic modulus of CBL foams is generally lower than that of conventional polymer foams of similar densities.

An Investigation into the Properties of Starch-Based Foams
Chapter 5. The Mechanical Properties of CBL & RPS Starch-Based Foams

162

5.2   Results of dynamic impact tests

From the multiple dynamic impact tests conducted on each set of samples in the three density ranges, peak deceleration were plotted against static stresses on the samples as shown in Figures 5.13, 5.14 and 5.15. The figure headings show the average density of all samples tested in each density range.
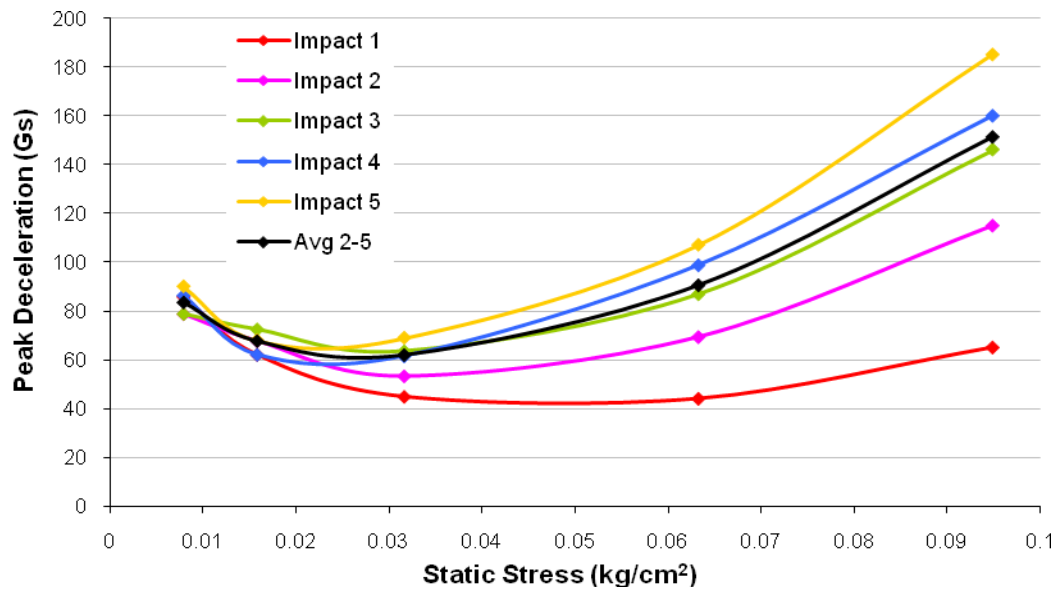
Figure 5.13: Multiple dynamic impact test results - CBL (43 kg/m³), drop height: 600mm
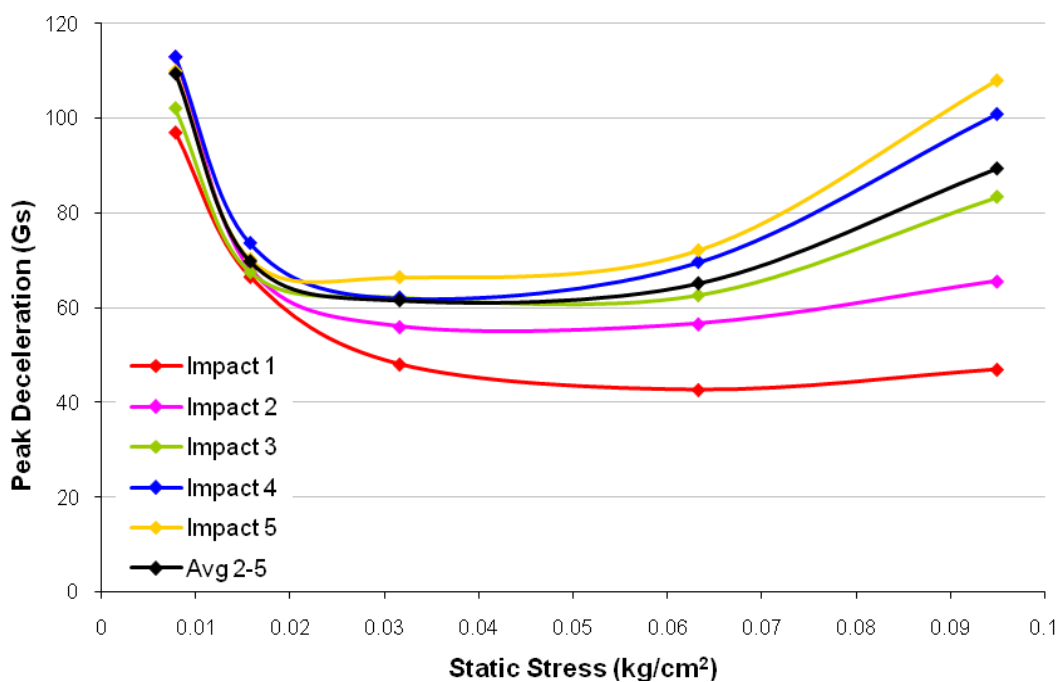
Figure 5.14: Multiple dynamic impact test results - CBL (61 kg/m³), drop height: 600mm

An Investigation into the Properties of Starch-Based Foams
Chapter 5. The Mechanical Properties of CBL & RPS Starch-Based Foams

163
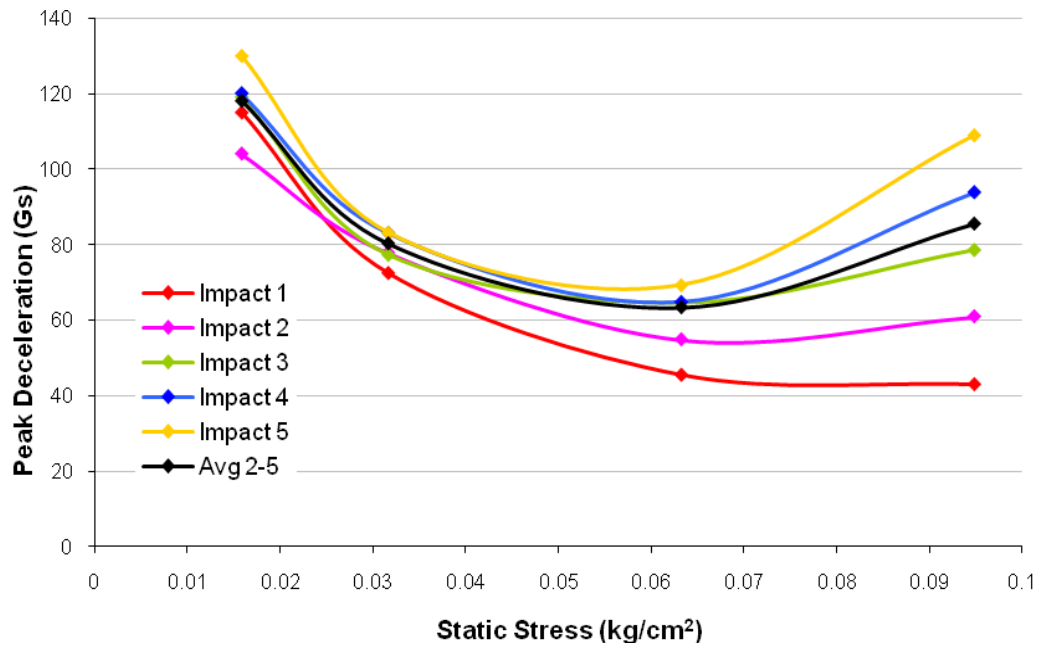
Figure 5.15: Multiple dynamic impact test results - CBL (80 kg/m³), drop height: 600mm

5.2.1 Interpretation of dynamic impact test results

Each cushion curve has a minimum peak deceleration value which illustrates the point of maximum cushion efficiency in terms of the energy absorption of the foam. As such, lower peak deceleration equates to greater energy absorption. An ideal energy absorbing foam would decelerate the entire range of stresses tested to minimum G values. However, whilst some energy absorbing foams may demonstrate low peak deceleration values at relatively broad ranges of static stresses, no ideal energy absorbing foam exists and peak deceleration will always vary with the level of static stress on the foam. This is a function of the softness or rigidity of the particular foam tested and is a key factor in the selection of foams for particular cushioning applications.

In Figures 5.13 – 5.15, the cushion curves generated for each density range demonstrated that peak deceleration varied with static stress. Figure 5.16 compares cushion curves from first dynamic impacts on the three densities of CBL foams tested.

An Investigation into the Properties of Starch-Based Foams
Chapter 5. The Mechanical Properties of CBL & RPS Starch-Based Foams

164
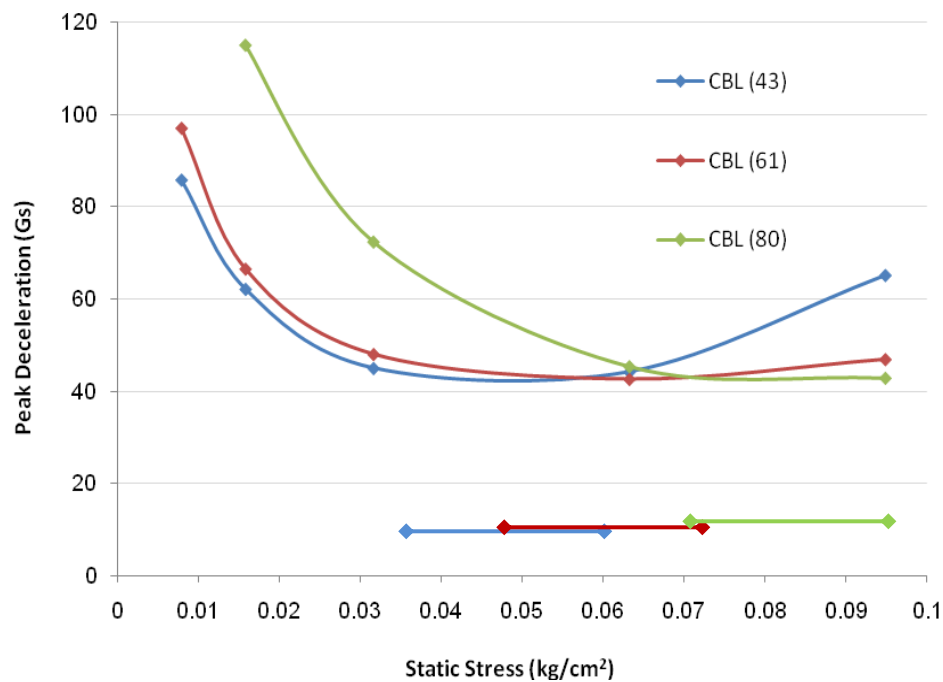
Figure 5.16: First impact cushion curve comparison - CBL (43, 61 & 80 kg/m³), drop height: 600mm (Bars show range of minimum static stresses for each foam)

By comparing the cushion curves generated from the first impacts on the three densities of CBL shown in Figure 5.16, it is possible to see that although peak deceleration does not vary significantly, as sample density increases there is a corresponding increase in static stress at minimum peak deceleration due to the increased rigidity of CBL foams at higher densities. In any practical cushioning application, the ideal range of static stresses that each foam is subject to from a single impact in order to achieve minimum peak deceleration from the drop height tested, are shown by the coloured bars corresponding to each density of CBL foam in Figure 5.16.

Figures 5.13 - 5.15 also demonstrated that repeated impacts on CBL foams resulted in increased peak deceleration values. As the cell walls of foams buckled in response to successive impacts they reached a level beyond which they could not recover and this loss of resilience reduced the cushion efficiency of the foams.

5.2.2   Dynamic impact performance - comparison with polymer foams

The dynamic impact test results for CBL foams can be compared with data for other conventional petrochemical-based polymer foams of similar densities which are typically used for cushion applications. The polymer foams used for this purpose were as follows:

- Ethafoam 220: closed-cell polyethylene foam with a density of 35.2 kg/m^3, manufactured by the Dow Corporation, USA. Applications include shock-absorption, vibration-dampening, insulation, buoyancy and cushioning components in packaging applications for loadings up to 17.5 kPa. (Quality Foam Packaging, 2010).

- Nopa Plank: polyethylene foams of two different densities - 35 kg/m^3 and 65 kg/m^3, manufactured by Pregis Corporation (Deerfield, IL, US). Applications include multiple shock and impact protection for sensitive and fragile items such as computers and electronis. (Pregis Corporation, 2010)

- Plastazote: nitrogen charged, cross-linked polyethylene foams of two different densities - 45 kg/m^3 and 70 kg/m^3, manufactured by Zotefoams plc (Croydon, Surrey, UK). Applications include packaging, protective padding in contact sports, automotive, health care and building (Zotefoams plc, 2010).

- Evazote: nitrogen charged, closed cell cross-linked copolymer foam with a density of 50 kg/m^3, manufactured by Zotefoams (Croydon, Surrey, UK). Evazote foams are generally tougher and more resilient than Plastazote foams. Applications include moulded or shaped impact absorbing components (Zotefoams plc, 2010).

Figures 5.17 and 5.18 compare the dynamic impact data (first impact and the average of 2nd-5th impacts respectively) for foams in the 35 – 50 kg/m^3 density range, whilst Figures 5.19 and 5.20 compare the dynamic impact data of foams in the 65 – 80 kg/m^3 density range.

An Investigation into the Properties of Starch-Based Foams
Chapter 5. The Mechanical Properties of CBL & RPS Starch-Based Foams

166
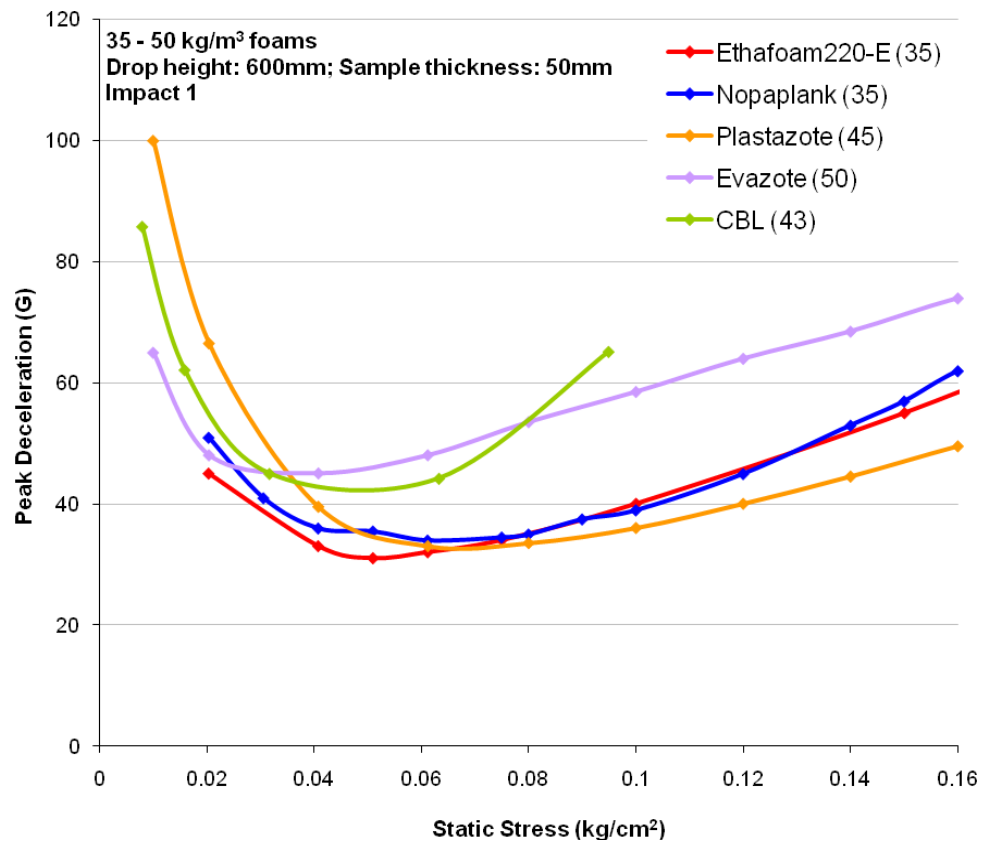
Figure 5.17: Comparison of 1st dynamic impact data for foams in 35 - 50 kg/m³ density range

Key to Figure 5.17: All figures given in parenthesis refer to foam densities (kg/m³).
Ethafoam220-E (35)
Nopaplank (35)
Plastazote (45)
Evazote (50)

Data for petrochemical polymer foams courtesy of James Wiles, Foam Engineers Ltd.

Figure 5.17 shows that for the first impact CBL (43) exhibits comparable peak deceleration values to the other polymer foams but at a slightly narrower range of static stresses at low to medium stress levels between 0.03 − 0.065 kg/cm². In practice this means that for cushion applications where protection against single shock is important, the CBL foam offers adequate cushion property within that particular range of static stresses. However, at higher stress levels Figure 5.17 shows that peak deceleration values of CBL foam rises, demonstrating that the CBL foam does not offer the cushioning performance of the polymer foams at those stress levels. This is due to the greater compressibility and reduced rigidity of CBL foams compared to these conventional polymer foams. In order to provide an equivalent performance either higher density or thicker CBL foams would be required.

An Investigation into the Properties of Starch-Based Foams
Chapter 5. The Mechanical Properties of CBL & RPS Starch-Based Foams

167
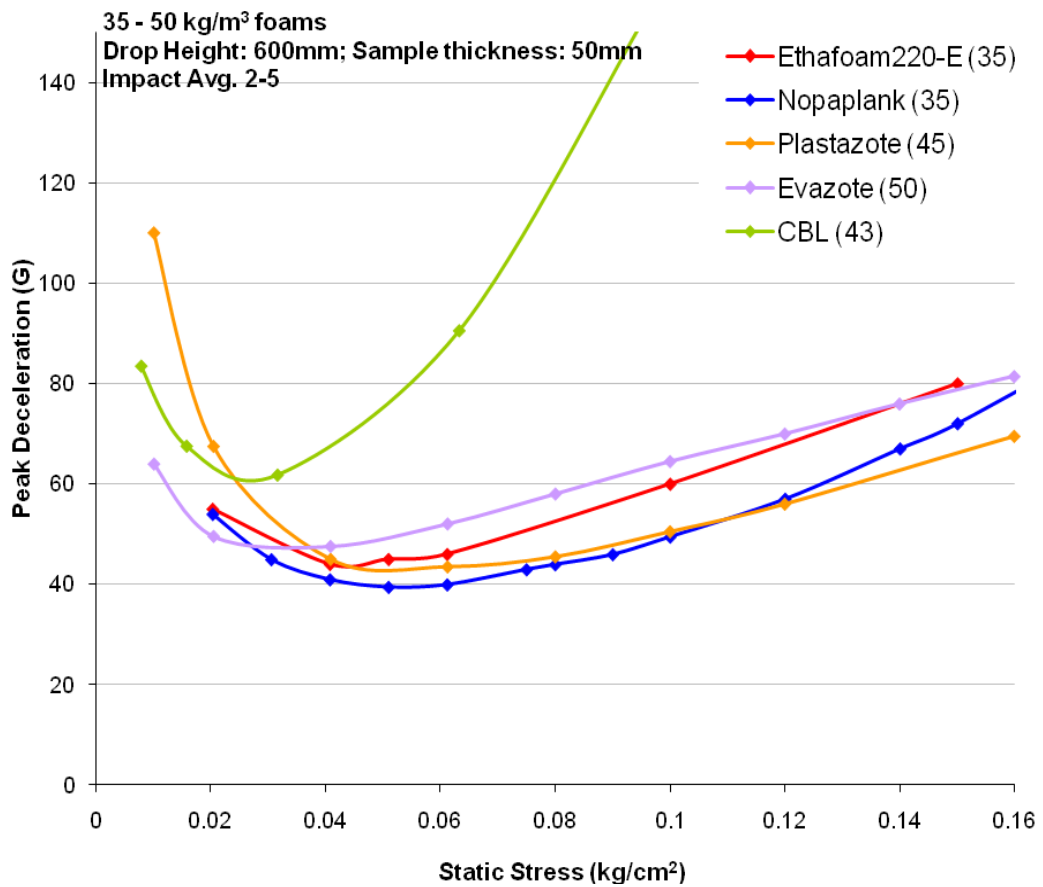
Figure 5.18: Comparison of 2nd - 5th dynamic impact data for foams in 35 - 50 kg/m^3 density range

> **Key to Figure 5.18:** All figures given in parenthesis refer to foam densities (kg/m^3).
> Ethafoam220-E (35)
> Nopaplank (35)
> Plastazote (45)
> Evazote (50)
>
> *Data for petrochemical polymer foams courtesy of James Wiles, Foam Engineers Ltd.*

Averaged cushion curves for impacts 2 – 5 shown in Figure 5.18 indicate that the peak deceleration for CBL (43) foam are higher but still comparable to the polymer foams at low static stresses below 0.03 kg/cm^2. At greater static stresses, successive impacts result in much higher deceleration values than those exhibited by the other polymer foams.

Figure 5.18 also demonstrates that repeated impacts on CBL foams result in increased peak deceleration values compared to the polymer foams used for comparison purposes. As cell walls of foams buckle in response to impacts they reach a level beyond which they cannot recover. This loss of resilience reduces the ability of the foam to recover in order to exhibit the required cushion efficiency to absorb the energy of successive impacts. Clearly in this respect starch-based CBL foams do not possess the resilience and recovery of the conventional polymer foams.

An Investigation into the Properties of Starch-Based Foams
Chapter 5. The Mechanical Properties of CBL & RPS Starch-Based Foams

168
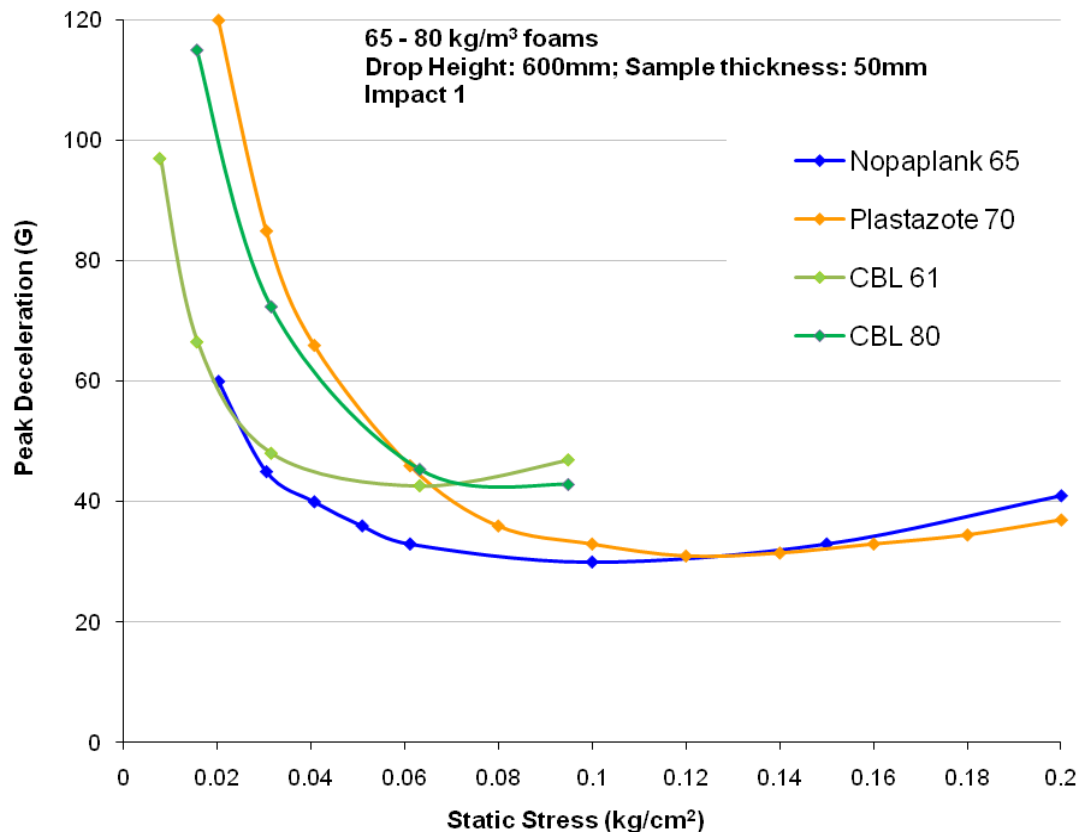
Figure 5.19: Comparison of 1st dynamic impact data for foams in 65 - 80 kg/m³ density range

Key to Figure 5.19: All figures given in parenthesis refer to foam densities (kg/m³).
Nopaplank (65)
Plastazote (70)

Data for petrochemical polymer foams courtesy of James Wiles, Foam Engineers Ltd.

The comparison of dynamic impact data in Figure 5.19 shows that Nopaplank (65) possesses the best cushion performance in terms of absorbing energy from the first impact across the broadest range of static stresses. CBL (61) foam exhibits lower peak deceleration values compared to Plastazote (70) foam in the low to medium stress range between 0.01 - 0.065 kg/cm². However, at higher static stresses the peak deceleration values of Plastazote (70) continue to fall, while at the same static stress level the peak deceleration values of CBL (80) begins to level off and for CBL (61) peak deceleration begins to rise.

This indicates relatively poor overall cushioning performance of CBL starch-based foams compared to the performance of the polymer foams examined. In practice this would mean that the cushioning applications of the CBL foam would be limited to the low to medium static stress range detailed above.

An Investigation into the Properties of Starch-Based Foams
Chapter 5. The Mechanical Properties of CBL & RPS Starch-Based Foams

169
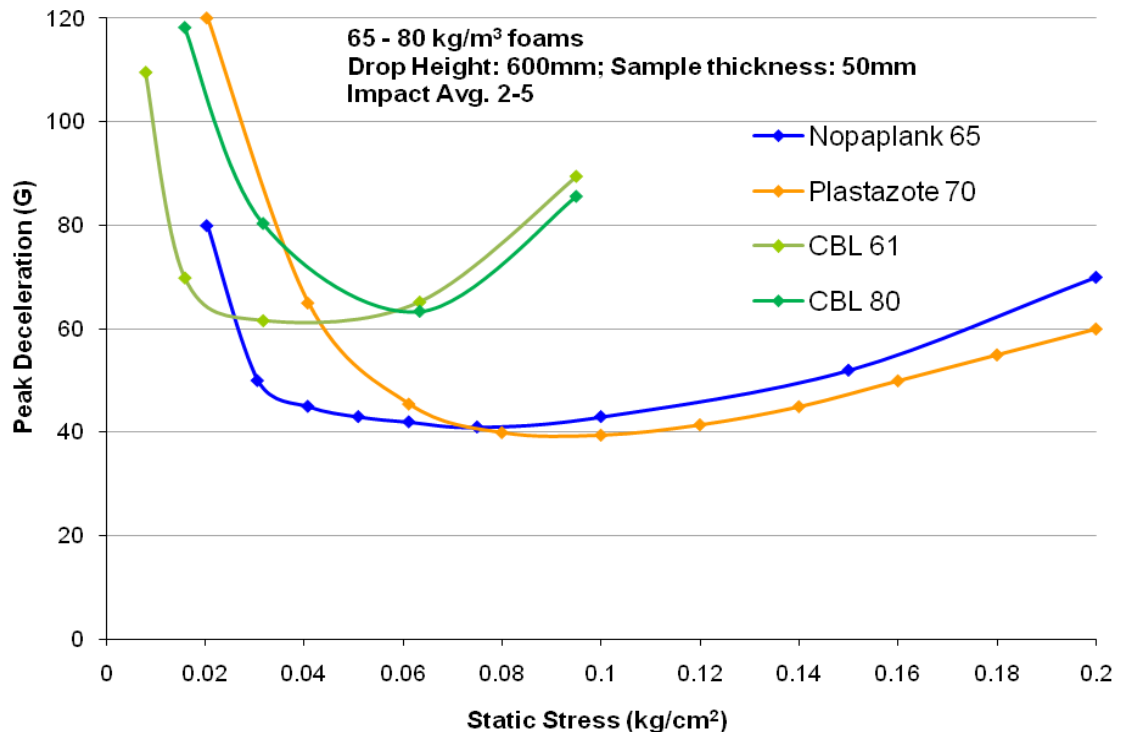
Figure 5.20: Comparison of 2nd - 5th dynamic impact data for foams in 65 - 80 kg/m^3 density range

Key to Figure 5.20: All figures given in parenthesis refer to foam densities (kg/m^3).
Nopaplank (65)
Plastazote (70)

Data for petrochemical polymer foams courtesy of James Wiles, Foam Engineers Ltd.

Similar trends are observed for the averaged cushion curves for impacts 2 - 5 shown in Figure 5.20. At lower stress levels below 0.04 kg/cm^2, CBL (61) and CBL (80) foams produced comparable cushioning performance to the other polymer foams and were able to demonstrate sufficient resilience to repeated impacts. However at higher stress levels repeated impacts raise deceleration values significantly for CBL foams, whilst at similar static stresses the polymer foams continue to exhibit lower peak deceleration values.

Although the elastic moduli of materials including foams is limited to describing their resistance to elastic deformation up to the point of yield, two categories of moduli may account for the greater elastic modulus of conventional polymer foams compared to starch-based foams of similar densities (as illustrated previously in Figures 5.11 and 5.12), which could contribute in part to the superior resilience and cushioning performance of the polymer foams shown in Figures 5.17 - 5.20 above.

1) *Material modulus* includes the elastic modulus of the solid material from which the cell walls or struts of the particular foam are made. Nopaplank and Plastazote foams are made from

An Investigation into the Properties of Starch-Based Foams
Chapter 5. The Mechanical Properties of CBL & RPS Starch-Based Foams

170

polyethylene and cross-linked polyethylene, which in their unfoamed solid forms have average elastic moduli of 1.08 GPa and 1.2 GPa respectively (CES Edupack, 2010).

This data can be compared to that of solid unplasticised starch film, reported to possess an elastic modulus of 3.15 GPa (Copeland et al, 2007). When viewed in the context of foam microstructures (cell walls or cell struts), the significantly lower elastic modulus of these polymers compared to solid starch cannot be a factor imparting the foams made from these conventional polymers with greater flexibility, resilience and energy absorption performance compared to starch-based foams.

2) The s*tructural modulus* of the foams including cell shapes, structure and topology (the connectivity of cell walls or struts, pore space and cell geometry), is the other factor which contributes toward their overall elastic modulus. In macro-composite foams such as CBL, both microstructure and macrostructure of the foam will influence the structural modulus of the foams.

One hypothesis in explaining the poor cushioning performance of CBL when compared to polymer foams may be that whilst the relatively uniform structure of conventional polymer foam will deform uniformly until it reaches the point at which the foam begins to "bottom out", voids and irregularities within the macrostructure of CBL foams results in compressive deformation to occur primarily at these areas of weakness, giving rise to poor resilience during repeated impacts. This inconsistent deflection may result in reduced overall cushion efficiency. Figure 5.21 shows a schematic representation of a cross-section of CBL foam illustrating the macrostructure of the foam which is characterised by irregular interfaces and large air pockets (in grey).
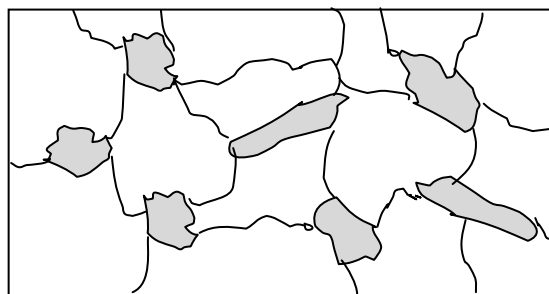
Figure 5.21: Schematic representation of the macrostructure of CBL foams

Another possibility for the reduced cushioning performance of CBL foams during repeated impacts, may be that on impact the inherent brittleness and reduced overall elastic modulus of starch foams results in a greater fracture of cell walls and increased compressive deformation occurring primarily in the portion of the foam closest to the site of impact (in this case the top

An Investigation into the Properties of Starch-Based Foams
Chapter 5. The Mechanical Properties of CBL & RPS Starch-Based Foams

171

portion of the sample), whilst the remainder of the sample at the base is not compressed by the force of impact. Partial deflection across the thickness of the sample would in effect produce a dynamic impact test result equivalent to that of a thinner sample being tested. Figure 5.22 illustrates a schematic representation of this hypothesis, which shows the deflected portion of the foam's cross section occurring in the darker shaded area.

impact direction

Deflected portion
Equivalent sample thickness
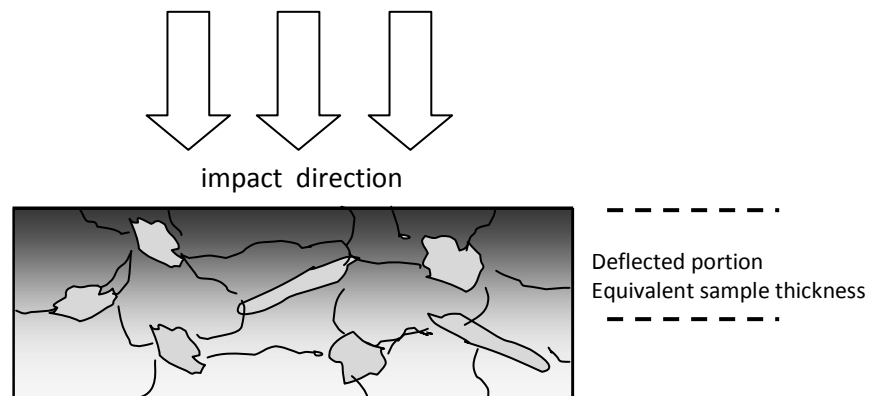
Figure 5.22: Schematic representation illustrating partial deflection hypothesis

The results of the dynamic impact tests have demonstrated that although peak deceleration does not vary significantly between different densities of CBL foams, as sample density increases there is a corresponding increase in static stress at minimum peak deceleration, due to the increased rigidity of CBL foams at higher densities. In any practical cushioning application this would limit the use of CBL foams to the particular range of stresses at which these foams were able to demonstrate cushion efficiency in terms of maximum energy absorption.

In comparison to the conventional polymer foams selected, the dynamic impact performance of CBL foams showed comparable peak deceleration values when subjected to initial impacts, but reduced cushioning performance when subjected to repeated impacts. It is possible that the inferior performance of CBL foams in comparison to the selected polymer foams results from a combination of their reduced overall resilience, as well as inherent material inconsistencies and partial deflection suppositions described above, but to what extent each factor may be responsible is currently unknown and obviously an area for further research.

An Investigation into the Properties of Starch-Based Foams
Chapter 5. The Mechanical Properties of CBL & RPS Starch-Based Foams

172

5.3   Results of creep tests

Figure 5.23 shows the creep performance of CBL foams of various densities.
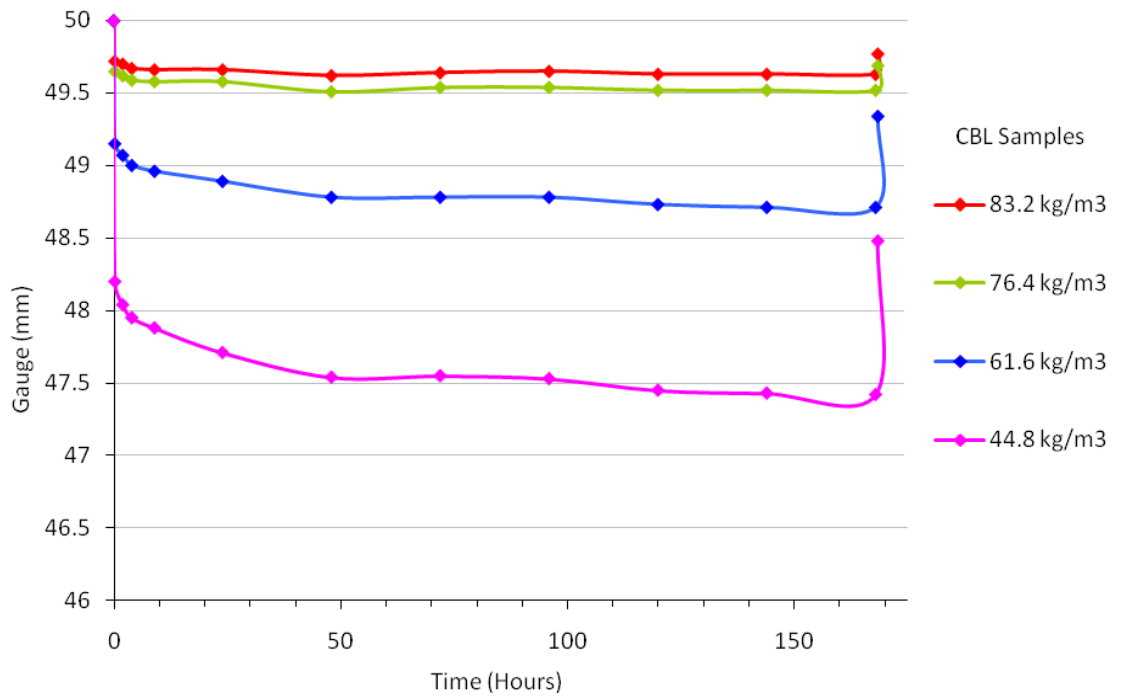
Figure 5.23: Creep gauge (sample thickness) as a function of time for CBL foams

5.3.1   Interpretation of creep test results

Figure 5.23 shows that in general, CBL foams of higher densities exhibited reduced creep deformation compared to CBL foams of lower densities. Figure 5.23 also indicates that the majority of creep deformation occurred within a relatively short time period at the beginning of the test and then stabilised to almost a constant sample thickness. Figure 5.24 below shows the initial 30 minutes of creep deformation in greater detail.

An Investigation into the Properties of Starch-Based Foams
Chapter 5. The Mechanical Properties of CBL & RPS Starch-Based Foams

173
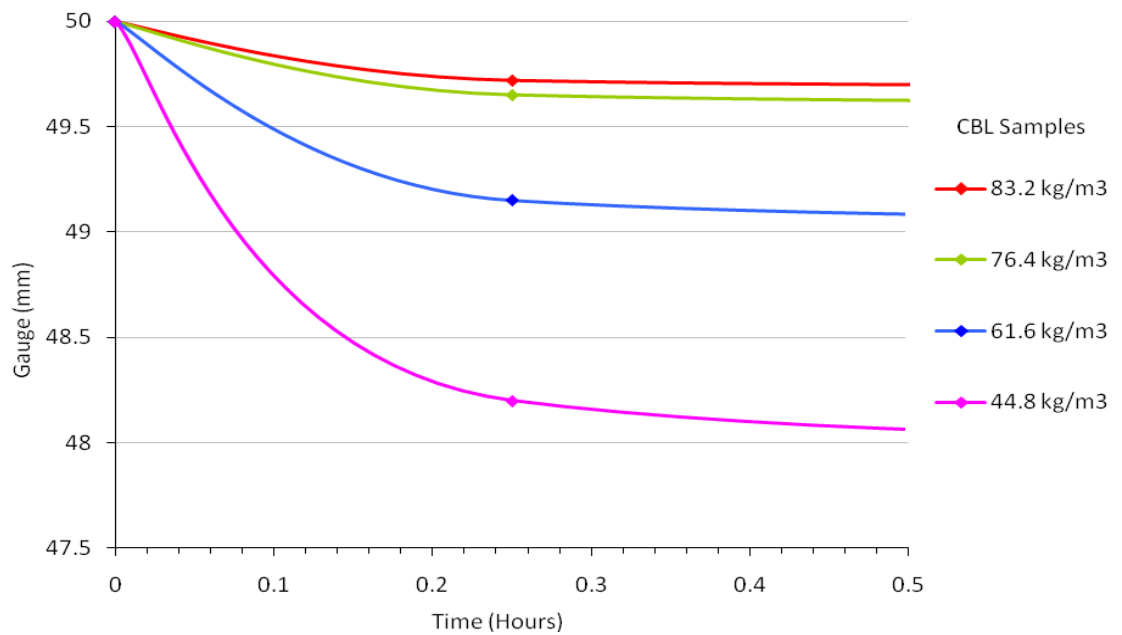
Figure 5.24 Creep gauge (sample thickness) as a function of time for CBL foams - initial 30 minutes

The recovery of deformation in CBL foam samples which occurred at the end of the creep test previously shown in Figure 5.23, was due to sample rebound as the load was taken off the sample during the final 30 minutes of the test. Table 5.1 summarises the creep behaviour of the CBL foam samples of different densities.

Table 5.1: Summary of the creep and recovery performance of CBL foam samples

Sample density (kg/m^3)	44.8	61.6	76.4	83.2
Start gauge (mm)	50	50	50	50
Final gauge before recovery (mm)	47.40	48.70	49.50	49.60
Creep deformation before recovery (%)	5.2	2.6	1.0	0.8
Final gauge post-recovery (mm)	48.48	49.34	49.69	49.77
Creep deformation post recovery (%)	3.0	1.3	0.62	0.46

Figures 5.23, 5.24 and Table 5.1 demonstrate that the creep performance of higher density CBL samples was superior to the lower density samples tested. Higher density foams generally exhibit increased levels of stiffness and therefore these results are to be expected. In percentage terms, the range of maximum creep deformation across the samples measured pre and post recovery (at 5.2% - 0.8% and 3% - 0.46% respectively), appear reasonable but will be evaluated against conventional polymer foams for the purposes of comparison.

An Investigation into the Properties of Starch-Based Foams
Chapter 5. The Mechanical Properties of CBL & RPS Starch-Based Foams

174

5.3.2   Creep performance - comparison with polymer foams

Figure 5.25 shows the results of creep deformation tests conducted on CBL foam samples of two different densities and a sample of RPS foam alongside the three polymer foam samples. For reasons of clarity, ETAS 40 which immediately "bottomed out" on commencement of the test beyond the measurable limits of the equipment is not shown in Figure 5.25.
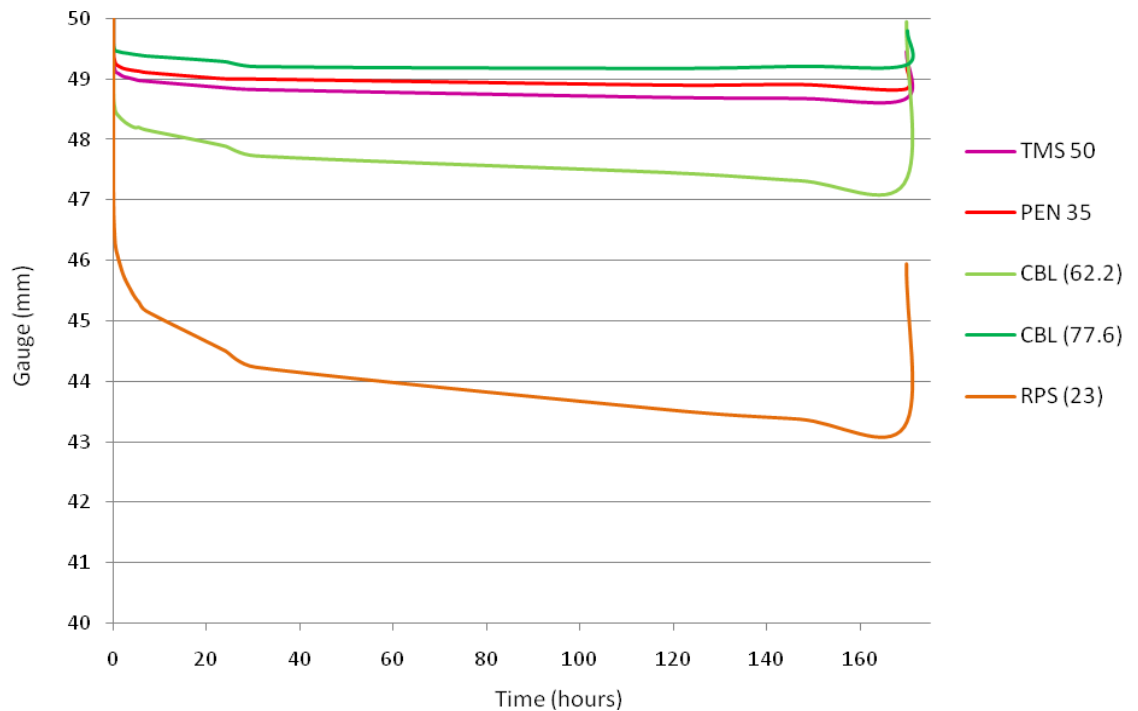
Figure 5.25 Creep performance of CBL and RPS starch-based foams compared to polymer foams

Table 5.2 summarises the creep behaviour of the samples tested.

Table 5.2: Summary of the creep and recovery performance of starch-based foam and conventional polymer foam samples

Samples and densities (kg/m^3)	ETAS 40	TMS 50	PEN 35	CBL (62.2)	CBL (77.6)	RPS (23)
Start gauge (mm)	50	50	50	50	50	50
Final gauge before recovery (mm)	*	48.66	48.83	47.27	49.23	43.24
Creep deformation before recovery (%)	*	2.68	2.34	5.46	1.54	13.52
Final gauge post-recovery (mm)	*	49.46	49.2	49.95	49.8	45.94
Creep deformation post recovery (%)	*	1.08	1.6	0.01	0.4	8.12

 * Sample immediately bottomed out beyond measurable limits of the equipment on commencement of the test.

An Investigation into the Properties of Starch-Based Foams
Chapter 5. The Mechanical Properties of CBL & RPS Starch-Based Foams

175

Figure 5.25 and Table 5.2 show that of the starch foam samples CBL (77.6) exhibited comparable creep performance to the polymer foams (PEN 35 and TMS 50), while despite its higher density, the creep performance of CBL 62.2 was relatively poor compared to the polymer foams. At a density of 23 kg/m^3, RPS foam exhibited inferior creep performance to the foams previously mentioned, but superior performance compared to ETAS 40 polymer foam which immediately "bottomed out" beyond the measurable limits of the equipment used. In general these tests show that starch foams have comparable creep performance when compared to certain polymer foams of similar densities.

Unlike the linear behaviour of foams in response to compression testing, creep testing produces a non-linear behaviour over time which gradually deforms cell walls or struts under constant loading. In this respect the high-density macrostructure of CBL foams may assist their creep performance.

An Investigation into the Properties of Starch-Based Foams
Chapter 5. The Mechanical Properties of CBL & RPS Starch-Based Foams

176

5.4   Results of tensile tests

Figure 5.26 shows a selection of stress-strain curves produced from the tensile tests conducted.
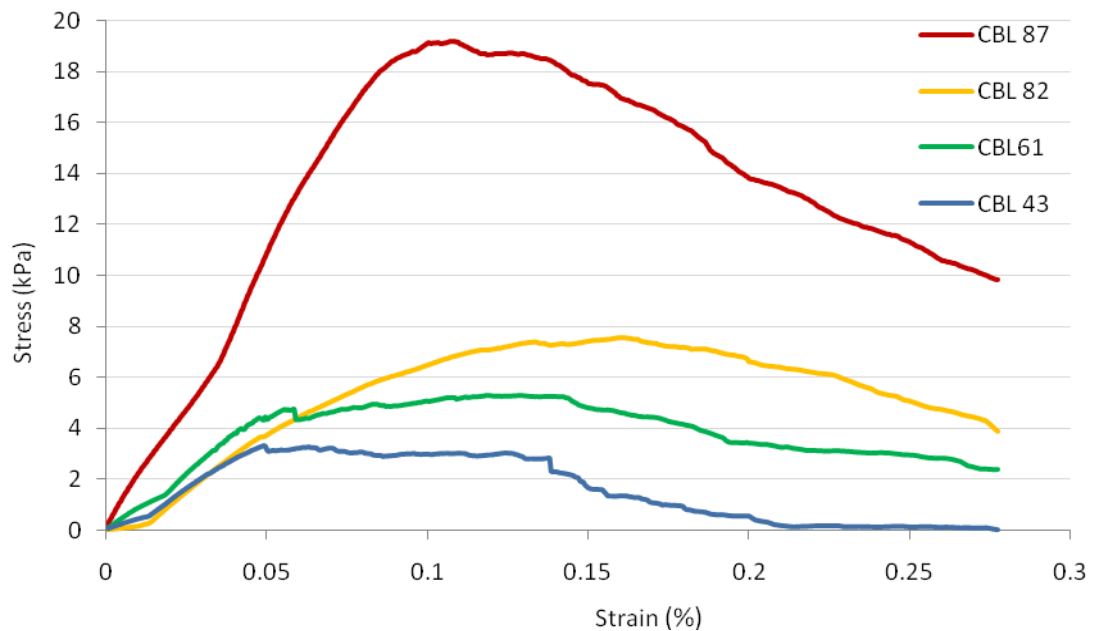
Figure 5.26: Stress-strain curves produced from a selection of tensile tests

As expected, Figure 5.26 shows that higher density CBL foam samples generally exhibited higher tensile strength (the peak stress in Figure 5.26), than lower density samples. This dependence of tensile strength on foam density is also confirmed by Figure 5.27 which incorporates all the tensile test results conducted.

An Investigation into the Properties of Starch-Based Foams
Chapter 5. The Mechanical Properties of CBL & RPS Starch-Based Foams

177
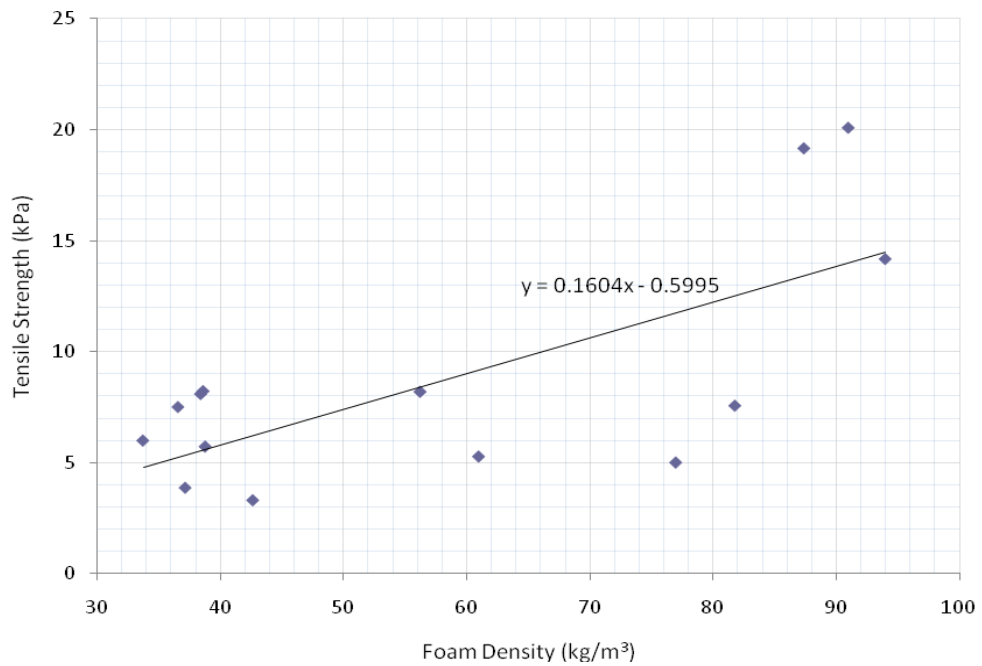
Figure 5.27: Tensile strength of CBL foams according to sample density (trendline generated by linear regression)

5.4.1   Interpretation of tensile test results

Although Figure 5.27 showed some correlation between sample density and tensile strength, the data is rather scattered. Compared to the results of previous mechanical tests conducted which showed much stronger correlations between the density of the material and particular mechanical properties, the correlation between foam density and tensile strength appears much weaker.

In tension, the small strain linear-elastic modulus of a foam with a relatively uniform cell structure is the same as that in compression and the moduli of open-cell foams are determined by cell edge bending. As strains increase the non-linear buckling of cell edges typically seen in compression cannot occur in tension. Instead, cell edges which initially lie at an angle to the tensile axis rotate towards the axis and the bending moment acting on them during the linear-elastic phase decreases. Figure 5.28 shows a schematic representation of the non-linear elastic alignment of cell edges under tensile loading (Gibson & Ashby, 1997).

An Investigation into the Properties of Starch-Based Foams
Chapter 5. The Mechanical Properties of CBL & RPS Starch-Based Foams

178
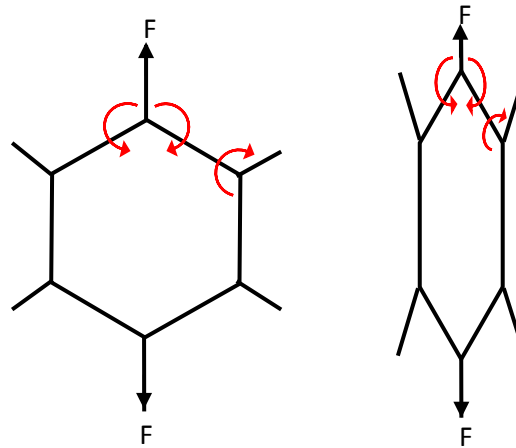
Figure 5.28: Schematic representation of non-linear elastic alignment of cell edges under tensile loading *Adapted from Cellular Solids – Structure and Properties, 2nd Edition, Gibson & Ashby (1997)*

A plastic foam with a relatively uniform cell structure generally yields in tension by the same mechanism and at essentially the same stress as in compression. Post-yield behaviour however, is quite different. In compression the rotation of cell walls or struts causes the bending moment to remain constant or even increase slightly, producing a long plateau phase on the stress-strain curve. In tension, rotation of cell edges during non-linear elasticity reduces the bending moment to approximately one-third of the strain, at which point the cell walls or struts are significantly aligned with the tensile axis as shown in Figure 5.28. Further strain then requires extension of the cell walls or struts themselves (Gibson & Ashby, 1997).

Brittle foams, which include most 'rigid' polymer foams, exhibit linear-elastic behaviour in tension right up to the point of fracture. *Brittle fracture* which occurs at the point of yield is quite different in tension from the gradual progressive crushing and collapse of cells which takes place in compression. In tension it occurs through the propagation of a single crack (Gibson & Ashby, 1997). Figure 5.29 shows a schematic representation of the propagation of a single crack through a brittle open-cell foam.

An Investigation into the Properties of Starch-Based Foams
Chapter 5. The Mechanical Properties of CBL & RPS Starch-Based Foams

179
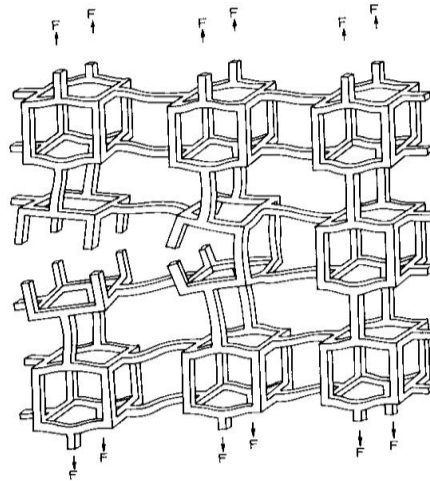
Figure 5.29: Schematic representation of the propagation of a single crack through a brittle open-cell foam *Cellular Solids – Structure and Properties, 2nd Edition, Gibson & Ashby (1997)*

However, the tensile behaviour of CBL starch-based foams is subject to a fundamental difference to the Gibson & Ashby model discussed above. Under tensile forces CBL samples will always separate at the interfaces between compressed and adhered loosefill chips, rather than separation through fracture of the foam which comprises the loosefill chips themselves. This phenomenon is shown in Figure 5.30.
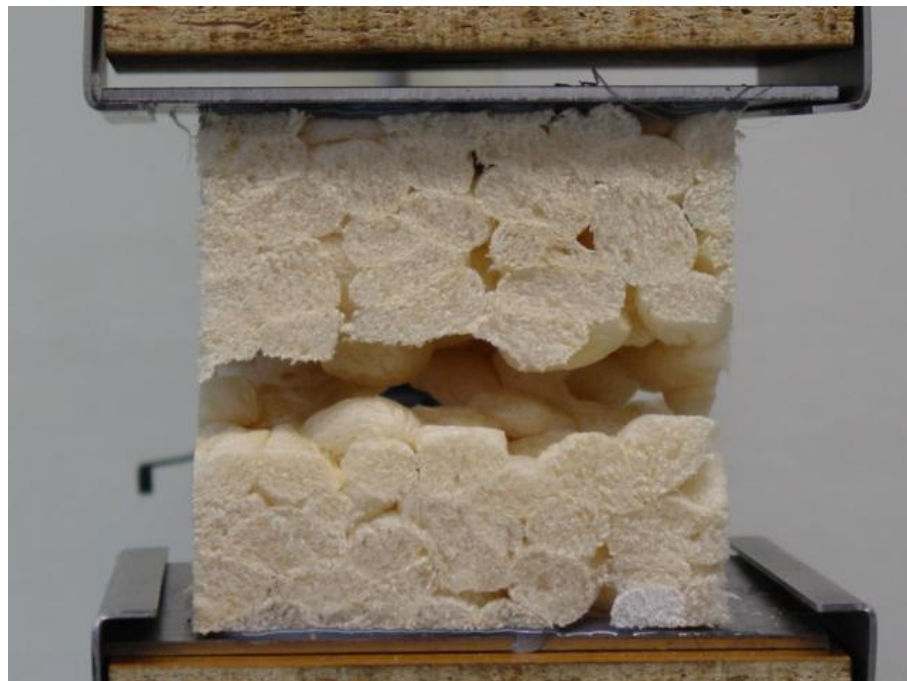
Figure 5.30: Macrostructure interface separation of CBL sample undergoing a tensile test

The tensile strength of materials is sensitive to flaws within samples and Figure 5.30 clearly shows the point of separation of a CBL foam sample under tensile forces occurred at the site of bonded interfaces between loosefill chips comprising the sample, rather than through brittle fracture of the cell walls or struts of the foam. This phenomenon may also explain the weak correlations found between tensile strength and the density of CBL samples tested.

The tensile test results given previously indicate that higher density CBL samples (created as a result of increased compression of wetted loosefill chips during fabrication as outlined in Chapter 3), will to some extent create stronger bonds between the internal interfaces of the material. The tensile strength of CBL is therefore to some degree a function of the strength of these interface bonds which in turn is dependent on the degree of compression during the CBL fabrication process. However, whilst the density of CBL may be modified as a consequence of variations in compression during fabrication, tensile test results indicate that this modification is largely the result of densification of the microstructure of the material and does not render the interface bonds between loosefill chips with bonding strength proportional to its density. Thus the macrostructure network of CBL will always represent weak points within the foam with respect to tensile and possibly shear forces.

It should be noted that although this macrostructure network represents weak points within the foam with respect to tensile forces, irregularities in the macrostructure in terms of flaws such as small air pockets, larger voids and irregular orientation of loosefill chips, produce much inconsistency and result in the weak correlations and the scattered tensile data illustrated.

In order to further analyse these results, the *elongation at break* of a sample undergoing a tensile test can be examined. Elongation at break refers to the extension in length of a specimen at the point of break as a percentage of its original length. Figure 5.31 shows the elongation at break of CBL samples tested according to sample density.

An Investigation into the Properties of Starch-Based Foams
Chapter 5. The Mechanical Properties of CBL & RPS Starch-Based Foams

181
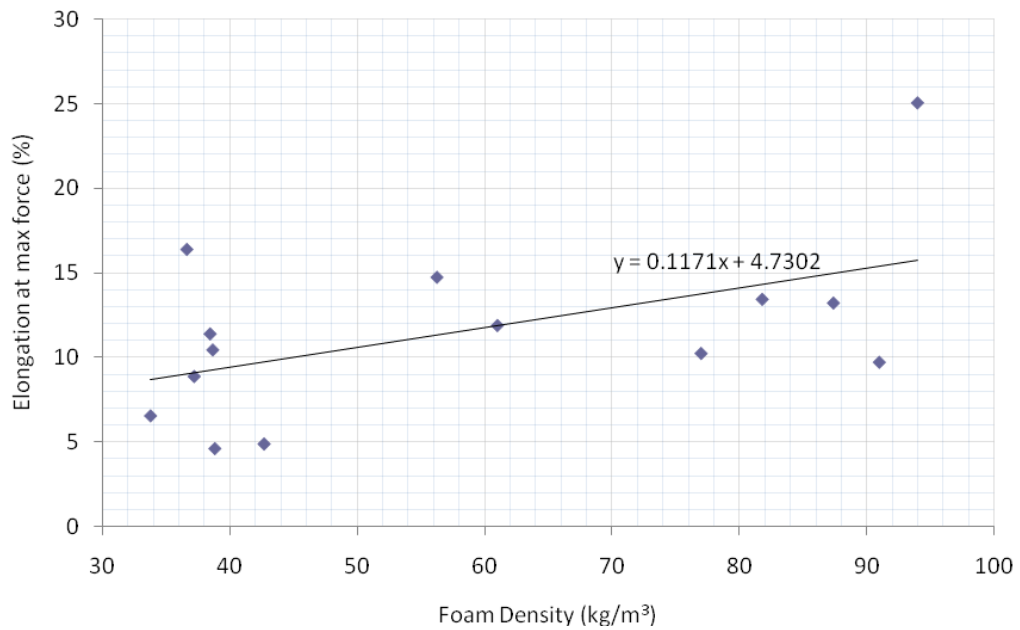
Figure 5.31: Elongation at break of CBL foams according to sample density (trendline generated by linear regression)

Given that the point of separation of a CBL foam sample under tensile loading occurs at the site of the bonded interfaces between loosefill chips comprising the sample, one may still have expected to see greater elongation of higher density CBL samples due to the probability of enhanced adhesion between the loosefill chips as a result of greater compression and increased contact area between loosefill chips during fabrication - all of which would then facilitate greater tensile deformation. However, Figure 5.31 shows only a very weak correlation between sample density and elongation at break, indicating that any increase in the strength of bonds between loosefill chips in higher density CBL foams is relatively limited. Whilst the density of CBL may be modified as a consequence of variations in compression during fabrication, tensile test results indicate that this modification is largely the result of densification of the microstructure of the material. Thus, the macrostructure network of CBL will always represent weak points within the foam with respect to tensile and possibly shear forces. It is also reasonable to conclude that tensile failure in CBL foams occurs without significant tensile deformation of the loosefill chips themselves, but rather is dominated by the de-bonding of the interfaces between them.

An Investigation into the Properties of Starch-Based Foams
Chapter 5. The Mechanical Properties of CBL & RPS Starch-Based Foams

182

5.4.2   Tensile performance - comparison with other foams.

Figure 5.32 shows the tensile strength of CBL starch foams in comparison with a selection of polymer foams of similar densities.
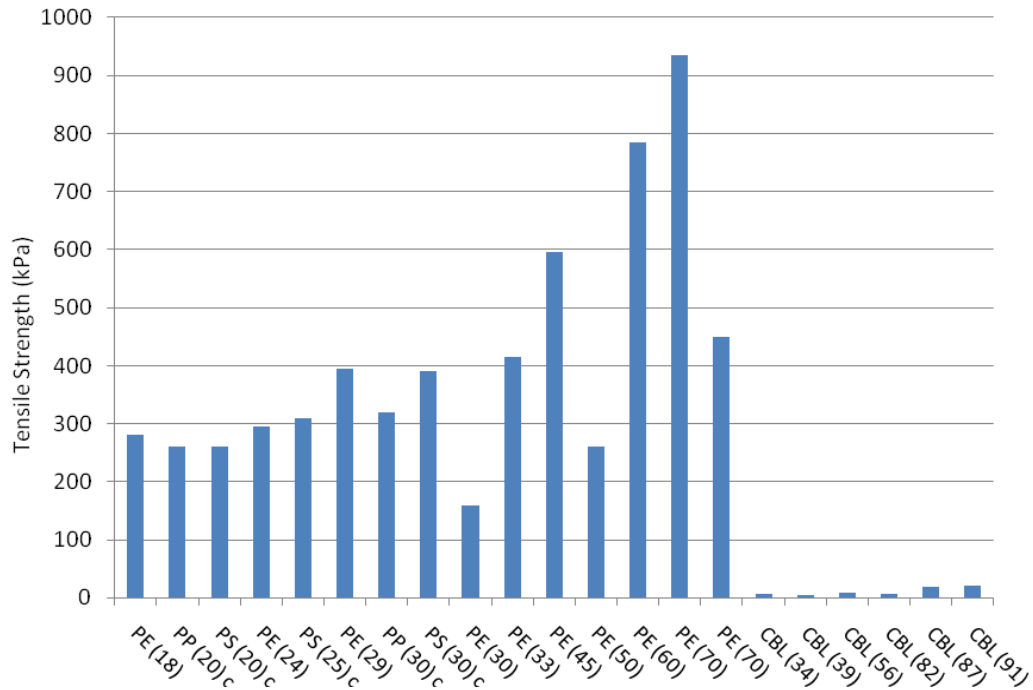
Figure 5.32: Tensile strength of CBL starch foams in comparison with polymer foams

Key to Figure 5.32: All figures given in parenthesis refer to foam densities (kg/m^3).
C denotes closed cell foams.

PE - Polyethylene foam
PP - Polypropylene foam
PS - Polystyrene foam
CBL - Compression Bonded Loosefill
Data for petrochemical polymer foams compiled from CES Edupack database (2008).

Figure 5.32 shows that the tensile strength of CBL foams is dramatically lower and not comparable to that of polymer foams. The reduced tensile performance of CBL foams when compared to polymer foams is clearly related to the weak interface bonding strength and structural irregularities previously discussed. Figure 5.33 shows the elongation at break of CBL starch foams in comparison with a selection of polymer foams of similar densities.

An Investigation into the Properties of Starch-Based Foams
Chapter 5. The Mechanical Properties of CBL & RPS Starch-Based Foams

183
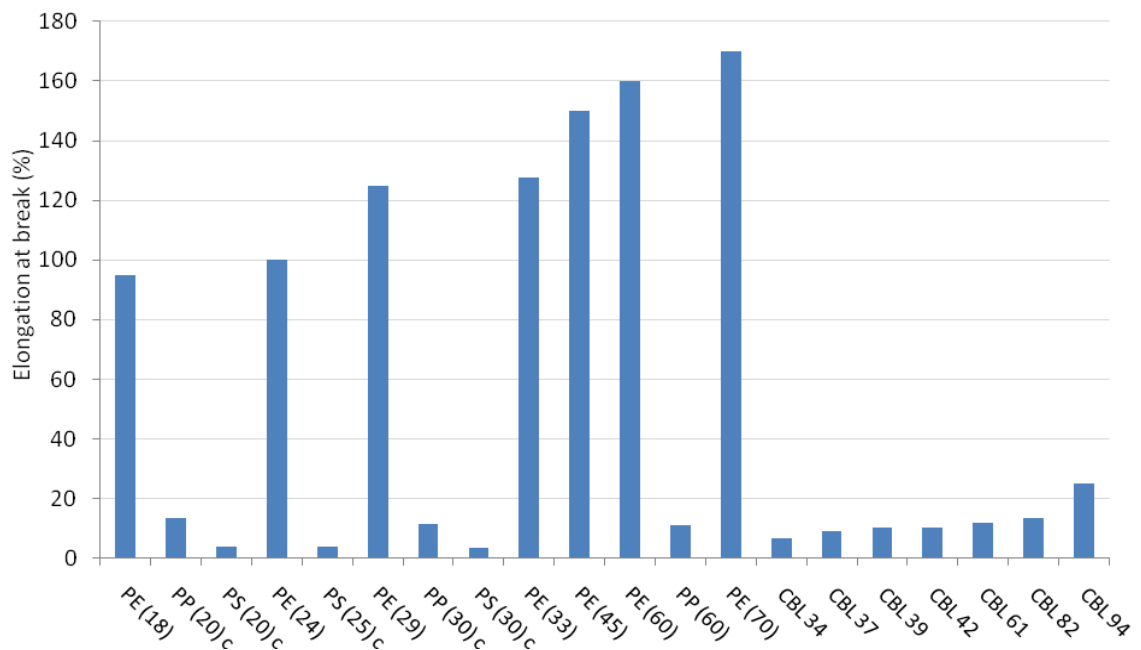
Figure 5.33: Elongation at break of CBL starch foams in comparison with polymer foams

Key to Figure 5.33: All figures given in parenthesis refer to foam densities (kg/m^3).
C denotes closed cell foams.

PE - Polyethylene foam
PP - Polypropylene foam
PS - Polystyrene foam
CBL - Compression Bonded Loosefill
Data for petrochemical polymer foams compiled from CES Edupack database (2008).

Figure 5.33 shows that in terms of elongation at break, CBL foams perform better than some rigid foams such as polystyrene while exhibiting comparable performance to polypropylene foams of similar densities. However CBL foams perform poorly in terms of elongation when compared to flexible foams such as polyethylene.

In general, the results of the tensile tests conducted on CBL foams show that these macro-composites suffer from significant limitations due to weaknesses at the interfaces which bond their constituent loosefill chips together. As such, CBL foams would be best utilised in applications which do not require good tensile strength performance, unless they can be laminated into sandwich structures with other materials such as corrugated fibreboard in order to obtain higher tensile (and bending) strengths.

An Investigation into the Properties of Starch-Based Foams
Chapter 5. The Mechanical Properties of CBL & RPS Starch-Based Foams

184

5.5   Results of high temperature & relative humidity compression tests

Figure 5.34 shows yield strength from compression tests conducted on high temperature and humidity conditioned samples, according to conditioned sample density. Since the mechanical properties of hygroscopic, moisture-sensitive material will be influenced by any absorbed moisture, the sample densities reported in Figure 5.34 refer to conditioned wet samples including any moisture absorbed into the samples during conditioning.
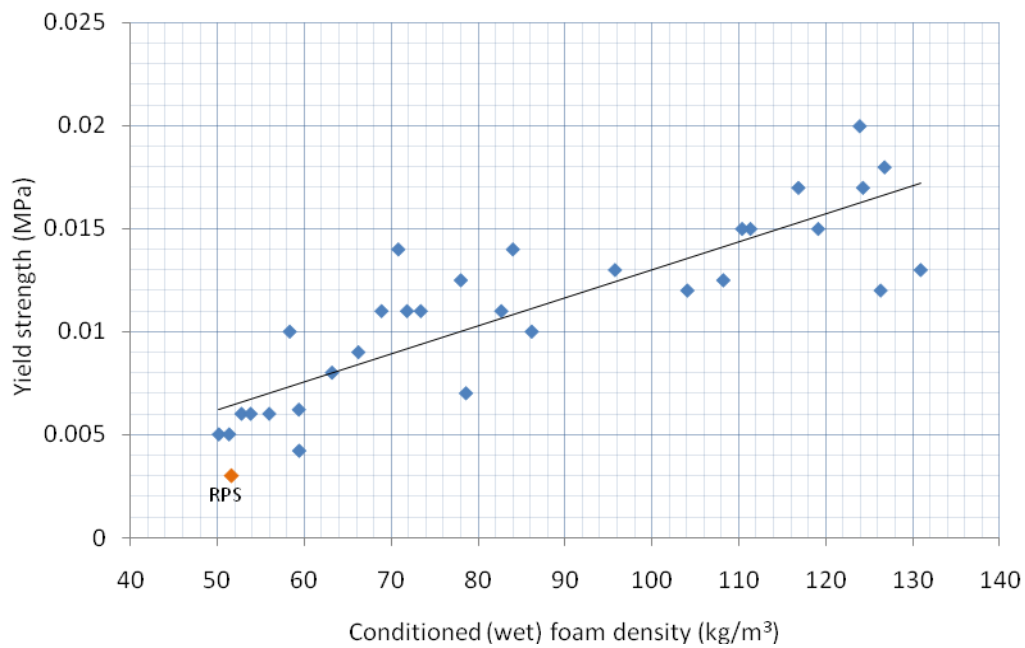
Figure 5.34: Yield strength of 38°C & 85% r.h. conditioned samples according to density (trendline generated by linear regression)

The yield strength values presented in Figure 5.34 appeared very low. Figure 5.35 compares this data to yield strength values from previous compression tests in which samples were conditioned and tests conducted at standard ambient conditions of 23°C and 50% r.h.
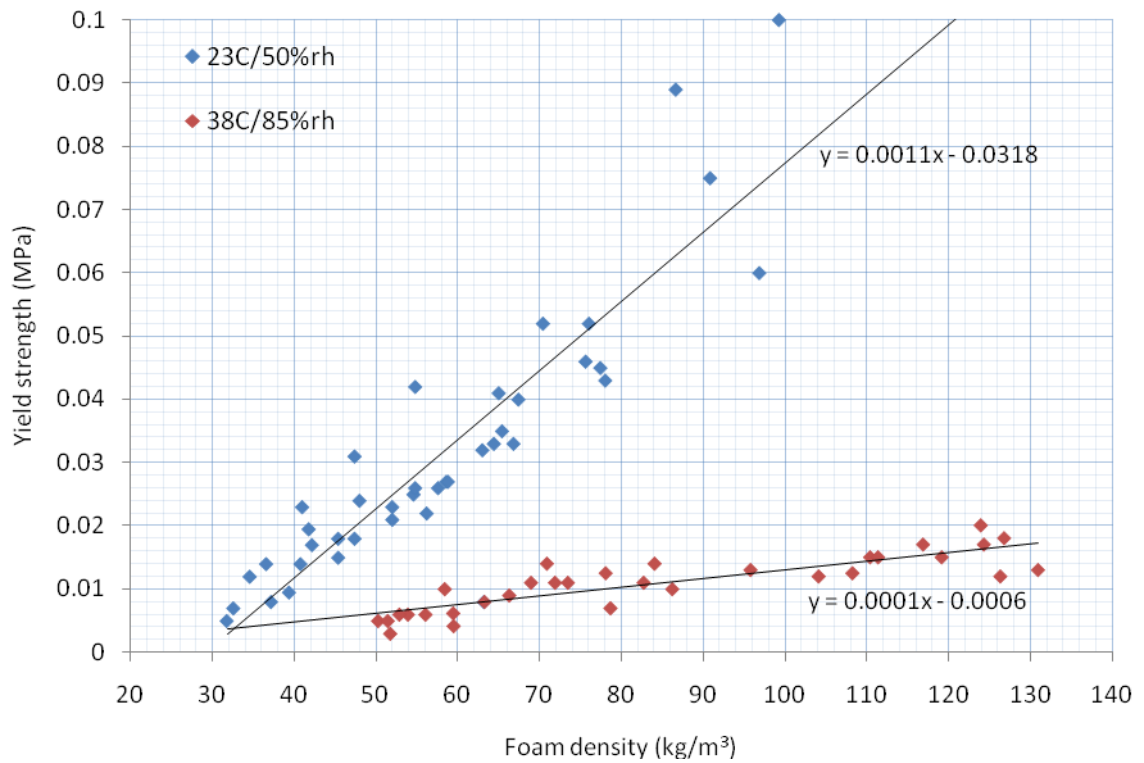
Figure 5.35: Comparison of yield strength values (38°C & 85% r.h) & (23°C & 50% r.h.) (trendlines generated by linear regression)

In contrast to studies conducted by Kang *et al* (as summarised Chapter 2, section 2.12), which reported enhanced mechanical properties of RPS foam blocks previously exposed to high humidity treatments and then tested under standard conditions, the tests reported in this study were conducted on high temperature and humidity treated starch foam samples under conditions of high temperature and relative humidity. The significantly decreased compressive yield strength performance of high temperature and humidity conditioned starch foam samples compared to samples conditioned at 23°C and 50% r.h are illustrated in Figure 5.35. The contrast is such that this comparison appears to feature the properties of two dissimilar and unrelated materials.

Sample shrinkage and an increase in foam density during high-humidity and temperature conditioning would be expected to enhance mechanical properties of starch foams if samples are first allowed to recondition under dry conditions before being tested. However, compression tests conducted under conditions of high humidity show that the absorption of moisture has *plasticised* the starch foam to the extent that it allows molecular mobility and reduced resistance to compression. Thus, when starch foam samples are mechanically tested under conditions of high humidity, plasticisation is the dominant effect leading to a reduction in compression strength.

An Investigation into the Properties of Starch-Based Foams
Chapter 5. The Mechanical Properties of CBL & RPS Starch-Based Foams

186

5.6   Results of high temperature & relative humidity creep tests

Figure 5.36 shows the results of creep deformation tests conducted in tropical conditions on samples previously specified in Chapter 4, section 4.2.5.5. For reasons of clarity, two foams (RPS and ETAS 40) which immediately "bottomed out" on commencement of the test beyond the measurable limits of the equipment are not shown.
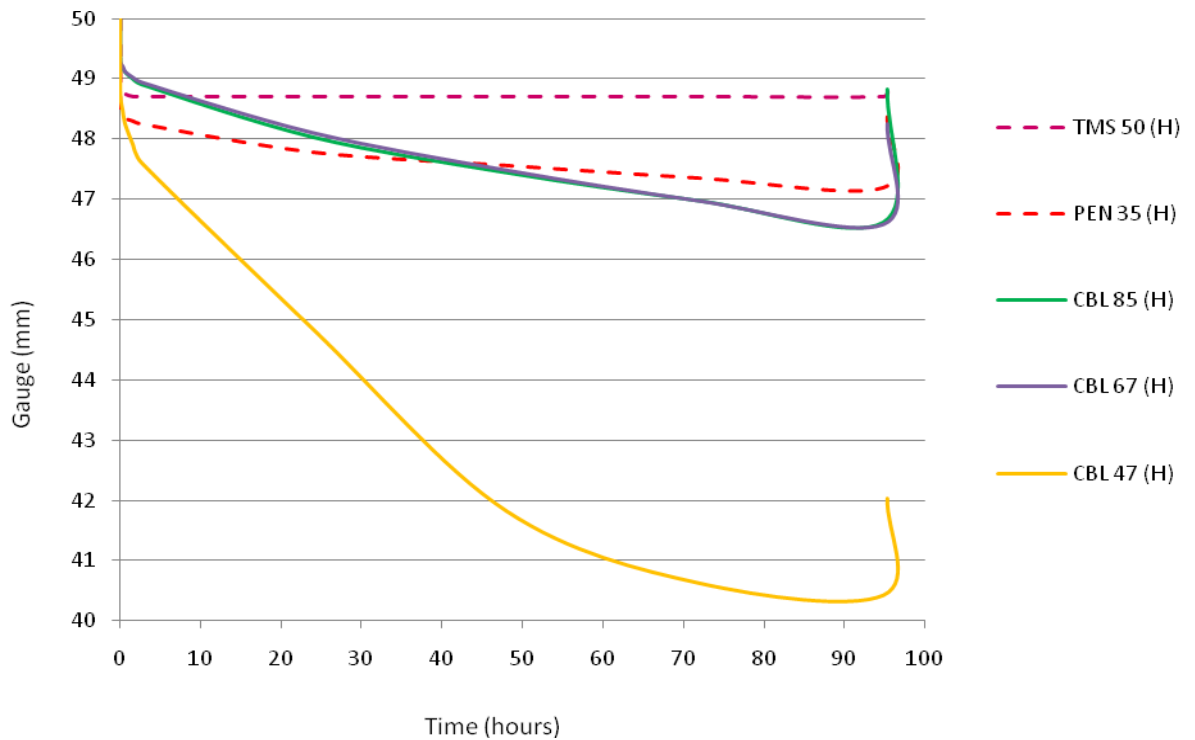
Figure 5.36: Creep deformation of CBL starch foams in high temperature and humidity conditions compared with polymer foams

Figure 5.36 shows that the foam which exhibited the best performance in terms of resistance to creep deformation under conditions of high temperature and humidity was TMS 50, followed by PEN 35, CBL 85 and CBL 67, all of which were within a fairly close range of gauge deformations. CBL 47 exhibited almost 20% gauge creep deformation over the 100 hour test period prior to load removal and rebound, whilst both ETAS 40 and RPS 23 foams both failed the test, 'bottoming out' beyond measurable limits of the creep rigs and are thus not shown in these results. Table 5.3 shows total post-test deformation of the samples tested after rebound (load removed for 30 minutes prior to sample gauge measurement).

An Investigation into the Properties of Starch-Based Foams
Chapter 5. The Mechanical Properties of CBL & RPS Starch-Based Foams

187

Table 5.3: Post-test creep deformation of high temperature & humidity conditioned samples

	ETAS 40(H)	TMS 50(H)	PEN 35(H)	CBL 85(H)	CBL 67(H)	CBL 47(H)	RPS 23(H)
Start gauge (mm)	50	50	50	50	50	50	50
Finish gauge (mm)	*	48.86	48.37	48.83	48.26	42.03	Fail *
Post-test deformation (mm)	*	1.14	1.63	1.17	1.74	7.97	-

(H): Sample conditioned & tested under high temperature & high humidity conditions.
* Sample immediately "bottomed out" beyond measurable limits of equipment on commencement of test.

In order to compare the creep deformation behaviour of CBL starch foams in standard ambient conditions (23°C & 50% r.h), with their behaviour in high temperature and humidity conditions (38°C & 85% r.h), Figure 5.37 shows the creep deformation of two density ranges of CBL foam under standard ambient conditions (from data previously presented in section 5.3), alongside the creep deformation test results given in Figure 5.36 above.
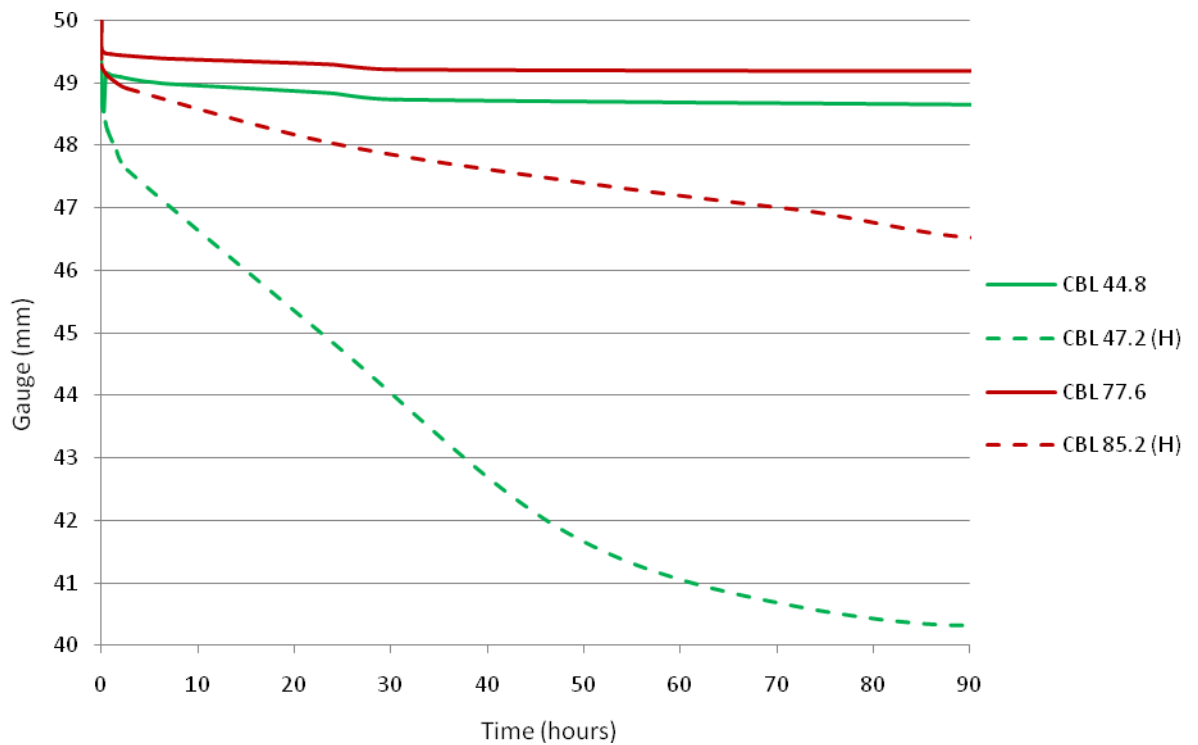
Figure 5.37: Creep behaviour of CBL starch foams under standard ambient conditions (23°C & 50% r.h) compared to high temperature & humidity conditions (38°C & 85% r.h)
(H): Sample conditioned & tested under high temperature & high humidity conditions

An Investigation into the Properties of Starch-Based Foams
Chapter 5. The Mechanical Properties of CBL & RPS Starch-Based Foams

188

In contrast to compression tests conducted on starch foam samples at high tempeature and humidity conditions, the results of these creep tests indicated more moderate reductions in the mechanical performance of the foams, compared to tests conducted under standard conditions. The compression tests continued to deform the cells within foam samples beyond their yield strengths, while the creep tests utilised relatively low loads below that of the samples yield strengths.

Comparison of higher density CBL foams shown in Figure 5.37 illustrated a moderate reduction in creep performance when tested under high temperature and relative humidity conditions compared to standard conditions. This data demonstrated that lower density CBL foams were more adversely affected by the high temperature and humidity conditions which reduced the mechanical resistance of the starch-based foams to creep deformation.

Despite high temperature and high relative humidity conditioning resulting in shrinkage of samples and producing starch foams with a greater number of cell walls per unit volume (a phenomenon which would be expected to enhance the mecanical strength of the samples if tested under dry conditions), absorption of moisture into the foams has plasticised the samples to the extent that it allows molecular mobility and reduced resistance to creep when tested under conditions of high relative humidity. The high temperature and relative humidity creep and compression test findings presented are of significance as it suggests that these starch foams would be not be suitable for applications in which resistance to deformation is required if these materials are also exposed to high temperatures and humidities typically found in tropical regions.

An Investigation into the Properties of Starch-Based Foams
Chapter 5. The Mechanical Properties of CBL & RPS Starch-Based Foams

189

5.7 Scanning electron microscopy (SEM) analysis of high temperature & relative humidity conditioned CBL foam structures

In order to analyse the shrinkage of CBL foam samples exposed to high temperature and high humidity conditioning, SEM imaging was used to investigate the mechanisms of shrinkage.

Figures 5.38 a), b) and c) show a set of SEM images taken at various magnifications of CBL samples conditioned at 'standard' conditions of 23°C & 50% r.h for a minimum of 48 hours as previously described in Chapter 4, section 4.2.5.3.
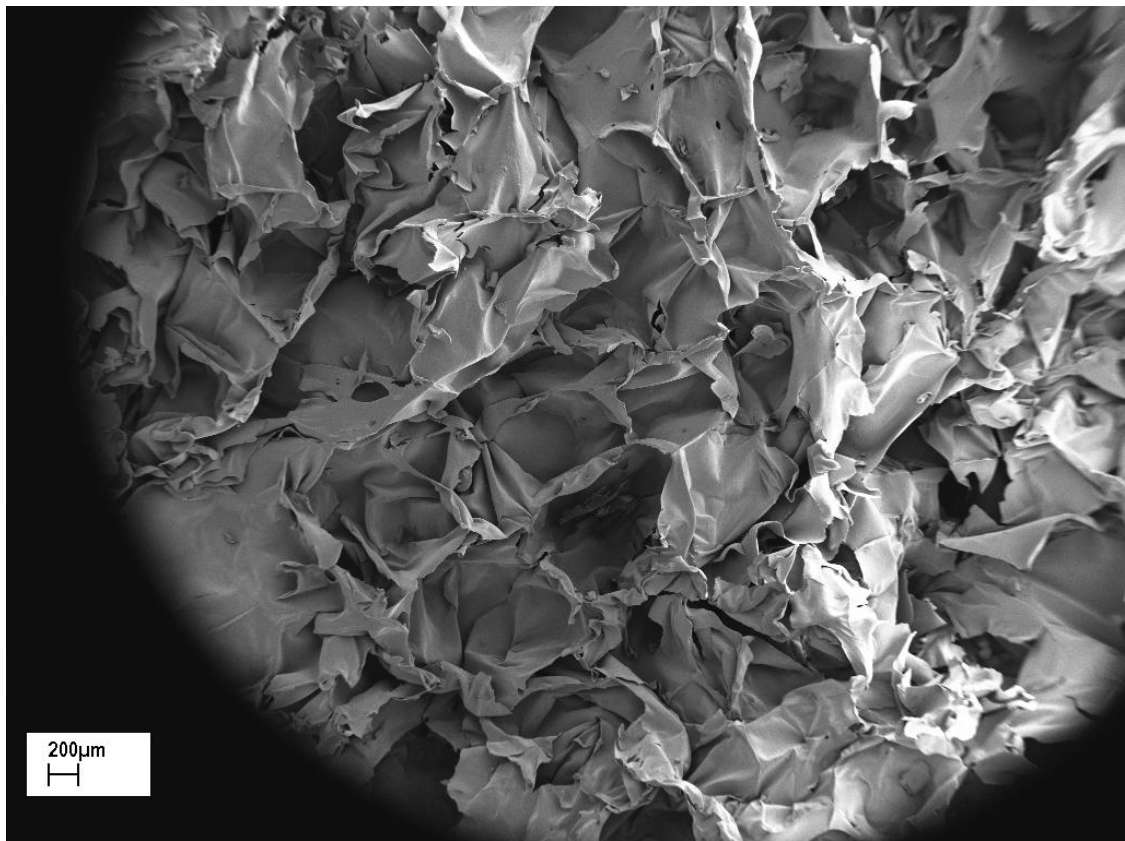
Figure 5.38 a) SEM image of CBL foam sample (density 43 Kg/m^3) conditioned at 23°C & 50% r.h.

An Investigation into the Properties of Starch-Based Foams
Chapter 5. The Mechanical Properties of CBL & RPS Starch-Based Foams

190
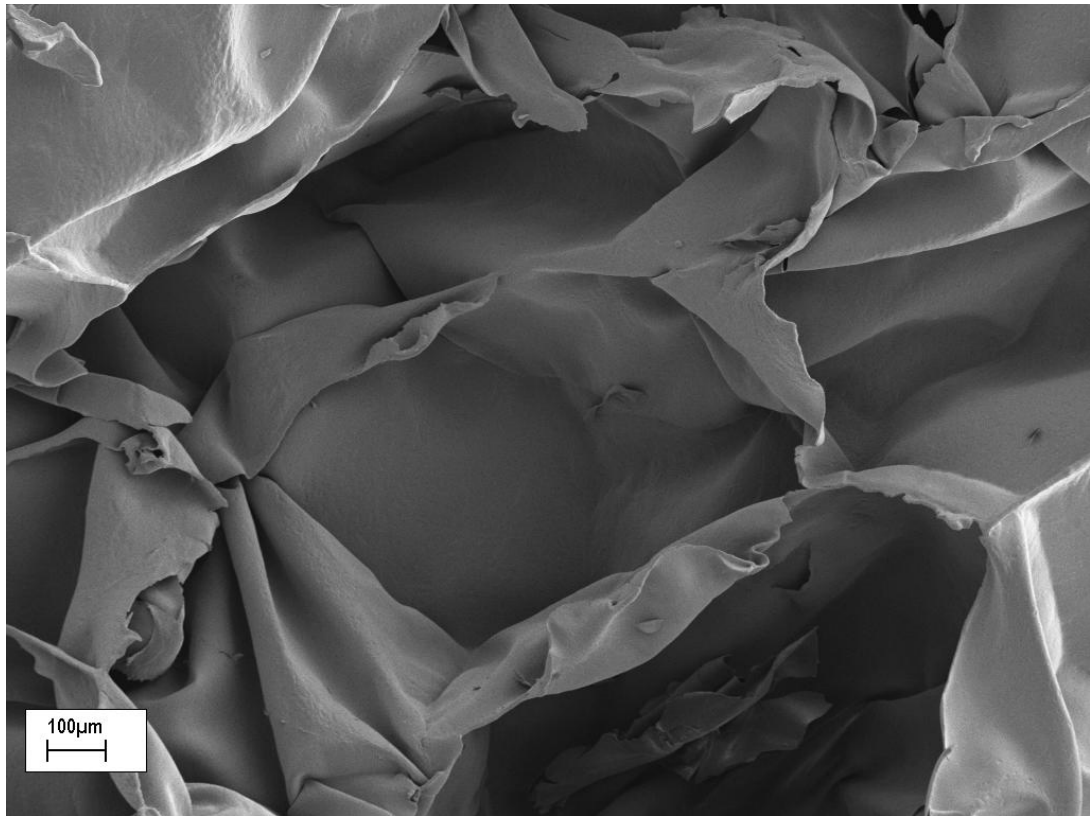
Figure 5.38 b) Higher magnification SEM image of CBL foam cells (density 43 Kg/m^3) conditioned at 23°C & 50% r.h.
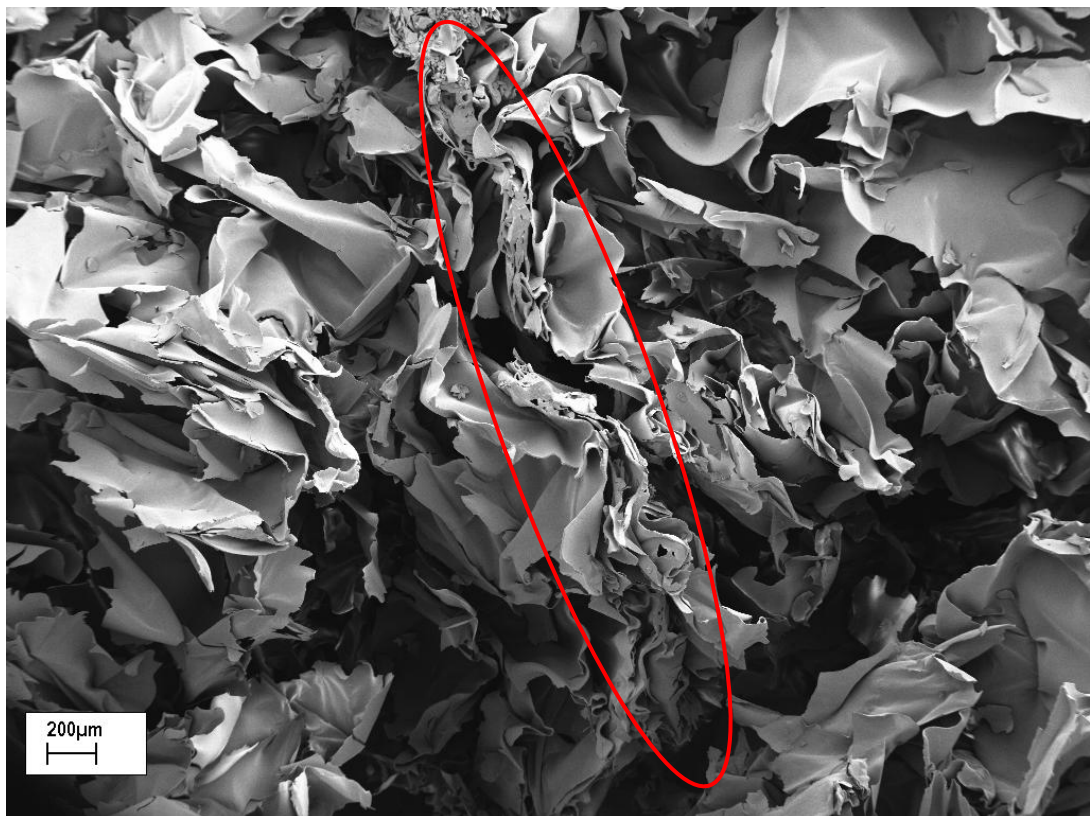
Figure 5.38 c) SEM image of CBL foam sample (density 43 Kg/m^3) conditioned at 23°C & 50% r.h., showing area of interface bonding between adhered loosefill chips (highlighted in red)

An Investigation into the Properties of Starch-Based Foams
Chapter 5. The Mechanical Properties of CBL & RPS Starch-Based Foams

191

Figures 5.39 a), b), c) and d) show a set of SEM images at various magnifications of CBL samples subected to high temperature and humidity conditioning at 38°C & 85% r.h for a minimum of 48 hours before being reconditioned at 'standard' conditions of 23°C & 50% r.h. for a minimum of 48 hours as previously described in Chapter 4, section 4.2.5.3.
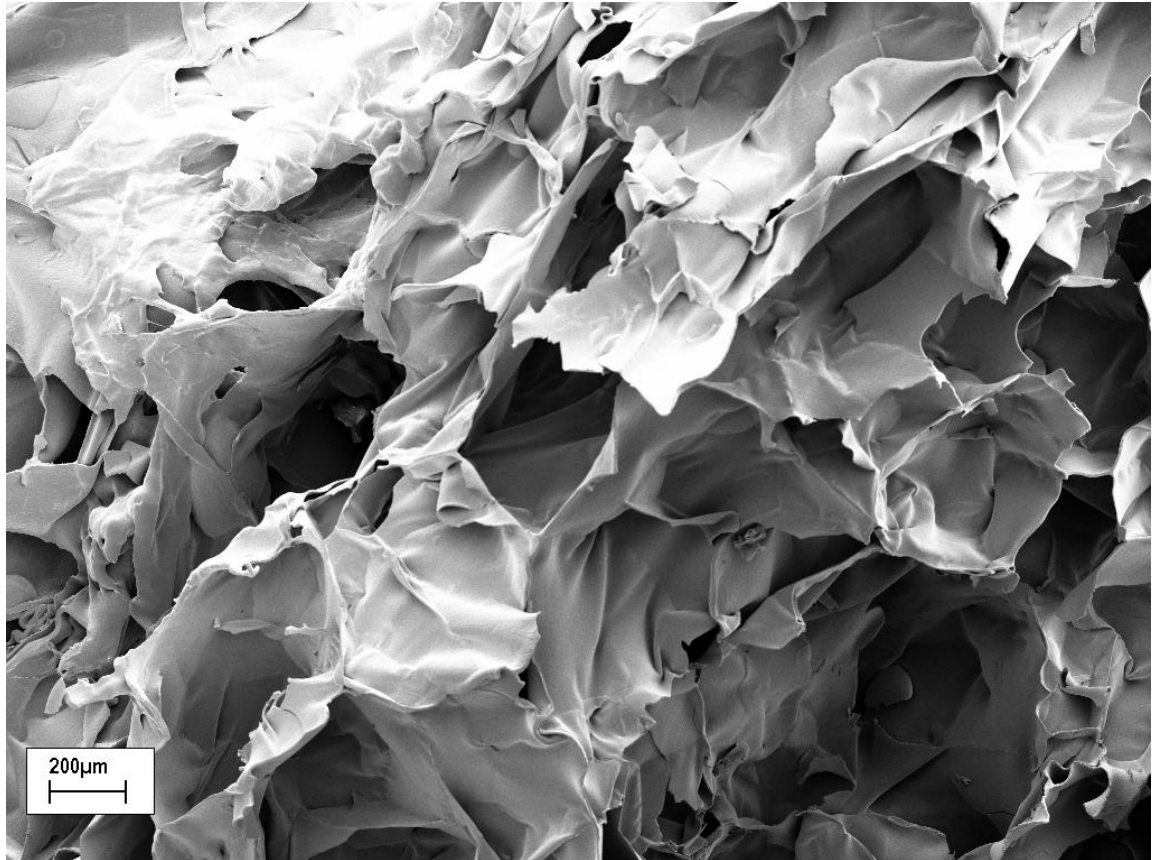
Figure 5.39 a) SEM image of 38°C & 85% r.h conditioned CBL sample (pre-conditioning density 43 Kg/m^3)

Figure 5.39 a) appears to show a similar cell structure to the SEM images given in Figures 5.38 a) and b). However, at the top left of the image some areas of the cell structures have become distorted and show a loss of structure.

An Investigation into the Properties of Starch-Based Foams
Chapter 5. The Mechanical Properties of CBL & RPS Starch-Based Foams

192
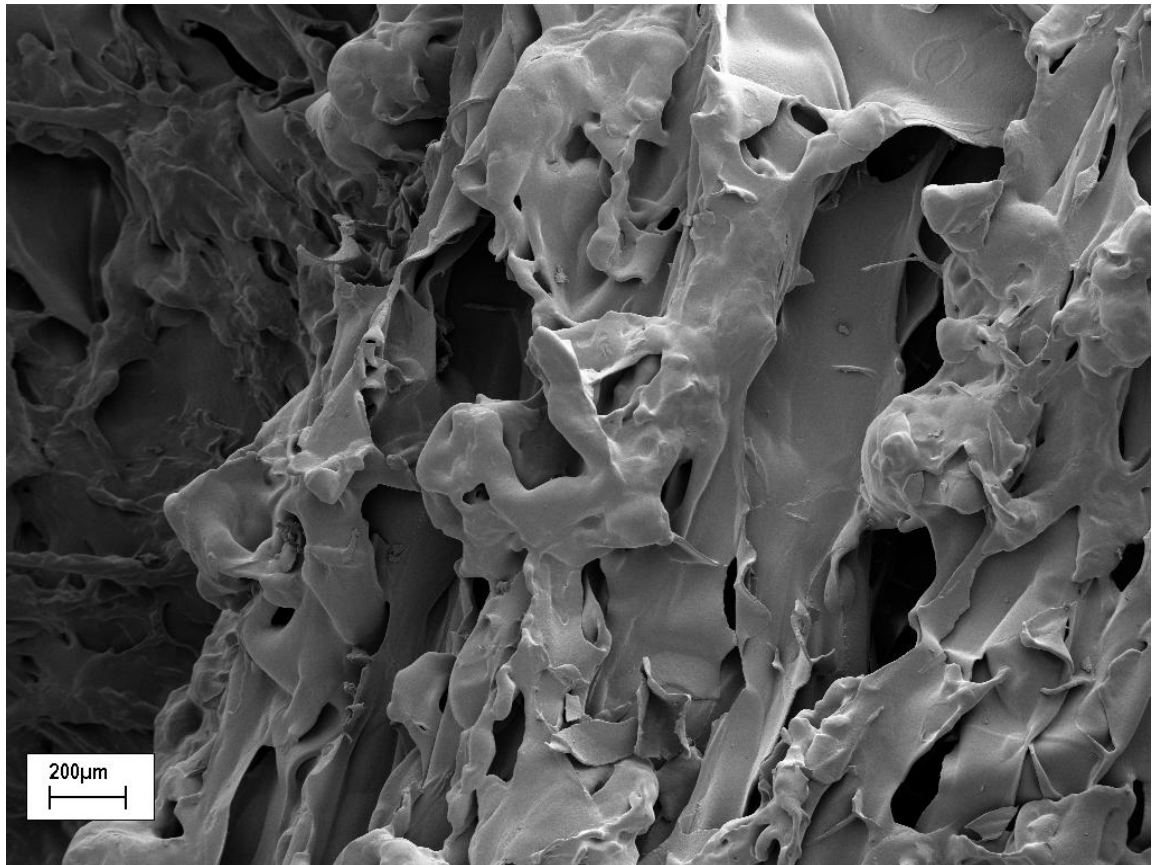
Figure 5.39 b) SEM image of 38°C & 85% r.h conditioned CBL sample (pre-conditioning density 43 Kg/m^3), showing area of cell wall plasticisation & distortion

Figure 5.39 b) shows an area of cell wall plasticisation and distortion in which cell walls have shrunk and collapsed due to high temperature and humidity conditioning. In these areas, exposure to moisture has plasticised cell structures which were previously expanded and "fixed" in a meta-stable state during extrusion foaming. This plasticisation has allowed the cell structure to relax and retract. Since some areas of the foam are subject to cell wall distortion whilst other areas remain largely unaffected by moisture ingress as shown in Figure 5.39 a), this may help to explain the differential rather than uniform nature of sample shrinkage.

An Investigation into the Properties of Starch-Based Foams
Chapter 5. The Mechanical Properties of CBL & RPS Starch-Based Foams

193
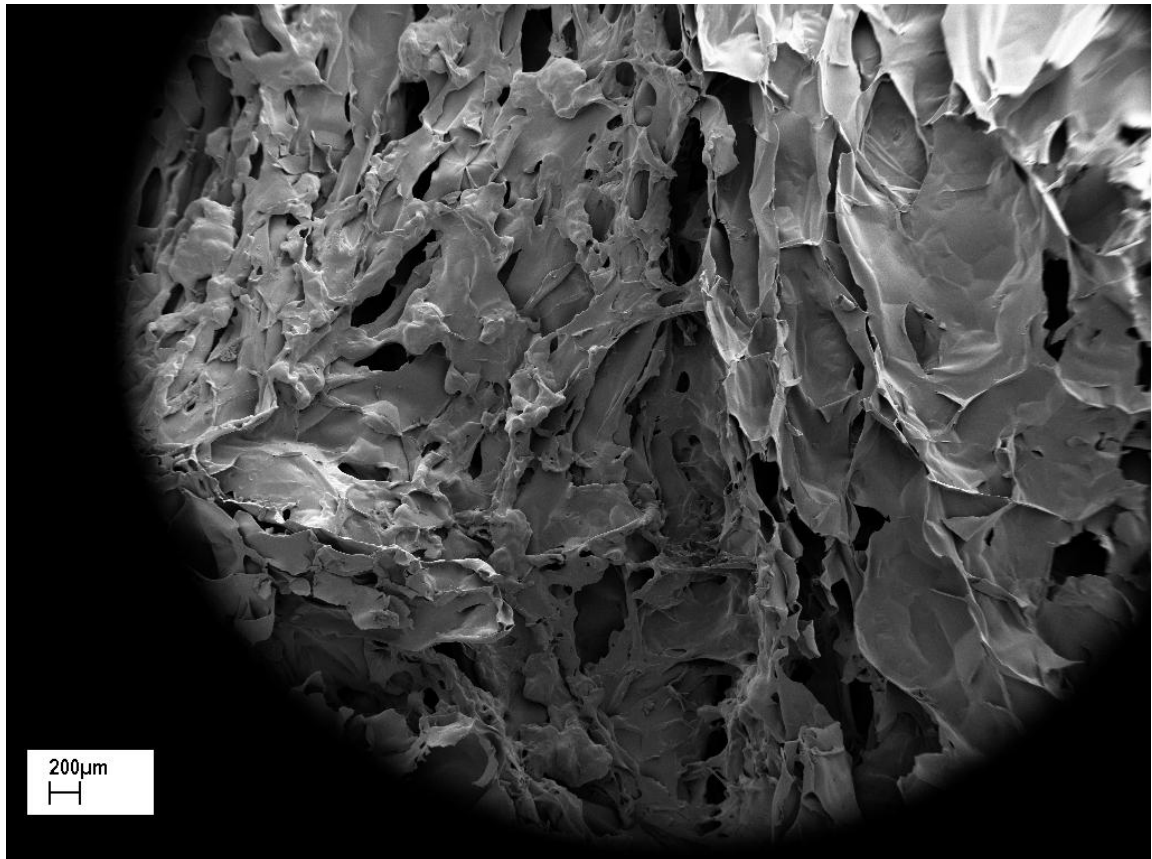
Figure 5.39 c) SEM image of 38°C & 85% r.h conditioned CBL sample (pre-conditioning density 43 Kg/m^3), showing area of interface bonding and cell wall distortion to the left

Figure 5.39 c) shows an area of interface bonding within the sample. Cell wall distortion due to high temperature and humidity conditioning appears to have occurred to the left of the interface in this image, which may indicate some blocking effects by the higher density interface to ingress of moisture into the sample, again perhaps serving to explain the differential nature of sample shrinkage.

An Investigation into the Properties of Starch-Based Foams
Chapter 5. The Mechanical Properties of CBL & RPS Starch-Based Foams

194
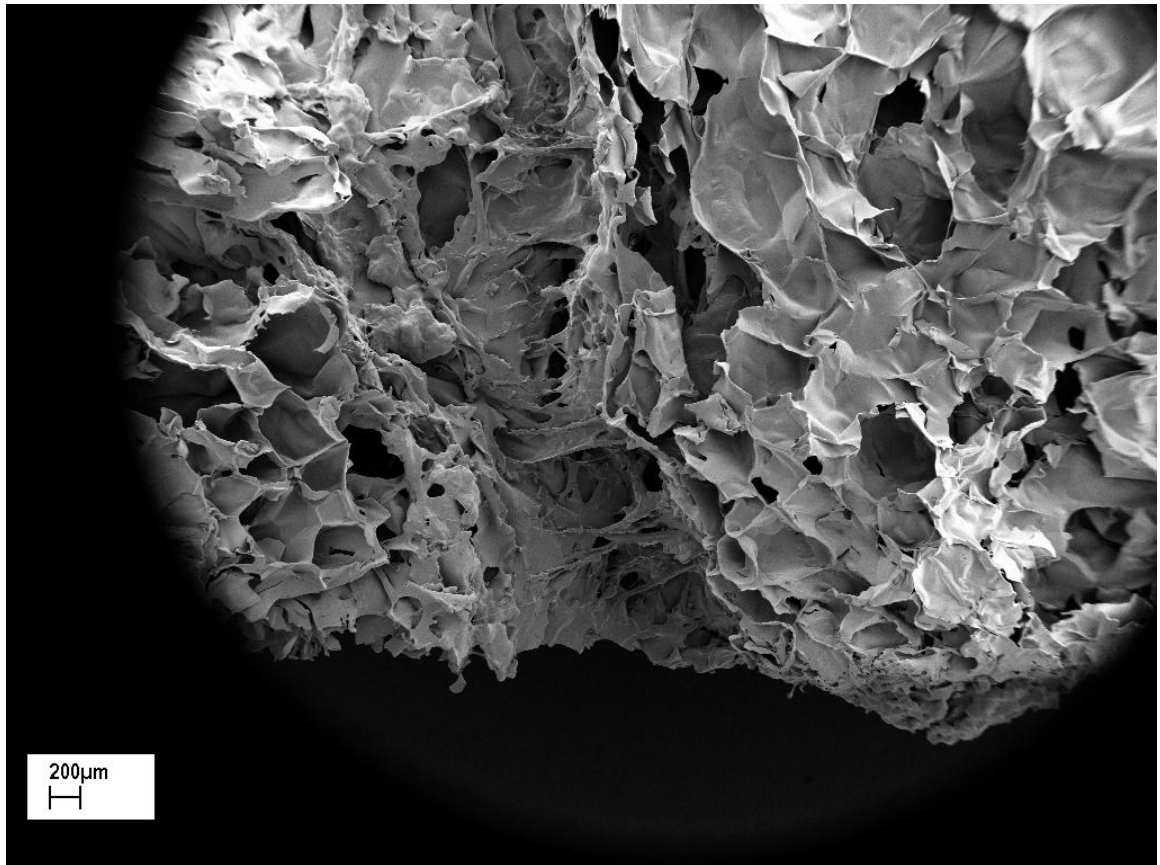
Figure 5.39 d) SEM image of 38°C & 85% r.h conditioned CBL sample (pre-conditioning density 43 Kg/m^3), showing area of interface cleavage

Figure 5.39 d) shows an area of interface bonding in which cell wall collapse and sample shrinkage appears to have resulted in physical cleavage across the interface, pulling the bond apart. Figure 5.39 e) shows this phenomenon in more detail.

An Investigation into the Properties of Starch-Based Foams
Chapter 5. The Mechanical Properties of CBL & RPS Starch-Based Foams

195
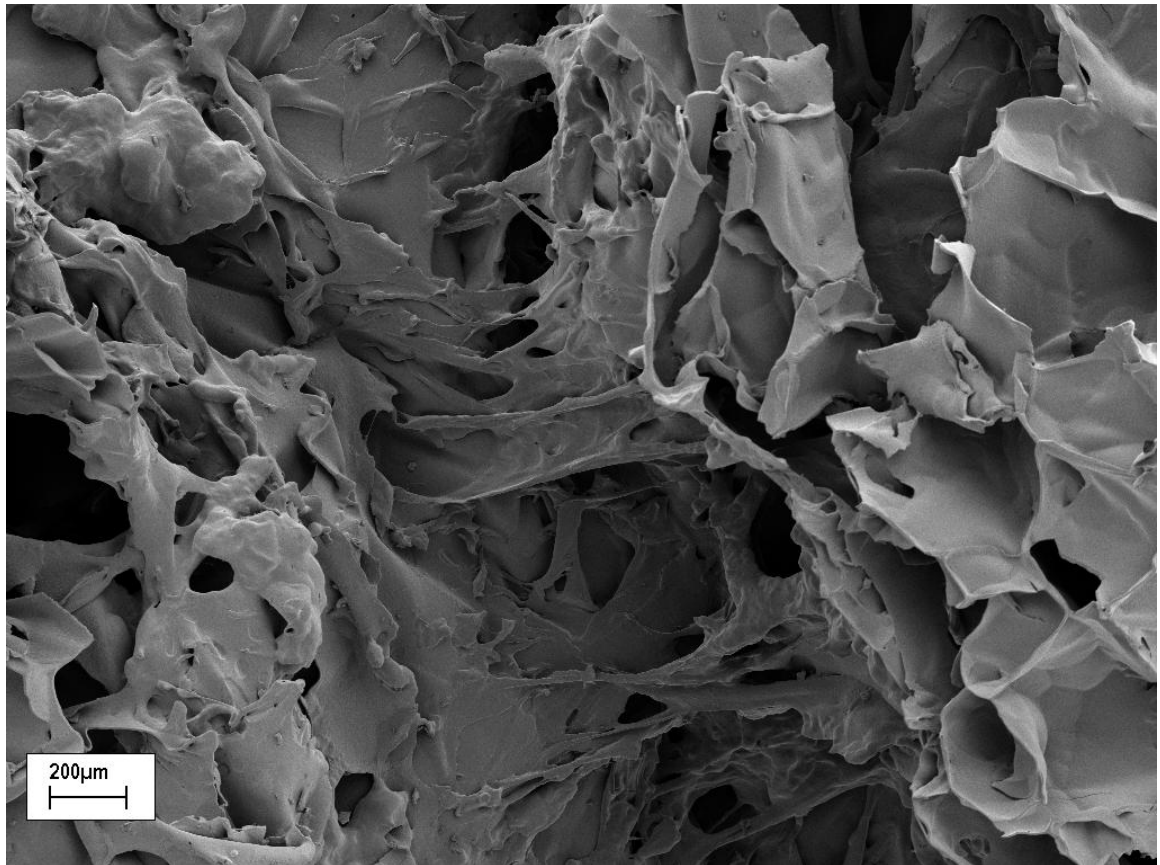
Figure 5.39 e) Higher magnification SEM image of 38°C & 85% r.h conditioned CBL sample (pre-conditioning density 43 Kg/m^3), showing area of interface cleavage

Figure 5.39 e) appears to show strands of plasticised material stretched in an axis perpendicular to the interface, indicating tensile forces across the interface which have forced the bond between loosefill chips to separate. This cleavage and separation phenomenon may be due to cell wall collapse and sample shrinkage from high temperature and humidity conditioning.

5.8 X-ray diffraction analysis of CBL foam crystallinity

In order to analyse the crystallinity of samples exposed to different conditioning regimes, XRD analysis was used to investigate the crystallinity of a range of samples. Using baseline samples taken from two different densities of untreated CBL foams conditioned at 23°C & 50% r.h. for a minimum of 48 hours, Figure 5.40 shows a comparison of X-ray diffraction patterns between the baseline samples and two CBL samples of different densities subected to high temperature and humidity conditioning at 38°C & 85% r.h for a minimum of 48 hours. The treated samples were reconditioned at standard ambient conditions of 23°C & 50% r.h. for a minimum of 48 hours prior to testing, as previously described in Chapter 4, section 4.2.5.4.
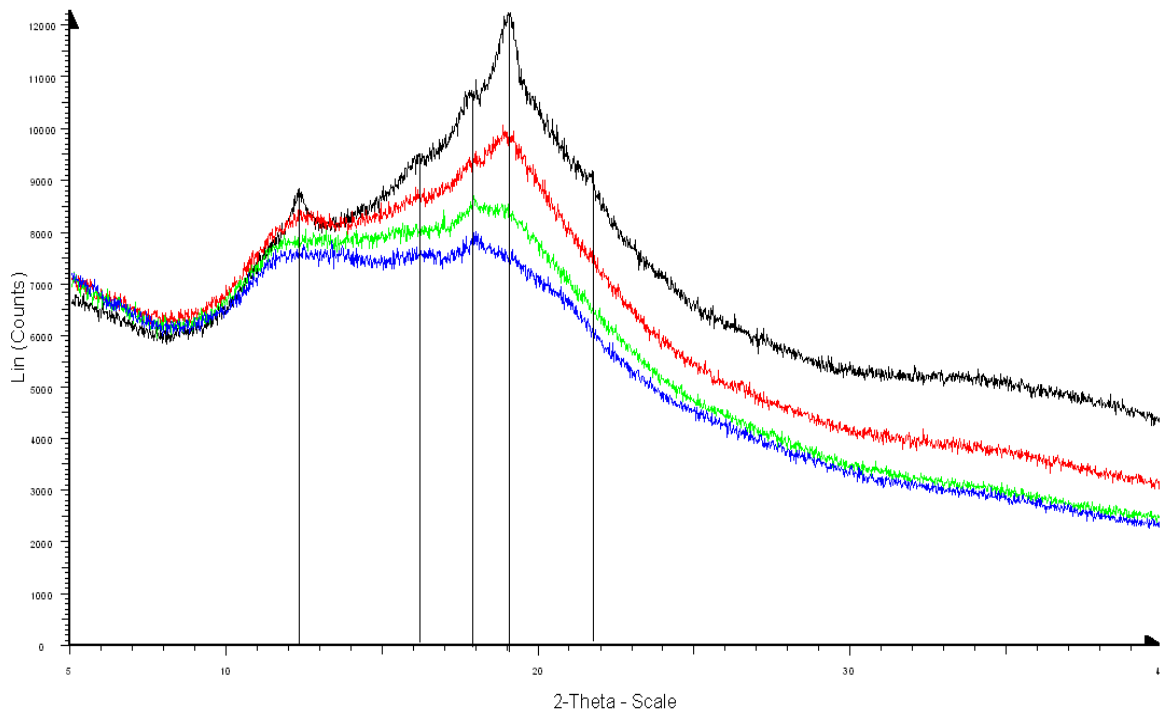
Figure 5.40: X-ray diffraction patterns of CBL samples

Key to Figure 5.40:	—— CBL 72 Kg/m^3 38°C & 85% r.h. (high temp & high r.h. conditioned)
	—— CBL 42 Kg/m^3 38°C & 85% r.h. (high temp & high r.h. conditioned)
	—— CBL 70 Kg/m^3 23°C & 50% r.h. (untreated baseline)
	—— CBL 43 Kg/m^3 23°C & 50% r.h. (untreated baseline)

The comparison of X-ray diffraction patterns shown in Figure 5.40 indicated an overall upward shift of curves representing the high temperature and high humidity conditioned samples. This is due to the shrinkage and density increases in the foams imparted by the conditioning regime (as previously described in Chapter 4, sections 4.2.5.2 & 4.2.5.4), which results in a larger quantity of cell walls and a greater proportion of material per unit volume tested.

An Investigation into the Properties of Starch-Based Foams
Chapter 5. The Mechanical Properties of CBL & RPS Starch-Based Foams

197

Higher crystallinities observed in the high temperature and relative humidity conditioned samples, as illustrated by increases in peak intensities shown in the diffraction patterns, indicate changes in the material's morphology characterised by more ordered and less amorphous crystalline arrangements. These changes were facilitated by increased mobility of the molecular structures of samples under high temperature and relative humidity conditioning.

The diffraction parameters of the processing induced crystallinities of CBL foams are summarised in Table 5.4

Table 5.4: Diffraction parameters of processing induced crystallinities of CBL foams

Type	2θ (°)	Intensity
V	12.34 19.06 21.66	Very strong Very strong Medium
E	17.90	Strong
A	16.23	Medium

Table 5.4 shows that the CBL foams tested have the characteristic diffraction patterns dominated by V and E-type structures typical of processed starch materials, as well as residual A-type structures typical of native cereal starch. These modified V and E type crystallinities are produced by the rapid recrystallisation of single-helical structures of amylose during retrogradation (van Soest & Vliegenthart, 1997).

5.9   Discussion of the mechanical properties of CBL & RPS starch-based foams

Although clear correlations exist between the density of starch-based CBL foams and their mechanical properties, inconsistencies exist due largely to local density variations within CBL samples and hence considerable scattering of data is also observed.

Yield strengths of CBL foams are comparable to many grades of polyethylene and polyurethane foams, but are relatively lower than other grades of polyethylene, polypropylene and polystyrene foams. With the exception of the polyurethane foam examined, the elastic modulus of CBL foams is generally lower than that of most rigid polymer foams used for comparative purposes.

Dynamic impact tests indicated that CBL foams exhibited comparable or lower peak deceleration values to a range of polymer foams at low to medium static stresses. In practice this means that the CBL foams would be good candidates for cushioning products with high to medium fragility factors. For higher static load cushioning, thicker gauges of CBL foams would need to be used to give the equivalent cushioning performance of high performance polymer foams.

The repeated dynamic impact performance of CBL foams tested were inferior to that of the polymer foams used for performance comparison purposes as shown by significant increases in peak deceleration values particularly in the response to high static loads. This is due chiefly to the relatively poor recovery of CBL foams after each impact, thus indicating that the materials are most suitable for cushioning where protection against a single drop is required.

The superior performance of the polymer foams to repeated impacts may be attributable to several factors: a) Their greater resilience compared to starch-based foams of similar densities which gives rise to better recovery in response to repeated impacts. b) Voids and irregularities within the macrostructure of CBL foams which cause compression to occur primarily at these areas of weakness, the inconsistent deflection resulting in reduced overall cushion efficiency. c) The relatively high brittleness of starch foams also results in localised deflection closest to the plane of impact. Partial deflection across the thickness of the foam sample in response to impacts would in effect result in the cushioning performance a thinner gauge of energy absorbing foam.

It is possible that the dynamic impact performance of CBL foams observed results from a combination of their reduced resilience, as well as inherent material inconsistencies and partial deflection suppositions, but to what extent each may be responsible is currently unknown and thus an area for further research.

An Investigation into the Properties of Starch-Based Foams
Chapter 5. The Mechanical Properties of CBL & RPS Starch-Based Foams

199

As is the case with other mechanical properties of CBL foams, strong correlations exist between the creep performance of CBL foam samples and their densities, with higher density CBL samples subject to reduced deformation than lower density samples. As previously discussed, higher density foams generally exhibit increased levels of resistance to mechanical deformation and therefore these results are to be expected. In general, creep tests showed that CBL foams have comparable creep performance when compared to certain polymer foams of similar densities. In this respect the high-density macrostructure which reinforces CBL foams may assist their creep performance.

In contrast to the majority of mechanical tests which show strong correlations between the density of CBL foams and particular mechanical properties, correlations between foam density and tensile strength properties appeared much weaker. These weaker correlations are attributable to the fact that under tensile stress CBL samples will always fail at the interfaces between the compressed and adhered loosefill chips comprising the sample, rather than rupture of the chips themselves. The tensile strength of CBL is therefore a function of the interface bonds which are surrounded by an irregular distribution of voids (as stress concentration sites), which cannot be completely removed.

In general, the results of the tensile tests conducted on CBL foams show that these macro-composites suffer from significant limitations due to weaknesses at the interfaces which bond their constituent loosefill chips together. As such, CBL foams would be best utilised in applications which do not require good tensile strength performance, unless they can be laminated into sandwich structures with other materials such as corrugated fibreboard in order to obtain higher tensile (and bending) strengths.

High temperature and relative humidity conditioning of starch foam samples for mechanical tests, in order to simulate the tropical environments in which these materials might realistically be expected to function, featured a tendency for conditioning to affect samples in terms of shrinkage, resulting in significant increases in sample density. Although the ingress of moisture into conditioned samples leads to shrinkage of the foams, it was found that it is the reduction in sample dimensions rather than the additional mass of moistue which were chiefly responsible for the density increases observed. However, high temperature and relative humidity conditioning of samples conducted at different facilities behaved very differently in terms of shrinkage and density increases, leading to the conclusion that in addition to the temperature and humidity conditions themselves, the volume of the conditioning chamber may affect the intensity of conditioning which in turn may also be responsible for varying rates of sample shrinkage.

In contrast to previous studies which reported enhanced mechanical properties of RPS foam blocks previously exposed to high humidity treatments and then tested under standard conditions, the mechanical tests reported in this study were conducted on high temperature and humidity treated starch foam samples under conditions of high temperature and relative humidity. Despite high temperature and high relative humidity conditioning resulting in the shrinkage of samples and producing starch foams with a greater number of cell walls per unit volume (a phenomenon which would be expected to enhance the mecanical strength of the samples if tested under dry conditions), absorption of moisture into the foams plasticised the samples allowing molecular mobility and reduced mechanical performance in both compression and creep tests when tested under conditions of high relative humidity.

Starch foams are dynamic materials in terms of their behaviour under different environmental conditions. High temperature and relative humidity conditioning produces a material with a dissimilar structure, morphology and mecahnical properties to those tested under standard conditions. The high temperature and relative humidity creep and compression test findings presented are of significance as it suggests that CBL and RPS starch foams would be not be suitable for applications in which resistance to mechanical deformation is required if these materials are also exposed to high temperatures and humidities typically found in tropical regions.

Scanning electron microscopy imaging conducted in order to determine the mechanisms of shrinkage on samples of CBL foams subjected to high temperature and humidity conditioning, revealed that plasticisation of cell walls caused distortion, collapse and loss of cell structure. Exposure to moisture plasticised cell structures which were previously expanded and "fixed" in a *meta-stable* state during extrusion foaming, allowing the cell structure to relax and retract resulting in sample shrinkage.

In contrast to studies conducted on single strand sections of extruded starch foams exposed to high humidity conditioning by Kang *et al* (2006), in which uniform moisture penetration and sample shrinkage was observed, blocking effects to the ingress of moisture by higher density interfaces within CBL foams were in evidence in the SEM images, which may contribute towards non-uniform sample shrinkage. Plasticisation, loss of cell structure and shrinkage of CBL samples subjected to high temperature and high humidity conditioning resulted in evidence of tensile forces across the interfaces within the materials which pulled the bonds between loosefill chips apart and forced them to separate.

X-ray diffraction examination of CBL samples indicated higher overall crystallinities in high temperature and high relative humidity conditioned foams compared to untreaed CBL samples.

An Investigation into the Properties of Starch-Based Foams
Chapter 5. The Mechanical Properties of CBL & RPS Starch-Based Foams

201

This was due to shrinkage and density increases in treated samples which resulted in a larger quantity of cell walls and a greater proportion of material per unit volume, thereby increasing the mechanical strength of reconditioned dry samples. Changes in the material's morphology as characterised by re-ordering of the crystalline structures and an increase in peak intensities may be an additional factor explaining the increased mechanical strength of the material under dry conditions.

Chapter 6   The Thermal Properties of CBL & RPS Starch-Based Foams

Previous work conducted to determine the thermal conductivity of starch-based foams focussed primarily on RPS foams, as described in Chapter 2 of this thesis. This chapter describes the results of thermal conductivity tests conducted on CBL and high-density RPS foams. In addition, the results of a series of case studies is presented which investigated the potential for RPS foam to be employed in a current commercial application for the packing and transit of temperature-sensitive food products in which a degree of thermal insulation is required.

6.1   Results of CBL thermal conductivity tests

Thermal conductivity is a measure of how a material transfers heat, determined by recording the steady state heat flux flowing through a material of thickness, under the influence of a fixed temperature gradient.

Assuming steady-state one-dimensional heat flux the thermal conductivity of materials can be derived from Fourier's law of heat conduction:

$$q = -\lambda \frac{\partial T}{\partial x} = \lambda \frac{(T_1 - T_2)}{x} \qquad (5.1)$$

Where: q = heat flux (W)

λ = thermal conductivity (W/m.K)

$\partial T / \partial x$ = temperature gradient (deg./m)

x = sample thickness (m)

Serth, 2007

Using this equation the results of thermal conductivity tests conducted on CBL foams at the selected temperatures are plotted in Figure 6.1 a). For comparison purposes, previous thermal conductivity values from tests conducted on RPS foam (Wang, 2008), as described in Chapter 2, (section 2.11.2) are also included.

An Investigation into the Properties of Starch-Based Foams
Chapter 6. The Thermal Properties of CBL & RPS Starch-Based Foams

203
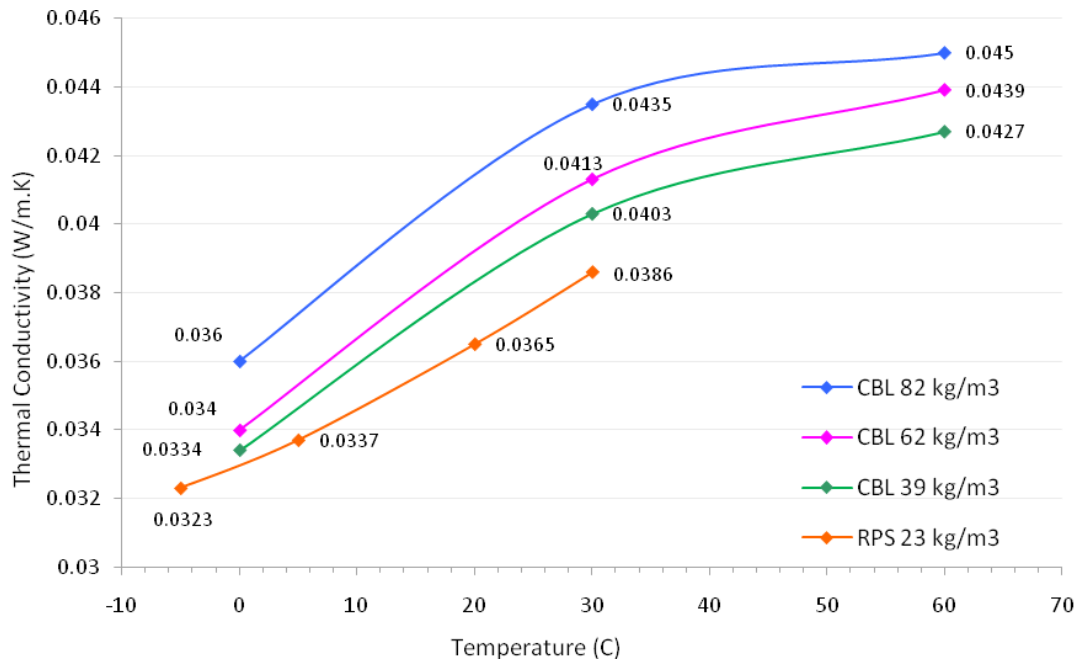
Figure 6.1 a): Thermal conductivity of CBL foams tested at increasing temperatures (0°C, 30°C, 60°C) & thermal conductivity of RPS foam previously tested
Thermal conductivity of RPS foam (Wang, 2008)

For all foam samples tested, thermal conductivity values varied according to the temperature at which they were tested. Unlike conventional polymer foams, starch foams are hygroscopic, the material's density and thus thermal conductivity being somewhat moisture dependent. The effects of moisture loss on the thermal conductivity of CBL samples tested can be seen by comparing Figure 6.1 a) where the CBL foams where tested at three temperatures, with Figure 6.1 b) in which the 30°C data were retested after the samples were exposed to 60°C and had thus lost some moisture.

An Investigation into the Properties of Starch-Based Foams
Chapter 6. The Thermal Properties of CBL & RPS Starch-Based Foams

204
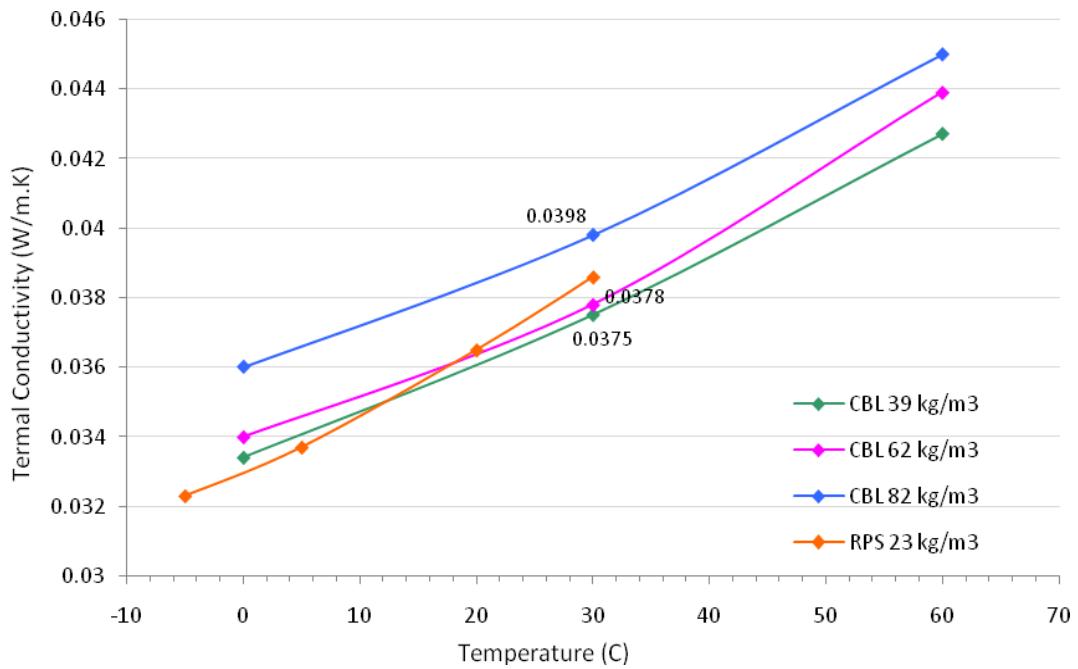
Figure 6.1 b): Thermal conductivity of CBL & RPS foams with final retest of CBL foams at 30°C
Thermal conductivity of RPS foam (Wang, 2008)

The retested 30°C values shown in Figure 6.1 b) were compared to the original 30°C test data shown in Figure 6.1 a). This comparison clearly showed that the thermal conductivity - temperature (λ - T) gradients were dependent on moisture content of the starch foam.

Due to the moisture sensitivity of these starch-based foams, in order to obtain more accurate thermal conductivity gradients, samples should either be preheated prior to testing to remove moisture, or they should be retested at lower test temperatures so that the effect of moisture level variation is taken into account. In these thermal conductivity tests the 30°C tests were again retested after testing at 60°C, however the 0°C tests were not retested and thus these values were adjusted to allow for moisture loss.

Figure 6.1 c) shows thermal conductivity with 0°C test data adjusted by the same amount as the retested 30°C values shown in Figure 6.1 b). The adjusted 0°C values shown in Figure 6.1 c) can be compared to the original 0°C test data previously shown in Figure 6.1 a).

Figure 6.1 c) also provides trendlines for each sample, formulated from thermal conductivity values at the three temperatures tested which illustrate the thermal conductivity - temperature (λ - T) relationships. The *thermal conductivity constants* are also given as equations describing the gradient of each trendline. These can be used to calculate the thermal conductivity of the foams as a function of temperature.

An Investigation into the Properties of Starch-Based Foams
Chapter 6. The Thermal Properties of CBL & RPS Starch-Based Foams

205
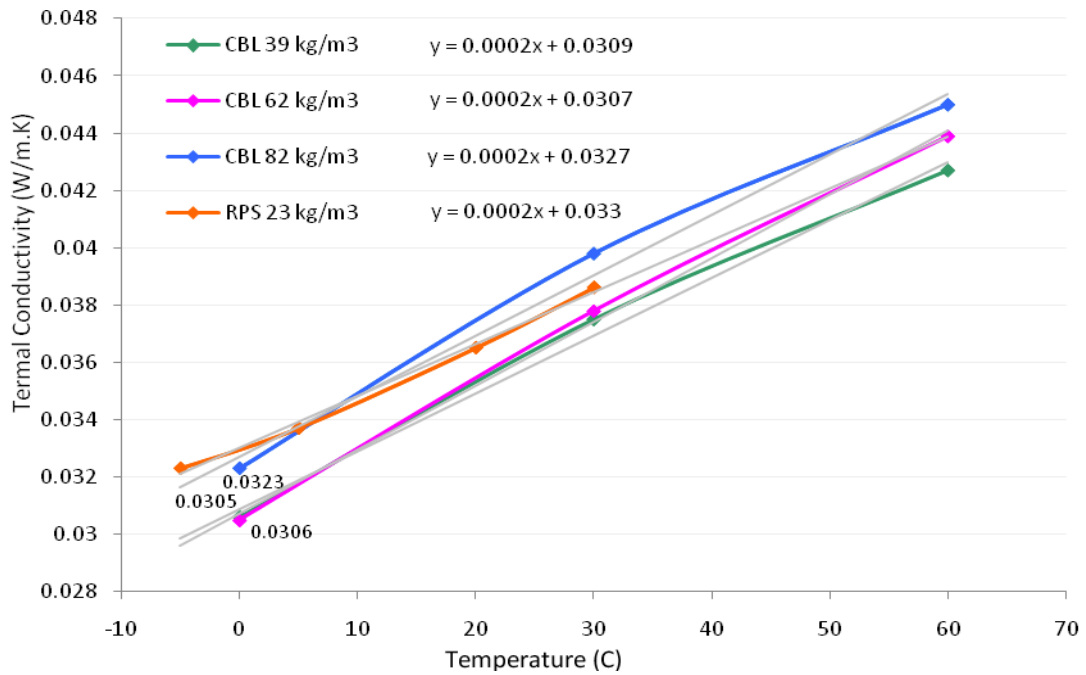
Figure 6.1 c): Thermal conductivity of CBL & RPS foams with final retest of CBL foams at 30°C & adjusted 0°C values (trendlines generated by linear regression)
Thermal conductivity of RPS foam (Wang, 2008)

Figures 6.1 c) illustrates how temperature affects the thermal conductivity of the foams tested. As the test temperature was increased the thermal conductivity of the foams increased. The thermal conductivity - temperature (λ - T) relationships for all samples shown in Figure 6.1 c) followed fairly similar gradients.

The density of the foams also influence their thermal conductivity. Amongst CBL foam samples, higher density foams displayed higher thermal conductivities at any given temperature tested. Data from previous tests conducted to characterise the thermal conductivity of low-density RPS foams (23 kg/m^3), indicated slightly higher thermal conductivity values than the (moisture loss) adjusted values of two higher-density CBL foams (CBL 39 kg/m^3 & CBL 62 kg/m^3), shown in Figure 6.1 c). In the previous tests the specimens of RPS foam were wrapped in a polyethylene film of approximately 0.01 mm thickness after conditioning to prevent further loss or gain of moisture prior to testing. However, no adjustment was made for moisture loss from the samples during testing and this may account for the slightly higher thermal conductivity values of low-density RPS foams shown in Figure 6.1 c).

Figure 6.1 d) shows the thermal conductivity of CBL foams as function of their density, formulated from thermal conductivity values across the three foam densities at each temperature tested. Trendlines are also shown which illustrate the thermal conductivity - density (λ - ρ) relationships. The *thermal conductivity constants* are also given describing the

An Investigation into the Properties of Starch-Based Foams
Chapter 6. The Thermal Properties of CBL & RPS Starch-Based Foams

206

gradient of each trendline. These can be used to calculate the thermal conductivity of the foams as a function of their density.
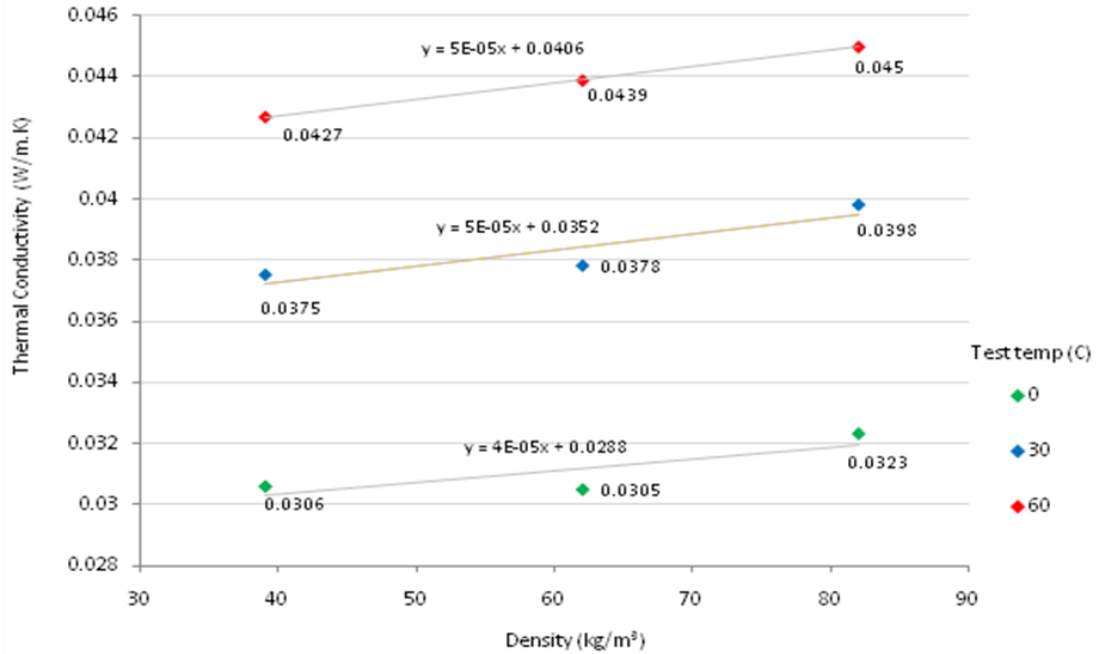
Figure 6.1 d): Thermal conductivity of CBL foams as a function of density (trendlines generated by linear regression)

The trendlines shown in Figure 6.1 d) describe the thermal conductivity - density (λ - ρ) relationship for each CBL foam sample at each temperature tested. This analysis showed a trend for increased thermal conductivity values of higher density samples. The thermal conductivity - density relationships for all CBL samples shown in Figure 6.1 d) followed fairly similar gradients.

6.1.1 Thermal conductivity of CBL & RPS - comparison with polymer foams

Figure 6.2 shows thermal conductivity data for CBL and RPS foams from the tests conducted, compared to a selection of polymer foams of similar densities, tested at approximately 23 °C.

An Investigation into the Properties of Starch-Based Foams
Chapter 6. The Thermal Properties of CBL & RPS Starch-Based Foams

207
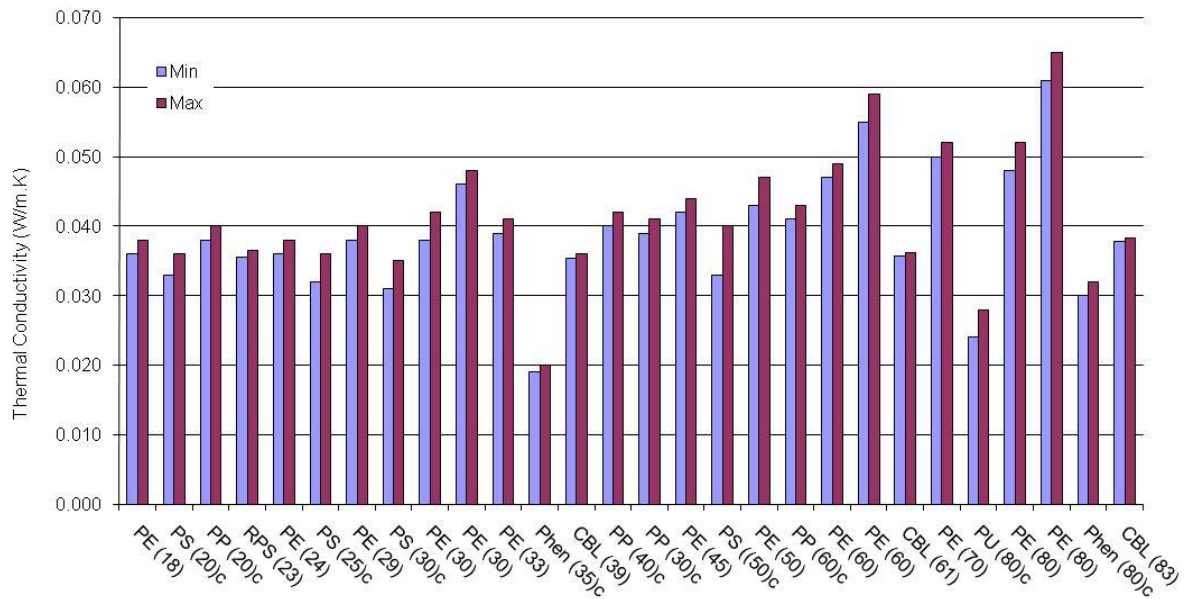
Figure 6.2: Thermal conductivity of CBL & RPS foams compared to selected polymer foams
Data for polymer foams compiled from CES Edupack database 2007.

Key to Figure 6.2: (c denotes closed-cell foam)

Foam	Density (Kg/m3)	Chart Label	k (W/m.K) Min	Max
Polyethylene Foam (LD18)	18	PE (18)	0.036	0.038
Polystyrene Foam: Closed Cell (0.020)	20	PS (20)c	0.033	0.036
Polypropylene Foam: Closed Cell (0.02)	20	PP (20)c	0.038	0.040
Regular Packing & Stacking	23	RPS (23)	0.036	0.037
Polyethylene Foam (LD24)	24	PE (LD24)	0.036	0.038
Polystyrene Foam: Closed Cell (0.025)	25	PS (25)c	0.032	0.036
Polyethylene Foam (LD29)	29	PE (29)	0.038	0.040
Polystyrene Foam: Closed Cell (0.03)	30	PS (30)c	0.031	0.035
Polyethylene Foam (PE30)	30	PE (30)	0.038	0.042
Polyethylene Foam (HD30)	30	PE (30)	0.046	0.048
Polyethylene Foam (LD33)	33	PE (33)	0.039	0.041
Phenolic Foam: Closed Cell (0.035)	35	Phen (35)c	0.019	0.020
Compression Bonded Loosefill	39.2	CBL (39)	0.035	0.036
Polypropylene Foam: Closed Cell (0.04)	40	PP (40)c	0.040	0.042
Polypropylene Foam: Closed Cell (0.03)	40	PP (30)c	0.039	0.041
Polyethylene Foam (LD45)	45	PE (45)	0.042	0.044
Polystyrene Foam: Closed Cell (0.05)	50	PS ((50)c	0.033	0.040
Polyethylene Foam (PE50)	50	PE (50)	0.043	0.047
Polypropylene Foam: Closed Cell (0.06)	60	PP (60)c	0.041	0.043
Polyethylene Foam (LD60)	60	PE (60)	0.047	0.049
Polyethylene Foam (HD60)	60	PE (60)	0.055	0.059
Compression Bonded Loosefill	60.7	CBL (61)	0.036	0.036
Polyethylene Foam (LD70)	70	PE (70)	0.050	0.052
Polyurethane Foam: Closed Cell (0.08)	80	PU (80)c	0.024	0.028
Polyethylene Foam (PE80)	80	PE (80)	0.048	0.052
Polyethylene Foam (HD80)	80	PE (80)	0.061	0.065
Phenolic Foam: Closed Cell (0.080)	80	Phen (80)c	0.030	0.032
Compression Bonded Loosefill	83.5	CBL (83)	0.038	0.038

6.1.2 Interpretation of thermal conductivity performance of CBL

The results of the tests conducted to determine the thermal conductivity of CBL showed a strong correlation between foam density and termal conductivity. Higher-density CBL foam samples displayed higher thermal conductivity values at any given temperature tested.

In comparison to the thermal conductivity of polymer foams of similar densities, starch-based foams performed well. At higher densities particularly, the superior thermal conductivity performance of CBL foams over several conventional polymer foams is notable.

The overall thermal conductivity of foamed materials (λ) can be attributed to four main factors: 1) thermal conduction through the solid materials from which the foam is made (λ_s); 2) thermal conduction through the gas within the cells of the foam (λ_g); 3) thermal convection within the cells of the foam (λ_c), and radiation through cell walls and across cell voids (λ_r).

Thus:

$$\lambda = \lambda_s + \lambda_g + \lambda_c + \lambda_r \qquad \text{(Gibson \& Ashby, 1997)}$$

According to Gibson & Ashby, of these four mechanisms a relatively low proportion (7.5%) of overall thermal conductivity through a closed-cell polystyrene foam with a thermal conductivity of 0.04 W/m.K comes from conduction through the solid (0.003 W/m.K), while the biggest contribution (60%) comes from conduction through the air contained within the cells of the foam (0.024 W/m.K). The remainder then (32.5%), must be contributed by radiation and thermal convection (0.013 W/m.K), although for the majority of foams used in thermal insulation applications, the proportion of overall thermal conductivity attributable to convection is negligible.

Using other examples of a range of closed-cell polyurethane foams with thermal conductivities of approximately 0.021 W/m.K, Gibson & Ashby illustrate how the relative contributions to overall thermal conductivity change according to the relative density of the foams. As the density of these foams increases, the contribution to overall thermal conductivity from conduction through the solid also increases, whilst the contribution to overall thermal conductivity from conduction through gas remains fairly constant.

These examples also illustrate that as foam density increases, the contributions from radiation towards increases in the overall thermal conductivity of the foams, are shown to decrease. Other radiative mechanisms which influence overall thermal conductivity include increases in the thermal conductivity of closed-cell foams with larger cell sizes. This is due to a reduction in the frequency of radiation-blocking reflections from cell walls of foams with larger cells - a characteristic of foams containing fewer cell walls per unit volume.

An Investigation into the Properties of Starch-Based Foams
Chapter 6. The Thermal Properties of CBL & RPS Starch-Based Foams

209

In general, the optimum thermal conductivity of closed-cell polymer foams is achieved at relative densities of between 0.03 - 0.07. At lower relative densities thermal conductivity increases due to the increased transparency of cell walls to radiation, and also because at such densities the cell walls may rupture producing foams with a proportion of open cells (Gibson & Ashby, 1997). These factors have obvious implications for foam structures such as CBL which feature a significant proportion of open cells comprised by cell struts rather than cell walls.

Only in the case of foams with very large cells (>10mm), does thermal convection begin to contribute towards overall thermal conductivity. The proportion of open-cells is another factor affecting the thermal conductivity of foams through thermal convection, but in this respect open-cells are of less significance than cell size (Gibson & Ashby, 1997). Since CBL has a significant proportion of open-cells including relatively large cells and voids, it therefore seems reasonable to assume that thermal convection may contribute, even if only to a very minor degree, towards the overall thermal conductivity of the foam.

Despite the fact that CBL starch foams are comprised by a significant proportion of open-cell structures, Figure 6.2 showed that they present similar or lower thermal conductivities in comparison to their conventional polymer counterparts. In some cases CBL foams displayed reduced thermal conductivity values compared to closed-cell polymer foams of similar densities, potentially signifying the suitability of these materials for thermal insulation applications.

Thus, the excellent thermal conductivity performance of CBL foams cannot be reasonably attributed to thermal resistivity of the cell micro-structure in terms of thermal conduction through the gas within the cells of the foam (λ_g); thermal convection within the cells of the foam (λ_c); or radiation through cell walls and across cell voids (λ_r).

In addition to the standard thermal characterisation of foams (as described by Gibson & Ashby and others), CBL starch foams may require further analysis due to their macrostructures - the interfaces which bond the compressed loosefill chips into the block foams and are characterised by dense areas of compressed foam (as outlined in Chapter 3 of this thesis). Although these dense interfaces may have some influence in increasing thermal resistivity to convection and radiation through the foam, these effects play comparatively minor roles in overall thermal conductivity. It is also possible that resistance to thermal conduction through the air held within CBL foams may be enhanced by the foam macrostructure, perhaps by closure of the pores at the surface of its constituent loosefill chips - in effect imparting CBL foams with some of the characteristics of closed-cell foams.

An Investigation into the Properties of Starch-Based Foams
Chapter 6. The Thermal Properties of CBL & RPS Starch-Based Foams

210

The other factor which may contribute to the thermal conductivity performance of CBL foams may be due to resistance to thermal conduction through the solid material from which these foams are comprised. However, despite data from some studies which have investigated the thermo-physical properties of starch sheets (Frandas et al, 2000; San Martin-Martinez et al, 2008), data pertaining to the particular thermal conductivity of the solid starch used in the production of CBL foam is currently unavailable. The issues highlighted thus clearly represent areas for further research.

An Investigation into the Properties of Starch-Based Foams
Chapter 6. The Thermal Properties of CBL & RPS Starch-Based Foams

211

6.2   Results of tests to determine thermal properties of high-density RPS

The Hot Disk[TM] Thermal Constants Analyser produces three parameters related to the thermal properties of materials tested - thermal conductivity (λ), thermal diffusivity (Td), and specific heat capacity (Cp).

Figure 6.3 shows the results of thermal conductivity testing of high-density RPS foams, including a trend line generated by linear regression.
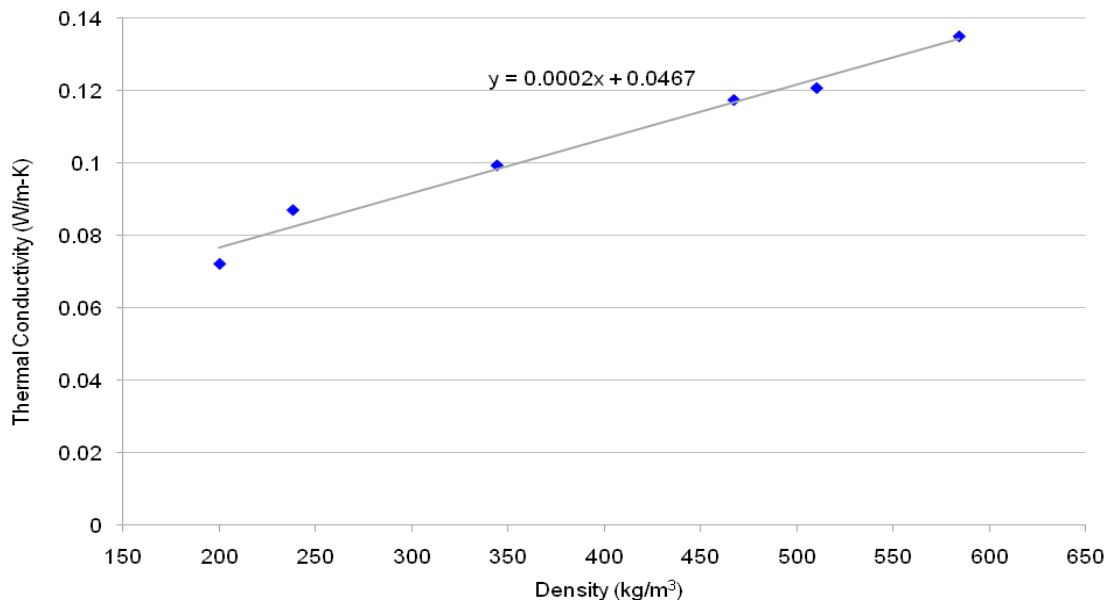
Figure 6.3: Thermal conductivity of high-density RPS foams

Figure 6.3 illustrates the increased thermal conductivity of high-density RPS foams as the sample density tested was increased. These results will be discussed in greater detail in section 6.2.2.

An Investigation into the Properties of Starch-Based Foams
Chapter 6. The Thermal Properties of CBL & RPS Starch-Based Foams

212

Thermal diffusivity can be defined as the ratio of the thermal conductivity to the specific heat capacity per unit volume of material. The thermal diffusivity of materials is closely related to their thermal conductivities and describes the speed of heat propagation through the material. Thermal diffusivity can be expressed:

$$Td = \frac{\lambda}{\rho C_\rho}$$
(5.2)

Where: Td = thermal diffusivity (mm^2/s)

λ = thermal conductivity (W/m.K)

ρ = density (kg/m^3)

C_p = specific heat at constant pressure (Jkg^{-1}K^{-1})

(Czichos *et al*, 2006)

Figure 6.4 shows the results of thermal diffusivity testing of high-density RPS foams, including a trend line generated by linear regression.
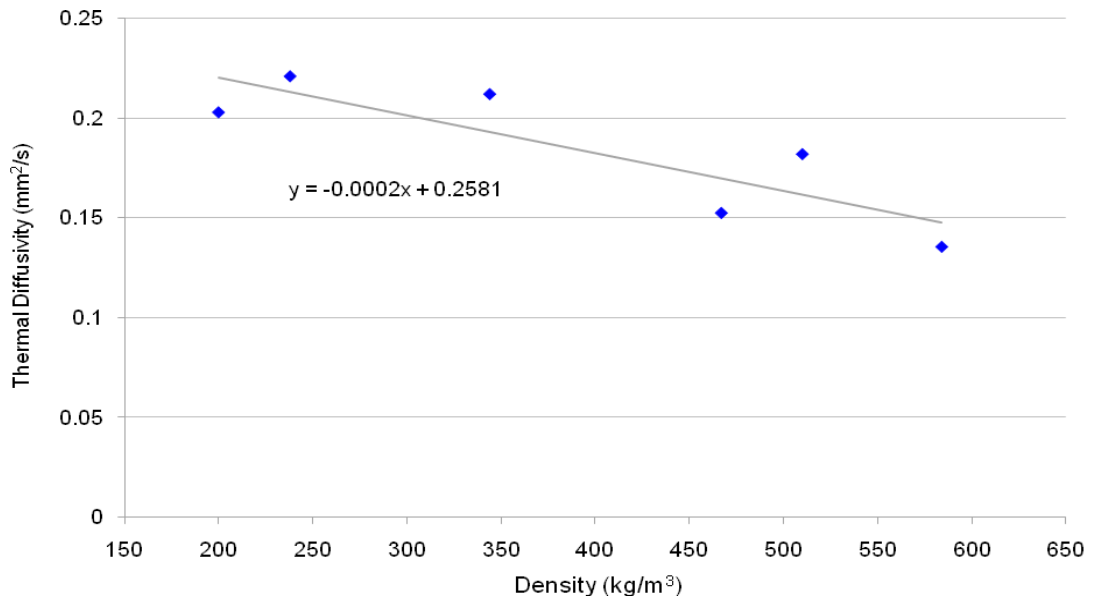
Figure 6.4: Thermal diffusivity of high-density RPS

Figure 6.4 illustrates that thermal diffusivity of high density RPS fell as sample density was increased, which indicated how heat propagation through higher density samples was slowed compared to heat propagation through lower density samples.

Specific heat capacity (*Cp*) is a measure of a material's ability to store heat and can be defined as the energy required to increase the temperature of a unit mass of material by one degree of temperature. If a specific amount of heat (d*Q*) is applied to a thermally isolated specimen of mass (*m*), the relationship between the heat applied and the temperature increase of the specimen (d*T*) can be given as:

$$ \mathrm{d}Q = mC_p\mathrm{d}T $$

(5.3)

(Czichos *et al*, 2006)

Figure 6.5 shows the specific heat capacity estimates as defined by the Hot Disk[TM] Thermal Constants Analyser, for high-density RPS (in units of MJ/m³-K), including a trend line generated by linear regression.
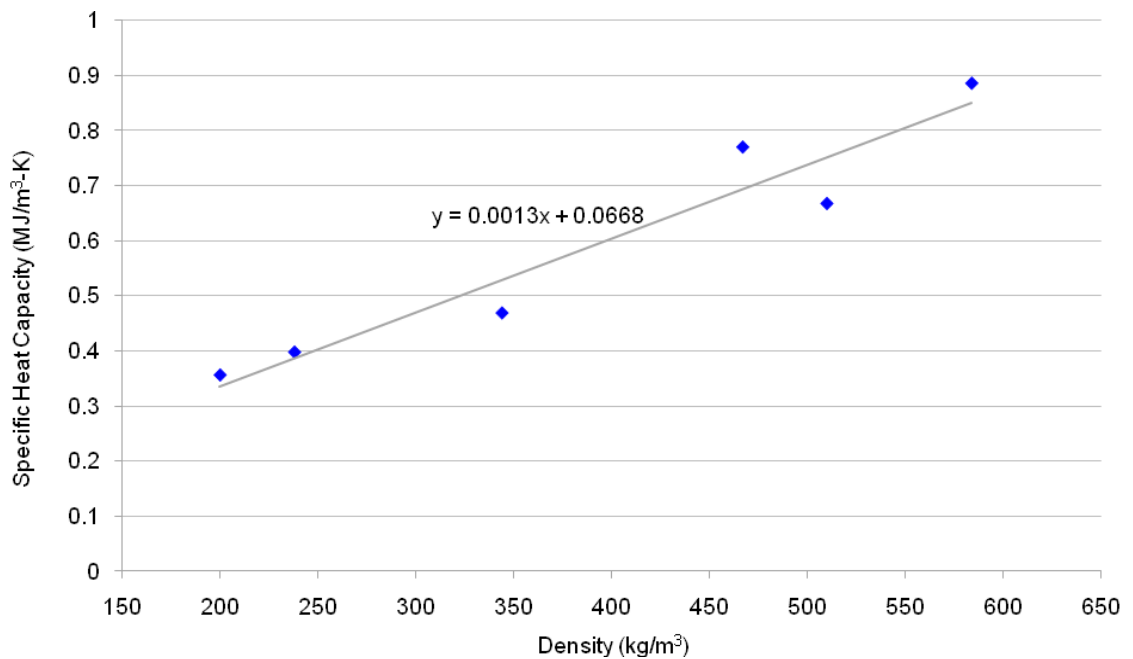
Figure 6.5: Specific heat capacity of high-density RPS

Figure 6.5 illustrates the relationship between sample density and specific heat capacity, in particular showing how the specific heat capacity of high density RPS foam increased as sample density was increased. These results indicate the greater ability of higher density samples to store heat compared to lower density samples.

6.2.1 Thermal conductivity of high-density RPS - comparison with polymer foams

Figure 6.6 shows the thermal conductivity of High Density RPS foams compared to a selection of polymer foams of similar densities, tested at approximately 23 °C.
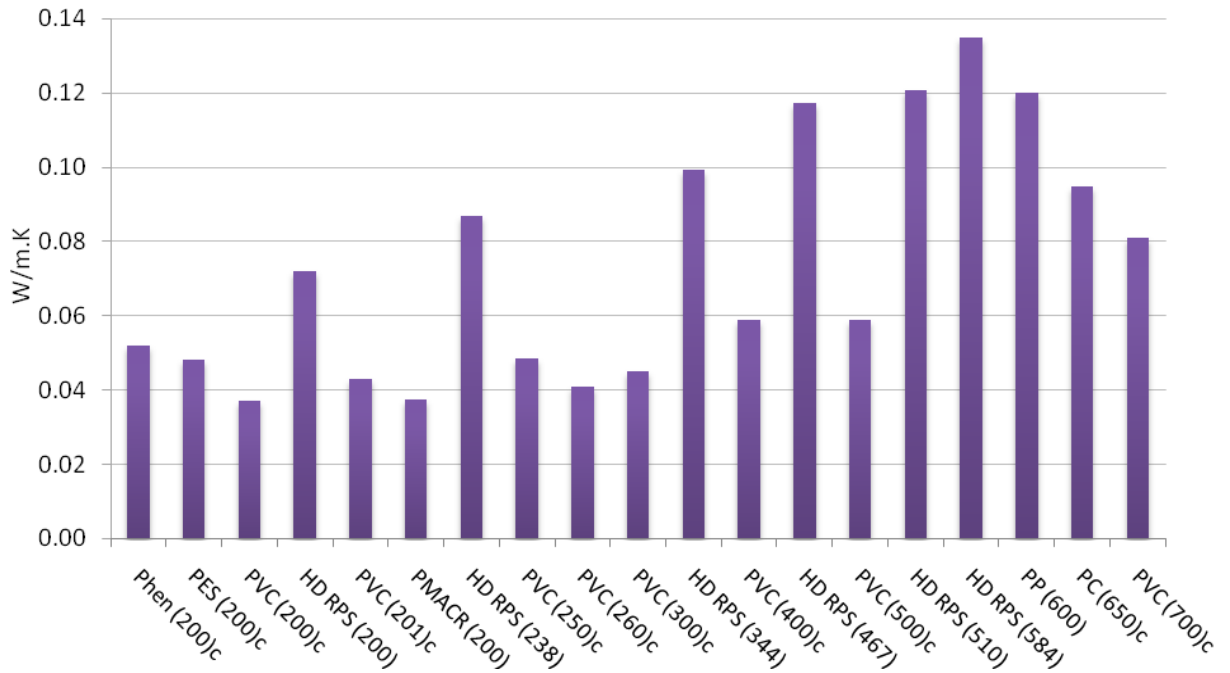
Figure 6.6: Thermal conductivity of High Density RPS foams compared to selected polymer foams of similar densities

Key to Figure 6.6: (c denotes closed-cell foam)

Foam	Density (kg/m3)	Chart Label	k (W/m.K)
Phenolic Foam: Closed Cell	200	Phen (200)c	0.0520
Polyethersulfone Foam: Rigid Closed Cell	200	PES (200)c	0.0480
Polyvinylchloride Foam: Rigid Closed Cell	200	PVC (200)c	0.0370
High Density RPS	200	HD RPS (200)	0.0722
Polyvinylchloride Foam: Rigid Closed Cell	201	PVC (201)c	0.0430
Polymethacrylimide Foam: Rigid PMACR	202	PMACR (200)	0.0375
High Density RPS	238	HD RPS (238)	0.0871
Polyvinylchloride Foam: Rigid Closed Cell	250	PVC (250)c	0.0485
Polyvinylchloride Foam: Rigid Closed Cell	260	PVC (260)c	0.0410
Polyvinylchloride Foam: Rigid Closed Cell	300	PVC (300)c	0.0450
High Density RPS	344	HD RPS (344)	0.0994
Polyvinylchloride Foam: Rigid Closed Cell	400	PVC (400)c	0.0590
High Density RPS	467	HD RPS (467)	0.1175
Polyvinylchloride Foam: Rigid Closed Cell	500	PVC (500)c	0.0590
High Density RPS	510	HD RPS (510)	0.1208
High Density RPS	584	HD RPS (584)	0.1350
Polypropylene Foam: Structural	600	PP (600)	0.1200
Polycarbonate Foam: Rigid Closed Cell	650	PC (650)c	0.0950
Polyvinylchloride Foam: Rigid Closed Cell	700	PVC (700)c	0.0810

Data for polymer foams compiled from CES database 2009.

An Investigation into the Properties of Starch-Based Foams
Chapter 6. The Thermal Properties of CBL & RPS Starch-Based Foams

215

Figure 6.6 shows that high-density RPS samples have higher thermal conductivity values compared to polymer foams of similar densities. Whilst RPS foams were tested at 25 - 27 °C, the data for polymer foams pertains to testing at 23 °C. Although the thermal conductivity of materials is temperature dependent, the slightly higher temperature at which high-density RPS was tested does not invalidate this comparison of its thermal conductivity performance with that of other foams.

6.2.2   Interpretation of high-density RPS thermal test results

The tests conducted on high-density RPS showed strong correlations between the density of the material and its thermal conductivity, thermal diffusivity and specific heat capacity.

Unlike the lower-density CBL samples previously examined (section 6.1), which exhibited comparable or lower thermal conductivity values compared to polymer foams of similar densities, in general the high-density RPS samples tested had comparable or higher thermal conductivity values when viewed against polymer foams in their density range.

As previously discussed, the overall thermal conductivity of foamed materials (λ) can be attributed to four main factors: 1) thermal conduction through the solid materials from which the foam is made (λ_s); 2) thermal conduction through the gas within the cells of the foam (λ_g); 3) thermal convection within the cells of the foam (λ_c), and radiation through cell walls and across cell voids (λ_r). Thus the main focus of any analysis must look at the particular cell structures of the foams as well as the thermal conductivity of the solid materials from which the foams are made.

The high-humidity treatment of RPS foams (as outlined in Chapter 4, section 4.3.2.1), produces foam samples with significantly increased densities. Microscopic examination of high-density RPS showed that modification of the foam's cellular structure during high-density RPS treatment is responsible for these density increases (Wang, 2008). Figure 6.7 shows a SEM image of the typical cell structure of RPS foam prior to the high-density RPS treatment.

An Investigation into the Properties of Starch-Based Foams
Chapter 6. The Thermal Properties of CBL & RPS Starch-Based Foams

216
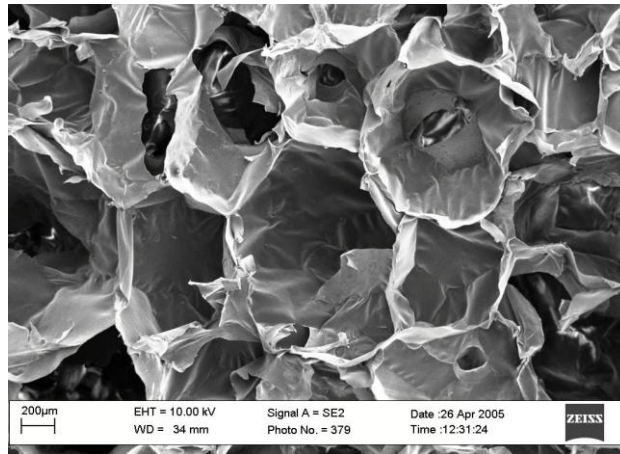
Figure 6.7: SEM image of cross-section of RPS foam prior to high-density treatment showing typical cell structure (14 kg/m³) *Wang, 2008*

Figure 6.7 shows fully-expanded cells with some cell wall membranes ruptured resulting in interconnected and open cells. During high humidity treatment, the cells undergo a reduction in size due to the shrinkage and relaxation of the expanded cell walls under conditions of high-humidity (as previously described, Chapter 2, section 2.12).

As shown in Figure 6.8 a), during the subsequent compression process of the high-humidity treatment, the relatively thin cell walls (circled), tend to be more susceptible to buckling and folding while the thicker walls and joints (rectangular box), tend to resist such a cell-wall deformation. With further increases in compression a more uniform and higher-density laminar structure is formed as shown in Figures 6.8 b) – 6.8 d) (Wang, 2008).

An Investigation into the Properties of Starch-Based Foams
Chapter 6. The Thermal Properties of CBL & RPS Starch-Based Foams

217
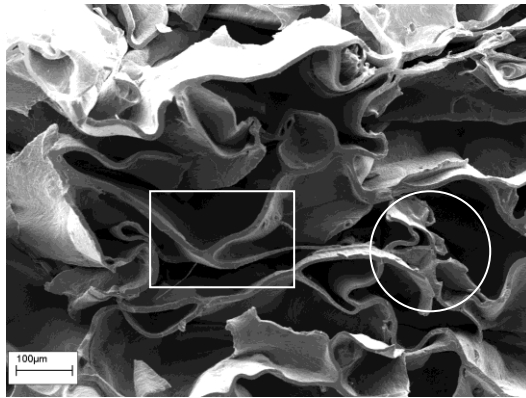
(a) ρ=224.6 kg/m^3 **(b)** ρ=350.5 kg/m^3
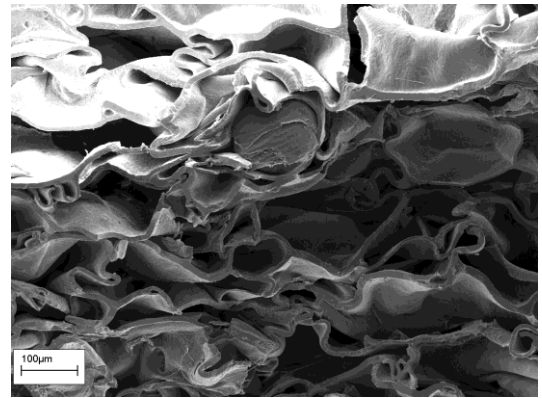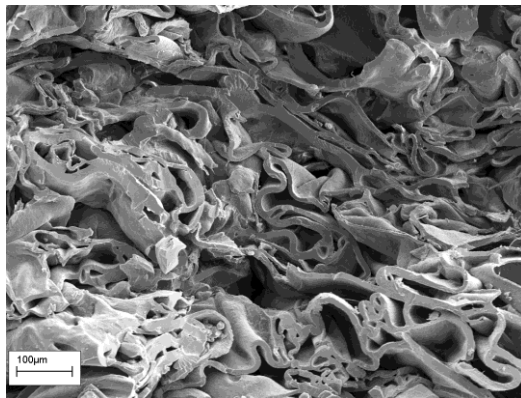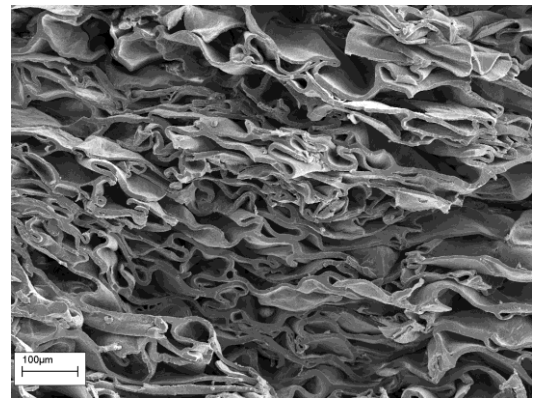
(c) ρ=488.7 kg/m^3 **(d)** ρ=590.7 kg/m^3

Figure 6.8 a), b), c) & d): SEM images of cross-sections of high-density RPS treated samples compressed to different densities, showing changes in cell structure. *Wang, 2008*

Such modifications of the density and cell structure of RPS foams will inevitably change the thermal properties of the material. As shown above in Figures 6.8 (a-d), the high-density treatment of RPS foams results in laminar structures in which adjacent cell walls are in contact with each other, allowing increased thermal conduction through the solid materials from which the foam is made and also through the reduced volumes of air between the modified cell structures of the foam. The correlation between the density of RPS foams and its thermal conductivity is reflected in Figure 6.9, which shows the thermal conductivity of high-density RPS foams in conjunction with thermal conductivity data from previous tests on untreated low-density RPS foam.

An Investigation into the Properties of Starch-Based Foams
Chapter 6. The Thermal Properties of CBL & RPS Starch-Based Foams

218
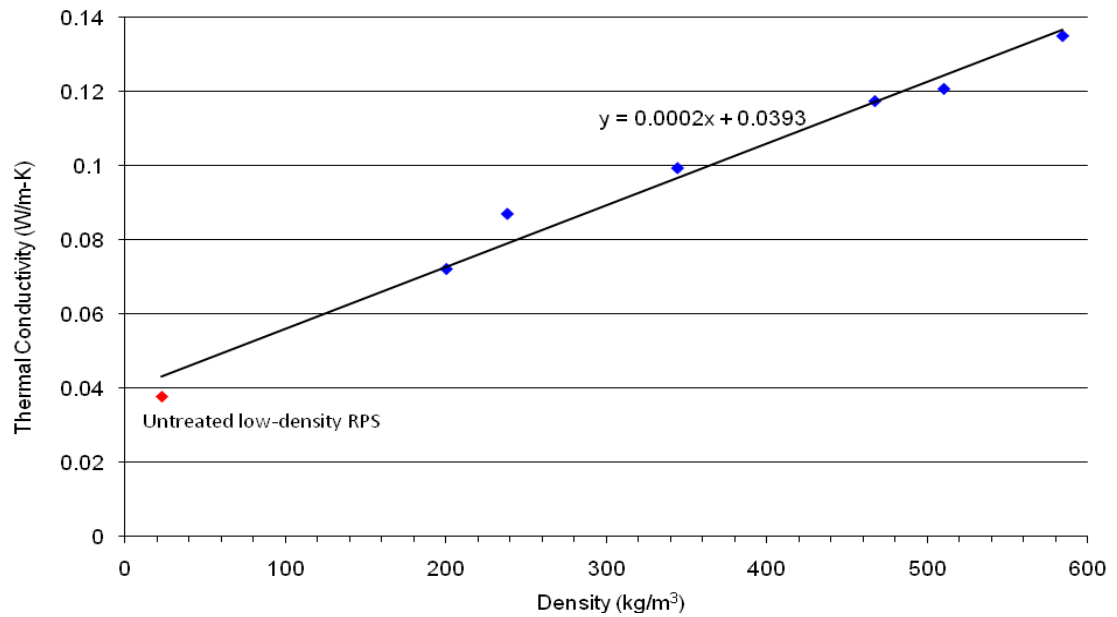
Figure 6.9: Thermal conductivity of low-density & high-density RPS (at 25-27°C)
(trendline generated by linear regression)
Thermal conductivity data of untreated low-density RPS foam (Wang, 2008)

Figure 6.9 shows a linear correlation between the thermal conductivity of RPS foams and their density, which extends over a wide density range from 23 kg/m^3 to 584 kg/m3. This analysis clearly shows that the increases in density of the modified RPS foams are responsible for their increased thermal conductivity values.

Whilst the densified cell structures of high-density RPS clearly contribute towards thermal conduction through the solids and air spaces of the foam, increasing their overall thermal conductivities, to what extent their non-uniform microstructures impart these foams with higher overall thermal conductivity values compared to polymer foams of similar densities is unclear. A comparison of the thermal conductivity of the solid material from which RPS starch-based foams are made with that of solid polymers is required in order to establish the relative contribution of the conductivity of starch towards the overall thermal conductivity of RPS foams. However, since data pertaining to the thermal conductivity of the solid starch used in the production of RPS is unavailable it is not currently possible to establish these relative contributions and this is clearly an area for further research.

An Investigation into the Properties of Starch-Based Foams
Chapter 6. The Thermal Properties of CBL & RPS Starch-Based Foams

219

6.3 Case study: Comparison of polyethylene & RPS starch foam in commercial thermal packaging application

Section 6.3 presents results from a series of tests and trials conducted to determine the performance of RPS starch-based foam in an existing commercial coolbox application as previously detailed in Chapter 4, section 4.3.3.

6.3.1 Results of static laboratory tests

Figures 6.10 a) - 6.10 d) present the results of the tests and are shown as a comparison between thermocouple readings in identical positions in the PE and RPS-lined coolboxes as previously described in Chapter 4, Figures 4.22 and 4.23.
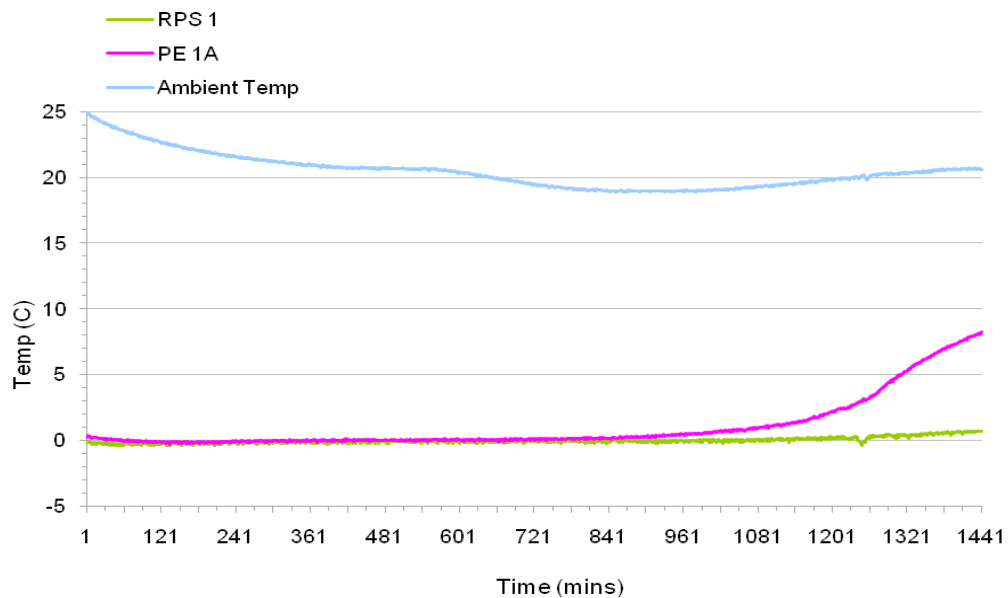
Figure 6.10 a): Temperature variations at thermocouple positions 1 and 1A

An Investigation into the Properties of Starch-Based Foams
Chapter 6. The Thermal Properties of CBL & RPS Starch-Based Foams

220
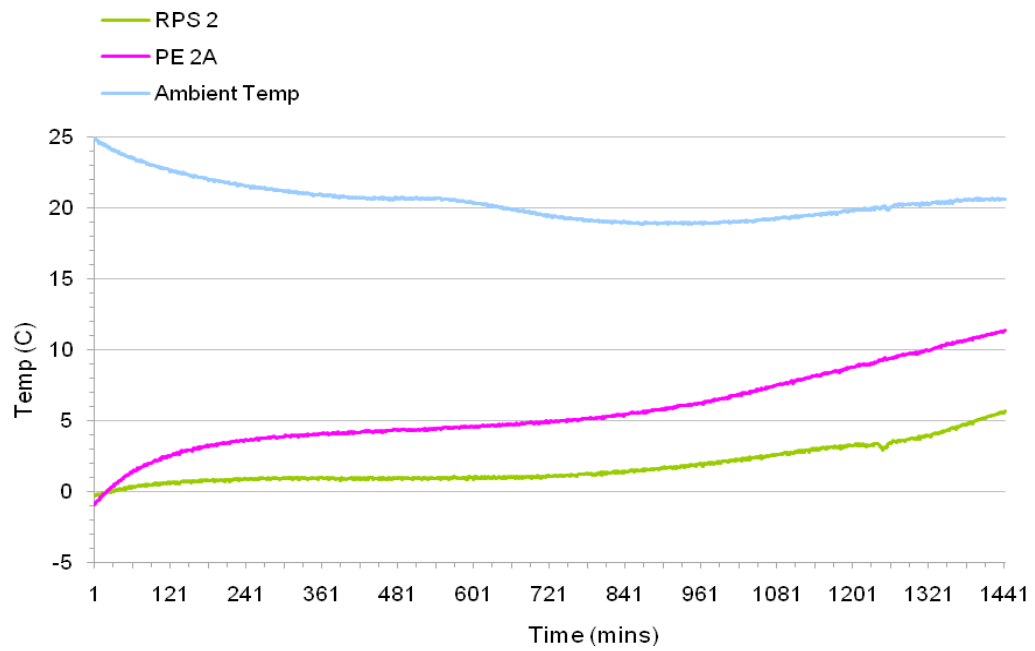
Figure 6.10 b): Temperature variations at thermocouple positions 2 and 2A
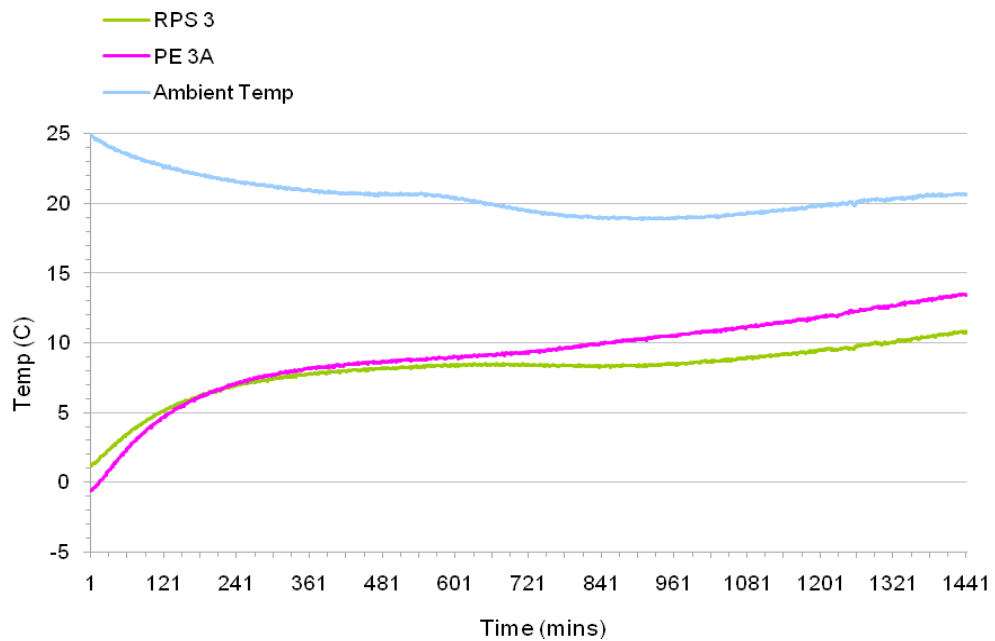
Figure 6.10 c): Temperature variations at thermocouple positions 3 and 3A

An Investigation into the Properties of Starch-Based Foams
Chapter 6. The Thermal Properties of CBL & RPS Starch-Based Foams

221
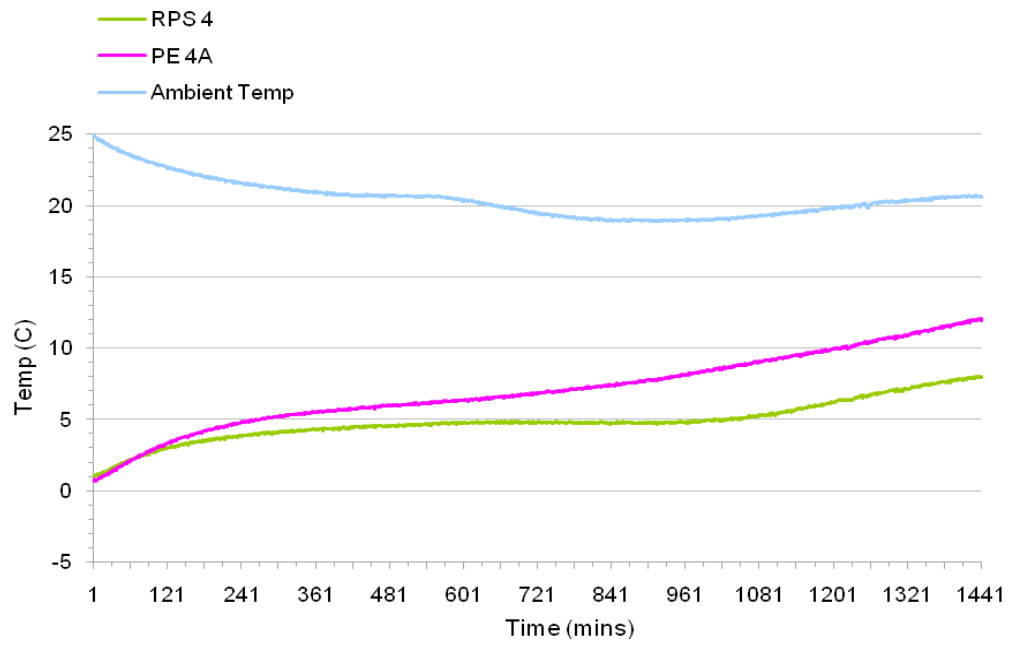
Figure 6.10 d): Temperature variations at thermocouple positions 4 and 4A

An Investigation into the Properties of Starch-Based Foams
Chapter 6. The Thermal Properties of CBL & RPS Starch-Based Foams

222

6.3.2   Interpretation of static laboratory test results

Figures 6.10 a) - 6.10 d) showed that in each case the RPS-lined coolbox performed better than the PE-lined coolbox, maintaining lower product temperatures at all thermocouple positions during the test period. The RPS foam-lined coolbox was able to maintain the required temperatures (below 5°C) during the 24 hour test period, at the point closest to the centre of the coolbox (thermocouple 1A) and on the shorter edge of the coolbox (thermocouple 2A). However, on the long edge of the coolbox (thermocouple 4A), the temperature rose faster and the required temperature was only able to be maintained below 5°C for 18 hours. In terms of maintaining product temperatures, the worst area measured was at the corner of the coolbox (thermocouple 3A) where it only took approximately 2 hours to reach 5°C.

Clearly uniform temperatures within coolboxes cannot be assumed and particular attention should be given to the insulation of chilled products at corners and edges of coolboxes, or the use of additional refrigerant adjacent to goods to compensate for the greater thermal losses in these locations. This is obviously an area requiring further investigation by means of temperature profile modelling within RPS-lined coolboxes in order to take account of the effects of thermal insulation and the packaging of goods and refrigerants.

An Investigation into the Properties of Starch-Based Foams
Chapter 6. The Thermal Properties of CBL & RPS Starch-Based Foams

223

6.3.3   Results of first transit trial

A comparison of core coolbox temperatures monitored by the Tinytags is shown in Figure 6.11.
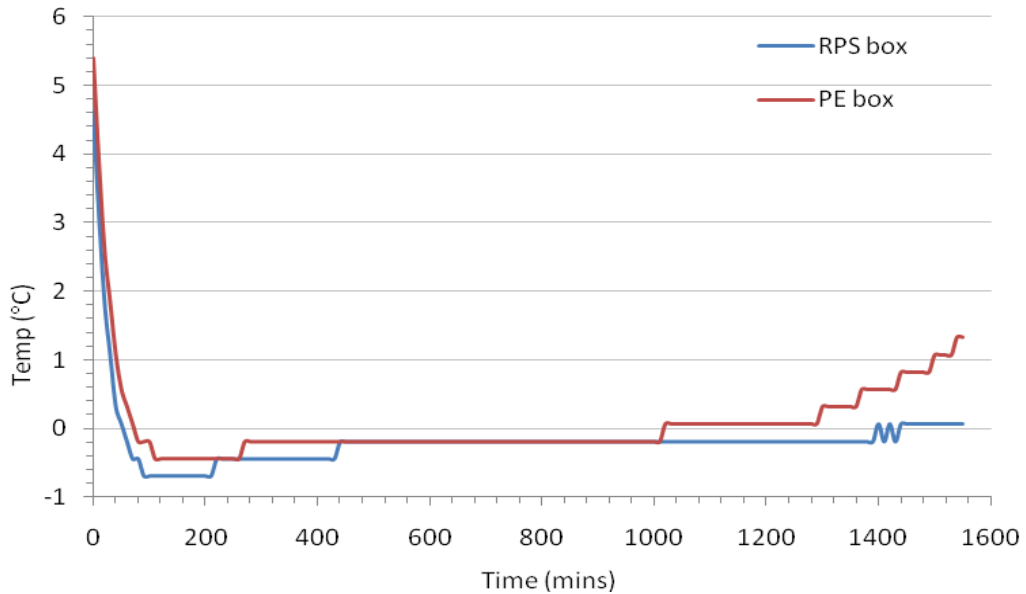
Figure 6.11: Comparison of product core temperatures (first transit trial)

6.3.4   Interpretation of the first transit trial results

The results of the first transit trial shown in Figure 6.11 demonstrated that both coolboxes exceeded expected performance requirements, maintaining core temperatures below 5 °C for a period of 24 hours. Comparison of core temperatures in the packed coolboxes appeared to indicate greater thermal insulation performance from the RPS-lined coolbox which maintained lower core temperatures for longer than the PE-lined coolbox. This divergence in performance is demonstrated by Figure 6.11 at times in excess of 1000 minutes.

However, it should be noted that in these trials the core temperatures of both coolboxes were reduced to below freezing point for a significant period of the trial. This possibly occurred as a result of the frozen ice sheets used as refrigerant coming into close proximity to the Tinytag data monitors.

An Investigation into the Properties of Starch-Based Foams
Chapter 6. The Thermal Properties of CBL & RPS Starch-Based Foams

224

6.3.5   Results of the second transit trial

Figure 6.12 shows the results of the second transit trial
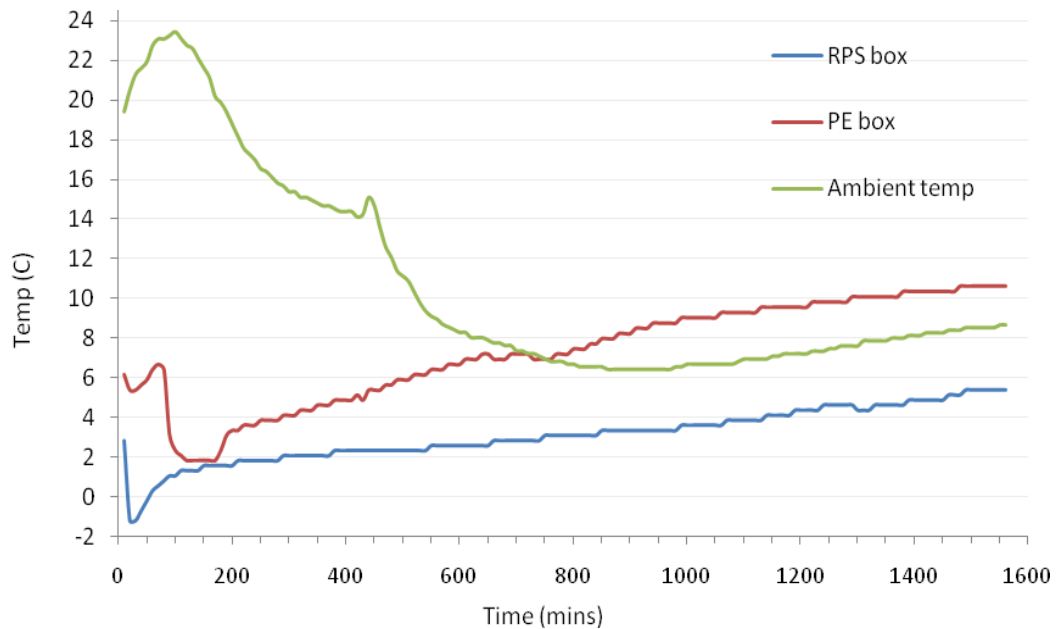
Figure 6.12: Results of the second transit trial

6.3.6   Interpretation of the second transit trial results

It should be noted that Tinytag data monitors were adhered to the exterior of the coolboxes and hence were affected by the low temperatures within the boxes. Figure 6.12 shows averaged monitor readings fell with time, reflecting the ambient air temperature around the coolboxes. Data monitors within the coolboxes were located at their outer edges - the point of highest temperature within the coolboxes.

Chilled product temperatures within a thermally insulated environment often fluctuate during the first hour or two of packing due to contents with different temperatures being packed together, which then stabilise as heat exchange takes place between them. Although the temperature monitored by the data monitor located inside the PE foam coolbox had registered values of approximately 3 °C higher at the start of the trial, by 150 minutes into the trial temperatures had settled and were approximately equal to those monitored inside the RPS coolbox. After this point during the trial period, the RPS coolbox maintained approximately a 5 °C lower temperature within the coolbox compared to the temperature monitored within the PE coolbox, effectively representing delivery of the product to the required condition (sub 5° C

An Investigation into the Properties of Starch-Based Foams
Chapter 6. The Thermal Properties of CBL & RPS Starch-Based Foams

225

within 24 hours). In contrast, the monitored temperature inside the PE coolbox rose above 5 ° C in a period of approximately 7 hours and would not have achieved this objective.

Since the product starting temperature inside the PE coolbox was slightly higher at the start of the trial, a more equitable comparison against the RPS coolbox was produced by means of temperature compensation, subtracting 3.33 °C from all monitored temperature measurements inside the PE coolbox as shown in Figure 6.12. Results of second transit trials with adjusted internal PE coolbox temperatures is shown in Figure 6.13.
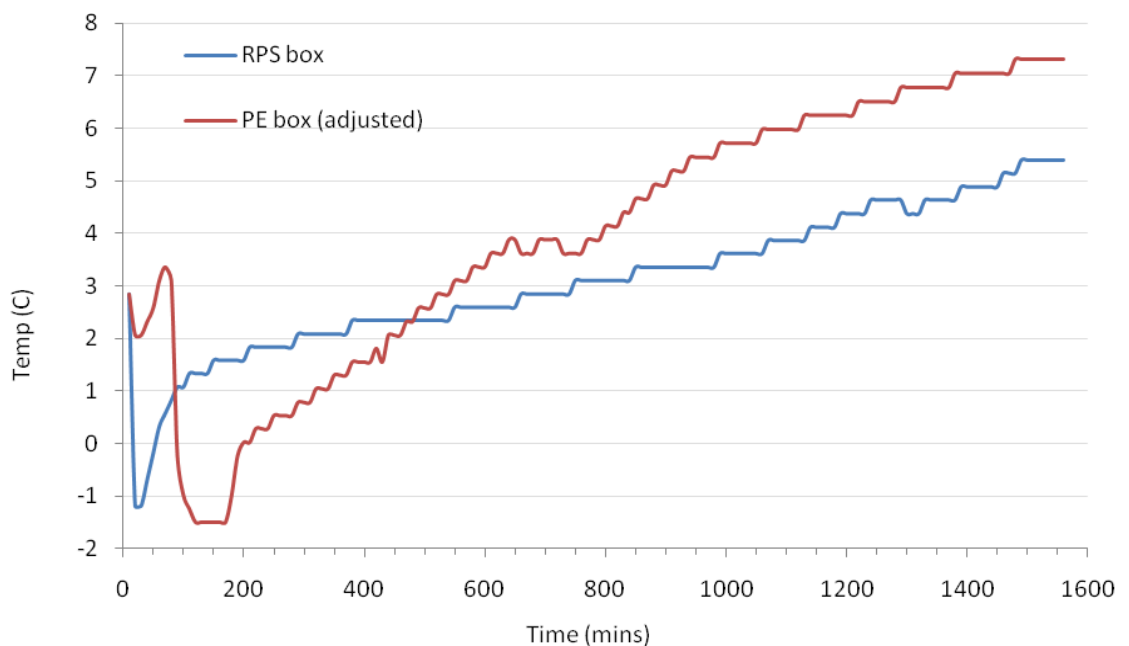
Figure 6.13: Results of second transit trial with adjusted internal PE coolbox temperatures

Despite the adjusted PE coolbox values, the comparison shown in Figure 6.13 demonstrated that the RPS coolbox nevertheless maintained a lower internal temperature than the PE coolbox and so can be said to have superior thermal insulation properties. It should also be noted that due to removal of the protective corrugated fibreboard inner liner within the RPS coolbox (as used in the first transit trials described in Chapter 4, section 4.3.3.1), in the second transit trials the total thickness of the RPS foam liner was only 26mm in comparison with 29mm for that of the PE foam liner. This extra thickness should have slightly benefitted the PE foam-lined coolbox in terms of its thermal insulation performance.

As outlined previously, one aspect of the second transit trails was to determine whether an unlined RPS coolbox without the protective cardboard lining (as used in the static laboratory

An Investigation into the Properties of Starch-Based Foams
Chapter 6. The Thermal Properties of CBL & RPS Starch-Based Foams

226

tests and first transit trials), would be adequately durable to resist the effects of condensation from the frozen ice sheets and chilled product inside the coolbox.

Following the second transit trials, the RPS foam inside the coolbox was examined and found to have slightly deformed in some areas where it had come into contact with the frozen ice sheets. In these areas of deformation it was observed that surfaces of the RPS in contact with ice sheets had formed a compacted skin which may have protected it against continued ingress of moisture and further deformation. Given the superior performance of the RPS-lined coolbox in the second transit trials, the deformation observed clearly did not compromise the thermal insulation performance of the RPS foam to a degree which impaired its performance in this application. The durability and resistance of unprotected RPS foam to condensation within the coolbox is thus deemed sufficient for this relatively short-timescale application. Figure 6.14 shows slight deformation of the RPS foam liner following the second transit trial.

Figure 6.14: Slight deformation of the unlined RPS foam following the second transit trial

6.4   Discussion of the thermal properties of CBL and RPS starch-based foams

In comparison to the thermal conductivity of polymer foams of similar densities, CBL starch-based foams performed well, particularly at higher densities, exhibiting similar or lower thermal conductivities in comparison to their polymer foam counterparts. Despite the fact that CBL starch-based foams are comprised by both open and closed cell structures, in some cases CBL foams displayed reduced thermal conductivity values compared to closed-cell polymer foams of similar densities, potentially signifying the suitability of these materials for applications in which a degree of thermal insulation is required.

Given the non-uniform open and closed cell structure of CBL foams, their excellent thermal conductivity performance cannot be reasonably attributed to thermal resistivity of their cell micro-structure. However, it is possible that resistance to thermal conduction through the air held within CBL foams may be enhanced by the foam macrostructure, in effect imparting CBL with the some of the characteristics of closed-cell foams.

The other factor which may contribute to the thermal conductivity performance of CBL foams may be resistance to thermal conduction through the solid material from which these foams are comprised. However, since data pertaining to the thermal conductivity of the solid starch used in the production of CBL foams is unavailable it is not currently possible to establish the relative contribution of this mode of thermal conduction towards the overall thermal conductivity of the foam. This is therefore an area for further research.

Tests conducted on high-density RPS showed strong correlations between the density of the material and its thermal conductivity, thermal diffusivity and specific heat capacity. Although still comparable to polymer foams of similar densities, the thermal conductivity of high-density RPS was generally higher than its polymer foam counterparts. Modifications of the density and cell structure of RPS foams by means of high-density treatment, changes the thermal properties of the material and the results in laminar structures in which adjacent cell walls are in contact with each other. This allows increased thermal conduction through the solid materials from which the foam is made and also through the reduced volumes of air between the modified cell structures of the foam.

To what extent the irregular microstructures of high-density RPS foams impart these materials with higher overall thermal conductivity values compared to the more uniform microstructures typically observed in polymer foams of similar densities is unclear. A comparison of the thermal conductivity of the solid material from which RPS starch-based foams are made against that of solid polymers is required in order to establish the relative contributions through this mode of

An Investigation into the Properties of Starch-Based Foams
Chapter 6. The Thermal Properties of CBL & RPS Starch-Based Foams

228

heat transfer. This reinforces the need for further research to establish the thermal conductivity of the solid starch used in the production of these starch-based foams.

Assimilation of thermal conductivity data from previous tests conducted on low-density RPS foams with data from tests conducted on high-density RPS foams, showed that all samples closely followed the trendline, illustrating how densification of starch-based foams results in increased thermal conductivity over a broad density range. These findings reinforce knowledge of the density/thermal conductivity relationship of these materials and indicate that the microstructures of these foams play a major role in determining their overall thermal conductivity performance.

The case study benchmarked RPS foam at standard density against a current commercial coolbox system comprising a polyethylene foam liner used to reduce thermal conductivity and maintain the temperature of its contents.

Thermocouple readings taken from the static laboratory tests which formed part of the case study, indicated that although the start temperatures were appropriate for chilled food, those temperatures rose too quickly and the validity of the tests was compromised. The results from these tests showed that the facilities available had not reduced *core* product temperatures adequately and as such these tests could not be considered commercially valid. However, despite this setback the results provided a good comparison between the two different coolbox systems and it was observed that in each case the RPS starch foam-lined coolbox maintained the product contained at a lower temperature for a longer period than the equivalent polyethylene foam-lined coolbox.

As part of the case study, the static laboratory tests were reinforced by findings of two transit trials, These trials showed that in addition to exhibiting sufficient durability to perform the shipping function required, the RPS starch-based foam coolbox liner out-performed the polyethylene foam coolbox liner in terms of maintaining product temperatures within a specified range.

The case study reinforced the findings of the thermal conductivity tests conducted on CBL and it can therefore be concluded that given sufficient research and development, these starch-based foams could potentially be utilised in applications requiring a degree of thermal insulation functionality.

Chapter 7   The Acoustic Properties of CBL & RPS Starch-Based Foams

7.1   Results of airborne sound absorption coefficient tests

Figure 7.1 shows the results of the sound absorption coefficient (α) tests conducted.

The PULSE ^{TM} analysis software has combined the frequency ranges from the two different sets of absorption coefficient tests covering 50 – 800 Hz and 800 – 6,400 Hz of each into a single combined frequency range of 50 – 6,400 Hz.
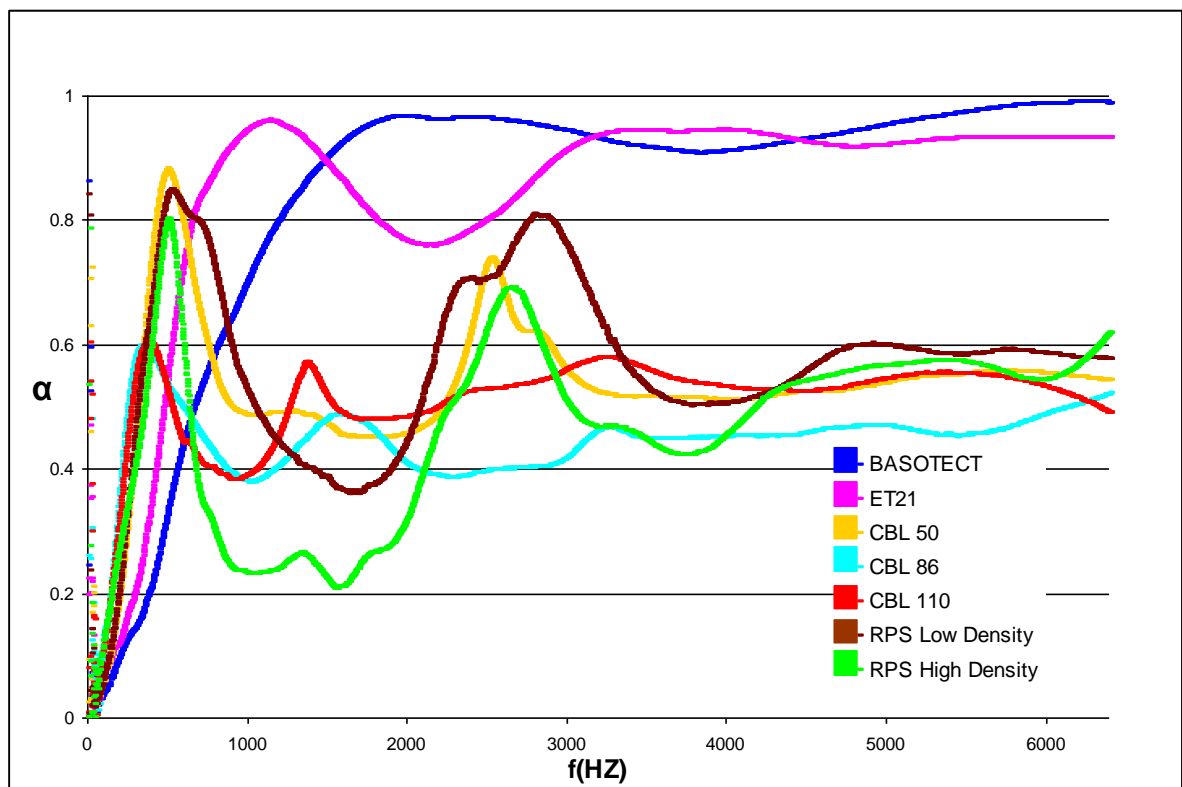
Figure 7.1: Sound absorption coefficient (α) results as function of frequency (f)

7.1.1   Interpretation of airborne sound absorption coefficient test results

An ideal acoustic sound absorbing material would absorb 100% of all audible frequencies tested and would be represented in Figure 7.1 by a straight horizontal line at 1 (or 100%) on the *y* axis ranging from zero to 6,400 Hz on the *x* axis. Thus, for sound absorption coefficient, units of measurement are given as a proportion of the ideal, and as such the scale is linear. In reality, no such ideal sound absorbing material exists. The sound energy absorption performance of cellular solids such as foams is dependent on vibrations within their cell structures in response to sound incidence in order to dissipate that sound energy.

An Investigation into the Properties of Starch-Based Foams
Chapter 7. The Acoustic Properties of CBL & RPS Starch-Based Foams

230

Figure 7.1 shows that the low-density polymer foams Basotect and ET21/250 were the best performing materials in these tests which demonstrated a higher sound absorption coefficient across a wider range of frequencies than the starch foams tested. In the case of cellular materials, any deformation in response to sound energy occurs at the cellular level, within the cell walls or struts of the material. This has obvious implications in terms of the architecture of the foam's cell structure. For example, closed cell foams tend not to absorb sound energy as well as open cell foams due to the presence of cell walls which restrict the permeation and absorption of sound energy. Foams of lower density typically exhibit higher sound absorption coefficients than foams of higher density due to the reduced resistance of the cell walls or struts from which these materials are comprised to be deformed elastically (non-permanently), under applied stresses. Thus, it is both the structure of cellular materials as well as the elastic modulus of the solid polymers from which they are comprised, which influence the sound absorption coefficient performance of foams and these are thus key determinants in the basis of any analysis.

Due to the unavailability of data pertaining to the elastic modulus of the solid polymers from which the foams Basotect and ET21/250 are derived, Table 7.1 compares previously published data for melamine formaldehyde, polyurethane resin and unplasticised starch film.

Table 7.1: Comparison of elastic modulus of solid polymers and solid starch

Foam	Solid Polymer	Density (kg/m3)	Elastic modulus (MPa)
Basotect	Melamine formaldehyde	1430	6730 - 7070
ET21/250	Polyurethane resin	1130	1310 - 2070
CBL & RPS	Unplasticised starch film	1300	3150

Melamine Formaldehyde: alpha cellulose filled, modified (CES Edupack database, 2010).
Polyurethane resin: unreinforced moulding grade (PUR molding) (CES Edupack database, 2010).
Solid unplasticised starch film (Copeland et al, 2007).

When viewed in the context of foam microstructure (cell walls or cell struts), the significantly higher elastic modulus of melamine formaldehyde may be one factor in explaining the superior sound absorption coefficient performance of Basotect foam as seen in Figure 7.1. However, unplasticised solid starch has a higher elastic modulus compared to solid polyurethane resin and therefore this does not explain the greater sound absorption coefficient performance of ET21/250 foam compared to CBL and RPS starch-based foams. Other factors which may account for the inferior sound absorption coefficient values of starch-based foams compared to ET21/250 foam may be due to

An Investigation into the Properties of Starch-Based Foams
Chapter 7. The Acoustic Properties of CBL & RPS Starch-Based Foams

231

differences in foam microstructures. The greater proportion of closed cells found in starch-based foams as compared to typical uniform open-cell polyurethane foams will result in reduced sound energy absorption. In addition, the non-uniform macrostructures of CBL and RPS starch-based foams comprise areas of much denser material and thus represent a reduced proportion of absorptive material in terms of sound energy absorption per unit volume. These microstructure and macrostructure characteristics of macro-composite starch-based foam and open-cell PU foam can be seen in Chapter 3, Figures 3.14 and 3.15.

When comparing the sound absorption coefficients of starch foams of different densities shown in Figure 7.1, the lower density starch foams can generally be seen to have exhibited higher sound absorption coefficients across a wider range of frequencies than starch foams of higher densities. Since these starch foams were all fabricated from the same material, this performance variation was due to the increased proportion of dense compressed macrostructure interfaces within higher density foams, resulting in a reduced proportion of absorptive material in terms of sound energy absorption per unit volume of foam.

The double peaks displayed by the plotted absorption coefficient measurements of both the CBL and RPS foams in Figure 7.1 may be explained by the non-homogeneous structures of the materials which influence local densities within the foams. Acoustic *boundary conditions* can occur in materials where juxtapositions of dramatically harder & softer surfaces are present (Vickers, 2006). Materials such as CBL and RPS foams are characterised by a network of high- density bonding interfaces encapsulating lower density foam domains and hence are subject to such boundary conditions which may account for the double peaks illustrated.

It is interesting to note that at a certain narrow range of low frequencies (approx. 50 - 750 Hz), the starch foams outperform the benchmark polymer foams and have absorbed a greater proportion of sound energy. Low frequency sound waves are notoriously difficult to attenuate, but the reasons for the higher absorption coefficient of starch foams at these frequencies is unclear. This phenomenon may be attributable to the existence of certain degree of open cells in the starch foams as a result of cell rupture during extrusion foaming. The ruptured cell walls may have been able to respond to low frequencies during the tests, which may have led to the increased absorption of low-frequency sound energy.

An Investigation into the Properties of Starch-Based Foams
Chapter 7. The Acoustic Properties of CBL & RPS Starch-Based Foams

232

7.2   Results of airborne sound transmission loss (STL) tests

Figures 7.2 a) and 7.2 b) show the results of the sound transmission loss tests conducted as sound loudness disparity on each side of the samples expressed in decibels (dB). Unlike the sound absorption coefficient results, the analysis software was unable to combine the frequency ranges from the two different size samples of each material tested. Thus the results for 50 – 800 Hz and 800 - 6,400Hz frequencies are displayed separately.
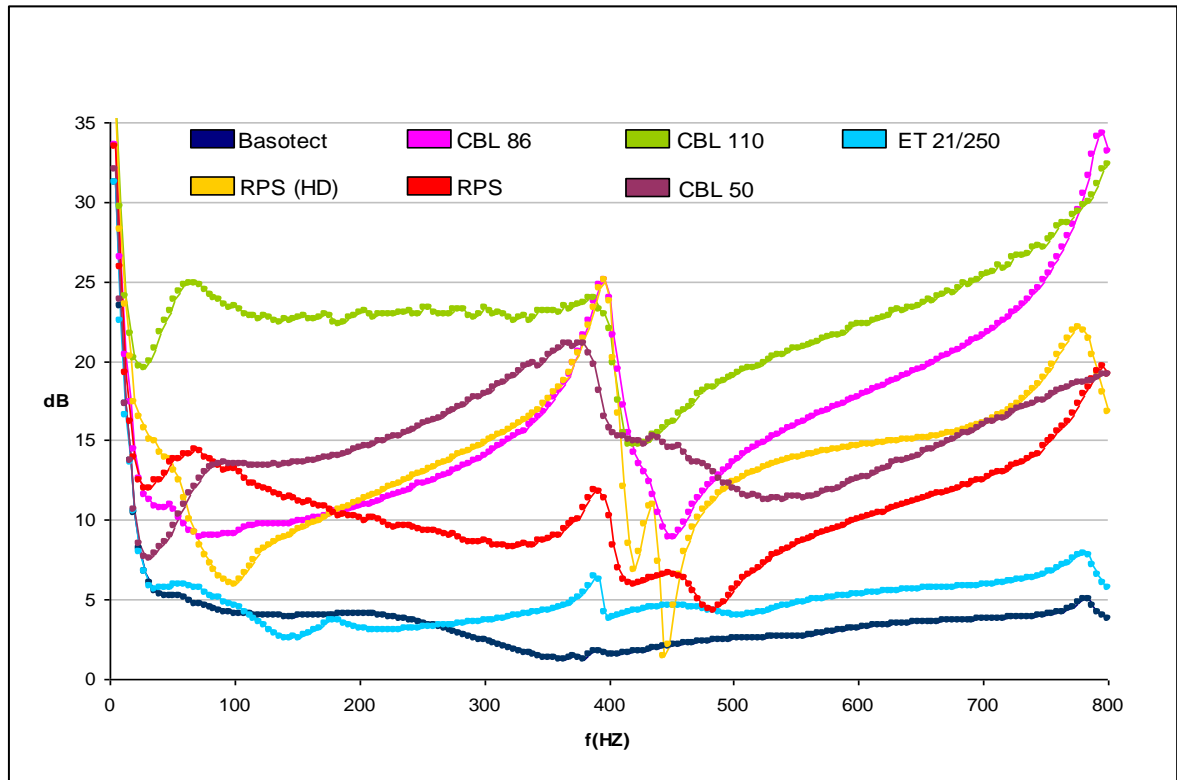
Figure 7.2 a): Sound transmission loss (STL) results (50 - 800 Hz) as function of frequency (f)

An Investigation into the Properties of Starch-Based Foams
Chapter 7. The Acoustic Properties of CBL & RPS Starch-Based Foams

233
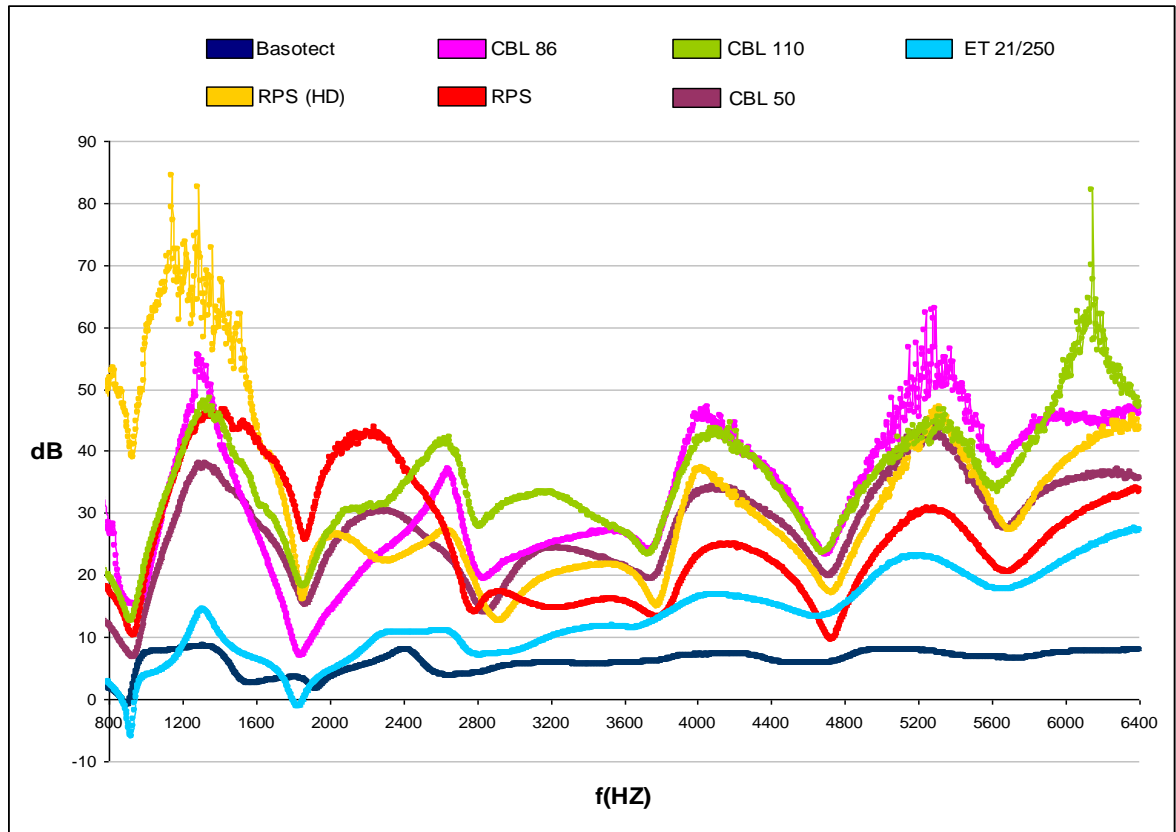
Figure 7.2 b): Sound transmission loss (STL) results (800 – 6400 Hz) as function of frequency (f)

7.2.1   Interpretation of airborne sound transmission loss (STL) test results

Unlike the linear scale used to display the sound absorption coefficient the test results shown previously, sound transmission loss measurements are given in decibels (dB), a non-linear logarithmic scale. These results in dB are based on the difference in the sound power level measurements on each side of the sample. Therefore, at any particular frequency, transmission loss measurements at higher decibels indicate that less sound energy has been transmitted through the sample than measurements shown at low decibels.

Figures 7.2 a) and 7.2 b) show that in general, higher density foams performed better than low density foams in sound transmission loss tests and in contrast to the sound absorption coefficient test results, the benchmark specialist acoustic foam Basotect and ET 21/250 which performed best in the sound absorption tests, have not performed as well as the starch foams in sound transmission loss tests, allowing a greater range of the frequencies tested to be transmitted.

An Investigation into the Properties of Starch-Based Foams
Chapter 7. The Acoustic Properties of CBL & RPS Starch-Based Foams

234

Efficient sound absorbing materials absorb rather than reflect sound energy which this does not necessarily mean they are effective at blocking the transmission of sound energy through a given thickness of material. Dense materials generally possess good sound transmission loss characteristics acting as sound barriers and effectively blocking transmission of sound by reflecting rather than absorbing the sound energy. In general, materials designed for sound absorption applications would not be used alone as sound barriers where denser materials are required. Lightweight specialist acoustic foams such as Basotect and ET 21/250 are primarily designed for sound absorption applications and are generally installed in front of an acoustic *hard wall*, or combined with denser materials in composite or laminate structures.

The undulations which can be seen to occur particularly across the 800 – 6400 Hz frequency range shown in Figure 7.2 b), result from *single degree of freedom systems* in which the natural resonant frequencies of the sample materials correspond with the sound frequencies generated and describe a condition in which the vibration input at those frequencies is amplified, resulting in an output value greater than the sum of all input values (Remington, 1998). From the data shown in Figure 7.2 b), the extremes of this phenomenon seem particularly prevalent in starch-based foams. Any susceptibility to such resonance on the part of CBL and RPS foams may be due to the considerable density variations inherent in these macro-composites which results in sound energy reverberations and oscillations within their structures at certain frequencies corresponding to the sound frequencies generated and leading to amplification of the sound energy at those frequencies. Some noise and distortion were also in evidence at the higher decibel peaks due to excess amplification at those frequencies (Vickers, 2006).

7.3   Discussion of the acoustic performance of CBL & RPS starch-based foams

Previous work to measure the airborne sound absorption coefficient of RPS and CBL starch foams was conducted by Malith Sumanasekera, a Mechanical Engineering graduate at the University of Manchester under the supervision of Dr. Bin Wang in 2006. The results of this work (as outlined in Chapter 2, section 2.11.3 of this thesis), differs from the data shown above, particularly since the sound absorption coefficients of both RPS and CBL starch-based foams do not demonstrate the double sound absorption coefficient peaks as described in Figure 7.1 of this thesis. Discrepancies between the two data sets may have been due to differences in test conditions or test methods used. For example, although a very limited range of low frequency tests (100 – 500 Hz), were conducted at the University of Manchester using the transfer function method as used in this thesis,

the more significant broader frequency range (100 – 5000 Hz), results were obtained using the standing wave ratio method (as outlined in Chapter 2, section 2.11.3).

Other factors contributing to discrepancies in the data may have been due to differences in the samples themselves. Although the thicknesses of the samples tested at the University of Manchester are given, the report does not specify the density of any of the materials tested - a factor that has a significant influence on the outcome of any acoustic testing.

In terms of potential acoustic applications, the performance of CBL and RPS starch-based foams would not provide sufficient functionality to be employed in applications in which dedicated sound absorption performance is required. However, it is apparent that these foams do have reasonable sound absorption capabilities when compared to specialised acoustic polymer foams. This, together with the sound transmission loss performance of these materials could help facilitate niche markets in acoustic barrier applications if used in conjunction with other higher-density materials known to perform well in airborne sound transmission loss tests. Such applications may be in laminate or composite partition boards or ceiling panels, for example as utilised in audio rooms or temporary music cabins at exhibitions or events in which the use of renewable materials and environmentally preferable post-use disposal is considered advantageous.

An Investigation into the Properties of Starch-Based Foams
Chapter 8. Discussion, Conclusions & Suggestions for Further Work

236

Chapter 8   Discussion, Conclusions & Suggestions for Further Work

Plastics are not normally renewable or degradable, most in fact are derived from finite petrochemical resources and are specifically formulated for stability. However, for some applications these plastics have increasingly become seen as over-engineered and in recent years greater efforts towards the creation of renewable and degradable materials have resulted in some new classes of synthetic plastics.

Despite improvements in the properties of starch-based plastics, the significance of these materials for large scale commercial applications has thus far mainly been limited to film products where research and development has led to significant improvements in their mechanical properties for applications such as supermarket carrier bags and other markets in the commercial packaging sector. In general, the development of starch-based foam materials still lags well behind those of their petrochemical counterparts, in part due to a lack of investment and technical knowledge.

As part of the overall efforts into greater research and development into starch-based materials, this investigation included a study of two novel types of starch-based block foams called RPS and CBL. While obstacles in the RPS fabrication process were identified and suggestions were made for improvement of the technique, the concept of CBL block foams comprised the main focus of the study and as such a feasibility study was conducted on aspects of the CBL fabrication process alongside studies on some key processing factors associated with development of the CBL technique towards an industrial process.

The study proved the feasibility of producing block foams in a range of densities from manually wetted and compressed loosefill chips, but it also highlighted key issues surrounding inconsistencies in sample density due to inadequate control of the technique. For this reason some preliminary studies were conducted with the objective of establishing an automated method to achieve greater uniformity of loosefill wetting which is a prerequisite of facilitating the efficiency of any subsequent automated compression system.

This objective was accomplished to some degree. The lab-scale equipment proved the overall feasibility of the wetting method and highlighted the significance of uniformity of wetting.

8.1   Identification of the potential applications of CBL & RPS starch-based foams

Given the mechanical properties of CBL and RPS, potential applications could include cushioning applications limited to the range of static loads within the capabilities of the materials. However, due to a propensity for the resilience of the materials to be compromised by successive impacts, this factor must be taken into account when determining cushioning applications. An additional

factor which should be considered when establishing suitable applications for these materials is the potential for tensile or shear forces to exploit weaknesses in the macrostructure of these materials.

Starch foams are dynamic materials in terms of their behaviour under different environmental conditions. Both CBL and RPS exhibited dimensional shrinkage, density increase and significantly reduced mechanical properties under conditions of high temperature and relative humidity. These findings suggest that these materials would not be suitable for applications in tropical regions where such conditions may be encountered, or for long-term applications unless used in conjunction with other protective materials which would not acutely increase the environmental burden of the product to the point where any positive environmental attributes of the starch-based foams are rendered negligable.

Low-density RPS and CBL foams exhibit lower thermal conductivity values and hence higher thermal insulation properties, compared to many commercially available polymer foams of similar densities. As such these foams have the potential to be used in applications in which a measure of thermal insulation is required. Thermal conductivity tests conducted on high density RPS were used to extend the extent of knowledge regarding the density/thermal conductivity relationship of this class of starch-based foams, which indicate that the structure of the foams play a major role in determining the thermal conductivity properties of these materials.

The case study which benchmarked RPS foam against a commercial chilled food distribution system reinforced the findings of the thermal conductivity tests, whilst also demonstrating that the materials have sufficient durability to perform the shipping function required. It can therefore be concluded that given sufficient research and development, starch-based foams could potentially be utilised in applications requiring thermal insulation functionality.

In terms of potential acoustic applications, neither CBL nor RPS starch foams are able to provide sufficient acoustic attenuation properties to be employed in applications in which dedicated acoustic performance is required. However, it is apparent that these open-celled foams do have reasonable sound absorption capabilities when compared to other polymer foams and this could help enhance their overall marketability for applications in which a degree of acoustic performance is desirable, especially if used in conjunction with other higher-density materials known to perform well in airborne sound transmission loss tests. Sound absorption products are generally comprised of multiple layers of different materials in laminate constructions in order to attenuate various sound frequencies, and applications could include laminated partition boards for example, in which the starch-based foams are protected from extremes of temperature and humidity.

An Investigation into the Properties of Starch-Based Foams
Chapter 8. Discussion, Conclusions & Suggestions for Further Work

238

It is anticipated that this work will make a significant contribution toward advances in the development of these novel technologies, specifically in terms of establishing an understanding of the properties of the starch-based materials in order to facilitate identification of potential applications. The research results should thus provide a fundamental element in the overall objective towards the future development of these renewable and biodegradable materials.

8.2 Suggestions for further work

While the work presented in this thesis gives some insight into the issues investigated, it has also raised some related issues requiring further investigation into this new class of materials in order to facilitate their future development. It is suggested that this work be extended and improved by further research into the following issues:

- Alternative rapid-spooling RPS foam fabrication techniques in order to expedite processing times and increase production efficiency.

- Automation and scaling up of CBL foam production in terms of loosefill wetting and compression in order to ameliorate problems surrounding local density variation within CBL foams and as a means of controlling overall density and uniformity of the foams produced.

- The extent to which the reduced cushioning performance of the starch-based foams results from material inconsistency and partial cushioning deflection suppositions as put forward in this thesis.

- The mechanisms of thermal resistivity responsible for the thermal conductivity performance of CBL and RPS starch-based foams, in particular the extent to which the thermal performance of the starch-based foams results from the structure of the foams as opposed to the material from which it is made.

Bibliography

Ager, A & Oakley, J., 2006. Marine & Coastal Litter (Marine Life Topic Note), Marine Life Information Network for Britain and Ireland, Marine Biological Association of the United Kingdom (Sept. 2006).

Anon, 1993. Degradable Plastics as Problem Solvers, Article: Australian Packaging, Vol. 41, No. 5, (May 1993).

Anon, 1998. SPI Defines Biodegradable & Compostable, Article: Paper Film Foil Converter, Nov. 1998. Article: Packaging World, 51, (May 2002).

Ansorge, T. & Nendel, K., 1998. Calculation of Cushion Diagrams Using a Physical Model, Institut für Allgemeinen Maschinenbau and Kunststofftechnik, Technische Universität, Germany. Packaging Technology & Science 11, 1-8, (Dec. 1998).

Asche, W., 1994. Biodegradable Plastics, Article: Seifen Ole Fette Washse, Vol. 120, No. 2-3, (Feb/Mar, 1994).

Atwell, W A, 2001. Wheat Flour. Eagan Press Handbook Series, Eagan Press. p 32 (2001).

Barnard, A. R. & Rao M. D., 2004. Measurement of Sound Transmission Loss Using a Modified Four Microphone Impedance Tube. Michigan Tech University, Houghton, MI 49931, USA. NOISE-CON 2004 (July, 2004).

Beynon, personal communication, 2008. Jonathon Beynon (Technical Manager), BETE Ltd, Lewes, East Sussex. (May, 2008).

Bhatnagar, S. & Hanna, M. A., 1996. Engineering and Processing Starch-Based Plastic Foams from Various Starch Sources. Cereal Chemistry 73(5):601-604 (May 1996).

Billington, personal communication, 2006. Ross Billington (Technical Director), Fairfax Meadow, 24 - 27 Regis Road, Kentish Town, London NW5 3EZ (Oct. 2006).

Bowcott, O., 1990. A Virtue of Plasticity, Article: The Guardian, (29 June, 1990).

Brüel &Kjær, 2008. Product Data Sheet BP1039.16 2008-04. DK-2850 Nærum · Denmark. (April, 2008).

Buleon, A., Colonna, P., Planchot, V. and Ball, S. Starch granules: structure and biosynthesis. International Journal of Biological Macromolecules. 23, 85-112 (1998).

Cairns, P., Morris, V. J., Singh, N. and Smith, A. C. X-ray diffraction studies on extruded maize grits. Journal of Cereal Science. **26**, 223-227 (1997).

Campbell, G. B., 1992. Package Cushion Design Data, D Pkg A/DR/4 Part 1/2, Directorate of Quality Assurance, Technical Support, Defence Packaging Authority, London p. C2, C7/8 (Feb. 1992).

CES Edupack database, 2006 – 2010. Cambridge University Engineering Dept & Granta Design Ltd, Cambridge, UK (2006 – 2010 editions).

Cha, J.Y., Chung, D.S. and Seib, P.A., 1999. Effects of Extrusion Temperature and Moisture Content on Mechanical Properties of Starch-Based Foams. Transactions of the ASAE American Society of Agricultural Engineers, 42 (6), 1765-1770 (1999).

Cornell, personal communication, 2007. Robert Cornell (Polymer Characterisation Technician), Polymer Characterisation Laboratory, Department of Materials Science, University of Cambridge (Nov. 2007).

Copeland, H; Qi, Kun; Song, J; Taverdi, K., 2007. Development of flour based biodegradable packaging composite. Wolfson Centre for Materials Processing, Brunel University. Proceedings of the 8th International Conference of Eco-Materials – ICM8, Brunel University, UK. (July, 2007).

Croy, D. E. & Dougherty, D. A.,1984. Handbook of Thermal Insulation Applications, EMC Engineers Inc, Denver Colorado, Noyes Publications, NJ,. 7, 17, 18, 27, 36, 9. (Jan, 1984).

Czichos, H; Saito, T; Smith, L., 2006. Handbook of Materials Measurement Methods. Springer Science & Business Media Inc., Leipzig, Germany. 8, 8.1, 400 (2006).

Daum M., 1999. A Simplified Process for Determining Cushion Curves: The Stress-Energy Method. Hewlett Packard (Packaging R&D), Boise, ID, 83714 USA (1999)

De Wilde, B.; De Baere, L., 1990. Methods to Determine Biodegradability of Solid Wastes, Paper: Exploring the Disposability Dilemma, Conference, Baltimore (June, 1990).

Eaves, D., 2004. Handbook of Polymer Foams, 2004, Rapra Technology. ix, 9, 1, 104, 2, 3, 106, 105, 9, 41, 179, 10-33 (2004)

ETSU/DTI, 1998. ETSU for the Department of Trade and Industry. An Introduction to Household Waste Management. Department of Trade and Industry (1998).

EuropaBio, 2006. The European Association for Bio-industries. Background Briefing: Genetically Modified Starch Potato (Amflora - EH92-527-1) (December 2006).

Evensen H.A. & Rao, M.D., 2002. Sound Fields & Room Acoustics, Section 3 in *Supplemental Notes to MEEM 4704 Acoustics and Noise Control*, edited by H.A. Evensen & M.D. Rao, Michigan Tech University, Houghton MI (2002).

Fang, Q; Hanna, M. A., 2001. Characteristics of Biodegradable Mater-Bi-Starch Based Foams as Affected by Ingredient Formulations. Industrial Crops and Products, 13 (3), 219–227 (2001).

Fang, Q, Hanna, M A, 2001[a]. Preparation and characterisation of biodegradable copolyester – starch based foams. Bio-resource Technology, 78, 115-122. (2001).

Frandas, A.; Paris, D.; Bissieux, C.; Chirtoc, M.; Antoniow, J.S.; Egée, M., 2000. Classical and photopyroelectric studies of optical and thermophysical properties of starch sheets: dependence on water content and temperature. Applied Physics, B 71, 69 – 75 (2000)

LaserComp. Fox 314 Thermal Conductivity Instrument information sheet. LaserComp, Saugus, MA 01906, USA. (undated).

Gearing, personal communication, 2010. John W E Gearing (Managing Director), Gearing Scientific, Ashwell, Herts. (Feb. 2010).

Gibson, L. J. & Ashby M. F., 1997. Cellular Solids, Structure & Properties (second edition). Cambridge University Press. p 5, 49, 257, 52, 183, 184, 185, 198, 199, 217, 218, 219, 285, 287, 288, 289, 290, 292, (1997).

Glenn, G, M; Orts, W, J., 2001. Properties of Starch-Based Foam Formed by Compression/Explosion Processing, Industrial Crop and Products. 13, 135-143 (2001)

Goddard; Pidgeon; Hunt., 1993. Special Report – Bio-crops, Packaging Week, Vol. 8, No. 42, (May, 1993).

Hull, D, Clyne, T W, 1996. An Introduction to Composite Materials. Second edition, CambridgeUniversity Press, Cambridge, 12.5 (1996).

Incpen (undated). Degradable Packaging Factsheet, Industry Council for Packaging & the Environment, Reading, Berkshire.

Jung, S, S; Kim, Y, T; Lee, Y, B; Cho, S, I; Lee, J, K., 2008. Measurement of Sound Transmission Loss by Using Impedance Tubes. Journal of the Korean Physical Society, Vol. 53, No.2. 596-600 (August 2008).

Kang, Y. G., 2006. Biodegradable Starch-Based Foam Block for Cushion Packaging (PhD Thesis) School of Engineering & Design, Brunel University. 2-53, 2-51, 7-1, 7-2, 4-38, 5-5, 5-23, 5-1, 5-7, 1-7, 7-1, 7-5, 7-10, 7-2, 7-32, 7-33 (2006).

Kirby, A. R., Clark, S. A., Parker, R., Smith, A. C. The deformation and failure behaviour of wheat starch plasticized with water and polyolefins. Journal of Material Science. **28**, 5937-5942 (1993).

Klemchuk, P. P., 1989. Chemistry of Plastics Casts a Negative Vote, Article: Modern Plastics International, Vol. 19, No. 9 (Sept. 1989).

Lee, S. T., 2000. Foam extrusion Principles and Practice. Lancaster, PA ; Basel: Technomic Publishing co., inc., 172. (2000).

Lewis, personal communication, 2010. David Lewis (Production Manager), Green Light Products Ltd., Cardiff, Wales (Feb, 2010).

Lorcks, J., 1998. Properties and application of compostable starch-based plastic material. Polymer Degradation and Stability, 59, 245-249 (1998).

Loveridge, P; Mills, N. J., 1993. Prediction of Packaging Cushion Curves and Helmet Liner Responses. School of Metallurgy and Materials, University of Birmingham, Cellular Polymers II Conference, Edinburgh, RAPRA Technology, Paper 21 (1993).

Lox, F., 1992. Packaging and Ecology, PIRA International, Leatherhead, Surrey. 57, 60, 61 (1992).

Lui, W B, Peng, J., 2005. Physical, mechanical, biodegradable properties and energy absorption behavior of corn grit-polyvinyl alcohol cushioning extrudates. Journal of Food Engineering, 71, 73–84 (2005).

Matthews, personal communication, 2008. Toby St. G. Matthews, Managing Director, PotatoPak Ltd., Henstridge, Somerset. (July, 2008).

McCarthy, S. P., 2001. Aqueous processing of biodegradable materials from renewable resources (Final report). National Centre for Environmental Research, Technology for a Sustainable Environment, University of Massachusetts. (Dec. 2001).

McCarthy-Bates, L., 1993. Biodegradables Blossom into Field of Dreams for Packagers, Article: Plastics World, Vol. 51, No. 3. (March, 1993).

Naguib, H. E., Park, C. B., Reichelt, N., 2004. Fundamental Foaming Mechanisms Governing the Volume Expansion of Extruded Polypropylene Foams. Journal of Applied Polymer Science, 91, 2661–2668 (2004).

Nawrath, C., Poirier, Y., Somerville, C., 1995. Plant polymers for biodegradable plastics: Cellulose, starch and polyhydroxyalkanoates. Carnegie Institution of Washington, Department of Plant Biology, 290 Panama Street, Stanford, CA. Molecular Breeding Vol. 1, No. 2: 105-122, (June 1995).

Nolan-ITU Pty Ltd., 2002. Biodegradable Plastics: Developments and Environmental Impacts, East Kew Victoria (in association with ExcelPlas, Australia) Ref: 3111-01. 1, 3 (Nov, 2002).

Ollett, A.-L., Parker, R., Smith, A. C., Miles, M. J., Morris, V. J. Microstructural changes during the twin-screw extrusion cooking of maize grits. Carbohydrate Polymers.. **13**, 69-84 (1990)

Park, C.P, Garcia G. A.; Watson R.G., 2003. (The Dow Chemical Company) Expandable Foam from Amorphous Polyester Resin. Journal of Cellular Plastics 2003; 39; 229 (2003).

Parker, R., Ring G.S., 2001. Aspects of the Physical Chemistry of Starch, Journal of Cereal Science, 34 (1),1. (2001).

Perchard, D., 1991. Packaging – The Environment and the Consumer, PIRA International, Leatherhead, Surrey. 72 – 81 (1991).

Poll, A. J., 1995. Opportunities and Barriers to Recycling of Compostable Wastes. (Consultation Report) AEA Technology, Abingdon, Oxfordshire. (1995).

Poutanen, K , Forssell, P. Modification of starch properties with plasticizers. Trends in Polymer Science. **4**, 128-132 (1996)

Rao, M.A & Hartel, R.W., 1998. Phase/State Transitions in Food, Marcel Dekker, New York. 151 (1998).

Remington, P. J., 1998. Handbook of acoustics (Edited by M.J. Crocker). John Wiley & Sins Inc.. 48. 559-564 (1998).

Roylance, D., 2001. Stress-Strain Curves. Department of Materials Science and Engineering, Massachusetts Institute of Technology, Cambridge, MA.. 1 (Aug. 2001).

Schnabel, Prof. Dr. W., 1981. Polymer Degradation – Principles and Practical Applications, Macmillan. 24, 31, 33 (1981).

Selke, S., 1990. Biodegradation and Packaging, PIRA International, Leatherhead, Surrey. 16, 18, 28 (1990)

Selke, S., 1996. Biodegradation and Packaging, (2nd Edition), PIRA International, Leatherhead, Surrey. 24, 25, 27, 38 (1996).

San Martin-Martinez, E; Aguilar-Mendez, M.A.; Cruz-Orea, A; Garcia-Quiroz, A. Photothermal techniques applied to the study of thermal properties in biodegradable films (2008). The European Physics Journal, Special Topics 153, 179 – 182, 2008.

Serth R. W., 2007. Process Heat Transfer, Principals & Applications, Academic Press, Kidlington, Oxford, UK. 1.2, 2 (2007).

Shires, personal communication, 2009. David Shires, (Environmental & Distribution Testing), Pira International, Leatherhead, Surrey, UK (Nov. 2009).

Shogren, R. L.; Jasberg, B. K. Ageing properties of extruded high-amylose starch. Journal of Environmental Polymer Degradation. **2**, 99-109(1994)

Shogren, R. L; Lawton J W; Tiefenbacher, K F; Chen, L., 1998. Starch-Polyvinyl Alcohol Foamed Articles Prepared by Baking Process. Applied Polymer Science, 68, 2129–2140 (1998).

Shogren, R. L.; Willett, J. L., 2002. Processing and properties of extruded starch/polymer foams. Plant Polymer Research Unit, US Department of Agriculture, National Center for Agricultural Utilization Research, Agricultural Research Service, Peoria, IL. US (2002).

Simmons, S. and Thomas, E. L. Structural characteristics of biodegradable thermoplastic starch/polyethylene-vinyl alcohol blends. Journal of Applied Polymer Science. **58**, 2259-2285 (1995)

Slater, R., Frederikson, J., Gilbert, E., 1999. The State of Composting 1999. The Composting Association, Coventry. 63-65 (1999).

Sokatch, J. R., 1969. Bacterial Physiology and Metabolism, Academic Press, London. 102 (1969).

Soroka, W., 1996. Fundamentals of Packaging Technology (Revised UK edition), Institute of Packaging, Leicester. 372-373, 364, 372, 370 (1996).

Stevens, E. S., 2002. Green Plastics: An Introduction to the New Science of Biodegradable Plastics, Princeton University Press, NJ. 76 (2002).

Suhanek, M; Jambroši, K; Horvat, M., 2008. A comparison of two methods for measuring the sound absorption coefficient using impedance tubes. Faculty of Electrical Engineering and Computing, Unska 3, 10 000 Zagreb, Croatia. 50th International Symposium ELMAR-2008, 10-12 September 2008, Zadar, Croatia. (2008).

Sumanasekera, M, 2006. Investigation of the Acoustic Properties of a Biodegradable Foam, Dept of Mechanical Engineering, University of Manchester, School of Mechanical, Aerospace & Civil Engineering (May, 2006).

Swinkels, J. J. M., 1985. Sources of Starch, Its Chemistry and Physics, Carbohydrate Polymers Volume 26, Issue 1, 1995, Pages 47-54 (1985).

Timoshenko S. & Goodier J.N., 1970. Theory of Elasticity, McGraw-Hill, New York (1970).

Tinius Olsen, 2010. Benchtop Materials Testing Machines (Bulletin140-D), Tinius Olsen 1065 Easton Road, Horsham, PA 19044 USA (2010).

Unilever Research / National Starch and Chemical Co., 2000. Production of very high-amylose potato starch by inhibition of SBE A and B, Nature Biotechnology, Volume 18, Number 5, 551 – 554 (May, 2000).

van Soest, J. J. G., Hulleman, S. H. D., De Wit, D., Vliegethart, J. F. G. Crystallinity in starch bioplastics. Industrial Crops and Products **5**, 11-22 (1996 [a]).

van Soest, J.J. G., De Wit, D., Vliegethart, J. F. G. Mechanical properties of thermoplastic waxy maize starch. Journal of Applied Polymer Science. **61**, 1927-1937 (1996 [b]).

van Soest, J. J. G., Benes, K. De Wit, D., Vliegenthart, J. F. G. The influence of starch molecular mass on the properties of extruded thermoplastic starch. Polymer **37**, 3543-3552 (1996 ᶜ).

van Soest, J. J. G. and Vliegenthart, J. F. G. Crystallinity in starch plastics: consequences for materials properties. TIB Tech. **15**, 208-213 (1997)

Vickers, personal communication, 2006. Keith Vickers (Sound Technician), Bruel & Kjaer UK Ltd., Stevenage, Herts. (Nov. 2006).

Wang, Y., 2008. A Study of the Structure & Properties of Starch Foam & Eco-Composites for Industrial Applications (PhD Thesis), School of Engineering and Design, Brunel University, p 67, 57, 104, 122. (July 2008).

Wiles, personal communication, 2006. James Wiles (Managing Director), Foam Engineers, Ltd., High Wycombe, Bucks. (Feb. 2006)

Wollerdorfer, M, Bader, H.,1998. Influence of natural fibres on the mechanical properties of biodegradable polymers. Industrial Crops and Products, 8 (2), 105–112 (1998).

Zobel, H. F. X-ray analysis of Starch granules. Methods in Carbohydrate Chemistry. Vol.4. Starch. R. L. Academic Press, New York, pp 109-113 (1964)

Zhang E; Song J., 2003. Puff Moulding of Starch Foams. Internal Report, Brunel University, School of Engineering & Design, Dept of Mechanical Engineering, Uxbridge, Middx. (2003).

Zhou, J., 2004. Microwave assisted moulding of starch-based foams, PhD Thesis, School of Engineering & Design, Dept of Mechanical Engineering, Brunel University, Uxbridge, Middx. (2004). Ch 2, p4

Zhou, J; Song, J & Parker, R., 2006. Structure and Properties of Starch-Based Foams Prepared by Microwave Heating from Extruded Pellets, Carbohydrate Polymers, 63**.** 466-475 (2006).

Zhou, J; Song, J & Parker, R., 2007. Microwave-Assisted Moulding Using Expandable Extruded Pellets from Wheat Flours and Starch, Carbohydrate Polymers, 69**.** 445-454 (2007).

Web References

Anter Corporation, 2009. Principal Methods of Thermal Conductivity Measurements (Technical Note #67) http://www.anter.com/TN67.htm

Aperion audio, 2008. http://www.aperionaudio.com/AperionU/physics_sound.aspx

Auralex, 2010. Auralex Acoustics, Inc. 6853 Hillsdale Court, Indianapolis, US. http://www.auralex.com/

Auto Reel, 2010. http://autoreel.co.uk/news.html

BPF, 2007. British Plastics Federation, http://www.bpf.co.uk/Plastipedia/Processes/Moulding_EPS.aspx

Canadian Plastics, 2009. http://sustainableplastics.org/news/canadian-researchers-turn-potato-starch-bioplastics

CRC Press LLC, 1989. http://composite.about.com/library/glossary/b/bldef-b712.htm

DEFRA, 2003. Environmental Protection, Municipal Waste Management Statistics (2003) Municipal Waste Management Statistics 2001/2, Waste and Recycling Bulletin http://www.defra.gov.uk/environment/statistics/wastats/bulletin/index.htm#WasteManagementDisposal

Demichelli, M., 1996. Biodegradable Plastics from Renewable Sources, IPTS Report No. 10, 1996. http://www.jrc.es/iptsreport/vol10/english/Env1E106.htm

Environment Council, 2002. The External Costs of Landfilling, The Stakeholders Guide to Sustainable Waste Management, http://www.wasteguide.org.uk/waste/mn_wmo_landfil_external.stm

ERG, 2008. Energy Research and Generation, Inc. http://www.ergaerospace.com/foamproperties/matspecificproperties.htm

Foam Design, 2008. http://www.foamdesign.com/materials.htm

Green Light Ltd, http://www.greenlightpackaging.com/pages/greenfill.html

Green Light, 2010. http://www.greenlightproducts.co.uk/our-products/biodegradable-loose-fill/

Hay, M, 2002. The Extent of Gelatinisation and Change to the Microstructure of Starch as a Result of Extrusion Processing (Thesis), The University of Queensland, Dept. of Chemical Engineering. http://www.cheque.uq.edu.au/ugrad/theses/2002/pdf/Thesis%20Hay.pdf

IENICA, 2003. Summary Report for European Union: Carbohydrate Crops, http://www.ienica.net//reports/BIGCARBS.pdf

Michigan Tech, 2010. Hot Disk[TM] Thermal Constants Analyzer Model TPS 2500 http://www.chem.mtu.edu/org/ctc/Hot%20Disk%20Summary%20for%20ctc%20web%20dec%202007.doc

National Starch & Chemical Co., 2003[a] http://www.eco-foam.com/structure.asp

National Starch & Chemical Co., 2003[b] http://www.eco-foam.com/processing.asp

NEFAB, 2009. http://www.nefab.com/Packaging_Information_Product_Fragility_G-factor-
.aspx

Official Journal of the European Communities, 2001
http://eur-lex.europa.eu/LexUriServ/LexUriServ.do?uri=CELEX:32001D0524:EN:HTML

Physics classroom, 2008. http://www.physicsclassroom.com/class/sound/u11l1c.cfm

Plastics Technology, 2009. http://www.ptonline.com/articles/kuw/9783.html

PFA, 2000. Polyurethane Foam Association
Flexible Polyurethane Foam: Industry at a Glance (www.pfa.org) Accessed: January, 2006.
http://www.pfa.org/intouch/new_pdf/lr_IntouchV5.2.pdf

Pregis Corporation, 2010. 1650 Lake Cook Road, Suite 400, Deerfield, Illinois 60015. USA.
http://www.pregis.com/PregisHome/ProtectivePackaging/AstroFoamPEsheetfoam/TechnicalF
oam/NOPAPLANK/tabid/173/language/en-GB/Default.aspx

Quality Foam Packaging, 2010. 31855 Corydon Street, Lake Elsinore, CA, 92530. USA.
http://www.qualityfoam.com/ethafoam-220.asp

Raynaud, L. (undated). New Commercial Developments in the Field of Starch-Based Plastics,
National Starch & Chemical Co., UK.
http://formacion.aimplas.es/seminariobio/Ludovic%20Raynaud.doc

Schueneman, H H, [(a)] (undated) Cushion Material Testing, Westpak Inc, San Jose, CA.
(www.westpak.com/techpapers/11_cushion_material_testing.pdf) p 9, 11, 7, 17

Schueneman, H H, [(b)] (undated) Cushion Engineering, Design & Testing, Westpak Inc, San Jose,
CA. (www.westpak.com) p 16

Sealed Air Corp, 2006.
http://www.sealedair.com/products/protective/instapak/instapak.html

Sengpiel audio, 2006. Decibel Table – Loudness Comparison Chart
http://www.sengpielaudio.com/TableOfSoundPressureLevels.htm

Silex, 2002. Sound Attenuation www.silex.com/pdfs/Sound%20Attenuation.pdf 1.16, 3.16

Talk Packaging, 2007. The online packaging community
http://talkpkg.com/Learning-Center/Mat-Tech/Foam/foam.htm#EPE

UNEP, 2010. United Nations Environment Programme, Distribution of Marine Litter
http://www.unep.org/regionalseas/marinelitter/about/distribution/default.asp

Nature, 2000. (Nature - Biotechnology) Production of very-high-amylose potato starch by
inhibition of SBE A and B
http://www.nature.com/cgitaf/DynaPage.taf?file=/nbt/journal/v18/n5/full/nbt0500_551.html

University of York, 2001. Friendly Packaging,
http://www.friendlypackaging.org.uk/schoolstarch.htm

US Department of Energy, Consumer Guide, 2009.
http://www.eere.energy.gov/consumer/your_home/insulation_airsealing/index.cfm/mytopic
=11620

Waste Watch, 2006. 56-64 Leonard Street, London EC2A 4JX
http://www.wasteonline.org.uk/resources/InformationSheets/Plastics.htm

Zotefoams plc, 2010. 675 Mitcham Road, Croydon, Surrey, CR9 3AL UK.
http://zotefoams.com/pages/EN/site-map.asp